This is to certify that the
dissertation entitled

SURFACE INITIATED ATRP OF SUBSTITUTED STYRENES AND FUNCTIONAL MONOMERS ON FLAT SURFACES

presented by

Sampa Saha

has been accepted towards fulfillment
of the requirements for the

Ph.D. degree in Chemistry

Major Professor's Signature

6 May 2010

Date

MSU is an Affirmative Action/Equal Opportunity Employer

SURFACE INITIATED ATRP OF SUBSTITUTED STYRENES AND FUNCTIONAL MONOMERS ON FLAT SURFACES

By

Sampa Saha

A DISSERTATION

Submitted to
Michigan State University
in partial fulfillment of the requirements
for the degree of

DOCTOR OF PHILOSOPHY

Chemistry

2010

ABSTRACT

SURFACE INITIATED ATRP OF SUBSTITUTED STYRENES AND FUNCTIONAL MONOMERS ON FLAT SURFACES

Surface initiated atom transfer radical polymerization (ATRP) of substituted styrenes leads to rapid synthesis of uniform and thick substituted polystyrene brushes (>100 nm in 1 hour) from gold and silicon surfaces. High growth rates were observed for styrenes substituted with electron withdrawing groups in meta/para positions. The effects seen in surface and solution polymerizations are similar for styrenes with electron withdrawing groups, and for electron donors in ortho and para positions. However, electron donors at meta sites have surprisingly fast growth rates, which may be due to steric inhibition of termination. The overall surface polymerization rates for substituted styrenes was analyzed and found to follow the Hammett relation with $\rho = 0.51$. The ratio of k_p to k_t, is as an indicator of the likelihood that a reaction will reach high degrees of polymerization before termination.

During surface initiated polymerization, thiols desorb from gold surfaces at low temperatures (< 60 $^{\circ}$C) and terminate growing polymers during surface initiated ATRP. Thiol desorption was prevented by forming a cross-linked poly(siloxane) primer layer on the gold surfaces prior to attaching the initiator layer. These modified surfaces provide polymer film thicknesses comparable to films grown from silicon surfaces. This strategy above 100 $^{\circ}$C since the film delaminates from the substrate. Usually, difficult monomers,

such as 2-vinyl pyridine, a polyelectrolyte precursor, cannot be grown from thio-initiators anchored on gold, but the cross-linked initiator enabled growth of thick polymer films.

Polyacrylate brushes with pendent terthiophenes (PTTMM) were successfully grown from ITO and gold using surface initiated ATRP. Using cyclic voltammetry, the PTTMM brush was electrochemically cross-linked to form a conjugated polymer network. The conjugation lengths in the film were short, but were increased via heterocoupling. These uniformly grafted conducting polymer brushes may find use in photovoltaic devices.

Click chemistry was used for the post-functionalization of hydrophilic polymer brushes. The polymer brushes were random copolymers of AZPMA (azidopropyl methacrylate), a functional monomer with a pendent azo group, and oligo ethylene glycol methyl ether methacrylate (PEGMA) with varying ethylene oxide chain lengths, which enabled control over the hydrophilicity and functional group density in the copolymer. Subsequent post-functionalization of homo and copolymer brushes was demonstrated by appending an alkyne-modified dye to AZPMA via click reactions. Kinetic studies showed that the modification of surface-grafted homo/copolymer brushes was fast (> 60% conversion in 1 min) irrespective of the copolymer composition. In the case of water soluble high molecular weight alkynes, surface-grafted copolymers with highest amount of hydrophilic monomer (PEGMA) gave the highest degree of immobilization, which indicates its potential application in bioconjugation.

To My Beloved Family

ACKNOWLEDGMENTS

I would like to thank my advisor, Professor Gregory L. Baker for being great mentors during my graduate study at Michigan State University. He has been an excellent research advisor who really taught me how to think and come up with own ideas. The openness to ask questions, propose solutions and the emphasis for critical thinking were important attributes that made the work environment both fun and challenging. I express my deep gratitude to all my committee members, Dr. Merlin Bruening, Dr. C.K. Chang and Dr. William Wulff. Professor Merlin Bruening has a great science attitude and critical thoughts. He is exceptionally good at math. I found plenty of helpful suggestions from him to achieve my research goal. As my second reader, I want to thank Professor William Wulff for his great suggestions especially toward my seminar and a great party with lot of delicious food at his home.

I would like to thank all past and present Baker group members: Bao, Ying, DJ, Erin, Qin, Gina, Hui, Heyi, Yiding, Wen and Quanxuan. I also enjoyed working with Bruening group members especially Fei, Weihan, David and Parul. I really enjoyed my life here with my husband and all of my friends. Special thanks to Debbie Roper for her kindness to me during my stay in Chemistry Department, especially in my last semester. She has been always a big help for me.

Though last year I lost my father, I believe his blessings are always with me. Whatever I am today, it's all because of my parent's encouragement. Finally, I would like to thank my husband who was my second mentor during my graduate study. Last but not

least I would like to thank my sister Dona and brother-in law Apurba for constant positive support. My beloved family deserve the greatest thank and love.

TABLE OF CONTENTS

LIST OF TABLES

Table **Page**

LIST OF FIGURES

Images in this dissertation are presented in color.

LIST OF SCHEMES

LIST OF ABBREVIATIONS

A	Absorbance
AIBN	2,2'-Azobisisobutyronitrile
AFM	Atomic force microscopy
ATR	Attenuated total reflectance
ATRA	Atom transfer radical addition
ATRP	Atom transfer radical polymerization
A_p	Average cross-sectional area of polymer chains
Azpma	Azidopropyl methacrylate
2-BPB	2-Bromopropionyl bromide
bpy	2,2'-Bipyridine
CL	ε-Caprolactone
C_M	Chain transfer constant to monomer
CV	Cyclic Voltammetry
CYCLAM	1,4,8,11-Tetraazacyclotetradecane
DMF	N,N-dimethylformamide
dNbpy	4,4′-Di(5-nonyl)-2,2′-bipyridine
dnNbpy	4,4′-Di(*n*-nonyl)-2,2′-bipyridine
DP	Degree of polymerization
ε	Molar extinction coefficient
EDOT	3,4 ethylenedioxy thiophene

Egma	Ethylene glycol methyl ether methacrylate
EtOAc	Ethyl acetate
f	free energy
FTIR	Fourier transform infrared
Γ	Grafting density
GC	Gas chromatography
GPC	Gel permeation chromatography
HEMA	2-Hydroxyethyl methacrylate
HMTETA	1,1,4,7,10,10-Hexamethyltriethylenetetramine
ITO	Indium tin oxide
k_p	Polymerization rate constant
k_{pabs}	Absolute propagation rate constant
k_{papp}	Apparent polymerization rate constant
k_t	Termination rate constant
k_{tapp}	Apparent termination rate constant
k_{act}	Activation rate constant
k_{deact}	Deactivation rate constant
Lactide	3,6-Dimethyl-1,4-dioxane-2,5-dione
LB	Langmuir-Blodgett
LCST	Lower Critical Solution Temperatures

MA	Methyl acrylate
Me	Methyl
Me_4Cyclam	1,4,8,11-tetramethyl-1,4,8,11-tetraazacyclotetradecane
Me_6TREN	*tris*[2-(Dimethylamino)ethyl]amine
iCP	Microcontact printing
MMA	Methyl methacrylate
M_n	Number average molecular weight
mPEG	methoxy Poly(ethylene glycol)
MS	Mass spectroscopy
MPS	Mercaptopropyltrimethoxysilane
MTM	3-Methylthienyl Methacrylate
MUD	Mercaptoundecanol
M_w	Weight average molecular weight
MWNT	Multiwalled carbon nanotubes
N_A	Avogadro's number
NMP	Nitroxide-mediated polymerization
NMR	Nuclear magnetic resonance
Nb	Norbornene
OTf	Triflate
PAA	Poly(acrylic acid)
PBA	Poly(*n*-butyl acrylate)

PCL	Poly(ε-caprolactone)
PDI	Polydispersity index calculated as M_w/M_n
PDMS	Polydimethylsiloxane
PEI	N-propionylethylenimine
PEG	Poly(ethylene glycol)
Pegma	Poly(ethylene glycol methyl ether methacrylate)
PGMA	Poly(glycidyl methacrylate)
Ph	Phenyl
PHEMA	Poly(2-hydroxyethyl methacrylate)
phen	1,10-Phenanthroline
PLA	Poly(lactide)
PLED	Photo light emitting diode
PMA	Poly(methacrylate)
PMEMA	Poly(2-(N-morpholino)-ethyl methacrylate)
PMMA	Poly(methyl methacrylate)
PMDETA	N,N,N′,N′,N″-pentamethyldiethylenetriamine
PNIPAAM	Poly(N-isopropylacrylamide)
POEGMA	Poly(oligoethylene glycol methyl ether methacrylate)
PPZ	Poly(phosphazenes)
PS	Polystyrene
PtBA	Poly(*tert*-butyl acrylate)
PVK	Poly(vinyl carbazole)
PVP	Poly(4-vinyl pyridine)

φ	Volume fraction
QR	Quenching and re-initiation
r	Random copolymer
RAFT	Reversible addition-fragmentation chain transfer
ROMP	Ring-opening metathesis polymerization
ROP	Ring-opening polymerization
R_p	Rate of polymerization
R_g	Radius of gyration
σ	Hammett constant
SAM	Self-assembled monolayer
SEM	Scanning electron microscopy
SI	Surface initiated
tBA	*tert*-Butyl acrylate
TEAP	Tetraethyl ammonium perchlorate
TEM	Transmission Electron Microscopy
TEMPO	2,2,6,6-Tetramethylpiperidinyloxy
THF	Tetrahydrofuran
TMEDA	Tetramethylethylenediamine
TREN	*Tris*[2-aminoethyl]amine
TTMM	[2, 2':5', 2''-Terthiophen]-3'-ylmethyl methacrylate
UV	Ultraviolet
4-VP	4-Vinyl pyridine

XPS	X-ray photoelectron spectroscopy
ρ	Reaction constant

Chapter 1
Introduction

1.1. Polymer Brushes – a brief definition

The term "polymer brush" refers to an assembly of polymer chains tethered at one end to a surface and packed sufficiently dense that the polymer chains are forced into an extended conformation. Polymer brushes can be formed by using either a 'grafting to' technique, where the polymers are absorbed onto a surface,[1] or a 'grafting from' technique, where the polymers are grown directly from the surface (Figure 1.1).[2,3,4] This study emphasizes the 'grafting from' technique due to its ease of synthesis, and the high density of polymer chains in the resulting film. A number of polymerization methods have been used to synthesize polymer brushes by the 'grafting from' technique, including free radical polymerization,[5] as well as controlled polymerizations such as reversible addition-fragmentation polymerization (RAFT),[6] nitroxide mediated radical polymerization (NMP),[7] ionic polymerization,[8] ring opening metathesis polymerization (ROMP),[9] and atom transfer radical polymerization (ATRP).[10] Surface-initiated ATRP is one of the most important techniques for generating polymer brushes[11] from surfaces such as gold[10] or silica.[12]

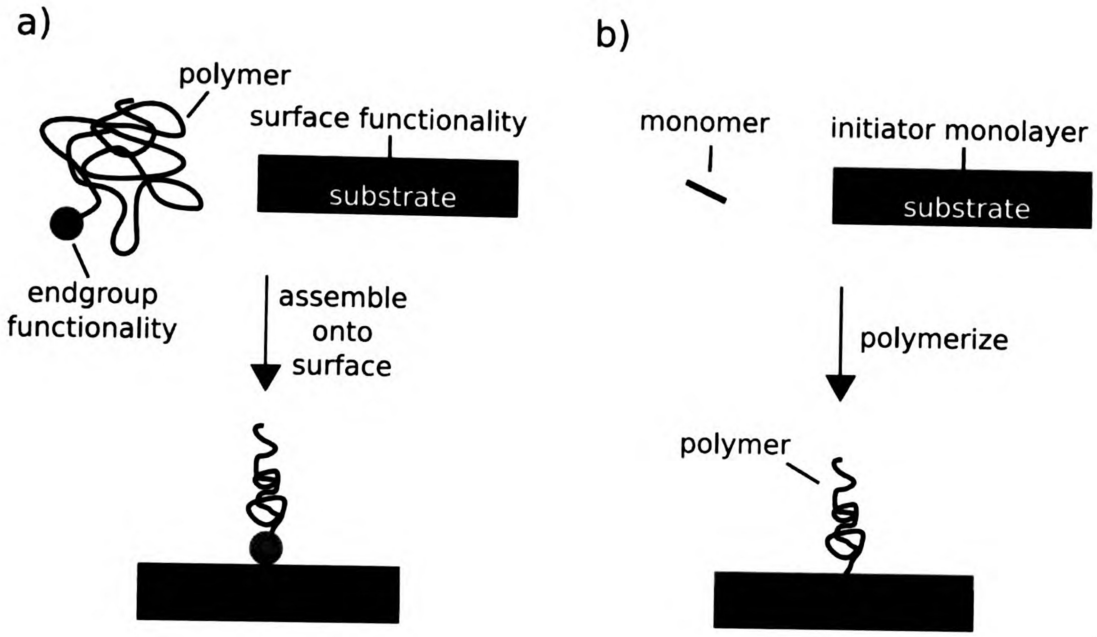

Figure 1.1: Graphical representation of a) the 'grafting to' technique, and b) the 'grafting from' technique (Reprinted with permission from Gregory L. Whiting, *Ph.D. thesis* **2006**, University of Cambridge).

1.2. Structure of Polymer Brushes

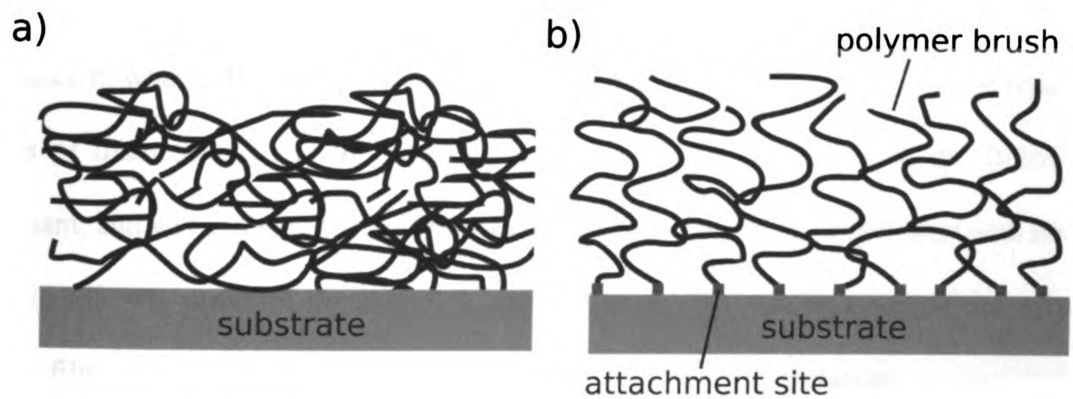

Figure 1.2: a) Schematic showing a thin film comprised of polymer chains in a random conformation. b) Schematic showing a thin film comprised of polymer chains in a brush conformation (Reprinted with permission from Gregory L. Whiting, *Ph.D. thesis* **2006,** University of Cambridge).

Due to steric interactions, the surface-attached polymer chains in a dense polymer brush film are expected to be more extended than randomly coiled polymers. Figure 1.2 compares the morphology of polymer chains in a random conformation (spin coated polymer) and in a brush conformation. A simple energy balance model can be constructed to compare the deformation of a polymer chain in a brush conformation and a randomly coiled polymer. Generally, maximization of entropy for polymer chains can be achieved by adopting a random coil conformation. However, this is not possible for polymer brushes due to the end-grafted chains and steric interactions from the overlap of other polymers. The Alexander model takes these two considerations into account for an end grafted polymer chain.[13,14] This model, developed using the Flory approximation (from random walk experiments), shows that the free energy, f, for a polymer chain in a good solvent in the brush conformation is given by Equation 1.1.The model assumes that the concentration of repeating units is constant throughout the polymer brush film, so that $\varphi = N\sigma/h$ (φ= volume fraction of the grafted polymer chains) and that there is a fixed distance h, where all of the polymer chains terminate. Here, N is the number of repeating units of diameter a, σ is the grafting density, T is temperature, k is the Boltzmann constant, and ν is an excluded volume parameter. Minimizing this expression with respect to h (df/dh =0), provides Equation 1.2, which indicates that the thickness of the polymer brush film, in solution, varies linearly with the degree of polymerization.

$$f \sim kT\left(\frac{3h^2}{2N\,a^2} + \nu N\varphi\right) \qquad 1.1$$

$$\frac{df}{dh} \sim kT\left(\frac{3h}{N a^2} - \frac{\nu\sigma N^2}{h^2}\right), \quad h\left(\frac{df}{dh} = 0\right) \sim N\left(\nu\sigma a^2\right)^{1/3} \qquad 1.2$$

This result implies that when the distance between the grafting sites is less than the radius of gyration, the chains stretch somewhat to minimize this steric energy. This is actually observable when the unstretched chain dimension increases as $N^{1/2}$ (since $R_g = N^{1/2}a$), the brush thickness increases linearly with respect to N. So, it seems reasonable to accept that the polymer chains must be deformed somewhat from a completely random conformation, and the deformation will become more pronounced for higher degrees of polymerization (N). A similar strategy can be applied to a polymer brush film in a dry state. In this case it can be shown that the equilibrium thickness increases as $N^{2/3}$, implying that the polymer chains are also stretched and deformed from a random configuration in the dry state. This deformation leads to changes in physical properties of the brush film.

Yamamoto, *et al.*[15] showed that poly(methyl methacrylate) (PMMA) brushes consistently have higher glass transition temperatures (T_g) than spin-coated PMMA films of similar thickness, and the corresponding brush films consistently have 8 °C higher T_gs at higher thickness. Though the mechanism is obscure, the increased T_g must be due to the stretched nature of the polymer brush chains.[14] It should be pointed out that the authors formed spin-coated films from free polymer synthesized from the same polymerization as the surface-attached films. Therefore, the two polymer films (brush

and spin-coated) are expected to have similar properties, and the T_g difference can not be due to differences in chain length, polydispersity or stereochemistry.[16] Overall, these data suggest that polymer brushes exist in a stretched configuration different from that of a free chain in solution.

1.3. Synthesis of Polymer Brushes – recent advances

There are two distinct pathways to achieve polymer brush architectures, the "grafting to" and "grafting from" approaches. "Grafting to" utilizes preformed polymers with an end functionality that interacts or anchors with the substrate surface. This generally involves a chemical or physical adsorption process. A limitation to this type of application is that the process is diffusion limited so that as more and more polymer chains are attached to the surface, the ability for a new polymer chain to diffuse to the surface of the substrate is greatly hindered (Figure 1.1a). On the other hand, the "grafting from" or surface initiated polymerization approach places the initiating groups directly on the surface, eliminating the diffusion problem to a great extent and providing control of the polymer chain length as well as the grafting density. Locating the initiator on the surface means that the growing polymer is attached to the surface and the monomer diffuses to the growing chain end throughout the reaction; i.e., the growing chain eventually extends from the substrate (Figure 1.1b). This technique is amenable to a large number of surface initiators as well as various polymerizations mechanisms[17] as discussed below.

1.3.1 Polymer brushes by free radical polymerizations

Surface initiated free radical polymerization was investigated in detail by Minko and coworkers using both theoretical and experimental approaches.[18] They attached azo

and peroxide initiators to solid substrates by either physisorption or chemical immobilization, and grew polystyrene via a free radical pathway. The kinetics for polystyrene grown from a silica surface with attached azo-initiators was followed by *in situ* ellipsometric measurement of the film growth. The resulting kinetics showed a linear dependence of the polymerization rate on the concentration of the immobilized initiator, and an inverse square root dependence on the initiator concentration in bulk, which is in accord with conventional free radical polymerization. However, their method for anchoring initiators led to a low grafting density and side reactions. Later, Rühe *et al.* developed a one-step initiator anchoring strategy and initiated free radical polymerization of styrene from surfaces. [5] Scheme 1.1 shows the polymerization reaction and the method used to detach the polymer chains from silica gel. The initiator has three important functionalities: (1) an azo group that generates free radicals upon heating or UV irradiation, (2) a chlorosilane that allows the initiator to be anchored to the surface through reaction with silanol groups of the silica substrate, and (3) an ester that can be hydrolyzed to detach the polymer brushes from the surface. After polymerization of styrene, the ester bonds that connect the polystyrene to the surface are easily cleaved to determine the molecular weights of the polymers, which allow comparisons between the free radical polymerization in solution and from a surface. From the molecular weight and grafting density, they found that the average distance between tethered polystyrene chains was 2-3 nm, smaller than the radii of gyration of the corresponding polymer molecules.

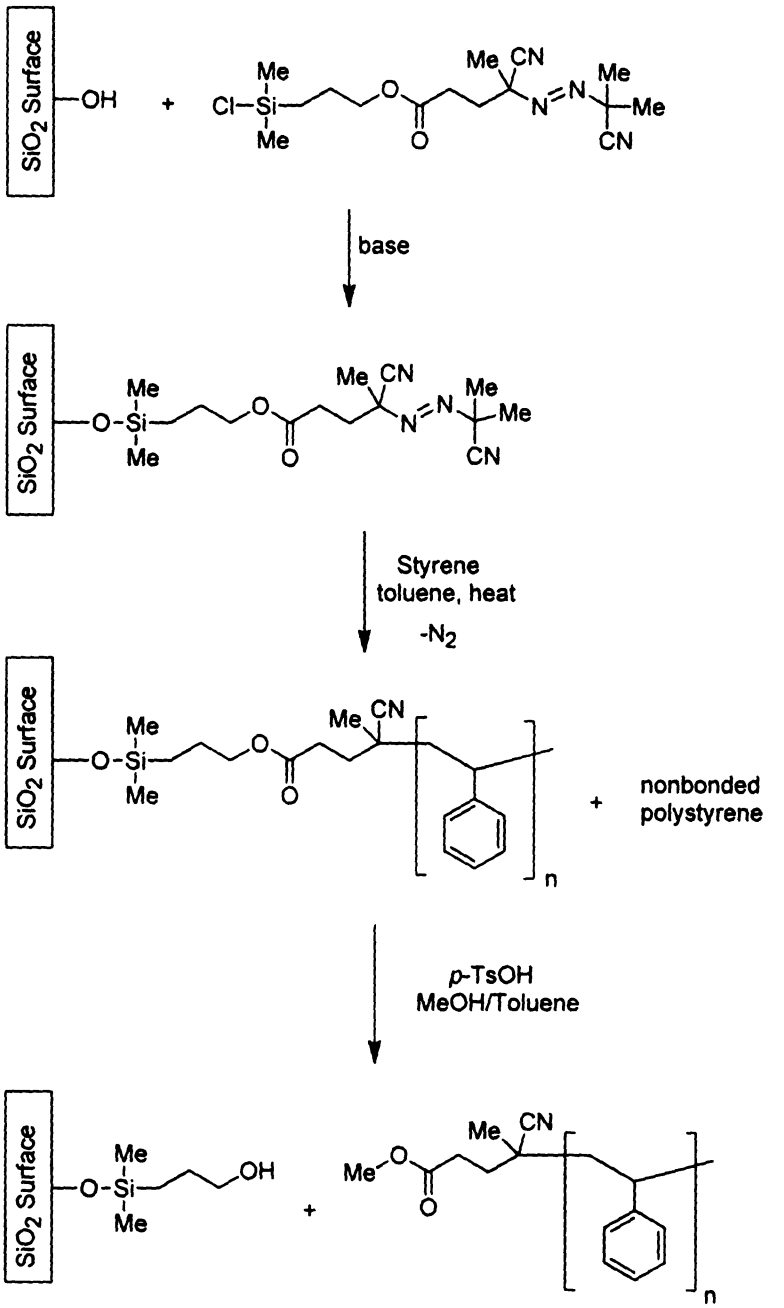

Scheme 1.1: Synthesis of polystyrene brushes on silica and cleavage of the polymers from the surface

Prucker and Rühe also investigated the kinetics and mechanism of surface-initiated free radical polymerization from a self assembled monolayer of azo initiators attached to the surface of silica particles.[19] The rate of decomposition of the surface-immobilized initiator was monitored by DSC, as well as by quantifying the amount of nitrogen generated from the azo component during decomposition. After polymerization, the polymer chains were detached from the surface and the molecular weights of the de-grafted polymers and their distribution were studied as a function of the reaction parameters during polymerization. They also irradiated selected areas of surfaces with UV to pattern thin polymer layers by surface-initiated free radical polymerization.[20] Other substrates have been studied. For example, Velten *et al.* anchored cation-bearing peroxides to mica surfaces via ion exchange, and initiated styrene polymerization from the initiators to obtain surface-bound polymers.[21]

Wittmer and coworkers predicted strong differences between polymer brushes grown from surfaces and polymers generated in solution.[22] They assumed that long chains are more efficient at adding monomers than short chains because they are more mobile and more accessible to monomers, and thus polymer brushes formed at the surface should have a higher polydispersity than the same reaction occurring in solution. However, the experimental data of Prucker and Rühe for polymers cleaved from surfaces indicate a small or no effect, with PDIs ranging from 1.5 to 2, which is close to the PDI of free radical polymerizations in solution. Figure 1.3 shows the molecular weights and polydispersities of the detached polymer brushes.

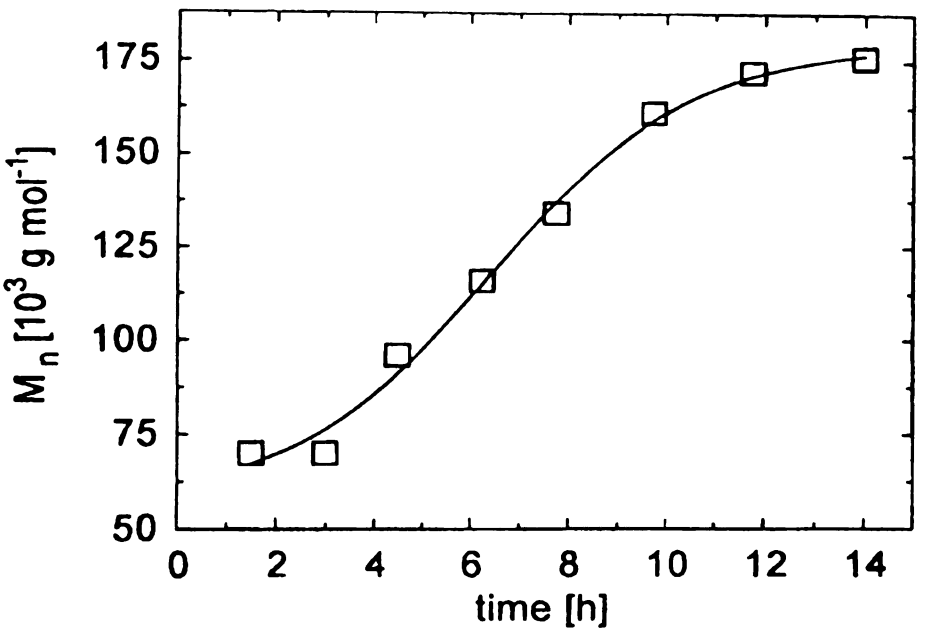

Figure 1.3: Time-dependent properties of polymer chains grown by surface-initiated free radical polymerization of styrene: molecular weight M_n. (Reprinted with permission from *Macromolecules* **1998**, *31*, 602-613. Copyright 1998 American Chemical Society)

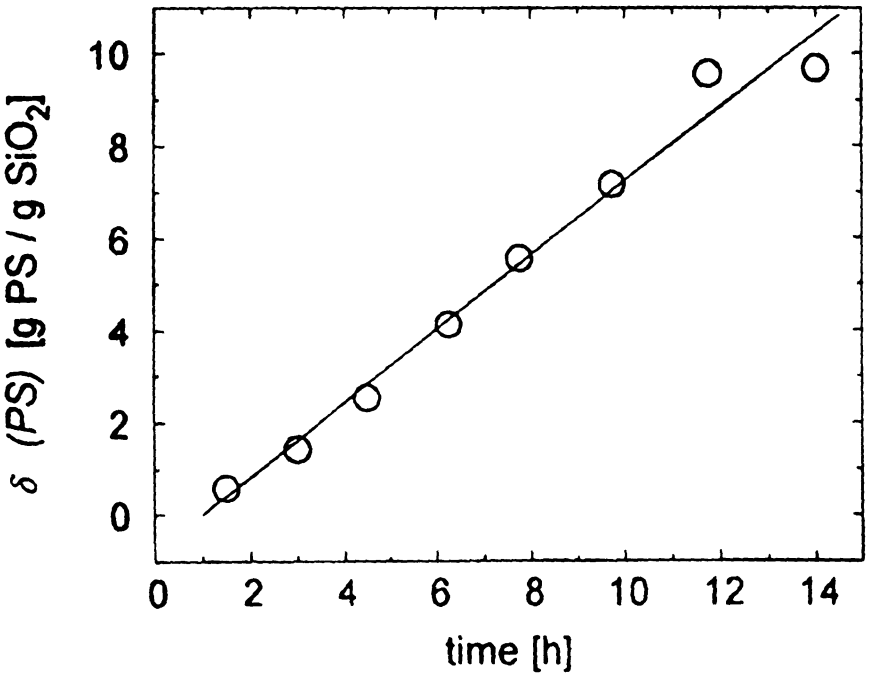

Figure 1.3: Time-dependent properties of polymer chains grown by surface-initiated free radical polymerization of styrene: Grafting densities δ(PS) (PS=Polystyrene). (Reprinted with permission from *Macromolecules* **1998**, *31*, 602-613. Copyright 1998 American Chemical Society)

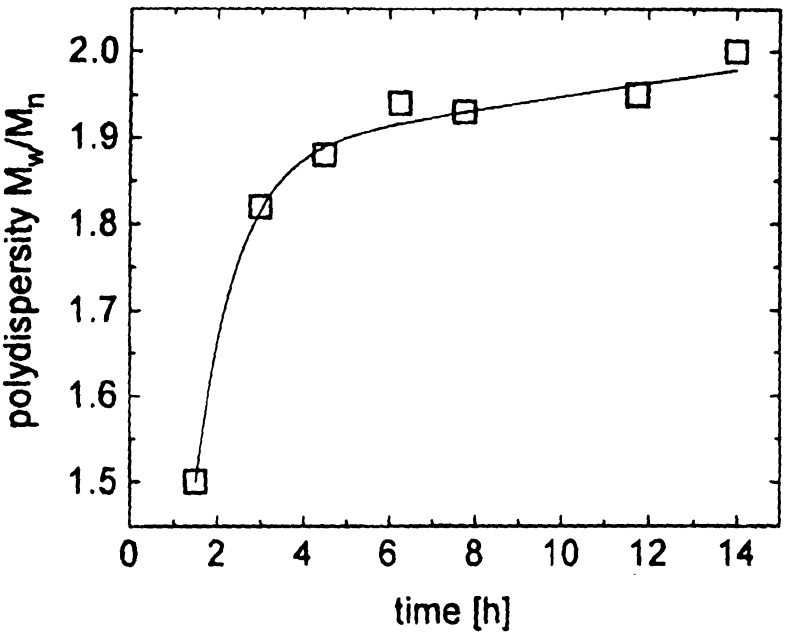

Figure 1.3: Time-dependent properties of polymer chains grown by surface-initiated free radical polymerization of styrene: Polydispersity of the covalently attached polymers. (Reprinted with permission from *Macromolecules* **1998**, *31*, 602-613. Copyright 1998 American Chemical Society)

Rühe and coworkers expanded surface-initiated free radical polymerization to the preparation of block copolymer brushes, where one block was synthesized by ROP.[23] A PCL (poly(caprolactone)) macroinitiator containing azo groups was physisorbed on a silicon oxide surface to initiate the radical polymerization of the other monomer to create hydrophobic layers on hydrophilic surfaces. Zhao *et al.*[24] later applied this strategy to the synthesis of amphiphilic Janus silica particles. Azo initiators were anchored to silica

particles, and the modified particles were suspended in a mixture of styrene and water. The particles were adsorbed at the liquid-liquid interface, with one hemisphere of each particle immersed in an aqueous phase, and the other in a styrene phase. After initiation at an elevated temperature (90 $^{\circ}$C), poly(sodium methacrylate) grew from the hemisphere immersed in water, and polystyrene chains grew from the particle surface immersed in styrene. Thermogravimetric analysis and IR spectral data confirmed the grafting of polymer brushes on the surfaces.

1.3.2 Surface-initiated controlled radical polymerization

Of the various polymerization methods used for polymer brush synthesis, controlled free radical polymerization (CRP) has attracted much attention due to its simplicity, wide functional group tolerance, and versatility compared to ionic processes. CRP provides control over the polymer chain length and length distribution, and also offers the possibility to design grafted polymer chains with controlled architectures. The most widely used CRP techniques are ATRP, RAFT, and NMP. All of these techniques have been used to build up highly dense polymer brushes from surfaces of various architectures (planar and nanoparticles).

1.3.2.1 Polymer brushes by Atom Transfer Radical Polymerization (ATRP)

ATRP is a versatile technique for the polymerization of various vinyl monomers, primarily acrylates and methacrylates. Most aspects of ATRP have been reviewed.[25,26,27] The mechanism for ATRP is shown schematically in Scheme 1.2. In ATRP systems, reversible termination is used to reduce the steady state concentration of growing radicals and suppress bimolecular radical termination reactions. Once a radical is generated from a dormant initiator, it can either add monomer or deactivate by reacting

with a metal complex (such as Cu(II)) to regenerate the dormant initiator and a metal in a lower oxidation state. The controlled nature of ATRP results from the equilibrium strongly favoring the dormant species.

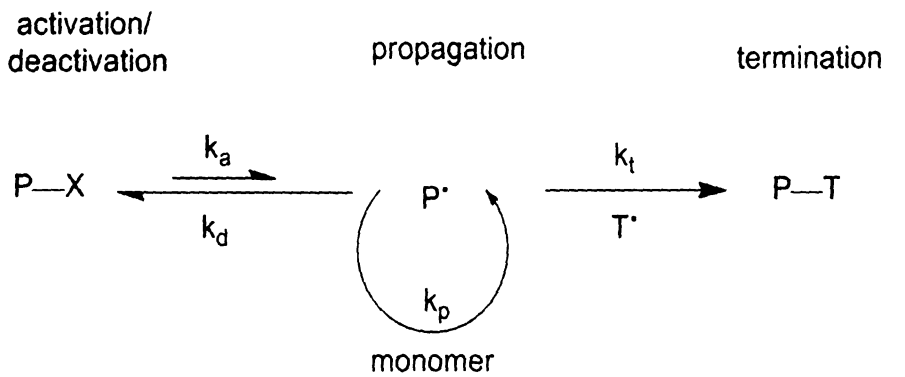

Scheme 1.2: Mechanism of ATRP

Polymers with low polydispersities are produced by ensuring that the initiation rate is faster than propagation with minimal termination. Since the dormant species is a growing polymer chain capped with a halogen atom, it is possible for a polymer chain to act as a macroinitiator, making ATRP a readily applicable technique for producing block copolymers. The kinetics of ATRP is shown in Equation 1.3.[18] In this expression [M], [P·], [Cu(I)], [Cu(II)X], and [PX] are the concentrations of monomer, active polymer radicals, copper(I), copper(II) halide, and halide-capped polymer chain respectively. The rate constants k_{app}, k_p, k_{act} and k_{deact} refer to the apparent rate constant, the propagation rate constant, the activation rate constant and the deactivation rate constant respectively and finally, K_{eq} is the equilibrium constant. As per this expression, ATRP follows first order kinetics with respect to monomer concentration ([M]).

$$R_P = K_{app}[M] = K_p[P^\bullet][M] = k_p K_{eq}[I]\frac{[Cu^I]}{[Cu^{II}X]}[M] \qquad 1.3$$

where,

$$K_{eq} = \frac{k_{act}}{k_{deact}} = \frac{[P^\bullet][Cu^{II}X]}{[Cu^I][PX]}$$

However, during surface initiated polymerization, the total amount of polymer synthesized on the surface is very small, and the concentration of monomer in solution remains essentially constant. This constant monomer concentration should lead to linear kinetic plots for surface-initiated polymer brush film thickness (proportional to the polymer molecular weight) with respect to time.[28]

1.3.2.1 Examples of Polymer Brushes via ATRP

Surface-initiated ATRP has been the most widely employed methodology for the formation of polymer brushes, and Figure 1.4 shows examples of common monomers used to synthesize polymer brushes via ATRP.

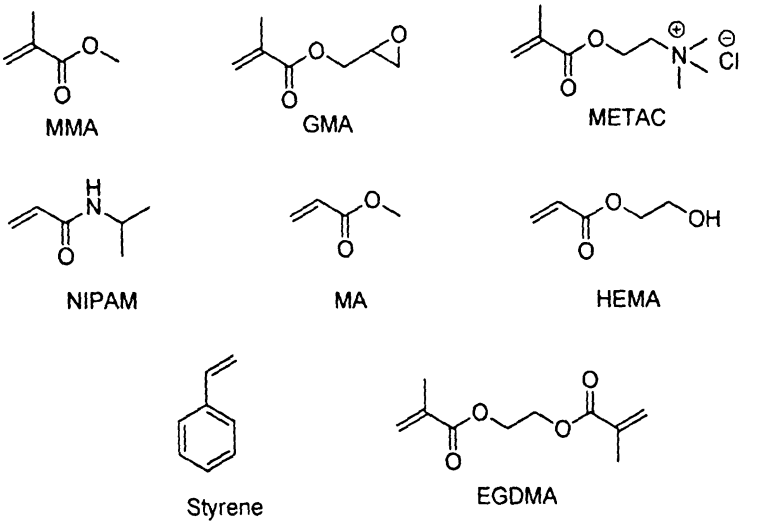

Figure 1.4: Examples of monomers that have been used to synthesize polymer brushes via ATRP.

Surface initiated ATRP can be applied to nonplanar surfaces such as nanoparticles. In an early example, Huang, *et al.*[29] used ATRP to grow polyacrylamide brushes from silica gel, and obtained a ~10 nm thick film after 40 hours at 130 °C. Husseman *et al.*[7] improved control over the growth of polymer brushes by adding a sacrificial initiator to decrease the concentration of active chains, and therefore reduced chain termination by coupling and disproportionation. However, the free initiators produced significant amount of polymer in solution that must be removed. An alternative method is to add a Cu(II) salt to the polymerization solution,[30] and shift the equilibrium more toward dormant chains. This is a 'surface confined' polymerization since no initiator is explicitly added to the solution, and therefore only small amounts of polymer is generated in solution.

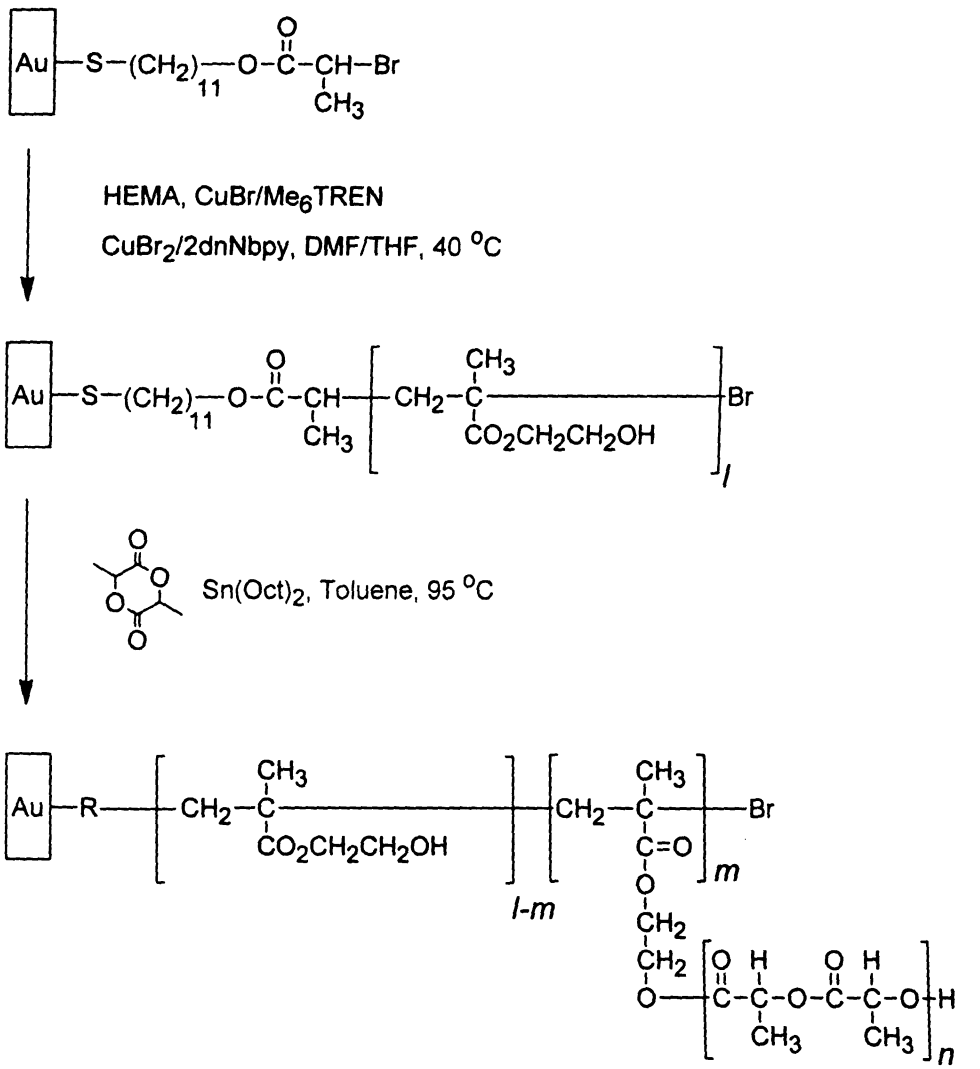

Scheme 1.3: Synthesis of PMA-*b*-PMMA-*b*-PHEMA triblock copolymer brushes

Similarly, styrene and methyl acrylate were polymerized from an initiator layer of 2-bromoisobutyrate immobilized on silicon wafers. The polymerizations showed a linear increase in the polymer thickness with reaction time.[31] Controlled growth was achieved by the addition of a deactivating Cu(II) species. A combined study of the control of initiator density on gold and silicon substrates was carried out by Bao *et. al.*[32] They prepared Au and SiO_2 substrates with various immobilized initiator densities using systems (size of initiator and diluent were matched) that should lead to a homogeneous

distribution of the initiator on the surface. Variations in the polymerization rate on both substrates were observed as a function of initiator density and it was found to be consistent with the decrease in bimolecular termination as well as a decrease in the number of chains on the surface when the initiator density drops below 10% on Au surfaces.

A related effect of initiator density was reported by Wu *et al.*[33] In their study, an initiator density gradient was formed on a silica surface, brushes were synthesized from the surface, and the thickness was found to vary systematically (as measured by ellipsometry) at different positions along the substrate. These results show that the polymer brush thickness decreases slightly with the reduction of the initiator density until a crossover point, where the polymer film thickness decreases markedly. At the crossover point the density of polymer is too low to force the polymer chains into a stretched conformation. As a result, the polymer chains do not interact with one another, and are present in the 'mushroom' regime as randomly coiled chains on the top of the surface. Since the polymer chains are already spaced far enough apart to not interact with each other in the mushroom regime, the thickness of the polymer chains does not correlate with initiator density.

Though room temperature polymerizations are desirable to avoid thermal polymerization, ATRP has been carried out at elevated temperature to increase the rate of polymerization. However, thiol on gold SAMs are unstable at temperatures above 60 $^{\circ}$C.[34] One way to increase polymerization rates and decrease the reaction temperature,

is to use aqueous polymerization systems.[10, 35] It is thought that the high dielectric constant of the polar solvent increases the activity of the ATRP catalyst system.

Another useful method for increasing the polymerization rate is to use ligands with high stability constants such as Me_4Cyclam. Moreover, ATRP catalysts based on Me_4Cyclam can grow 100 nm thick film of poly(*tert*-butyl acrylate) (P*t*BA) in 5 minutes.[36] ATRP is also a useful technique for the formation of block copolymers, since the polymer chains can act as macroinitiators for a new monomer. Several examples of block copolymer brushes via ATRP have been shown. Kim *et al.* used a simple quench and re-initiation (QR) approach to grow PMA-*b*-PMMA-*b*-PHEMA triblock copolymer brushes on Au (Scheme 1.3).[37] Growing polymer brushes were quenched with a concentrated $CuBr_2$/ligand solution, preserving the Br atoms at the chain ends for subsequent re-initiation of the next polymer block. The efficiency of the QR scheme was found to be superior over a simple solvent washing procedure, which resulted in a higher loss of active chains. In another example, ABA triblock copolymer brushes of polystyrene and poly(methyl methacrylate) were synthesized on silica surfaces.[38] Treatment with different solvents reversibly altered the surface morphology leading to applications in switchable and responsive surfaces. As the synthesis of polymer brushes via ATRP has become more controlled and an increasingly large number of monomers have been used, potential applications of this film morphology is now being explored.

1.3.2.2 Polymer brushes by Nitroxide Mediated Polymerization (NMP)

The livingness of NMP depends on the reversible capping of the active chain-end radical with a nitroxide leaving group. Husseman *et al.* demonstrated that polystyrene (PS) chains could be grown from the surface by NMP (Scheme 1.4).[7] They first attached alkoxyamine initiators onto the surface and then heated the system to 120 °C to initiate radical polymerization. During the initiating process, the stable nitroxide radical 2,2,6,6-tetramethylpiperidinyloxy (TEMPO) is cleaved and reversibly caps the chain-end radicals to control radical propagation. The addition of free alkoxyamine initiator provided more control over the molecular weight, but solution polymerization could not be avoided.

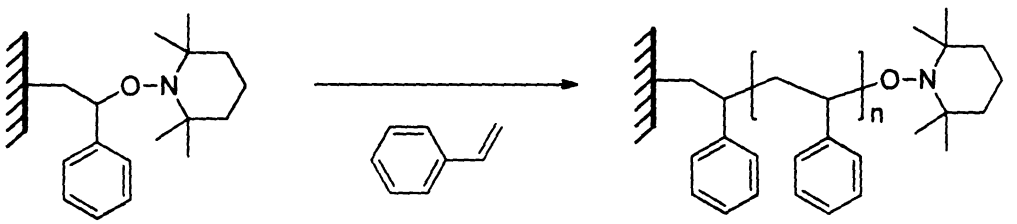

Scheme 1.4 Polystyrene brushes grown by nitroxide-mediated polymerization

Hawker and coworkers applied NMP to photolithography by patterning polymer brushes into well-defined hydrophobic and hydrophilic domains (Figure 1.5).[39] PtBA brushes (hydrophobic) were synthesized by surface-initiated NMP and then hydrolyzed to form hydrophilic poly(acrylic acid) (PAA) brushes. Recently, Konn *et al.*[40] grew polystyrene chains from the surface of synthetic Laponite clay platelets by nitroxide-mediated polymerization of styrene using N-*tert*-butyl-N-[1-diethylphosphono-(2,2-dimethylpropyl)] (DEPN) as mediator (Scheme 1.5). A novel water-soluble quaternary ammonium alkoxyamine was synthesized and intercalated into the clay galleries by

cation exchange. Polystyrene (PS) chains with controlled molecular weight and narrow polydispersities were then grown from the organoclay which displayed a high stability and dispersibility in organic solvent as well as into polar and nonpolar monomers.

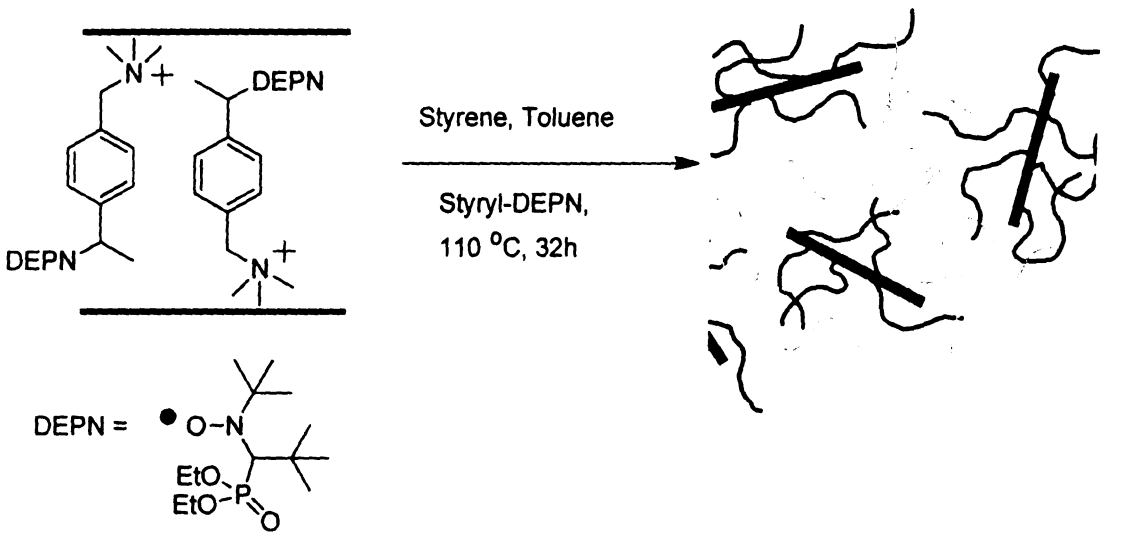

Scheme 1.5: Illustration of the intercalation of the quaternary ammonium alkoxyamine initiator into laponite by cation exchange and the subsequent formation of ionically bonded PS chains by surface-initiated NMP of styrene using a sacrificial alkoxyamine initiator. (Reprinted with permission from *Macromolecules* **2007**, *40*, 7464. Copyright 2007 American Chemical Society.)

1.3.2.3 Polymer brushes by reversible radical addition-fragmentation chain transfer

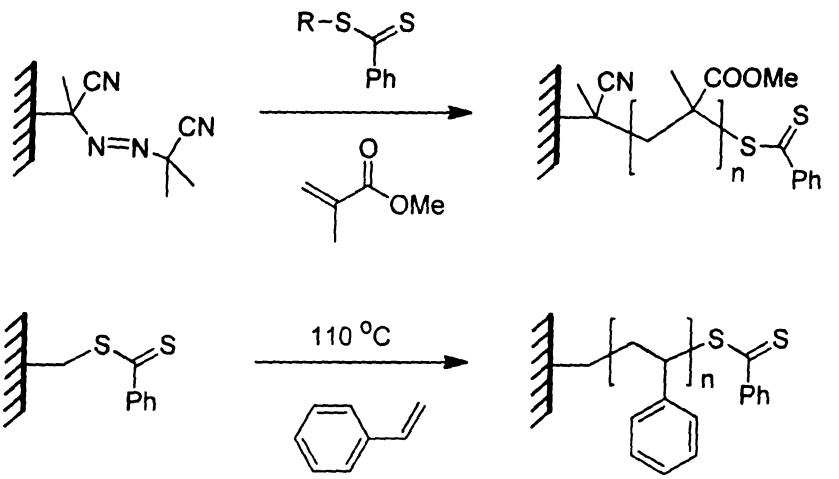

Scheme 1.6 Polymer brushes grown by RAFT polymerization of MMA

ATRP is arguably the most widely used controlled radical polymerization technique for the preparation of surface initiated polymer brushes. However, RAFT offers potential benefits over ATRP in the polymerization of functional monomers. RAFT is a versatile technique based on a reversible degenerative chain transfer mechanism in which thiocarbonylthio compounds act as chain transfer agents providing controlled growth of polymer chains (Scheme 1.6).[41,42,43,44] Boyes *et al.* modified surfaces with RAFT chain transfer agents and synthesized a series of homopolymer and diblock copolymer brushes (Scheme 1.7).[45] They cleverly converted an immobilized ATRP surface initiator to the RAFT chain transfer agent surface by an atom transfer addition reaction. RAFT chain transfer agents were anchored to the surface of silicon wafers, and then homopolymer brushes of PMMA and PS and diblock copolymer brushes of PMMA-*b*-PS, PMMA-*b*-PDMAEMA and PS-*b*-PMA were grown from the substrates.

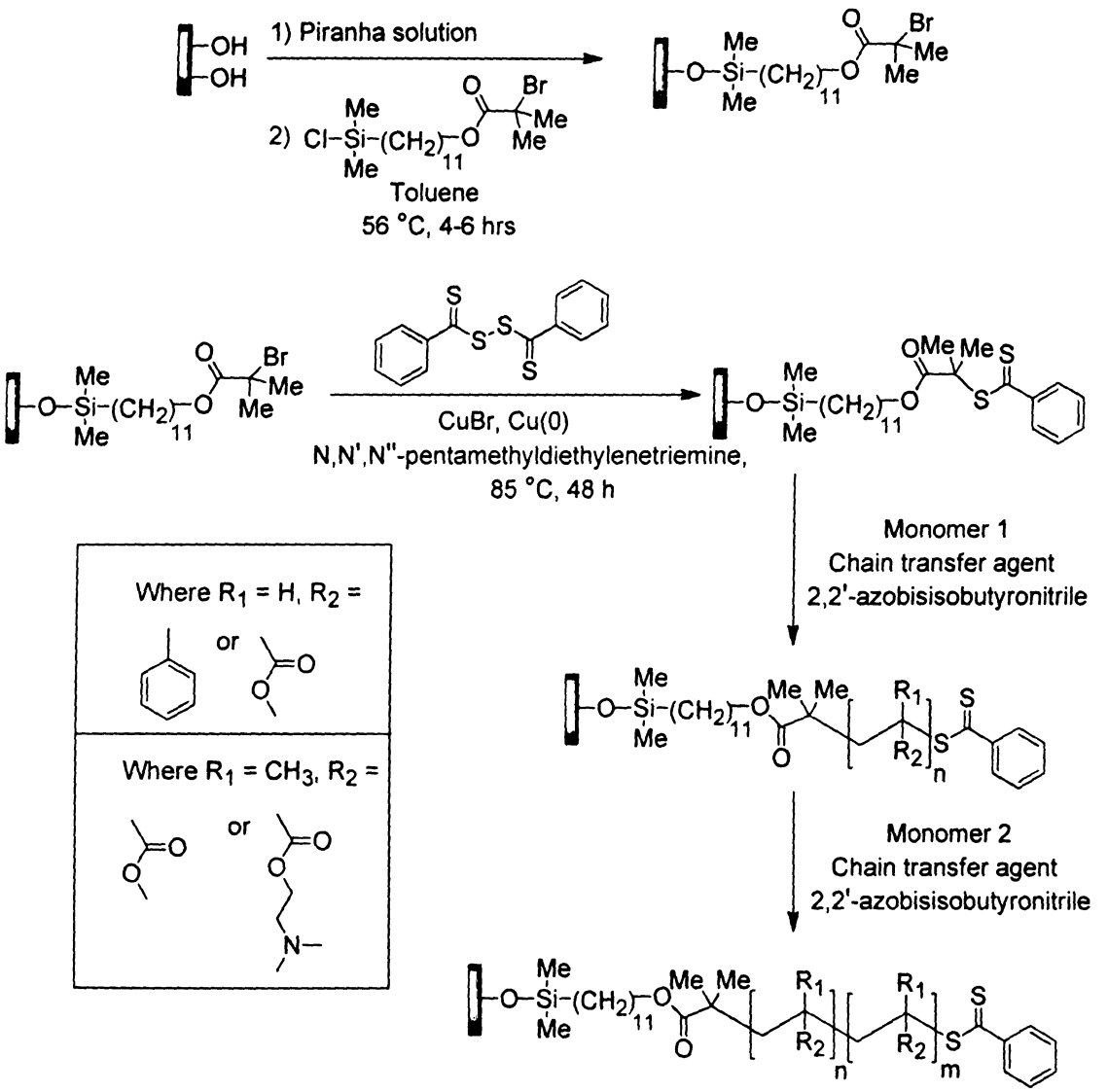

Scheme 1.7: General procedure for the preparation of atom transfer addition modified surfaces and subsequent diblock copolymer brush formation via Reversible Addition-Fragmentation Chain Transfer Polymerization.

1.3.3 Polymer brushes by Cationic Polymerizations

Substantially less work has been reported on the application of cationic polymerization for the synthesis of polymer brushes from surfaces. Jordan and Ulman[46] initiated cationic ring opening polymerization of 2-substituted 2-oxazolines from gold surfaces, resulting in a 10 nm poly(*N*-acylethylenimine) brush after 7 days of polymerization under reflux in chloroform (Scheme 1.8). They also showed that the polydispersity of the resulting linear polymers were narrow because of the highly living character of the ring-opening polymerization. This method allows block-copolymers synthesis by consecutive addition of different 2-substituted monomers. Furthermore, terminal functionalities are easily introduced by terminating the polymerization with nucleophiles. They extended this strategy to gold nanoparticles to the preparation of functional composites at the nanometer scale.[47] Zhao and Brittain[48] deposited SAMs terminated with cumyl methyl ether moieties on silicon wafer surfaces. Activation with $TiCl_4$ in the presence of styrene and di-*tert*-butylpyridine, a proton scavenger, led to 30 nm thick polystyrene brushes in less than an hour. The brush growth was carried out at -78 $^{\circ}C$ to suppress chain transfer reactions. The livingness of the polymerization was confirmed by re-initiating the polymer chains to grow additional polystyrene. Recently, Patton *et al.*[49] developed a new class of polymer brushes based on the hybrid inorganic-organic polymer backbone of poly(phosphazenes) (PPZs). PPZ brushes were synthesized using surface-bound phosphoranimines as active sites for living cationic surface-initiated polymerization of chlorophosphoranimines.

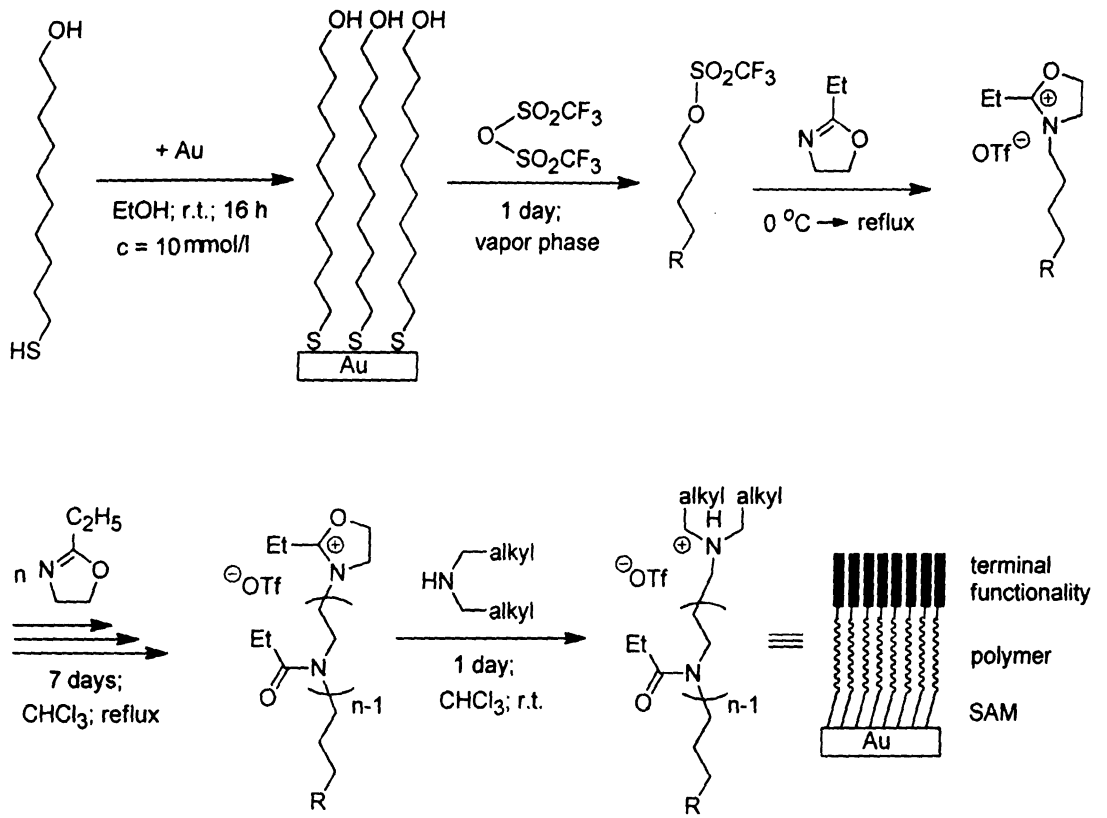

Scheme 1.8: Surface-initiated cationic polymerization of 2-oxazolines.

1.3.4 Polymer brushes by Anionic Polymerizations

The living nature of anionic polymerization has made it an attractive choice for the synthesis of well defined polymer brushes via the 'grafting from' approach. Early examples involving "grafting to" approaches such as the reaction of lithiated polystyrene chains with surfaces were first described in the 1970s.[50,51] This usually involved the reaction of carbanions of living polymers of polystyrene or polyvinylpyridine with surface bound chlorosilane groups to bind the macromolecule covalently to the silica surface. Later, Jordan *et al.*[52] initiated anionic polymerization of styrene from gold substrates. Initially, a bromobiphenyl SAM group was converted to the corresponding lithium species by metal-halogen exchange with *sec*-butyllithium, and after addition of

styrene, uniform 18 nm thick films grew in 3 days. The initiating efficiency and grafting density were calculated to be 8% and 3.2-3.6 nm^2/chain respectively. Ingall *et al.* polymerized acrylonitrile from SiO_2 using a similar strategy.[53] A bromine terminated SAM, formed from 3-bromopropyltrichlorosilane, was lithiated with lithium di-*tert*-butylbiphenyl, and subsequent addition of monomer resulted in a 245 nm thick film after 8 days of polymerization.

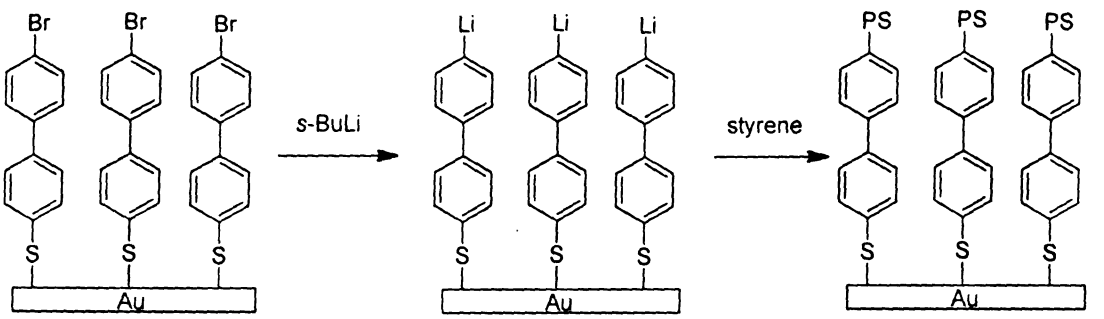

Scheme 1.9: Surface-initiated anionic polymerization of styrene on gold

Advincula *et al.* used *n*-butyllithium to activate diphenyethylene-terminated SAMs for the anionic polymerization of styrene[54] from gold and silicon substrates. The polymerization was slow, and reaction times of several days produced thin films (up to 16 nm). The results for silicon surfaces showed large variations in film thickness for similar reaction conditions. The addition of tetramethylethylenediamine (TMEDA) produced a thicker film (26 nm). To demonstrate the living nature of the polymerizations, polystyrene-*block*-polyisoprene and polybutadiene-*block*-polystyrene were synthesized by the sequential addition of monomers. Later, they[55,56,57] extended anionic surface-initiated polymerization to silica and clay nanoparticles. (Scheme 1.10). They confirmed

the "living" nature of the polymerization by demonstrating a linear relationship between monomer concentration and M_n.

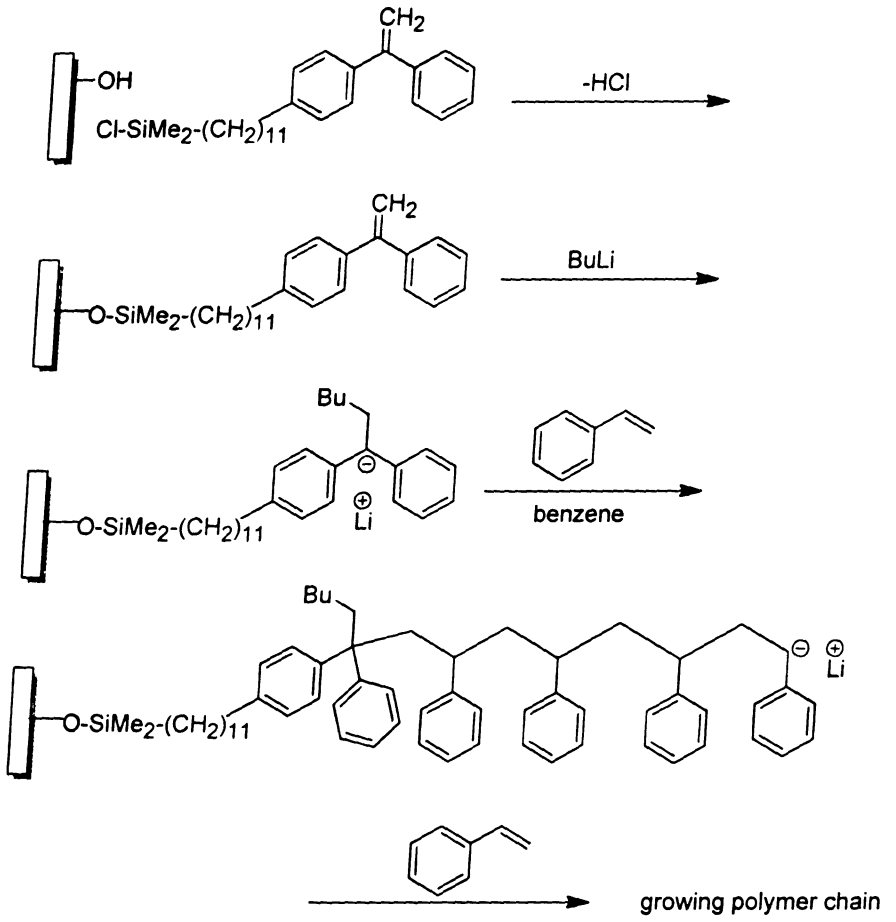

Scheme 1.10: Immobilization of the DPE initiator followed by polymerization of the styrene homopolymer to form PS brushes by SIP.

Baskaran *et al.*[58] used living surface-initiated anionic polymerization (Scheme 1.11) to synthesize poly(ethylene oxide) and polystyrene brushes from the surface of MWNTs. Using a "grafting from" strategy, MWNTs were covalently functionalized with 4-hydroxyethyl benzocyclobutene (BCB-EO) and 1-benzocylcobutene-1'-phenylethylene (BCB-PE) through [4 + 2] cycloaddition. Alkoxy anions and alkyllithium anions were generated from MWNTs-*g*-(BCB-EO)$_n$ and MWNTs-*g*-(BCB-PE)$_n$ using

triphenylmethane and *sec*-butyllithium for the polymerization of ethylene oxide and styrene in THF and benzene, respectively. The initiation of ethylene oxide and styrene from the surface alkoxy and alkyl anions respectively was found to be slow due to heterogeneous nature of the reaction. But with increasing reaction time, the polymerization of ethylene oxide from the surface of MWNTs-*g*-(BCB-EO)$_n$ exhibited linear growth as indicated by the monomer conversion and weight percent of PEO on the MWNTs. Moreover, this process provided surface grown polymers in high conversion. Mueller and coworkers[59] utilized a similar strategy for the grafting of MWNTs with the biodegradable and biocompatible polymers such as poly(ε-caprolactone) and poly(ethylene oxide). In their "grafting from" methodology, an initiator was covalently attached to the MWNT through a [4 + 2] Diels–Alder cycloaddition reaction. The resulting polymer-CNT hybrid materials contained a high percentage of polymers (as high as 98%), as revealed by TGA.

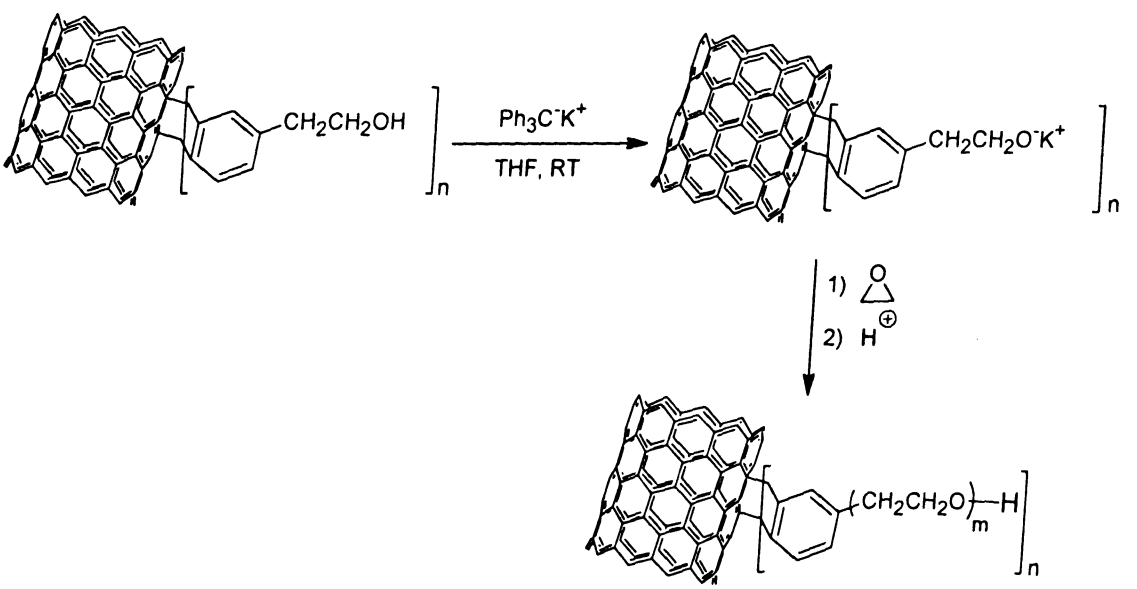

Scheme 1.11: Surface-initiated anionic polymerization of ethylene oxide from MWNTs-*g*-(BCB-EO)$_n$ surfaces.

Although living anionic polymerization is useful for the synthesis of well-defined brushes with low polydispersity, it has several disadvantages such as the extreme sensitivity of anionic polymerization to impurities, which necessitates the use of specialized glassware and rigorous purification and drying of reagents. Restricted monomer functionality, long reaction times and low values for final thickness of the polymer films also hinder the use of this technique for polymer brush growth.

1.3.5 Polymer brushes via surface-initiated Ring-opening Polymerization

Radical surface initiated polymerization is limited to vinyl monomers. However there is a need for biocompatible and biodegradable polymers such as polylactides and polylactones for medical applications[60]. These polyesters are usually synthesized by the ring opening polymerization of cyclic monomers initiated by organometallic reagents[61] in a living/controlled fashion, which is the prerequisite for the controlled grafting of polymers from surfaces. Surface initiated ring opening polymerization is generally performed after the formation of a hydroxyl- or amine terminated self-assembled monolayer which initiates the polymerization (Scheme 1.12). The most comprehensive article on polyester grafting by ring opening polymerization of lactones (ε-caprolactam) was reported by Carrot *et al.*[62] Covalent grafting of polyester chains was achieved by functionalizing silica surfaces with a trimethoxysilane agent containing an amine functionality. Initiation occurred selectively from the surface by activation of amine groups by an aluminum alkoxide, and the controlled polymerization proceeded via a

coordination-insertion mechanism involving the coordination of the carbonyl group of the ε-caprolactam by triethyl aluminum followed by the nucleophilic addition of the amine. In related work, Choi and Langer formed an oligo(ethylene glycol) terminated SAM on gold substrate and used tin(II) (2-ethylhexanoate)$_2$ (Sn(Oct)$_2$) to catalyze the ROP of L-lactide from Au and silicon substrates[63] (Scheme 1.12). Polymerization for 3 days provided 12 nm thick PLA brushes on Au surfaces, and 70 nm thick films on silicon surfaces. The PLA brushes were shown to be chiral and crystallized on the surface. Later, Choi and coworkers,[64, 65] used tin(II) octoate to grow biodegradable, aliphatic poly(ether-esters) such as poly(p-dioxane) (PPDX) and poly(1,5-dioxepan-2-one) (PDXO) from an oligo(ethylene glycol)-terminated SAM by the ring opening polymerization. However the polymerization was not "living" in nature as suggested from the imperfect shapes of the resultant particles. In another study,[63] the silanol groups of the silica particles were used to initiate polymerization. A 140 nm thick polylactide brush was obtained, which was consistent with thermogravimetric analysis (TGA).

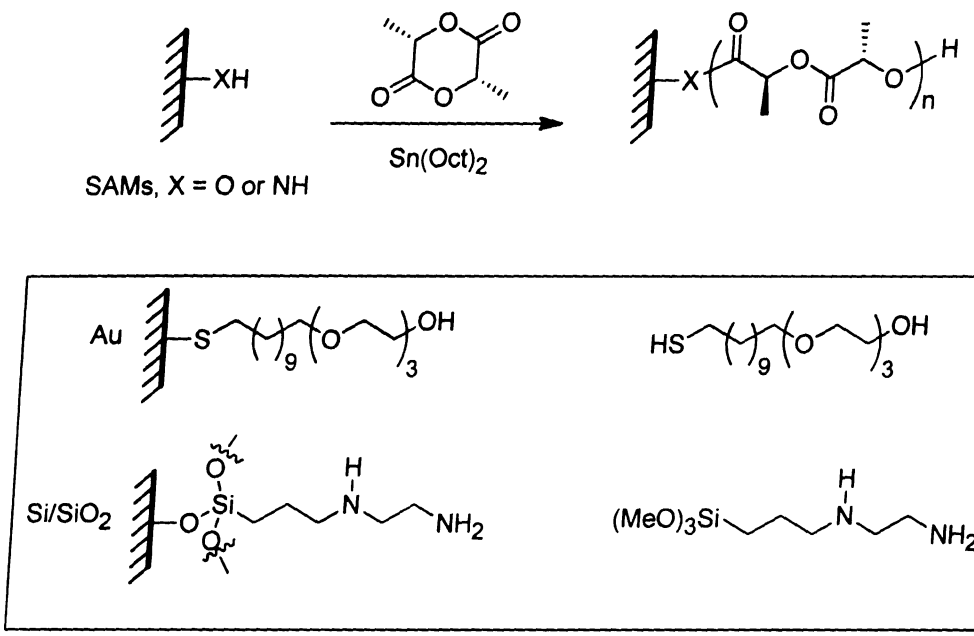

Scheme 1.12: Surface-initiated ring opening polymerization of lactide.

1.3.6 Polymer brushes by Ring-opening metathesis polymerization (ROMP)

ROMP is the transition metal catalyzed ring opening polymerization of strained cyclic olefins. Via ROMP, Whitesides and co-workers grew a variety of norbornene-derived polymer brushes from silicon surfaces.[66] The surface-bound catalytic sites were produced by forming a trichlorosilane-derived SAM containing norbornene groups, and then exposing the SAM to a solution of a Grubbs-type ROMP catalyst. The polymerization was controlled with rapid initiation, producing 90 nm thick brushes in 30 min. The formation of block copolymer brushes and the use of microprinting to produce patterned surfaces also were described. In related work, Mingotaud *et al.* immobilized a ruthenium catalyst on 200 nm silica nanoparticles[67] by reacting a methathesis catalyst bearing a hydroxyl group with silica particles modified with acyl chloride functional groups, and then performing ROMP of norbornene. The authors estimated that 30% of

the catalyst initiated polymerization. TEM characterization showed a core–shell morphology which suggested the presence of the catalyst on the silica surface. Using a recently invented ruthenium catalyst, $[(H_2IMes)(3\text{-}Brpy)_2(Cl)_2Ru{=}CHPh]$, Choi and coworkers demonstrated that surface-initiated ring opening metathesis polymerization (SI-ROMP) can be utilized for the formation of diblock copolymer brushes from surfaces (Scheme 1.13).[68] Taking advantage of the highly improved activity of the ruthenium catalyst and the rapid initiation step of SI-ROMP, they successfully formed thin films of well-defined diblock copolymers with 5-norbornene-2-*endo*,3-*endo*-dimethanol (Nb-diMeOH) and an endo/exo isomeric mixture (44:56) of norbornene carboxylic acid methyl ester (Nb-COOMe).

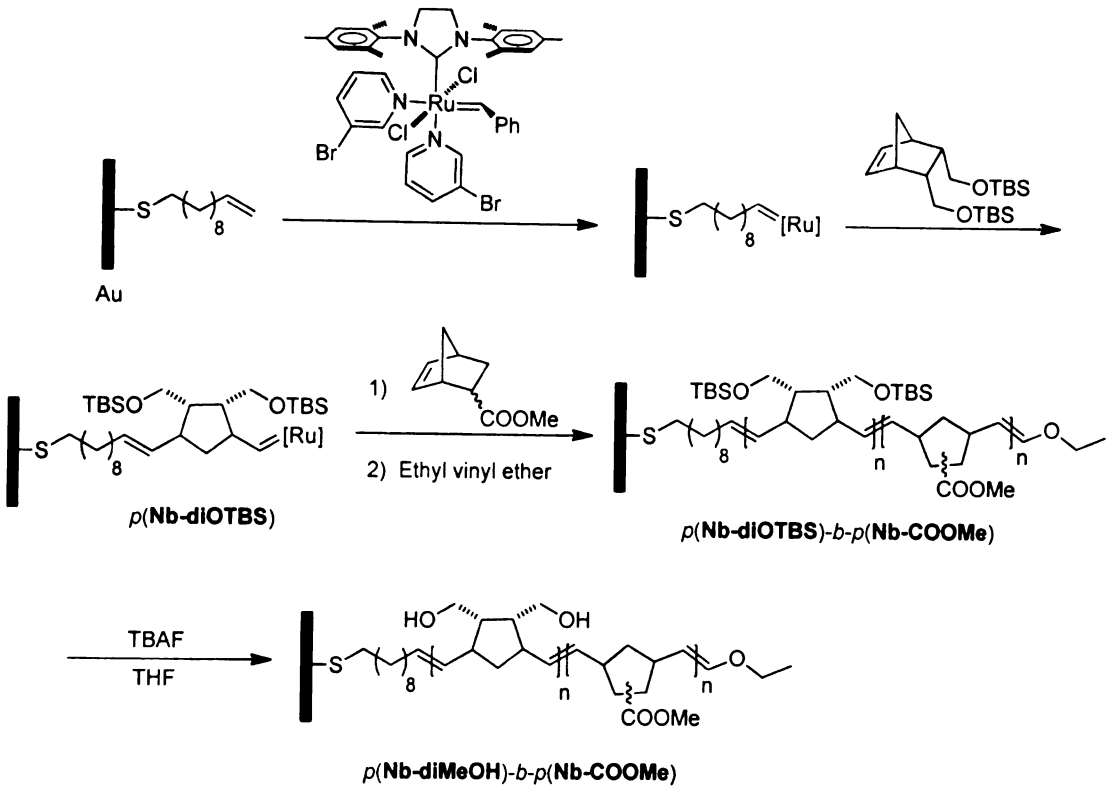

Scheme 1.13: Schematic description of the formation of *p*(Nb-diMeOH)-*b*-*p*(Nb-COOMe) diblock copolymer brushes on a gold surface.

1.4 Applications of Surface-initiated Polymerization

A significant advantage of polymer brushes compared to other surface modification methods is their mechanical and chemical stability, accompanied by a high level of synthetic flexibility towards the introduction of functional groups. This is in contrast to the physisorbed, non-bound polymer films where chemical modification by using wet chemistry is difficult to conduct. Additionally, it is now possible to grow brushes on virtually every surface (flat surfaces, particles or macromolecules), to any thickness, of every composition, incorporating a multitude of functional groups and containing series of blocks. More recent applications of polymer brushes include

nanopatterned surfaces,[69] photochemical devices,[70] new adhesive materials,[71] protein-resistant biosurfaces,[72] chromatographic devices,[73] lubricants,[74] polymer surfactants,[1] polymer compatibilizers[1] and many more.

One of the most attractive applications of surface-initiated polymerizations is the formation of nano-patterned surfaces by soft lithography techniques that combine microcontact printing (μCP) and graft polymerization. An elegant example is that of Hawker *et al.* who combined photolithography with nitroxide-mediated "living" free radical polymerization to obtain patterned polymer brushes with well-defined hydrophobic and hydrophilic domains (Figure 1.5).[49] They extended this concept to synthesize patterned polymer layers by aqueous ATRP.[75]

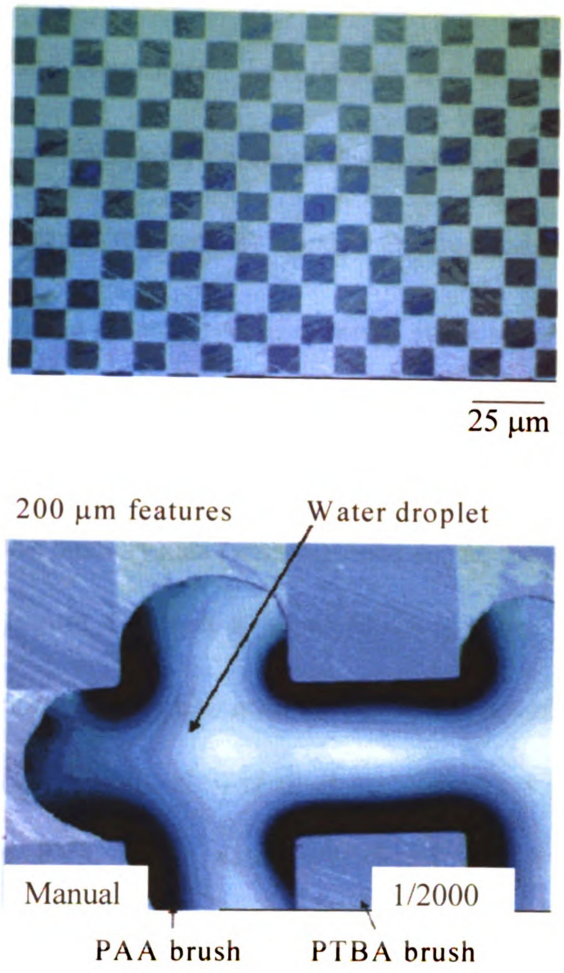

Figure 1.5: Optical micrographs of patterned surfaces: (left image) 10-μm features in a continuous polymer brush showing regions of poly(*tert*-butyl acrylate) (dark) and poly(acrylic acid) (light) and (right image) interaction of a water droplet with 200-μm features showing an unusual wetting profile and preferential interaction with poly(acrylic acid) brush domains.(Reprinted with permission from *J. Am. Chem. Soc.* **2000**, *122*, 1844-1845. Copyright 2000 American Chemical Society.)

Recently, Huck and coworkers[68] have shown that charge-transporting polymer brushes (polytriphenyl amine acrylate) can be synthesized from a variety of surfaces (ITO, SiO_2 and conducting polymer) relevant for organic electronic device fabrication. These polymer brush films contain a greater level of ordering at the molecular level and display higher charge mobility than spin-coated films of the same polymer, which was attributed to the controlled polymer brush architecture and morphology. They also demonstrated substantial uptake of CdSe nanocrystals (with diameter in the range 2.5-2.8 nm) into the polymer brush layers (Figure 1.6) and a photovoltaic quantum efficiencies of up to 50%.[76] In another report, Advincula and coworkers[77] successfully grafted hole-transporting PVK (poly(vinyl carbazole)) brushes on transparent ITO electrodes. Using cyclic voltammetry, the PVK brush was electrochemically crosslinked, to form a conjugated polymer network film. Covalent linkage of PVK led to a direct electroluminescent PLED device, in which the electroluminecent polymer layer can be simply solution-cast onto the modified ITO.

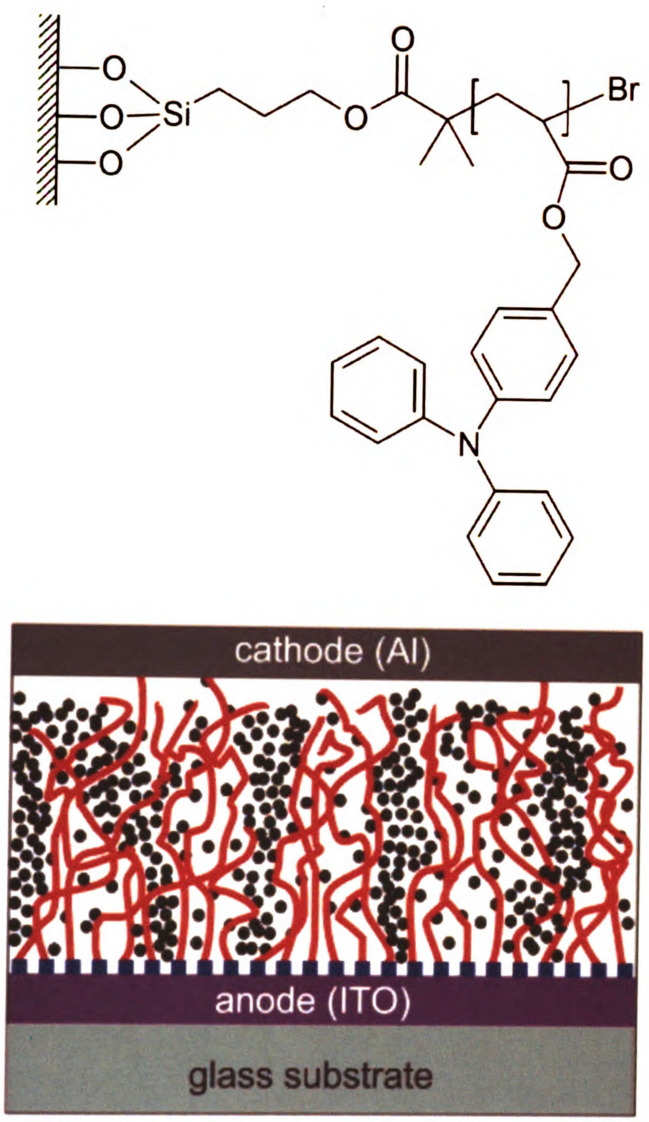

Figure 1.6: Top image: PTPAA brushes and bottom image: Cartoon of inferred structure for CdSe nanocrystal infiltrated polymer brush photovoltaic device (From bottom to top) ITO-coated glass slide modified by surface attachment of a bromine end-caped trichlorosilane self-assembled-monolayer (SAM) (blue squares), polymer brushes grown from the SAM (red lines), CdSe nanocrystals infiltrated into the brush network exhibiting some degree of phase separation in the plane of the film (small black circles), and caped with an aluminum cathode. (Reprinted with permission from *Nano Lett.* **2005**, *5*, 1653. Copyright 2005 American Chemical Society.)

A more ambitious challenge in surface science is the design of smart surfaces with dynamically controllable properties.[78] Such surfaces have characteristics that can be changed or tuned in an accurate and predictable manner by using an external stimulus. Recently, Huck and coworkers have shown that wetting properties of surfaces modified with cationic polyelectrolyte brushes strongly depend on the nature of the counter ion. Coordination of polyelectrolyte brushes bearing quaternary ammonium groups (QA^+) with sulfate anions resulted in highly hydrophilic surfaces,[79] whereas, coordination of similar brushes with ClO_4^- rendered the surface hydrophobic.[80]

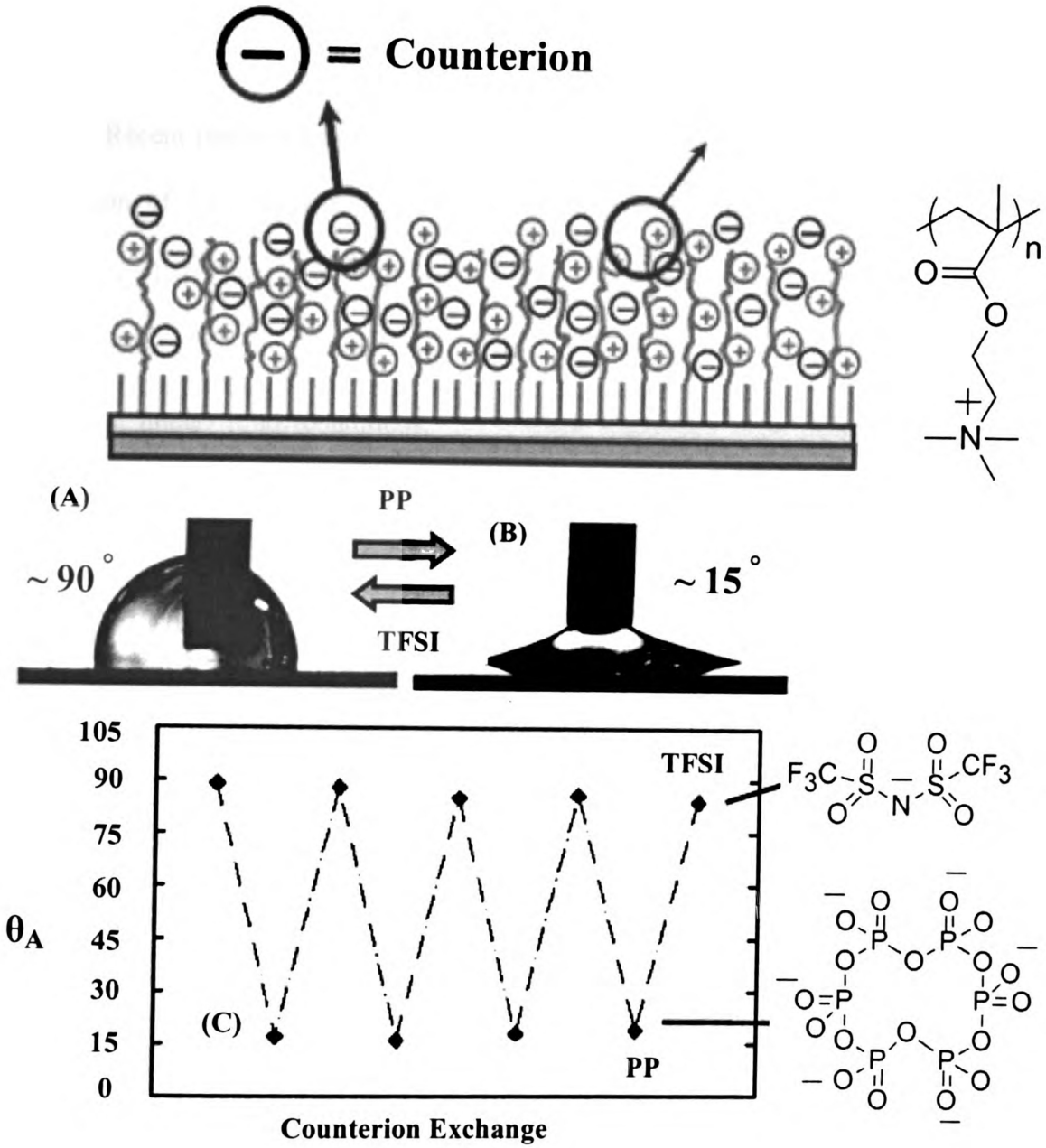

Figure 1.7: Top image: PMETAC brushes and bottom image: Change in the wetting characteristics of PMETAC brushes (height, *h* ~20 nm) after exchanging the two contrasting counterions: TFSI (a) and polyphosphate (PP) (b). c) Representation of θ_A as a function of counter ion (PP and TFSI). The plot depicts the reversible behavior of PMETAC brushes over repeated cycles of TFSI and PP counter ion exchange. On the

right the chemical structures of both counter ions are represented. (Reprinted with permission from *Angew. Chem. Int. Ed.* **2005**, *44*, 4578. Copyright 2005 Wiley-VCH.)

Recent research has focused on the Cu(I)-catalyzed, highly specific and efficient formation of 1,2,3-triazoles via the 1,3-dipolar cycloaddition of azides and terminal alkynes ("click"chemistry).[81] This methodology has been used to modify surfaces of solid metals and cells, because the reaction provides high yields, stereospecificity and proceeds under mild conditions.[82, 83] Click chemistry also has been used for functionalizing polymers in solution.[84,85] Research in nanobiotechnology and biomedical sciences often involves the manipulation of interfaces between manmade surfaces and biomolecules (and cells), which generally requires the construction of surfaces that present chemically active functional groups from non-biofouling supporting materials. Choi and coworkers[86] used "click" chemistry to couple azide groups at the terminal of the non-biofouling polymeric film of poly(oligoethylene glycol methacrylate) with incoming molecules of interest containing terminal acetylenes (Figure 1.8). As a model for bioconjugation, biotin was immobilized onto the poly(oligoethylene glycol methacrylate) film via click chemistry, and biospecific recognition of streptavidin was demonstrated.

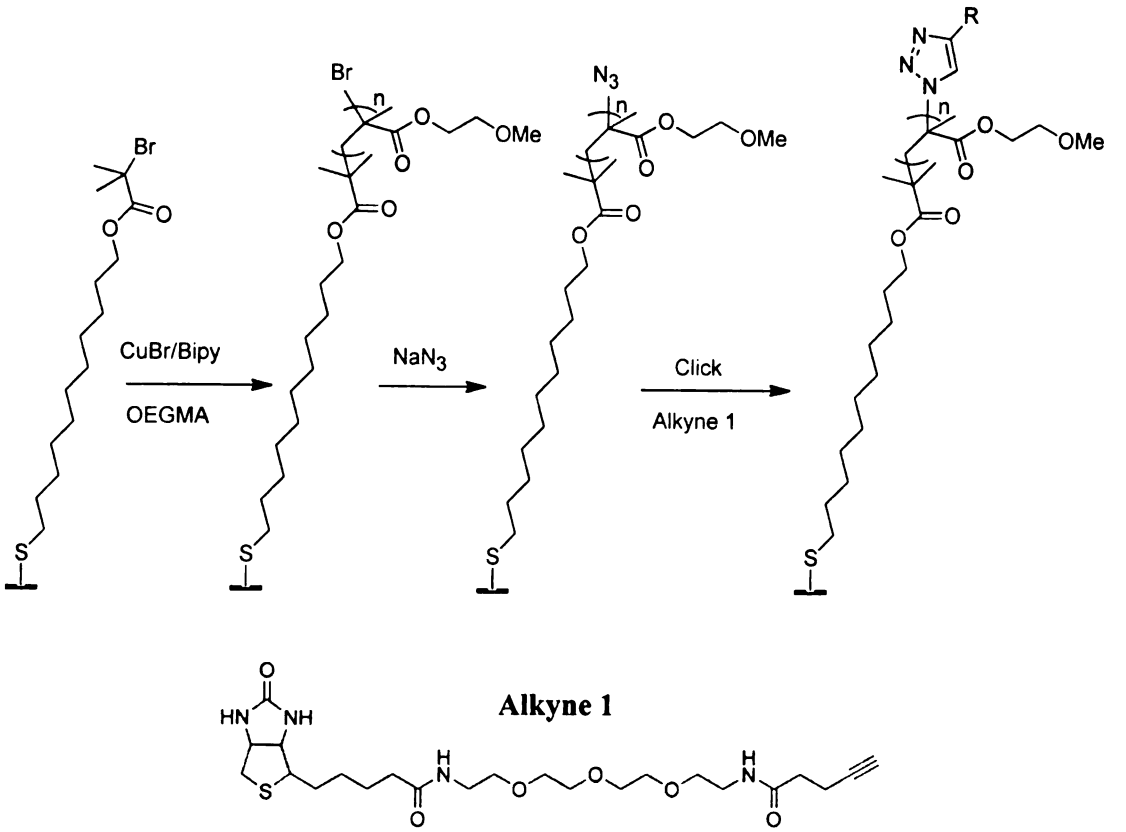

Figure 1.8: Schematic description of the attachment of biotin to polymer brush via click chemistry [Acetylene group-containing biotin compound: biotin-PEO-LC-N-pentynoate (**1**)].

1.5 References

1 Milner, S. T., *Science* **1991**, *251*, 905.

2 Zhao, B.; Brittain, W. J. *Prog. Polym. Sci.* **2000**, *25*, 677.

3 Edmondson, S.; Osborne, V. L.; Huck, W. T. S. *Chem. Soc. Rev.* **2004**, *33*, 14.

4 Pyun, J.; Kowalewski, T.; Matyjaszewski, K. *Macromol. Rapid Commun.* **2003**, *24*, 1043.

5 Prucker, O.; Rühe, J. *Langmuir* **1998**, *14*, 6893.

6 Baum, M.; Brittain, W. J. *Macromolecules* **2002**, *35*, 610.

7 Husseman, M.; Malmstrom, E. E.; McNamara, M.; Mate, M.; Mecerreyes, D.; Benoit, D. G.; Hedrick, J. L.; Mansky, P.; Huang, E.; Russell, T. P.; Hawker, C. J. *Macromolecules* **1999**, *32*, 1424.

8 Jordan, R.; Ulman, R. A.; Kang, J. F.; Rafailovich, M. H.; Sokolov, J. *J. Am. Chem. Soc.* **1999**, *121*, 1016.

9 Juang, A.; Scherman, O. A.; Grubbs, R. H.; Lewis, N. S. *Langmuir* **2001**, *17*, 1321.

10 Jones, D. M.; Huck, W. T. S. *Adv. Mater.* **2001**, *13*, 1256.

11 Patten, T. E.; Matyjaszewski, K. *Adv. Mater.* **1998**, *10*, 901.

12 Ramakrishnan, A.; Dhamodharan, R.; Rühe, J. *Macromol. Rap. Comm.* **2002**, *23*, 612.

13 Alexander, S., *J. Phys.* **1977**, *38*, 977.

14 De Gennes, P. G., *Macromolecules* **1980**, *13*, 1069.

15 Yamamoto, S.; Tsujii, Y.; Fukuda, T. *Macromolecules* **2002**, *35*, 6077.

16 Yamamoto, S.; Ejaz, M.; Tsujii, Y.; Matsumoto, M.; Fukuda, T. *Macromolecules* **2000**, *33*, 5602.

17 Advincula, R.; Rühe, J.; Brittain, W.; Caster, K. E. *Polymer Brushes: On the Way to Tailor-Made Surfaces*; 1st ed.; Wiley-VCH: New York, **2004**.

18 (a) Minko, S.; Gafijchuk, G.; Sidorenko, A.; Voronov, S. *Macromolecules* **1999**, *32*, 4525. (b) Minko, S.; Sidorenko, A.; Stamm, M.; Gafijchuk, G.; Senkovsky, V.; Voronov, S. *Macromolecules* **1999**, *32*, 4532. (c) Sidorenko, A.; Minko, S.; Gafijchuk, G.; Voronov, S. *Macromolecules* **1999**, *32*, 4539. (d) Luzinov, I.; Minko, S.; Senkovsky, V.; Voronov, A.; Hild, S.; Marti, O.; Wilke, W. *Macromolecules* **1998**, *31*, 3945. (e) Minko, S. S.;

Luzinov, I. A.; Evchuk, I. Y.; Voronov, S. A. *Polymer* **1996,** *37*, 177. (f) Luzinov, I.; Evchuk, I.; Minko, S.; Voronov, S. *J. Appl. Polym. Sci.* **1998,** *67*, 299.

19 Prucker, O.; Rühe, J. *Macromolecules* **1998**, *31*, 602.

20 Prucker, O.; Schimmel, M.; Tovar, G.; Knoll, W.; Rühe, J. *Adv. Mater.* **1998**, *10*, 1073.

21 Velten, U.; Tossati, S.; Shelden, R. A.; Caseri, W. R.; Suter, U. W.; Hermann, R.; Mueller, M. *Langmuir* **1999**, *15*, 6940.

22 Wittmer, J. P.; Cates, M. E.; Johner, A.; Turner, M. S. *Europhys. Lett.* **1996**, *33*, 397.

23 Stohr, T.; Ruhe, J. *Macromolecules* **2000**, *33*, 4501.

24 Zhang, J.; Jin, J.; Zhao, H. *Langmuir* **2009**, *25*, 6431.

25 Patten, T. E.; Matyjaszewski, K. *Adv. Mater.* **1998**, *10*, 901.

26 Tunca, U.; Hizal, G.; Acar, M. H.; Tasdelen, M. A.; Yagci, Y.; Mishra, M. K. *Plast. Eng. (Boca Raton, FL, United States)* **2009**, *73*, 231.

27 Pintauer, T.; Matyjaszewski, K. *Chem. Soc. Rev.* **2008**, *37*, 1087.

28 Edmondson, S.; Huck, W. T. S. *J. Mater. Chem.* **2004**, *14*, 730.

29 Huang, X. Y.; Wirth, M. J. *Anal. Chem.* **1997**, *69*, 4577.

30 Huang, W. X.; Kim, J. B.; Bruening, M. L.; Baker, G. L. *Macromolecules* **2002**, *35*, 1175.

31 Matyjaszewski, K.; Miller, P. J.; Shukla, N.; Immaraporn, B.; Gelman, A.; Luokala, B. B.; Siclovan, T. M.; Kickelbick, G.; Vallant, T.; Hoffmann, H.; Pakula, T. *Macromolecules* **1999**, *32*, 8716.

32 Bao, Z.; Baker, G. L.; Bruening, M. L. *Macromolecules* **2006**, *39*, 5251.

33 Wu, T.; Efimenko, K.; Genzer, J. *J. Am. Chem. Soc.* **2002**, *124*, 9394.

34 Huang, W. X.; Skanth, G.; Baker, G. L.; Bruening, M.L. *Langmuir* **2001**, *17*, 1731.

35 Jones, D. M.; Brown, A. A.; Huck, W. T. S. *Langmuir* **2002**, *18*, 1265.

36 Bao, Z.; Baker, G. L.; Bruening, M. L. *J. Am. Chem. Soc.* **2006**, *128*, 9056.

37 Kim, J. B.; Huang, W. X.; Bruening, M. L.; Baker, G. L. *Macromolecules* **2002,** *35*, 5410.

38 Boyes, S. G.; Brittain, W. J.; Weng, X.; Cheng, S. Z. D. *Macromolecules* **2002**, *35*, 4960.

39 Husemann, M.; Morrison, M.; Benoit, D.; Frommer, K. J.; Mate, C. M.; Hinsberg, W. D.; Hedrick, J. L.; Hawker, C. J., *J. Am. Chem. Soc.* **2000,** *122*, 1844.

40 Konn, C.; Morel, F.; Beyou, E.; Chaumont, P.; Bourgeat, E. *Macromolecules* **2007**, *40*, 7464.

41 Moad, G.; Solomon, D. H. *The Chemistry of Radical Polymerization,* 2nd fully revised ed.; Elsevier Ltd.: Amsterdam, **2006**.

42 Le, T. P.; Moad, G.; Rizzardo, E.; Thang, S. H. SH PCT Int. Appl. WO 98 01478 A1 980115, **1998**.

43 Moad, G.; Chiefari, J.; Chong, Y. K.; Krstina, J.; Mayadunne, R. T. A.; Postma, A.; Rizzardo, E.; Thang, S. H. *Polym. Int.* **2000**, *49*, 993.

44 Perrier, S.; Takolpuckdee, P. *J. Polym. Sci., Part A: Polym. Chem.***2005**, *43*, 5347.

45 Rowe, M. D.; Boyes, S. G. *Macromolecules* **2007**, *40*, 879.

46 Jordan, R.; Ulman, A. *J. Am. Chem. Soc.* **1998,** *120*, 243.

47 Jordan, R.; Nuki, W.; Yen-Ming, C.; Oskar, N.; Ulman, A. *Macromolecules* **2001**, *34*, 1606.

48 Zhao, B.; Brittain, W. J. *Macromolecules* **2000,** *33*, 342.

49 Jun, L.; Arthur, L.; Joel, H.; Derek, P. L. Abstracts of Papers, 237th ACS National Meeting, Salt Lake City, UT, United States, March 22-26, **2009**, POLY-228.

50 Horn, J.; Hoene, R.; Hamann, K. *Makromol. Chem.* **1975**, *1*, 329.

51 Donnet J.B.; Papirer, E. *Colloq. Int. CNRS.* **1975**, *231*, 117.

52 Jordan, R.; Ulman, A.; Kang, J. F.; Rafailovich, M. H.; Sokolov, J., *J. Am. Chem. Soc.* **1999,** *121*, 1016.

53 Ingall, M. D. K.; Honeyman, C. H.; Mercure, J. V.; Bianconi, P. A.; Kunz, R. R., *J. Am. Chem. Soc.* **1999,** *121*, 3607.

54 Advincula, R.; Zhou, Q. G.; Park, M.; Wang, S. G.; Mays, J.; Sakellariou, G.; Pispas, S.; Hadjichristidis, N. *Langmuir* **2002**, *18*, 8672.

55 Zhou, Q.; Fan, X.; Xia, C.; Mays, J.; Advincula, R. *Chem. Mater.* **2001**, *13*, 2465.
56 Zhou, Q.; Wang, S.; Fan, X.; Xia, C.; Mays, J.; Advincula, R. C. *Langmuir* **2002**, *18*, 3324.

57 Fan, X.; Zhou, Q.; Xia, C; Cristofoli, W.; Mays, J.; Advincula, R. C. *Langmuir* **2002**, *18*, 4511.

58 Sakellariou, G.; Ji, H.; Mays, J. W.; Baskaran, D. *Chem. Mat.* **2008**, *20*, 6217.

59 Priftis, D.; Sakellariou, G.; Hadjichristidis, N.; Penott, E. K.; Lorenzo, A. T.; Mueller, A. J. *J. Polym. Sci., Part A: Polym. Chem.* **2009**, *47*, 4379.

60 Nouvel, C.; Ydens, I.; Degee, P.; Dubois, P.; Dellacherie, E.; Six, J. L. *Macromol. Symp.* **2001**, *175*, 33.

61 Mecerreyes, D.; Jérôme, R.; Dubois, P. *Adv. Polym. Sci.*, **1999**, *147*, 1.

62 Carrot, G.; Rutot, D.; Pottier, A.; Degée, P.; Hilborn, J.; Dubois, P. *Macromolecules* **2002**, *35*, 8400.

63 Choi, I. S.; Langer, R., *Macromolecules* **2001**, *34*, 5361.

64 Yoon, K. R.; Koh, Y. J.; Choi, I. S. *Macromol. Rap. Comm.* **2003**, *24*, 207.

65 Yoon, K. R.; Lee, Y. J.; Lee, J. K.; Choi, I. S. *Macromol. Rap. Comm.* **2004**, *25*, 1510.

66 Kim, N. Y.; Jeon, N. L.; Choi, I. S.; Takami, S.; Harada, Y.; Finnie, K. R.; Girolami, G. S.; Nuzzo, R. G.; Whitesides, G. M.; Laibinis, P. E. *Macromolecules* **2000**, *33*, 2793.

67 Mingotaud, F.; Reculusa, S.; Mingotaud, C.; Keller, P.; Sykes, C.; Duguet, E.; Ravaine, S. *J. Mater. Chem.* **2003**, *13*, 1920.

68 Kong, B.; Lee, J. K.; Choi, I. S. *Langmuir* **2007**, *23*, 6761.

69 Shah, R. R.; Merreceyes, D.; Husemann, M.; Rees, I.; Abbott, N. L.; Hawker, C. J.; Hedrick, J. L. *Macromolecules* **2000**, *33*, 597.

70 Whiting, G. L.; Snaith, H. J.; Khodabakhsh, S.; Andreasen, J. W.; Breiby, D. W.; Nielsen, M. M.; Greenham, N. C.; Friend, R. H.; Huck, W. T. S. *Nano Lett.* **2006**, *6*, 573.

71 Raphael, E.; De Gennes, P. G. *J. Phys. Chem.* **1992**, *96*, 4002.

72 Amiji, M.; Park, K. *J. Biomat. Sci. Polym. Ed.* **1993**, *4*, 217.

73 Vanzanten, J. H. *Macromolecules* **1994**, *27*, 6797.

74 Joanny, J. F. *Langmuir* **1992**, *8*, 989.

75 Vidal, A.; Guyot, A.; Kennedy, J. P. *Polym. Bull.* **1980**, *2*, 315.

76 Snaith, H. J.; Whiting, G. L.; Sun, B.; Greenham, N. C.; Huck, W. T. S.; Friend, R. H. *Nano Lett.* **2005**, *5*, 1653.

77 Fulghum, T. M.; Prasad, T.; Advincula, R. C. *Macromolecules* **2008**, *41*, 5681.

78 Lahann, J.; Mitragotri, S.; Tran, T. N.; Kaido, H.; Sundaram, J.; Choi, I. S.; Hoffer, S.; Somorjai, G. A.; Langer, R. *Science* **2003**, *299*, 371.

79 Moya, S. E.; Azzaroni, O.; Farhan, T.; Osborne, V. L.; Huck, W. T. S. *Angew. Chem., Int. Ed.* **2005**, *44*, 4578.

80 Azzaroni, O.; Moya, S. E.; Farhan, T.; Brown, A. A.; Huck, W. T. S. *Macromolecules* **2005**, *38*, 10192.

81 Feldman, A. K.; Colasson, B.; Fokin, V. V. *Org. Lett.* **2004**, *6*, 3897.

82 (a) Rostovtsev, V.; Green, L. G.; Fokin, V. V.; Sharpless, K. B. *Angew. Chem., Int. Ed.* **2002**, *41*, 2596. (b) Tornoe, C. W.; Christensen, C.; Meldal, M. *J. Org. Chem.* **2002**, *67*, 3057.

83 Lewis, W. G.; Green, L. G.; Grynszpan, F.; Radić, Z.; Carlier, P. R.; Taylor, P.; Finn, M. G.; Sharpless, K. B. *Angew. Chem., Int. Ed.* **2002**, *41*, 1053.

84 Sumerlin, B. S.; Tsarevsky, N. V.; Louche, G.; Lee, R. Y.; Matyjaszewski, K. *Macromolecules* **2005**, *38*, 7540.

85 Gao, H.; Louche, G.; Sumerlin, B. S.; Jahed, N.; Golas, P.; Matyjaszewski, K. *Macromolecules* **2005**, *38*, 8979.

86 Lee, B. S.; Lee, J. K.; Kim, W. J.; Jung, Y. H.; Sim, S. J.; Lee, J.; Choi, I. S. *Biomacromolecules* **2007**, *8*, 744.

Chapter 2

Substituent effects in surface ATRP of polystyrene brushes

2.1. Introduction

The development of controlled radical polymerizations such as Atom Transfer Radical Polymerization (ATRP),[1,2] Reversible-Addition-Fragmentation Transfer Polymerization (RAFT)[3] and Nitroxide-Mediated Polymerization (NMP),[4,5] provide powerful methods for the growth of polymer brushes from surfaces. These polymerization methods limit radical concentrations during polymerization, minimize bimolecular termination reactions and provide control over M_n and the polydispersity (PDI). However, compared to traditional radical polymerization, control comes at the expense of a substantial reduction in the polymerization rate. Recently, we reported the remarkably rapid growth of well-defined poly(*tert*-butyl acrylate) brushes under mild conditions (50 °C) using ATRP. The key aspect of the polymerization was the use of a highly active ATRP catalyst [Cu(I)1,4,8,11-tetramethyl-1,4,8,11-tetraazacyclotetradecane (Cu(I)-Me_4Cyclam)] which provided 100 nm thick poly(*tert*-butyl acrylate) (P*t*BA) brushes on a flat Au surfaces in just 5 minutes (Scheme 2.1).[6] Such polymerization rates are several orders of magnitude greater than typical controlled polymerizations from surfaces. The Cu(I)-Me_4Cyclam) system also enabled rapid growth of thick brush layers from other vinyl monomers such as styrene, vinyl pyridine and methacrylates. Rapid

growth of brushes could expand the scope and applications for polymer brushes by greatly reducing the time required for their synthesis.

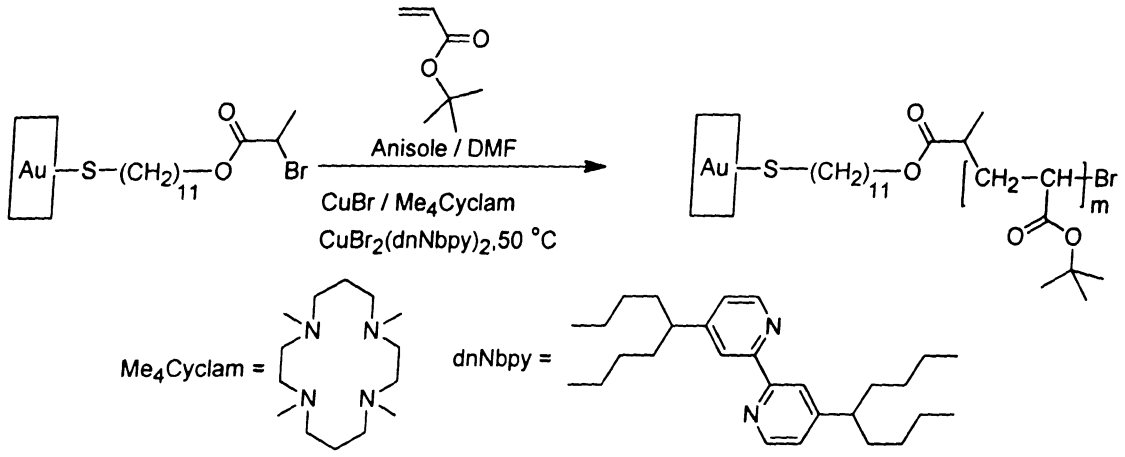

Scheme 2.1: Synthesis of tethered P*t*BA film on gold surface [6]

The unusually rapid growth of P*t*BA films compared to other vinyl monomers can be rationalized as a combination of *t*BA's fast propagation rate and reduced bimolecular coupling due to the steric bulk of the monomer. As shown in Scheme 2.2, sterically demanding monomers show a high propensity towards head to tail placement during polymer growth, and the same steric interactions would be expected to hinder termination by coupling (analogous to forming a head to head linkage). The generality of this phenomena can be seen in k_p (propagation rate constant) and k_t (termination rate constant) values for the methacrylate monomers shown in Table 2.1.[7,8] The first five entries show data for structurally related methacrylates obtained under similar experimental conditions. There are two important trends in the data; k_t decreases as the size of the ester increases because of the steric crowding depicted in Scheme 2.2, but a more surprising result is that in some cases, k_p also increases with the size of the ester group. Gilbert suggested that the

increases in k_p may be due to the increased momentum associated with collisions between higher molecular weight species.[9] Monomers with both high k_p and low k_t values, i.e. a high k_p / k_t ratio, should be the prime candidates for rapid polymerizations from surfaces. The last two entries show that there are limits to this approach. For example, k_t for trityl methacrylate is $<1\times10^{-6}$ L $mol^{-1}sec^{-1}$, but the extreme size of the ester group apparently hinders any enhancement in k_p. Ethylene is the least demanding vinyl monomer and the reported value for k_t, 540×10^{-6} L $mol^{-1}sec^{-1}$, indicates facile termination by coupling and disproportionation. When combined with a k_p ~242 $Lmol^{-1}sec^{-1}$, the k_p / k_t ratio for ethylene is 0.45×10^{-6}, which predicts ethylene as a poor candidate for rapid growth from surfaces by radical polymerization. The above arguments suggest that k_p and more importantly the k_p / k_t ratio could be used to identify promising monomers for the rapid growth of polymer brushes from surfaces.

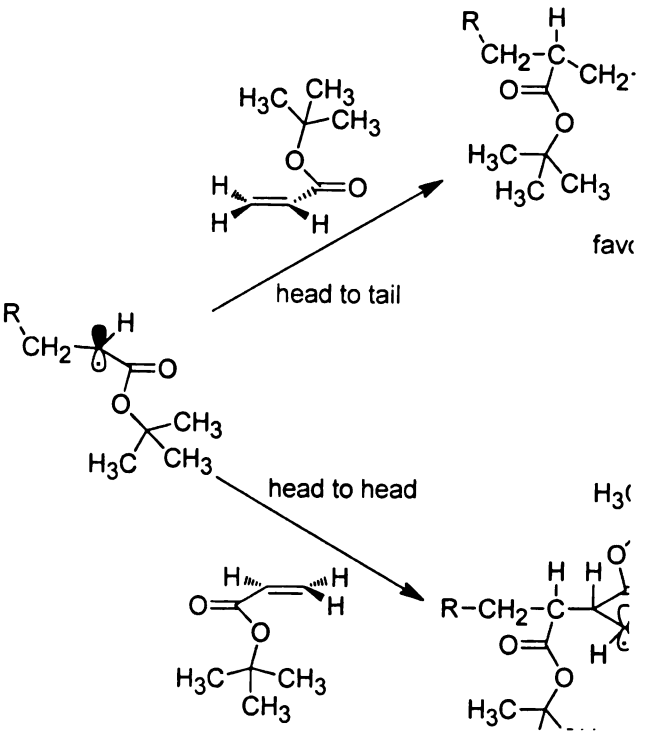

Scheme 2.2. Steric constraints favor head to tail addition and low k_t values.

The polymerization results for P*t*BA prompted us to examine other bulky monomers to see if they also would polymerize rapidly and provide thick films. Thick polystyrene brushes are difficult to grow via surface initiated ATRP (40 nm thick films in 1 hour compared to 100 and 200 nm films in 1 hour for MMA or *t*BA, respectively),[6] consistent with its small k_p / k_t ratio (4.3 at 60 °C)[8]. We studied substituted styrene derivatives (Scheme 2.3) to evaluate the effects of steric congestion and electronic effects on the polymerization rate under the same conditions used for *t*BA system. These monomers efficiently polymerize via free radical polymerization in solution,[10,11,12,13]

but there are no reports of their polymerization via surface-initiated ATRP or other controlled radical processes.

Table 2.1. Propagation and termination rate constants for representative methacrylates[8]

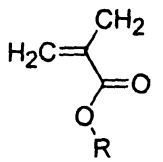	k_p (L mol^{-1}sec^{-1})	k_t ($\times 10^{-6}$) (L mol^{-1}sec^{-1})	k_p/k_t ($\times 10^6$)
—CH_3	649	25.5	25
—CH_2CH_3	723	7.35	98
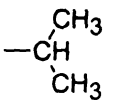	740	4.52	163
—$(CH_2)_3CH_3$	794	10	79
—$(CH_2)_{11}CH_3$	1011	0.6	1670
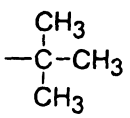	350	14	25
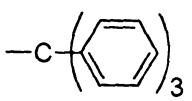	26	0.30	86

From data reported from other types of radical polymerizations in solution,[14,15,16] we expected that substituents on the styrene ring may affect the polymerization rate, and enable fast growth of polystyrene brushes from surfaces.

Furthermore, we expected that such a study would provide a better understanding of the mechanism of surface initiated polymerizations (especially the correlation between surface polymerization rate and monomer structure) as there has been no systematic investigation of substituent effects in substituted styrenes in surface initiated polymerizations.

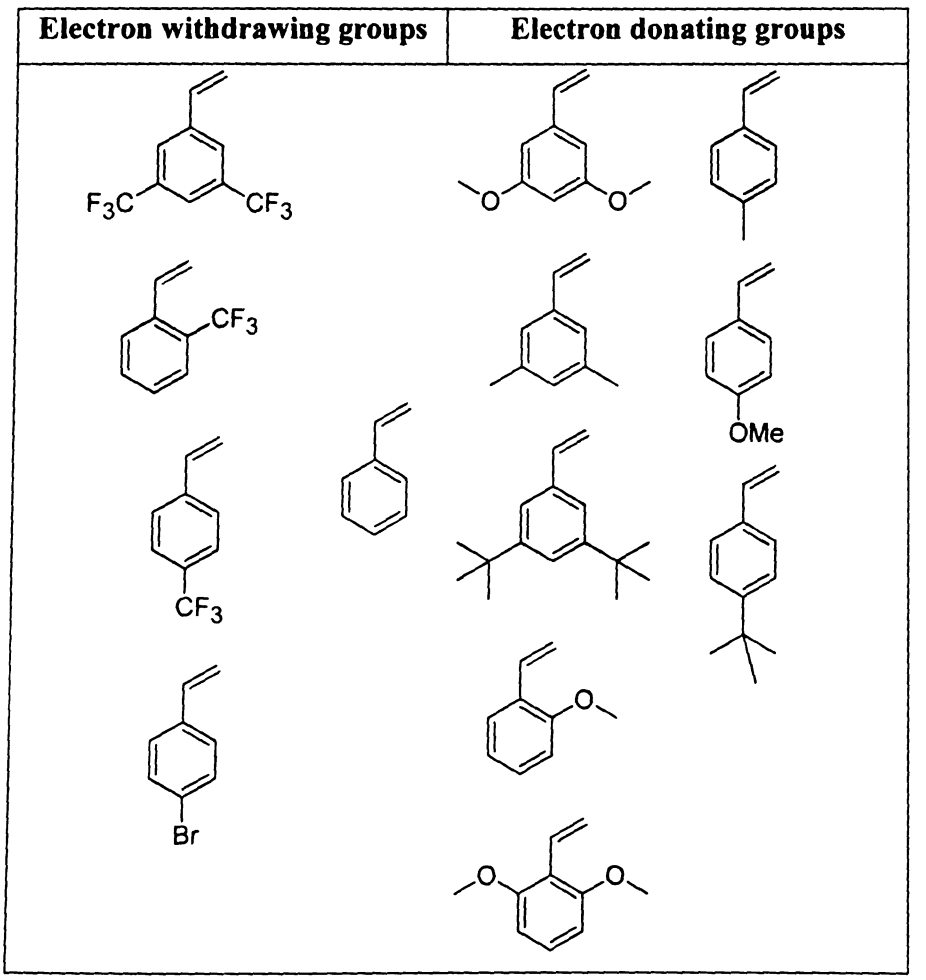

Scheme 2.3. Substituted styrene monomers polymerized in the study

Herein we report the rapid surface initiated polymerization of substituted styrenes, and the effect of various substituents on the polymerization kinetics studies. The data are discussed with regard to the Hammett equation: $\log (k_x/k_H) = \rho\sigma$

2.2. Experimental Section

2.2.1. Materials

Unless otherwise noted, all chemicals were obtained from Aldrich. 11-Mercapto-1-undecanol (MUD, 97%), 2-bromopropionyl bromide (2-BPB) (97%), anisole (99.7%), *N,N*-dimethylformamide (DMF, 99.8%), Cu(I)Br (99.999%), $Cu(II)Br_2$ (99.999%), $Me_4Cyclam$ (99%), and 4,4′-dinonyl-2,2′-bipyridine (dnNbpy, 97%) were used as received. Triethylamine was vacuum-distilled from calcium hydride. *tert*-Butyl acrylate (*t*BA) (98%), MMA (99%), styrene (99%), 2-vinylanisole (95%), 4-bromostyrene, pentafluorostyrene, 4-methylstyrene and 4-*tert*-butyl styrene were passed through a 10 cm long column of basic alumina followed by distillation to remove inhibitors. 3,5-Bis(trifluoromethyl)styrene (97%) and 3,5-dimethylstyrene were purified by passing through a 10 cm long basic alumina column. After purification, the monomers and solvents were transferred to Schlenk flasks, degassed using three freeze-pump-thaw cycles, and then transferred into a drybox. Other monomers such as 3,5-di-*tert*-butyl styrene, 3,5-dimethoxystyrene, 2,6-dimethoxystyrene, 4-vinylanisole and 4-(trifluoromethyl)styrene were prepared as previously reported mostly from their aldehyde precursors via the Wittig reaction.[11-13]

2.2.2. Characterization Methods

Film thicknesses were measured using a rotating analyzer ellipsometer (model M-44, J. A. Woollam) at an incident angle of 75°. The data were analyzed using WVASE32 software, and thickness and refractive index determinations were performed on at least three spots on each substrate. The refractive index of the films was assumed to be 1.5 and

then fitted with the film thickness. Reflectance FTIR spectroscopy was performed using a Nicolet Magna-IR 560 spectrometer containing a PIKE grazing angle (80°) attachment.

2.2.3. Preparation of Initiator Immobilized Gold Substrates

Gold-coated Si wafers (200 nm of Au sputtered on 20 nm of Cr on Si(100) wafers) were UV/O_3-cleaned for 15 min before use and then transferred into a N_2-filled glovebag. Hydroxy-terminated SAMs were formed by immersing the Au-coated substrates in a vial containing a 1 mM ethanolic solution of MUD for 24 h. After removing the vial from the glovebag, the substrates were rinsed sequentially with ethanol and water and dried under a stream of N_2. The ellipsometric thickness of the MUD layer was 10-15 Å. MUD-coated substrates were transferred to a drybox filled with N_2 and were dipped in a 10 mL solution of 0.12 M triethylamine in anhydrous THF at 0°C. After 1 min, 10 mL of a solution of 2-BPB in anhydrous THF (0.1 M) was added dropwise to the solution to form the immobilized initiator layer. The reaction time was limited to 2-3 min, since thiol-terminated SAMs could be unstable in the presence of the acyl bromide. After rinsing with THF, the Au substrates were removed from the drybox, and then rinsed sequentially with ethyl acetate, ethanol and deionized water (Milli-Q) and dried under a stream of N_2.

2.2.4. Preparation of Immobilized Initiators on Si Substrates

UV/O_3 cleaned Si wafers with an ellipsometrically determined oxide thickness of 20 Å were transferred to a glove bag filled with N_2 and immersed in a dry toluene solution (20 mL) containing 30 μL of [11-(2-bromo-2-methyl)propionyloxy]undecyl trichlorosilane. After 24 h without stirring, the samples were removed from the solution,

placed in fresh toluene and sonicated for 1 min. Following additional rinsing with toluene, acetone, and ethanol, the substrates were dried under a stream of N_2. The ellipsometric thickness of the initiator layer was ~ 20 Å.

2.2.5. Polymerization of Substituted Styrenes from Initiators Immobilized on Au Substrates – Kinetic Experiments

Note: For best results, solvents, initiators and monomers must be scrupulously purified and deoxygenated. In a N_2-filled drybox, CuBr (5.7 mg, 0.04 mmol) $CuBr_2$, (4.5 mg, 0.02 mmol), Me_4Cyclam (10.3 mg, 0.04 mmol) and dnNbpy (16.4 mg, 0.04 mmol) were added to a round-bottom flask containing 20 mL of a degassed solution of monomer in DMF/anisole (DMF/anisole ~1:1 (v:v), [styrene] ~ 4 M). The mixture was well-stirred and heated with an oil bath to 50 °C until a transparent, light green solution formed. The prepared solution was then transferred into a small vial containing an initiator-modified Au substrate to start the surface-initiated polymerization. After a predetermined reaction time at 50 °C, the substrate was removed from the vial, washed with ethyl acetate and THF sequentially, and then dried under a flow of N_2 in the drybox. The same conditions were used for the polymerization of other monomers.

2.3. Results and Discussion

2.3.1. Synthesis of Substituted Styrenes

The substituted styrenes used in this investigation are listed in Scheme 2.3. Most were available from commercial sources, however, 3,5-di-*tert*-butylstyrene, 3,5-dimethoxystyrene, 2,6-dimethoxystyrene, 4-vinylanisole and 4-(trifluoromethyl)styrene were synthesized according to literature procedures.[10-13,17] The synthetic protocols for 3,5-dimethoxystyrene, 4-vinylanisole and 4-(trifluoromethyl)styrene are outlined below (Scheme 2.4.).

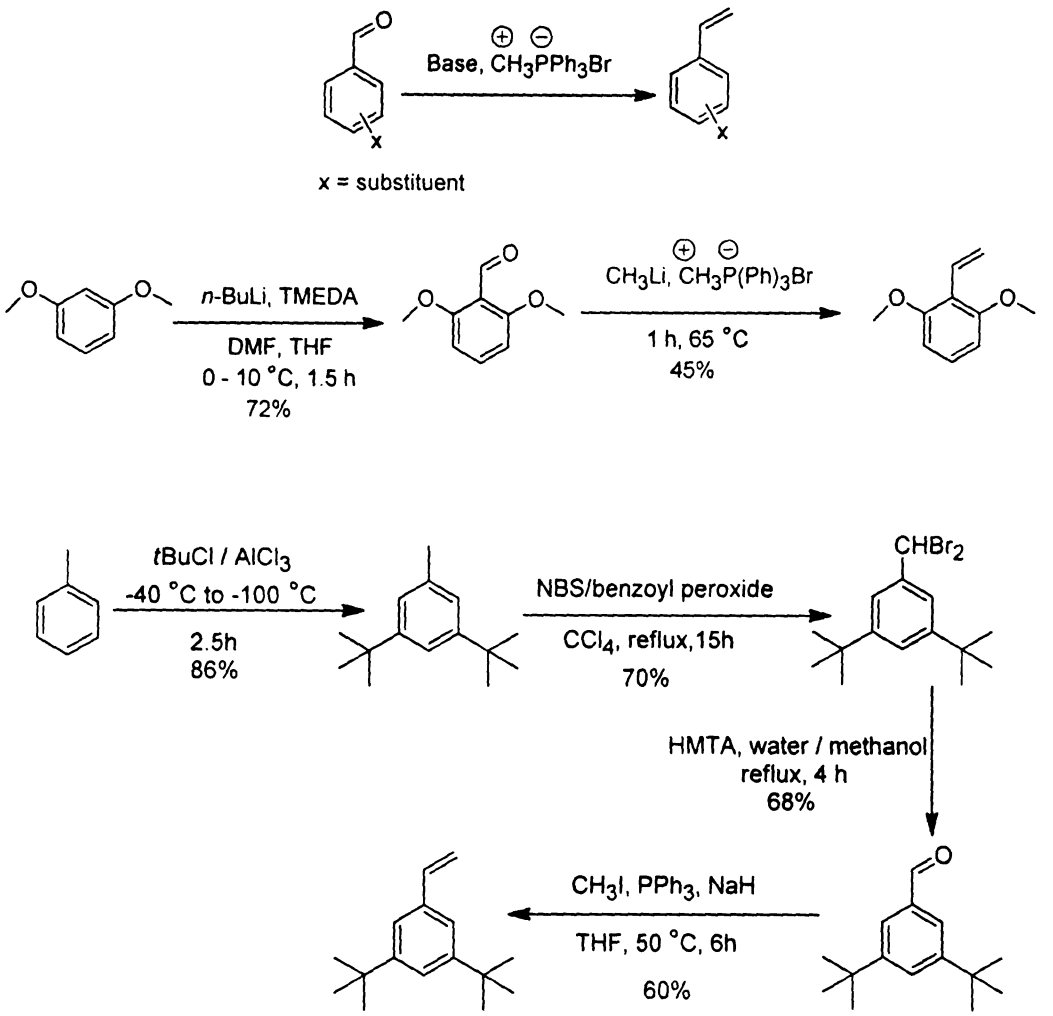

Scheme 2.4: The synthesis of substituted styrenes. (top) 3,5-Di-*tert*-butylstyrene, 3,5-dimethoxystyrene, 2,6-dimethoxystyrene, 4-vinylanisole and 4-(trifluoromethyl) styrene were synthesized via the Wittig reaction from commercially available aldehydes. (middle) Formylation of 1,3-dimethoxystyrene followed by Wittig olefination provided 2,6-dimethoxystyrene in moderate yield. Synthesis of 3,5-di-*tert*-butylstyrene (bottom) was prepared via a four step procedure.

2.3.2. Synthesis of Substituted Styrene Brushes via Surface Initiated Polymerization

Scheme 2.5. outlines the synthesis of substituted styrene polymer brushes grown from gold substrates. The experimental procedure is similar to that described by Bao *et al.* for the rapid growth of *tert*-butyl acrylate from gold surfaces.[6] A self assembled monolayer was prepared on the gold surface using MUD and converted into an initiator monolayer by reacting its terminal hydroxy group with 2-bromopropionyl bromide, as described previously. Initiator immobilization was apparent from the appearance of a carbonyl peak at 1743 cm^{-1} in the reflectance FTIR spectrum (Figure 2.2a). The purified substrates were transferred into a dry box, and the polymerization was performed inside the drybox to avoid contamination from oxygen. The catalyst system was a mixture of Cu(I)Br/Me_4Cyclam and Cu(II)Br_2/(dnNbpy)$_2$ in 1:1 (v/v) solutions of DMF and anisole. The Cu(II) complex ensures deactivation of active radicals and provided some control over the rapid polymerization. Polymerizations of substituted styrenes were run at 55 °C for 8 hours under identical conditions. The substrates were sonicated, and then washed with ethyl acetate and THF. The IR reflectance spectra of the dried films confirmed formation of polymer brushes by the appearance of characteristic peaks that correspond to the substituents on the styrene ring (Figure 2.2).

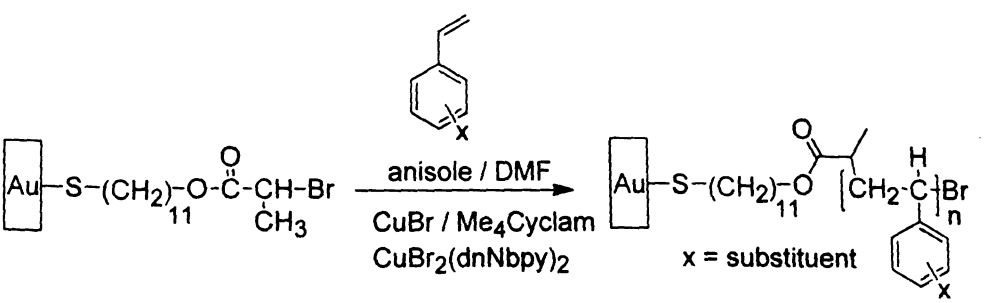

Scheme 2.5.: Surface initiated polymerization of styrene derivatives

2.3.3. Kinetic study of surface initiated polymerization of substituted styrene from gold surface.

Figures 2.1 and 2.3 show the evolution of film thickness with time for the polymerization of substituted styrenes. Figure 2.1 shows data for the surface polymerization of ortho and meta-substituted monomers while Figure 2.3 shows comparable data for para-substituted styrenes. The polymerization rates at 55 °C were unusually high for the ATRP of 3,5-disubstituted styrenic monomers, providing 100-350 nm thick layers in 4 hours.[18] In the early stages of polymerization, the nonlinear relationship between the film thickness and time suggests a relatively high concentration of radicals leading to some termination as well as a high polymerization rate. However, after >2 hours, growth in film thickness with time is roughly linear, indicating that some level of control was established during the polymerization. Polymerizations of ortho-substituted monomers were sluggish, likely due to steric effects, and none provided 100 nm thick films in 8 hours.

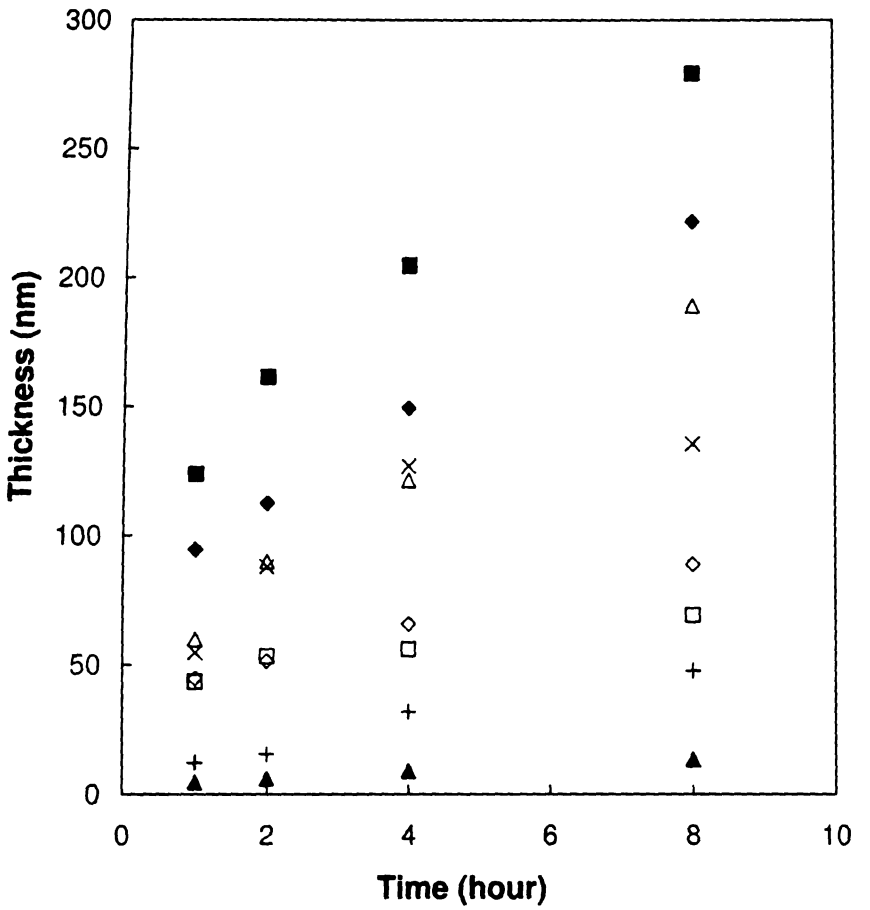

Figure 2.1: Evolution of the ellipsometric brush thickness with time for the polymerization of substituted styrenes from gold substrates. 3,5-bis-(trifluoromethyl)styrene (■), 3,5-dimethoxystyrene (◆), 3,5-dimethylstyrene (△), 3,5-di-*tert*-butylstyrene (×), styrene (◇), 2-(trifluoromethyl)styrene (□), 2-methoxystyrene (+), 2,6-dimethoxystyrene (▲).

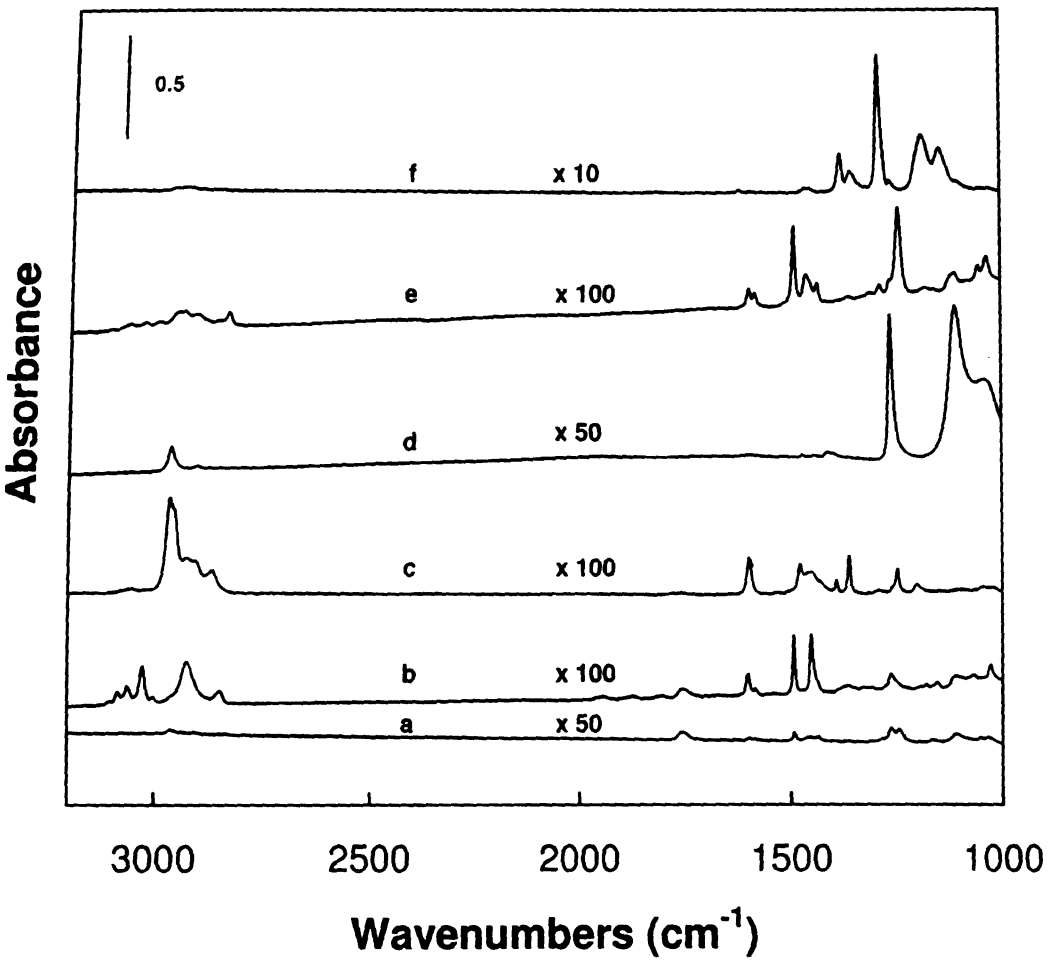

Figure 2.2: Representative reflectance FTIR spectra of gold surfaces coated with (a) the immobilized initiator (b) 70 nm of polystyrene (c) 55 nm of poly(3,5-*di-tert* butylstyrene) (d) 5 nm of poly(2,6-dimethoxystyrene) (e) 27 nm of poly(2-methoxystyrene) and (f) 130 nm of poly(3,5-bis-(trifluoromethyl)styrene).

The IR spectra in Figure 2.2 confirm the growth of polymers from Au surfaces. Furthermore, the spectral intensities agree well with the kinetic data. Spectrum b shows the four peaks (overtones and combinations) from 2000-1700 cm^{-1} characteristic of mono-substituted benzene rings (styrene). Strong methyl C-H stretching bands at 3000-2850 cm^{-1} and the characteristic doublet for *tert*-butyl groups, a strong peak at 1370 cm^{-1} and a weaker signal at 1390 cm^{-1} confirms the growth of 3,5-di *tert*-butyl styrene in spectrum c. The strong, broad, asymmetric (1280-1220 cm^{-1}) and symmetric (1050-1000 cm^{-1}) stretching modes for aryl ethers confirm the attachment of dimethoxy and monomethoxy styrene (spectra d and e). In spectrum f, a sharp strong peak at 1350 cm^{-1} (C-F stretching) identifies the CF_3 group of poly(3,5-bis-(trifluoromethyl)styrene).

In Figure 2.4, strong peaks between 1280-1220 cm^{-1} in spectrum b (C-O-C stretching of an alkyl aryl ether) confirm the growth of 4-methoxystyrene. A sharp strong peak at 1350 cm^{-1} (C-F stretching) identifies the CF_3 group in poly(4-trifluoromethyl styrene) (spectrum c). The spectrum of poly(4-methylstyrene) (d) is similar to that of styrene (a), except for the 2 peaks between 2000-1700 cm^{-1} (overtones and combinations) for a 1,4-disubstitutedbenzene ring. The strong, narrow peak seen at ~1000 cm^{-1} in spectrum e is characteristic of aromatic C-Br stretching expected for poly(4-bromostyrene). In spectrum c, the characteristic doublet for *tert*-butyl groups, a strong peak at 1370 cm^{-1} and a weaker signal at 1390 cm^{-1} confirms the growth of 4-*tert*-butyl styrene.

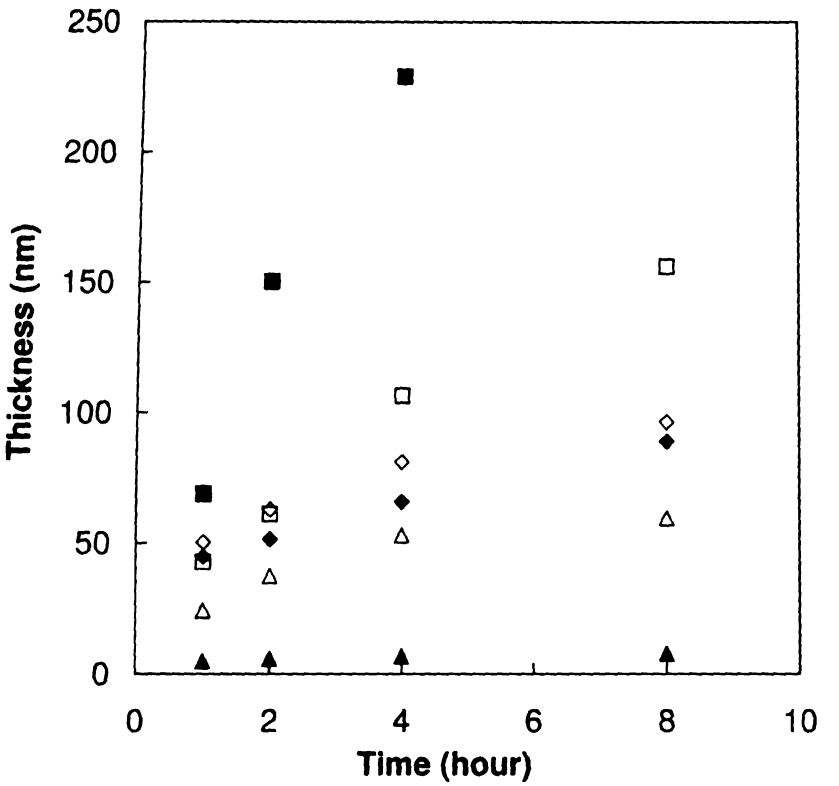

Figure 2.3: Evolution of the ellipsometric brush thickness with time for the polymerization of 4-substituted styrenes from gold substrates. 4-(trifluoromethyl)styrene (■), 4-*tert*-butylstyrene (◆), 4-bromostyrene (□), styrene (◇), 4-methylstyrene (△), 4-methoxystyrene (▲).

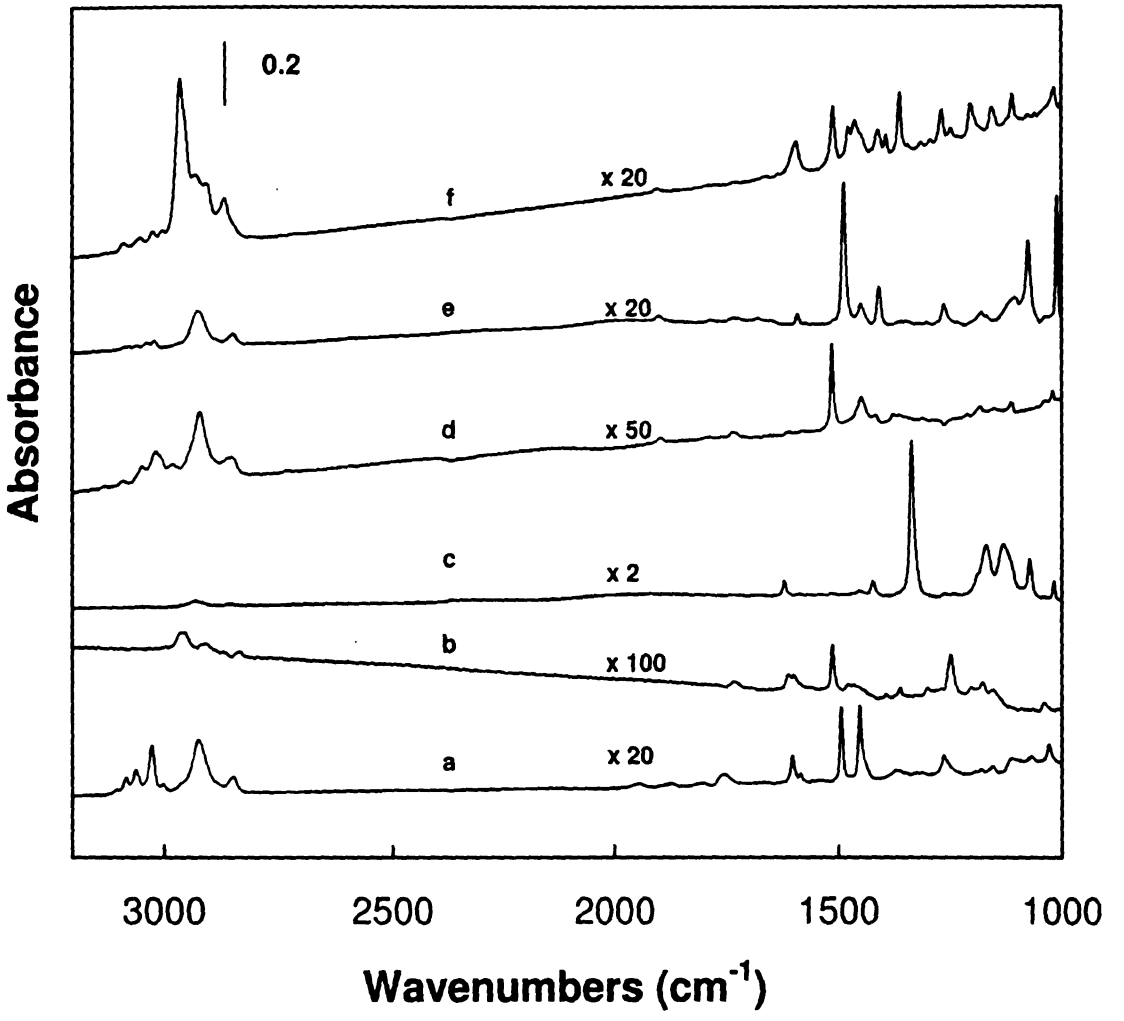

Figure 2.4: Representative examples of reflectance FTIR spectra of 4- substituted styrenes grown from gold substrates (a) 70 nm polystyrene (b) 10 nm poly(4-methoxystyrene) (c) 200 nm poly(4-(trifluoromethyl)styrene) (d) 55 nm poly(4-methylstyrene) (e) 100 nm poly(4-bromostyrene) (f) 150 nm poly (4-*tert*-butylstyrene).

2.3.4. Substituent effects on polymerization rate.

The data in Figures 2.1 and 2.3 show that monomers with electron withdrawing groups polymerize faster than monomers bearing electron donating groups, irrespective of the substitution pattern on the aromatic ring, (excluding ortho-substituted monomers where steric effects restrict propagation and termination. We also failed to grow α-methyl styrene from gold surface (data not shown) due to steric reasons.) Monomers with bulky electron donating groups (*tert*-butyl) at meta or para position polymerized faster than styrene and ortho-substituted monomers. Surprisingly, monomers with electron donating groups at meta sites polymerized faster than styrene or their ortho/para substituted analogues, irrespective of their steric demand. The observed film growth rates varied in the order of *m*-di-CF_3, *p*-CF_3> *m*-di methoxy> *m*-dimethyl, *m*-di-*tert*-butyl > *p*-*tert*-butyl > *p*-Br > H > *p*-methyl > *o*-methoxy > *o*-dimethoxy, *p*-methoxy. The results are consistent with solution polymerization rate data obtained from conventional radical polymerizations as well as controlled radical polymerizations such as ATRP[16] and living radical polymerizations initiated by TEMPO/BPO.[14,15]

To analyze the surface initiated polymerization rate data, we constructed a Hammett plot similar to the method used to analyze solution polymerizations.[16,19] A Hammett plot requires rate constants for the surface polymerization of para-substituted styrene because, only para-substituted styrene Hammett constants (σ) are known. The propagation and termination rate constants for surface polymerization can be estimated by using a model proposed by the Wirth group.[20]

The initiation and propagation steps of living radical polymerization have been well-documented and adopted for ATRP systems as shown in Scheme 2.6.

Initiation:

$$\sim R_n\text{-}X + (Cu(I)\ ligand)X \underset{k_d}{\overset{k_a}{\rightleftharpoons}} \sim R_n^{\bullet} + (Cu(II)\ ligand)X_2 \qquad (1)$$

Propagation:

$$\sim R_n^{\bullet} + M \xrightarrow{k_p} \sim R_{n+1}^{\bullet} \qquad (2)$$

Termination:

$$\sim R_n^{\bullet} + \sim R_m^{\bullet} \xrightarrow{k_t} \begin{matrix} \sim R_n \\ | \\ \sim R_m \end{matrix} \qquad (3)$$

Scheme 2.6: The initiation, propagation and termination steps of ATRP

According to this mechanism, the disappearance of monomer only occurs during propagation (step 2 of Scheme 2.6).

$$-\frac{d[M]}{dt} = k_p[\sim R^{\bullet}][M] \qquad (1)$$

If [R·] is constant, the monomer concentration can be reduced according to the first-order kinetics.

$$\ln \frac{[M_0]}{[M]} = k_p[R^{\bullet}]t \qquad (2)$$

However, [R·] usually is not constant due to termination, especially in case of surface polymerization which is clearly visible in Figures 2.1 and 2.3. Assuming only termination by coupling for surface-initiated ATRP, and ignoring possible contributions from surface

fouling or side reactions such as radical transfer to solvent, the rate of termination can be expressed[18] as:

$$\frac{d[R\cdot]}{dt} = -k_t[R\cdot]^2 \qquad (3)$$

$$[R\cdot] = \left(\frac{[R\cdot]_0}{1 + [R\cdot]_0 k_t t}\right) \qquad (4)$$

Recognizing that monomer-to-initiator ratio is so high that monomer concentration changes are negligible simplifies the solution of Equation 2.

$$\frac{[M]}{[M]_0} = 1 - k_p[R\cdot]t \qquad (5)$$

Substituting Equation 4 into Equation 5 reduces conversion to simple nonlinear time dependence:

$$\frac{[M]_0 - [M]}{[M]_0} = \frac{k_p[R\cdot]_0 t}{1 + [R\cdot]_0 k_t t} \qquad (6)$$

Realizing that the ellipsometric thickness is proportional to $[M]_0 - [M]$, the data of Figure 2.3 were fit to Equation 6. The fits to the data, as shown in Figure 2.5 for 4-bromostyrene, is reasonable and allows extraction of the apparent rate constants for propagation ($k_{p\,app} = [M]_0 k_p [R\cdot]_0$) and termination ($k_{t\,app} = [R\cdot]_0 k_t$). The data obtained for different para-substituted styrenes are tabulated in Table 2.2.

Table 2.2. Apparent rate coefficients in surface ATRP obtained from the Wirth model and absolute propagation rate constants for substituted styrenes[8]

Substituent	σ[21]	$k_{p\ app}$ (mol^{-1} Ls^{-1})	$k_{t\ app}$ (s^{-1})	$k_{p\ abs}$ (mol^{-1} Ls^{-1})[8]
4-CN	0.66	-	-	219
4-CF_3	0.54	649	7.23	-
4-Br	0.23	111	1.35	186
4-Cl	0.23	-	-	150
4-H	0.00	106	1.82	110
4-Me	-0.17	76	2.03	84
4-CMe_3	-0.20	288	6.81	-
4-OMe	-0.27	9.0	0.59	71

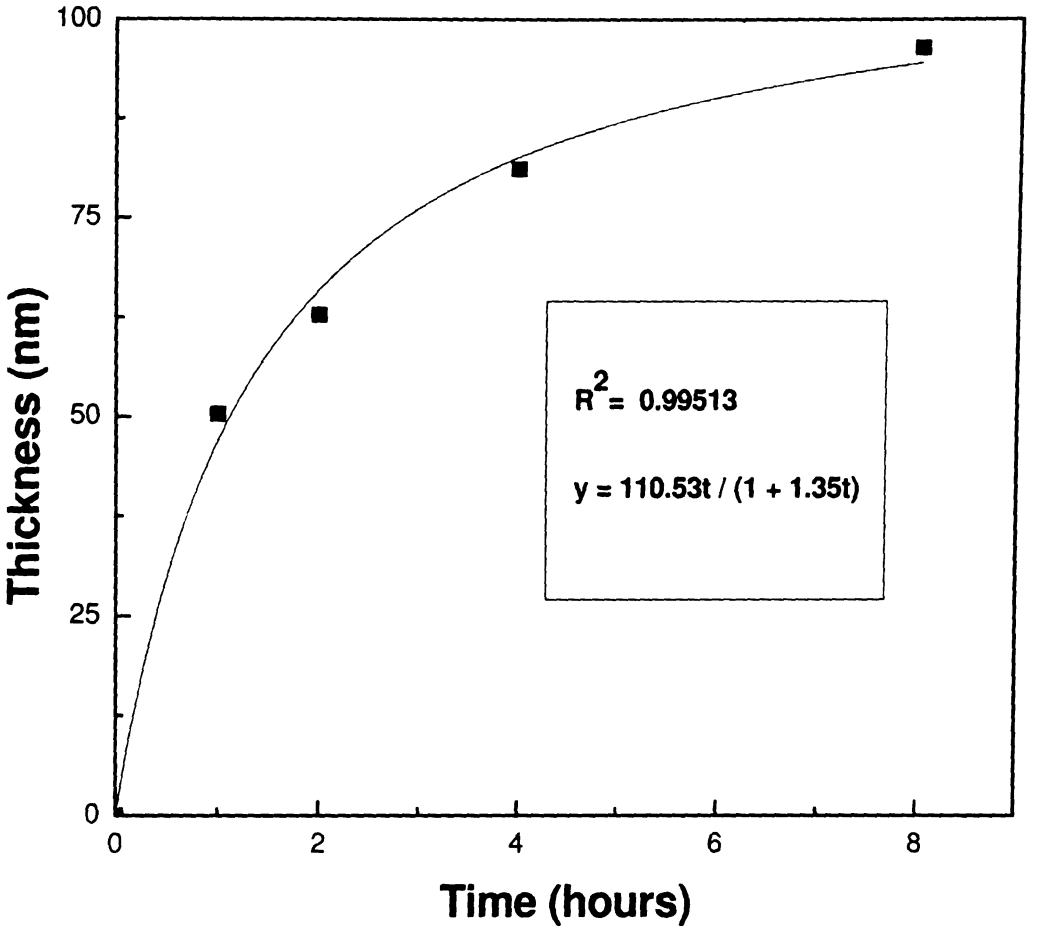

Figure 2.5: A representative example of the polymerization data for 4-bromo styrene fit to Equation 6. The polymer was grown from Au substrates at 55 °C.

Using the rate constants from fitting the data to Equation 6, we constructed a Hammett plot (Figure 2.6) relating the ratio of the apparent rate coefficients ($k_{p\ app}/k_{t\ app}$) (similar to analyzing product ratios, as applied by several authors to obtain Hammett plots)[22,23,24] and the Hammett constant, σ, for different para substituents. By using the ratio of the rate constants, we eliminate the radical concentration $[R\cdot]_0$, and in principle, $k_{p\ app}$ / $k_{t\ app}$ should reflect the ratio of absolute rate coefficients. Thus,

$k_{p\,app} / k_{t\,app} = [M]_0 k_p [R\cdot]_0 / [R\cdot]_0 k_t = [M]_0 k_p / k_t$ and

$\log (k_X / k_H) = \log [([M]_0 k_p / k_t)_X / ([M]_0 k_p / k_t)_H] = \log [(k_p / k_t)_X / (k_p / k_t)_H]$

where X and H refer to the substituted styrene and styrene respectively. For conventional radical polymerization of para-substituted styrenes, there is a linear correlation between $\log(k_{p\ app} / k_{t\ app})$ and the Hammett σ constants for different substituents. The value of ρ for our surface ATRP data ($\rho = 0.51$) was similar to that of conventional radical systems run in solution ($\rho = 0.55$, Figure 2.6),[25] but much smaller than the ρ value reported by Matyjaszewski for the solution ATRP ($\rho = 1.5$).[16] The difference between the solution and surface ATRP results is the use of different ordinates. In solution ATRP, the correlation was established with regard to the apparent propagation rate constant which comprises [R·], rather than the *ratio* of rate coefficients used for surface ATRP. Thus, the ρ values for surface ATRP and conventional (solution) radical polymerizations which also uses absolute rate coefficients as ordinate, are similar.

Based on the qualitative success of the simple Hammett equation similar to the solution polymerization via free radical pathway,[26] we conclude that these reaction constants are roughly correlated with Hammett parameters for the para substituents in surface polymerization with $\rho = 0.51$. Such substituent effects are mainly due to an increase in k_p / k_t for monomers substituted with electron-withdrawing substituents in para positions (Table 2.2). However, it does not exclude the possibility of a larger K_{eq} (in addition to larger k_p) for electron withdrawing monomers due to the decrease in the bond

dissociation energy (BDE) of the C-X bond by electron-withdrawing substituents and hence causes the additional enhancement of apparent polymerization rate coefficient with σ (similar to the solution polymerization)[16]. The energy graph in Scheme 2.7 provides a qualitative picture of the substituent effects on polymerization rates in surface ATRP of substituted styrenes.

Of the monomers studied, only 4-methoxystyrene failed to grow a significant surface film. Similar observations were made by Matyzasjewski *et al.*[16] in their study of the solution ATRP of 4-methoxystyrene, where they failed to obtain high molecular weight polymer. They suggested that the active growing species has a cationic nature due to the presence of strong electron-donating substituent. For this reason, we excluded 4-methoxystyrene from the Hammett plot.

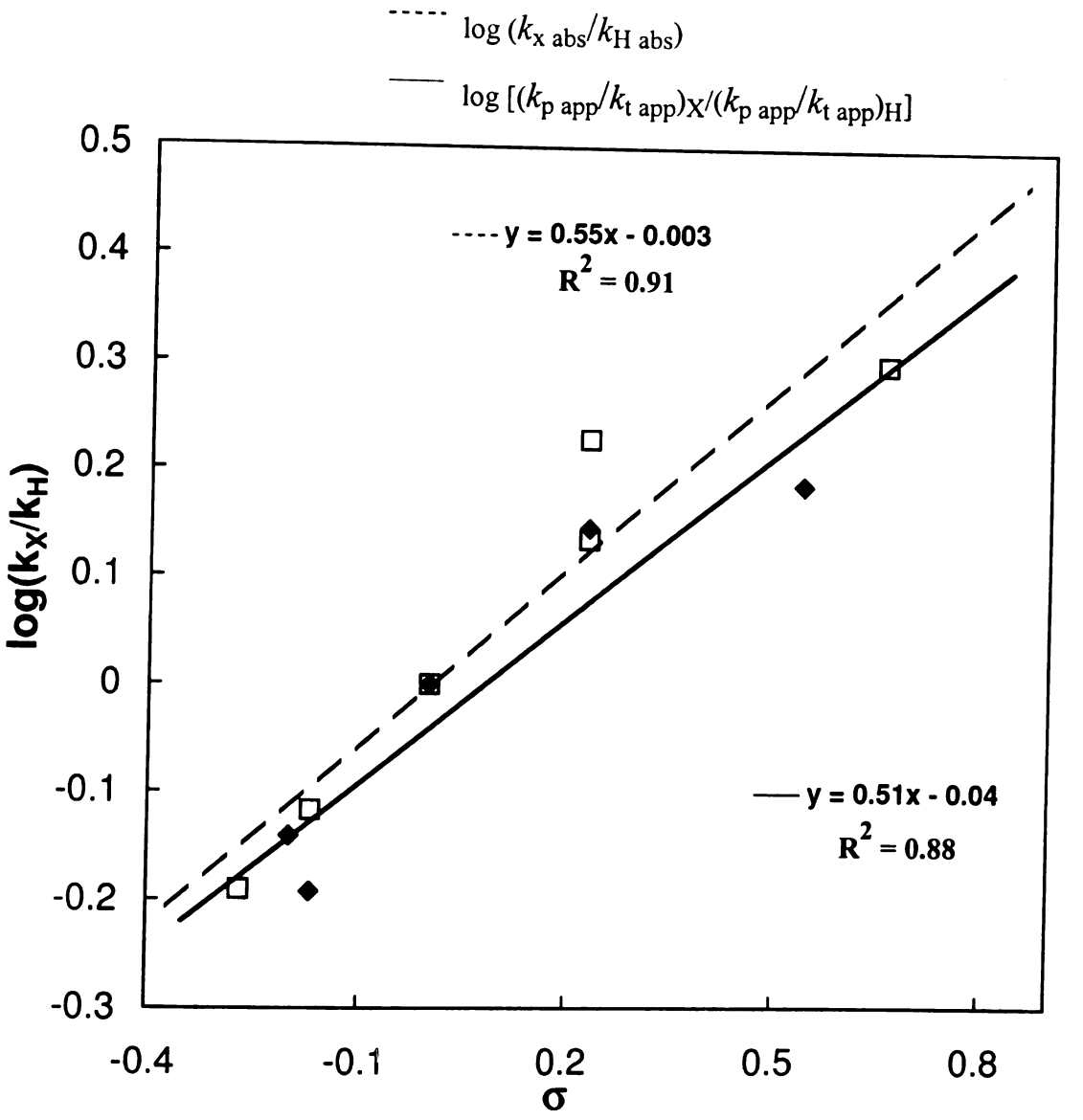

Figure 2.6: Hammett plots of (k_p/k_t) in surface-initiated ATRP of substituted styrenes (◆) and for absolute k_p values from conventional polymerizations (□) of substituted styrenes.[8]

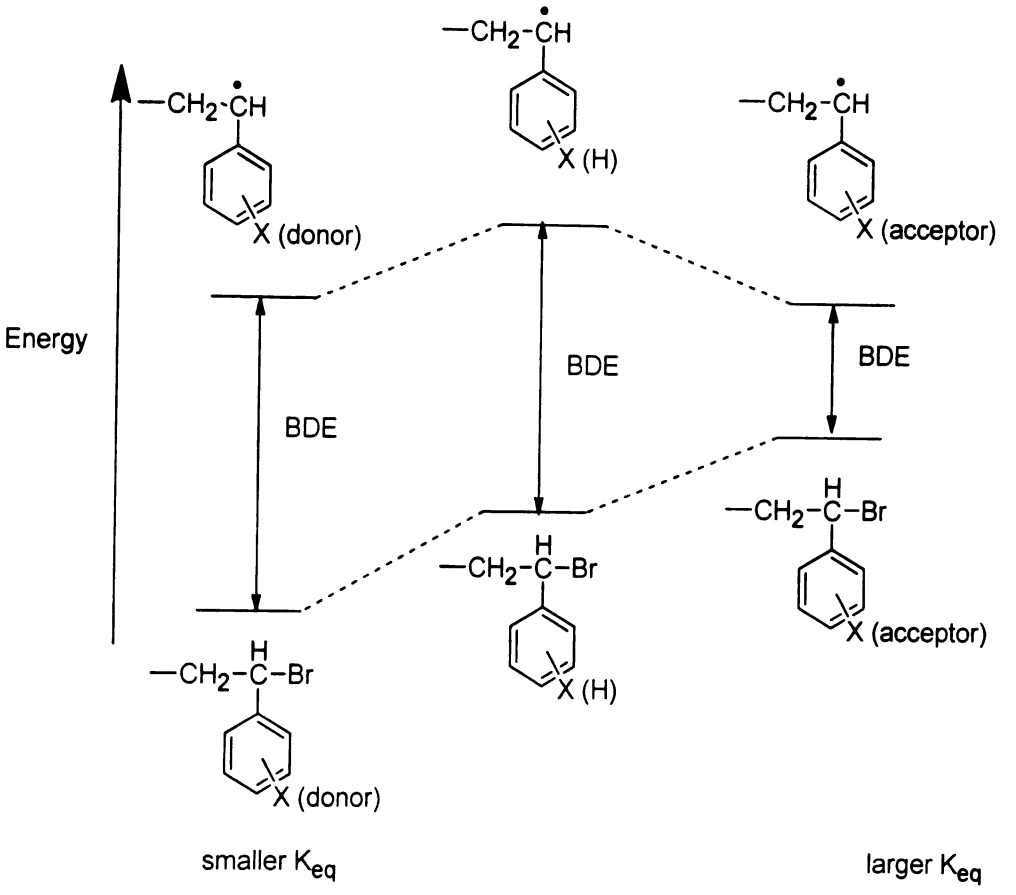

Scheme 2.7: Energy diagram for different substituents[16]

2.3.5 Synthesis of substituted styrene polymer brushes from SiO_2 substrates

This polymerization system was broadened to silica substrates as well. As expected, similar polymerization trends were observed (i.e. monomers with electron withdrawing substituents polymerize faster than those bearing electron donating substituents). One interesting observation was that polymerizations initiated from gold substrates were always slower than those from silica substrates, irrespective of monomer studied (Figure 2.7). This observation, previously reported by Bao *et al.*[6, 27] will be explained in detail in Chapter 3.

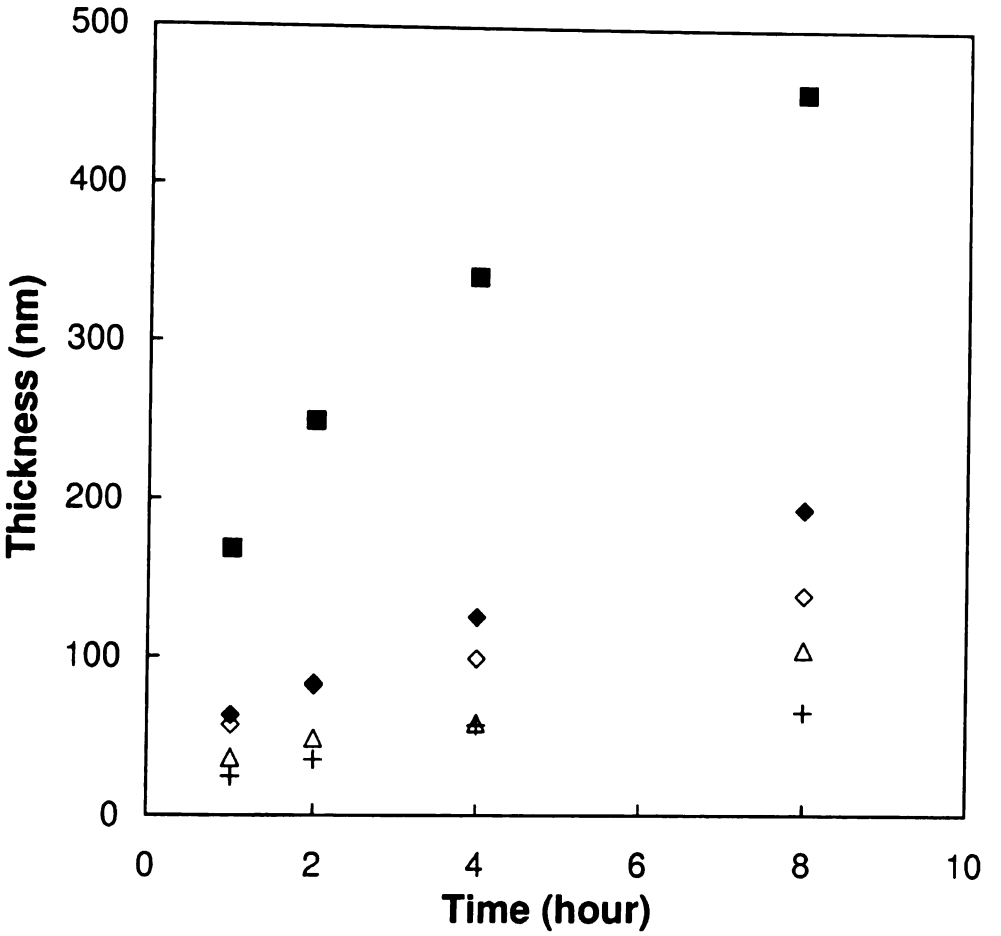

Figure 2.7: Evolution of the ellipsometric brush thickness with time for the polymerization of 3,5-bis(trifluoromethyl)styrene (■), 4-*tert*-butylstyrene (◆), styrene (◇), 4-methylstyrene (△),and 2-methoxystyrene (+) from silica surfaces.

2.4. Conclusions

Surface initiated atom transfer radical polymerization of substituted styrenes provides uniform and thick brushes (>100 nm in 1 hour) from gold and silicon surfaces. Styrenes substituted with electron withdrawing groups in meta and para positions exhibited high growth rates. The substituent effects seen in surface and solution polymerizations are similar for styrenes with electron withdrawing groups, and for electron donors in ortho and para positions, but donors at meta sites have surprisingly fast growth rates, possibly due to steric inhibition of termination. We also showed that the surface polymerization rate varies with different substituents follow the Hammett relation with $\rho = 0.51$. The ratio of k_p to k_t, acts as an indicator of the likelihood that a reaction will reach high degrees of polymerization before termination.

2.5. References

1 Matyjaszewski, K.; Xia, J. H. *Chem. Rev.* **2001**, *101*, 2921.

2 Kamigaito, M.; Ando, T.; Sawamoto, M. *Chem. Rev.* **2001**, *101*, 3689.

3 Chiefari, J.; Chong, Y. K.; Ercole, F.; Krstina, J.; Jeffery, J.; Le, T. P. T.; Mayadunne, R. T. A.; Meijs, G. F.; Moad, C. L.; Moad, G.; Rizzardo, E.; Thang, S. H. *Macromolecules* **1998**, *31*, 5559.

4 Couvreur, L.; Lefay, C.; Belleney, J.; Charleux, B.; Guerret, O.; Magnet, S. *Macromolecules* **2003**, *36*, 8260.

5 Grande, D.; Guerrero, R.; Gnanou, Y. *J. Polym. Sci. Polym. Chem.* **2005**, *43*, 519.

6 Bao, Z.; Bruening, M. L; Baker, G. L. *J. Am. Chem. Soc.* **2006**, *128*, 9056.

7 Odian, G. *Principles of Polymerization*. 3rd ed.; John Wiley & Sons: New York, **1991**.

8 Brandup, J.; Immergut, E. H.; Grulke, E. A. *Polymer Handbook*. 4th ed.; John Wiley & Sons: New York, **1999**.

9 Heuts, J. P. A.; Gilbert, R. G.; Radom, L. *Macromolecules* **1995**, *28*, 8771.

10 Pillow, J. N. G.; Halim, M; Lupton, J. M.; Burn, P. L.; Risch, N.; Meyer-Roscher, B.; Langhals, M. *Macromolecules* **1999**, *32*, 5985.

11 Risch, N.; Meyer-Roscher, B.; Langhals, M. *Z. Naturforsch., B: Chem. Sci.* **1994**, *49*, 141.

12 Overberger, C. G.; Burns, C. M. *J. Polym. Sc., Polym. Chem.* **1969**, *7*, 333.

13 Kawamura, T.; Uryu, T; Matsuzaki, K. *Makromol. Chem.* **1982**, *183*, 125.

14 Imoto, M.; Kinoshita, M.; Nishigaki, M. *Makromol. Chem.* **1965**, *86*, 217.

15 Kazmaier, P. M.; Daimon, K.; Georges, M. K.; Hamer, G. K. *Am. Chem. Soc., Polym. Prepr.* **1996**, *37*, *485*.

16 Qiu, Jian ; Matyjaszewski, K. *Macromolecules* **1997**, *30*, 5643.

17 Okuma, K.; Sakai, O.; Shioji, K. *Bull. Chem. Soc. Jpn.* **2003**, *76*, 1675.

18 Samadi, A.; Husson, S. M.; Liu, Y.; Luzinov, I.; Kilbey, M. *Macromol. Rap. Comm.* **2005**, *26*, 1829.

19 Coote, M. L.; Davis, T. P. *Macromolecules* **1999,** *32,* 4290.

20 Xiao, D. Q.; Wirth, M. J. *Macromolecules* **2002,** *35,* 2919.

21 Hansch, C.; Leo, A.; Taft, R. W. *Chem. Rev.* **1991,** *91,* 165.

22 Watkins, A. L.; Hashiguchi, B. G.; Landis, C. R. *Org. Lett.* **2008,** *10,* 4553.

23 Yajima, Tomoko; Okada, Kyoko; Nagano, H. *Tetrahedron,* **2004,** *60,* 5683.

24 Galardon, E.; Le Maux, P.; Simonneaux, G. *Tetrahedron,* **2000,** *56,* 615.

25 Walling, C.; Briggs, E. R.; Wolfstirn, K. B.; Mayo, F. R. *J. Am. Chem. Soc.* **1948,** *70,* 1537.

26 Coote, M. L.; Davis, T. P. *Macromolecules* **1999,** *32,* 4290.

27 Bao, Z.; Baker, G. L.; Bruening, M. *Macromolecules* **2006,** *128,* 9056.

Chapter 3

Surface effects in surface-initiated ATRP

3.1. Introduction

Surface initiated polymerization is a powerful technique for preparing chemically modified surfaces.[1,2,3,4,5,6] Studies aimed at understanding the fundamentals of polymer growth often use self-assembled monolayers (SAMs) as the initiator layer, because SAMs provide a closely packed, well-ordered and stable configuration on the surface. Most SAMs are generated on metal surfaces such as Au, Ag and Cu using thiol chemistry while alkyl siloxanes anchored to hydroxyl-terminated surfaces, such as SiO_2, Al_2O_3 and other oxides via alkoxy and chlorosilanes. Surface initiated radical polymerization can be carried out on a broad range of substrates, but most studies have focused on silicon and gold substrates. Gold surfaces are chemically homogeneous, virtually free of contamination, easy to clean, applicable to a wide variety of analytical techniques for thin film characterization. A disadvantage of Au surfaces is that the Au-S bond that links the initiator layer to the surface is labile above 60 °C[7,8,9] and hence polymerizations are typically limited to <60 °C. However, at such temperatures, the low propagation rates for radical polymerization of important aromatic monomers such as styrene and 4-vinyl pyridine limit their growth. In addition, Bao *et al.* observed that film growth rates from SiO_2 substrates were higher than those grown from Au substrates, regardless of monomer[10] even at temperatures < 60 °C.

Huang *et al.* [9a] investigated free-radical polymerization of styrene from azo-initiators immobilized on flat Au substrates, and showed that free-radical polymerization from Au is limited by the instability of alkanethiol monolayers. They reported that soluble free radicals accelerated thiol desorption from Au, and the desorbed alkanethiols appeared to be efficient chain-transfer reagents that terminate brush growth. To overcome monolayer instability, they utilized a simple cross-linking procedure to enhance the stability of SAMs, and made thermal radical polymerization from Au surfaces facile. Later Stephanie *et al.* [9b] restricted thiol desorption at elevated temperatures by coating gold electrodes with a layer of carboxylic acid functionalized polypyrrole, and in their work on one pot thermal polymerization from gold nanoparticles, Matyjaszewski *et al.* [11c] used a crosslinked polymer shell to prevent dissociation of linear brushes from gold nanoparticles at elevated temperatures.

There are other factors that may lead to different polymerization rates on Au and silica. One difference between Au and SiO_2 surfaces is the number and density of sites available on the surface for immobilizing initiator. Studies show that silica surfaces have a limiting area/chain of 0.6 nm^2,[11] roughly 40% of the density for a SAM on Au, while typical values for silica range from 0.65 nm^2 to 1.54 nm^2/chain. Bao *et al.* [12] investigated the effect of initiator density on polymerization rates for Au and silica surfaces, and observed that decreasing the initiator density on silica by 50% decreased the polymerization rate, but for gold, the rate was nearly unchanged. Additionally, gold is a

transition metal capable of quenching radicals,[13,14,15] which could reduce the number of active chains, resulting in thin films.

This chapter describes a systematic evaluation of three factors that may be responsible for the lower film growth rates from gold: 1) differences in the initiator densities for gold and silica substrates, 2) termination resulting from desorption of thiols from SAMs on gold surfaces, which is absent in silicon surfaces 3) and radical quenching by the gold surface.[13,14,15] Based on the work of Bao *et al.*, we suspected that desorption of thiols from SAMs on gold surfaces at ambient temperatures, followed by chain transfer of growing polymer chains to thiols was the likely cause of thinner film growth on Au compared to silica surfaces. We tested this hypothesis by examining polymerizations from a crosslinked initiator anchored on gold substrates, and by analysis of block copolymer growth from Au and silica surfaces.

3.2. Experimental Section

3.2.1. Materials

Unless otherwise noted, all chemicals were obtained from Aldrich and stored under nitrogen. 11-Mercapto-1-undecanol (MUD, 97%), 2-bromo-2-methylpropionyl bromide (2-BIB, 97%), 3-mercaptopropyltrimethoxysilane (MPS), anisole (99.7%), *N,N*-dimethylformamide (DMF, 99.8%), Cu(I)Br (99.999%), $Cu(II)Br_2$ (99.999%), $Me_4Cyclam$ (99%), and 4,4'-dinonyl-2,2'-bipyridine (dnNbpy, 97%) were used as received. (3-Aminopropyl)trimethoxysilane was distilled under vacuum prior to each use. Triethylamine was distilled from calcium hydride under a nitrogen atmosphere, and stored under nitrogen. *tert*-Butyl acrylate (*t*BA) (98%), MMA (99%) and styrene (99%)

were passed through a 10 cm column of activated basic alumina and then distilled from calcium hydride to remove inhibitors. The disulfide initiator (11-[(2-bromo-2-methyl)propionyloxy]undecyldisulfide)[7] [(Br-C(CH_3)$_2$-COO-(CH_2)$_{11}$S)$_2$], the trichloro-silane initiator (11-[(2-bromo-2-methyl)propionyloxy]undecyl trichlorosilane[11] and the trimethoxysilane initiator [2-bromo-2-methyl-*N*-(3-trimethoxysilylpropyl)propionamide] were synthesized using slightly modified versions of literature procedures.[16] Silane compounds were used and stored under nitrogen. Toluene was distilled under nitrogen in the presence of sodium/potassium alloy using benzophenone as an indicator. After purification, the monomers, liquid chemicals and solvents were transferred to Schlenk flasks, degassed by three freeze-pump-thaw cycles, and then transferred into a drybox. Silicon wafers and Au-coated wafers (electron-beam evaporation of 200 nm of Au on 20 nm of Ti on Si (100) wafers, or 200 nm of Au sputter-coated on 20 nm of Cr on Si (100) wafers) were cleaned in a UV/O_3 chamber for 30 min prior use.

3.2.2. Characterization Methods

Ellipsometric measurements were obtained with rotating analyzer ellipsometer (model M-44, J. A. Woollam) using WVASE32 software. The angle of incidence was 75° for all experiments. For the calculation of film thickness, a refractive index of 1.50 was used. Reflectance Fourier Transform Infrared (reflectance FTIR) spectroscopy was performed using a Nicolet Magna-560 FTIR spectrometer containing a PIKE grazing angle (80°) attachment. Spectra were typically collected with 128 scans using a MCT detector. Changes in surface morphology of the polymer film during thermal degradation

on gold surface were observed using a Keyence Digital Microscope equipped with a video camera.

3.2.3. Preparation of immobilized initiators on gold and silicon substrates

Gold-coated wafers were UV/O_3-cleaned for 30 min, washed with water and ethanol, and after transferred into a N_2 glovebag, immersed in a 1 mM ethanolic solution of the disulfide initiator [(Br-C(CH_3)$_2$-COO(CH_2)$_{11}$S)$_2$] for 24 h to form the self-assembled initiator monolayer. The films were then washed with ethanol and dried under a stream of N_2. A crosslinked initiator monolayer was formed by immersing Au-coated substrates in a vial containing a 2 mM methanolic solution of MPS for 12 h in a glovebag at room temperature. After deposition, the substrate was rinsed three times with 2 mL of methanol and dried with nitrogen. The attached silane monolayer was then hydrolyzed at room temperature with 0.1 M HCl for 15 h to afford a hydroxylated surface. The modified Au substrate was then treated with a 10 mM solution of trimethoxysilane initiator [2-bromo-2-methyl-*N*-(3-trimethoxysilylpropyl)propionamide] in toluene at 55 °C for 12 h under nitrogen. Following the deposition, the substrates were rinsed repeatedly with toluene and isopropanol, and then dried in a stream of nitrogen. The ellipsometric thickness of the crosslinked initiator layer on gold was 10-15 Å.

The trimethoxysilane initiator was immobilized on UV/O_3-cleaned silicon wafers by immersing the substrate in a 10 mM solution of [2-bromo-2-methyl-*N*-(3-trimethoxysilylpropyl)propionamide] in toluene at 55 °C under nitrogen. After 12 h, the wafer was rinsed repeatedly with toluene and isopropanol, sonicated in toluene for 1 min

and dried in a stream of nitrogen. The ellipsometric thickness of the crosslinked initiator layer on silicon surface was 10-15 Å.

3.2.4. Surface initiated polymerization

In a N_2-filled dry box, CuBr (5.7 mg, 0.04 mmol), $CuBr_2$ (4.5 mg, 0.02 mmol), Me_4Cyclam (10.3 mg, 0.04 mmol) and dnNbpy (16.4 mg, 0.04 mmol) were added to a round-bottom flask containing 20 mL of a degassed solution of monomer in DMF/anisole (monomer/DMF/anisole) 2:1:1 v:v:v, [monomer]~4.0 M). The mixture was well-stirred and heated with an oil bath to 50 °C until a transparent, light green solution formed. The prepared solution was then transferred into a small vial containing an initiator-modified Au / SiO_2 substrate to start the surface-initiated polymerization. After a predetermined reaction time at 50 °C, the substrate was removed from the vial, washed with ethyl acetate and THF sequentially, and then dried under a stream of N_2 in the dry box.

3.3. Results and discussion

3.3.1. Surface initiated polymerization from gold and SiO_2 substrates

Bao *et al.* had reported that "identical" polymerizations of MMA from Au and SiO_2 surfaces gave different polymer film thicknesses, with polymer films grown from SiO_2 systematically thicker than those grown from Au substrates.[12] To confirm Bao's observation, we polymerized MMA and styrene under identical conditions from initiators anchored on Au and SiO_2 surfaces (Scheme 3.1), and compared the evolution of the film thickness with time. Figures 3.1a and 3.1b show the growth of PMMA and polystyrene

brushes from flat Au and SiO_2 surfaces. Irrespective of the monomer, SiO_2 surfaces yield thicker films and higher apparent polymerization rates than those grown from Au surfaces under similar conditions. However, the film thickness vs. time profiles are similar, suggesting that the primary difference between growth from gold and growth from silica is fewer active chains when brushes are grown from gold surfaces. These data confirm the observations of Huang *et al.* and Bao *et al.*, that polymer films grown on Au substrates are systematically thinner than those polymerize on SiO_2.

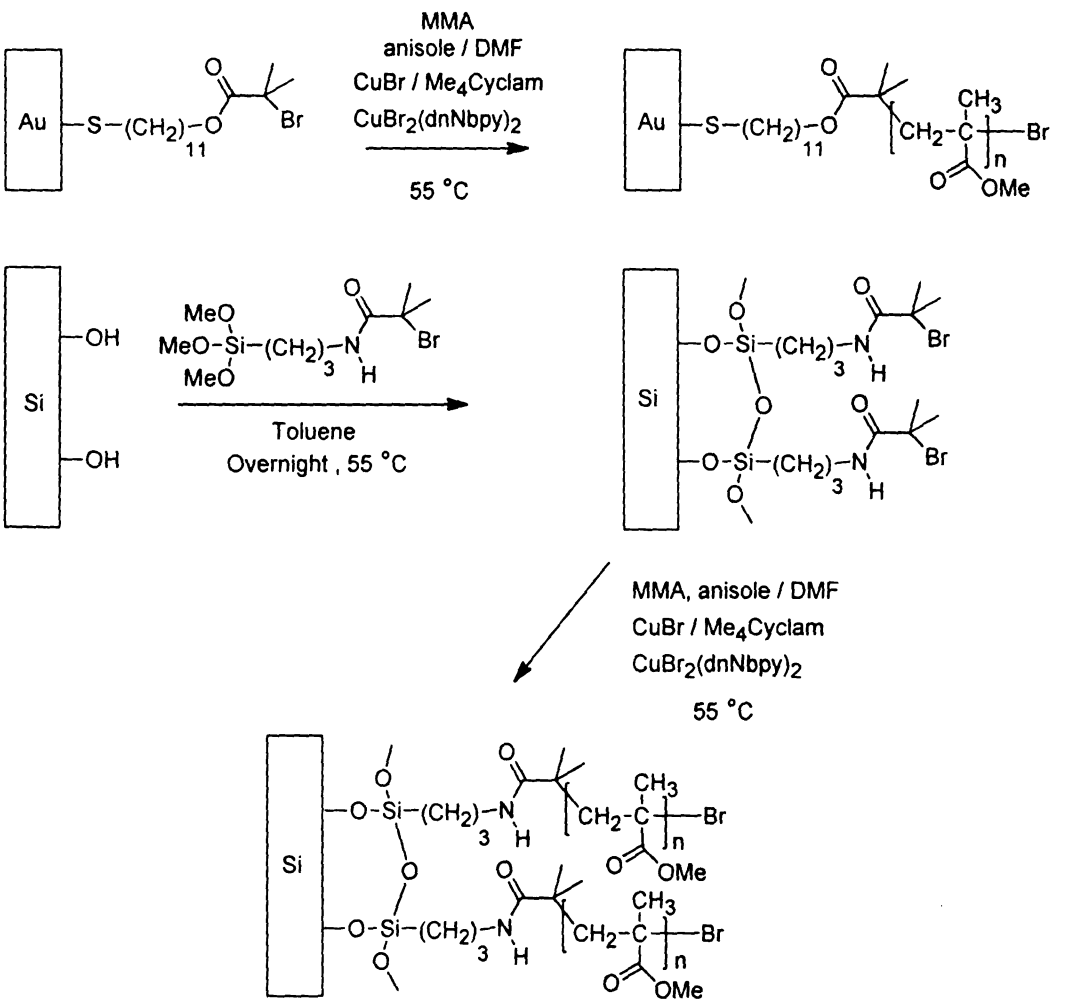

Scheme 3.1: Surface initiated polymerization of MMA from silicon and gold surfaces

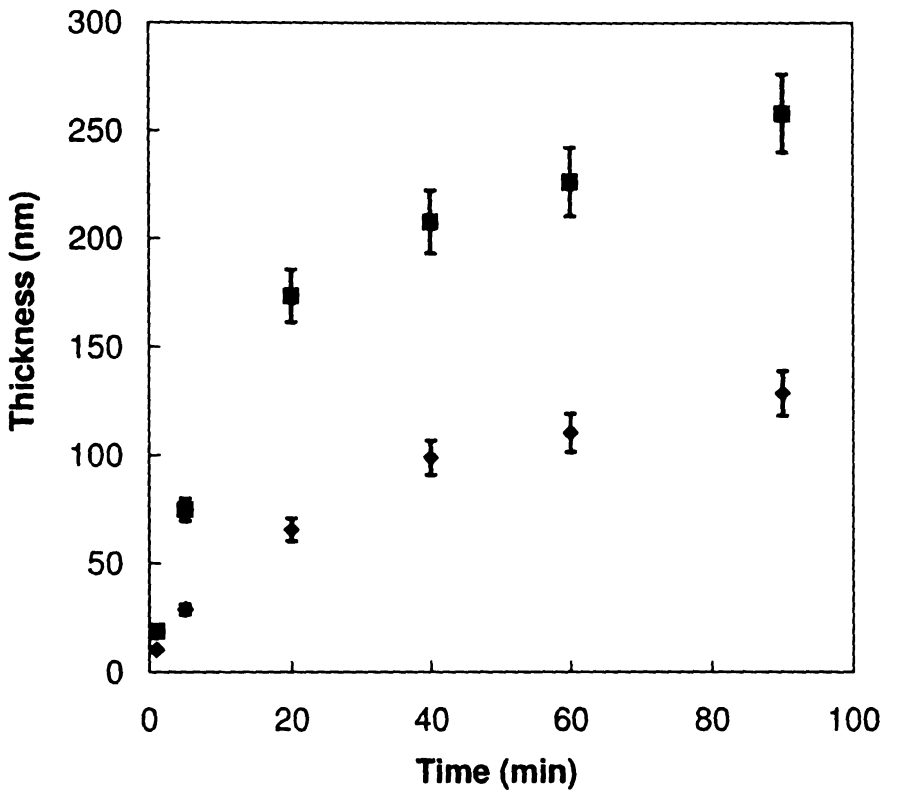

Figure 3.1a: Evolution of the ellipsometric brush thickness with time for the polymerization of MMA (methyl methacrylate) from ◆ gold and ■ silicon surfaces at 50 °C. The points are the average of data from two independent runs, and the limits of the error bars are the measured film thicknesses from the two runs.

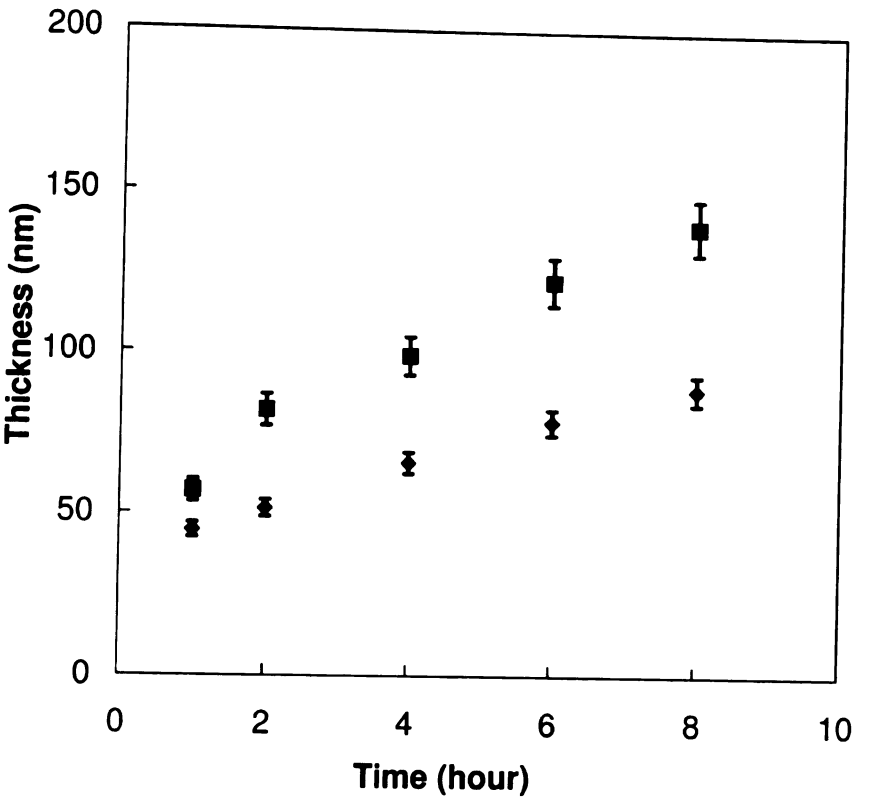

Figure 3.1b: Evolution of the ellipsometric brush thickness with time for the polymerization of styrene from ◆ gold and ■ silicon surfaces at 50 °C. The points are the average of data from two independent runs, and the limits of the error bars are the measured film thicknesses from the two runs.

3.3.2. Block copolymer formation on Au and SiO_2 substrates

It would be reasonable to expect that the different behaviors seen for films grown from Au and SiO_2 substrates would diminish when the growing polymer chains are distant from the substrate. This hypothesis can be tested by placing the initiator at increasing distances from the Au surface. One way to form an extended initiator is to use ATRP to grow polymers from the surface, and then quench the growing chain by adding

a large excess of $Cu(II)Br_2$ as shown in Scheme 3.2. The resulting Br-terminated chains can then be used as initiators for further polymerization. To that end, we grew poly(*tert*-butyl acrylate) (poly*t*BA) brushes from initiators anchored to a Au surface, and quenched the growing chains at various times. After washing the substrate to remove excess monomer, it was dried under a stream of N_2, removed from the dry box, and characterized by ellipsometry and FTIR spectroscopy. We then returned the substrates to the drybox and initiated polymerization of MMA for 1 hour from the dormant P*t*BA chains. The same process was carried out on a SiO_2 substrate, which served as a control.

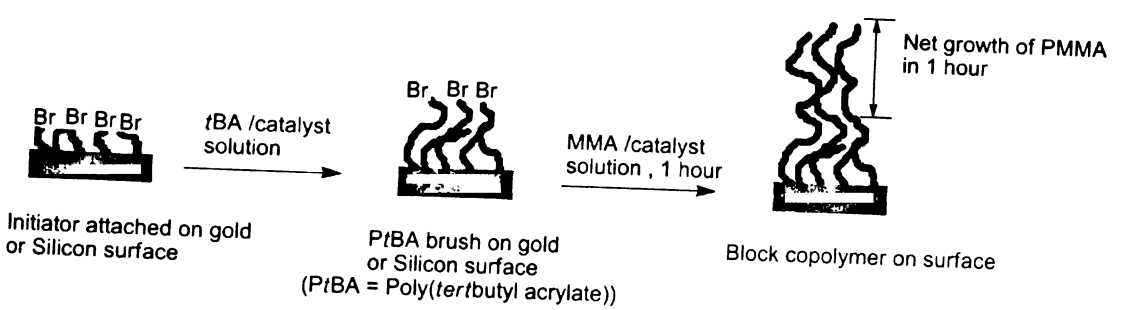

Scheme 3.2: Block copolymer formation on Au and SiO_2 surfaces

Figure 3.2 shows FTIR spectra of a 97 nm P*t*BA film and the P*t*BA-*block*-PMMA copolymer after growing 210 nm of PMMA from the initial P*t*BA film. The spectrum for the block copolymer is as expected; the intensity of the ester carbonyl increased, and the relative intensity of the *t*-butyl doublet decreased compared to the C-H rocking bands, ($1350 - 1500\ cm^{-1}$).

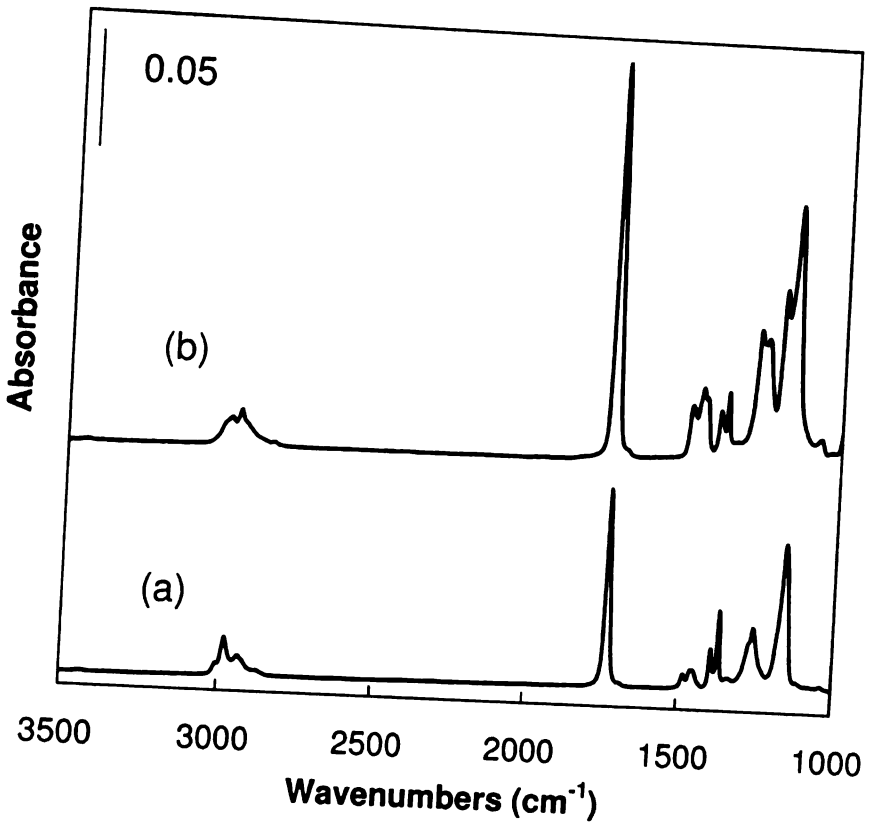

Figure 3.2: Reflectance FTIR spectra of gold substrates coated with (a) 100 nm P*t*BA brushes grown from the initiator layer; (b) a P*t*BA-*block*-PMMA copolymer brush, synthesized by growing 210 nm of PMMA from a 100 nm P*t*BA film.

Figures 3.3a and 3.3b show that PMMA blocks grown for 1 hr from P*t*BA brushes were ~200 nm thick, 2-3 times thicker than PMMA films grown directly from gold surfaces, but comparable to PMMA blocks grown directly from SiO_2. These results suggest that a substantial fraction of the P*t*BA chains were active after polymerization of the initial P*t*BA block, and directly confirm the role of the Au surface in reducing the

film thickness when polymers are grown from Au surfaces. For Au substrates, the thickness of the PMMA layer grown from P*t*BA films in 1 hour increased with the P*t*BA thickness, saturated at ~ 200 nm, and then slowly declined. The decline likely reflects fewer dormant P*t*BA chains available to form the P*t*BA-*block*-PMMA copolymer. Since the same effect is not seen for SiO_2 substrates, the decline can be identified with higher termination rates for the growth of P*t*BA on Au, presumably by radical quenching by electron transfer, or by the loss of growing chains via desorption of thiols from Au surfaces. Desorbed thiol may act as a chain transfer agent - for polymer brush syntheses, chain transfer is equivalent to termination. An alternative desorption scenario is that polymers anchored through Au-S bonds may be mechanically unstable, especially for highly solvated polymers of high molecular weight.

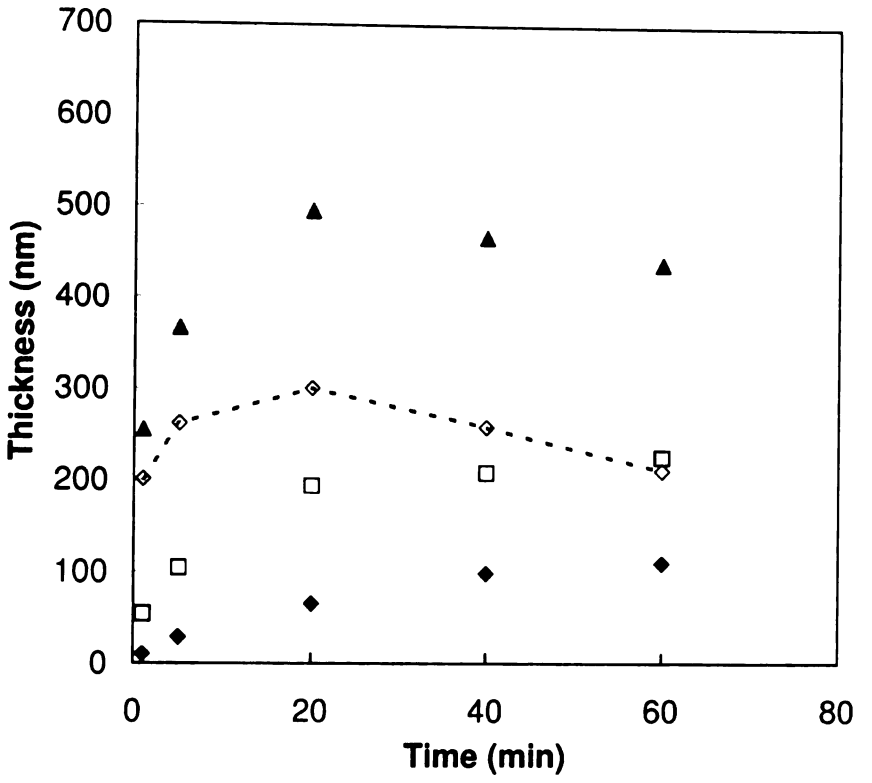

Figure 3.3a: Surface polymerization study of the formation of P*t*BA-*block*-PMMA films on gold surfaces. □ P*t*BA brushes grown from initiators anchored on gold for various times; ▲ Total film thickness after 1 hour growth of PMMA from P*t*BA brushes grown on gold; ◇ Net growth of PMMA from P*t*BA (total film thickness – P*t*BA brush thickness) after 1 hour of polymerization (The broken line drawn as a guide to the eye) ◆ PMMA grown from initiators anchored on gold for various times, shown for comparison.

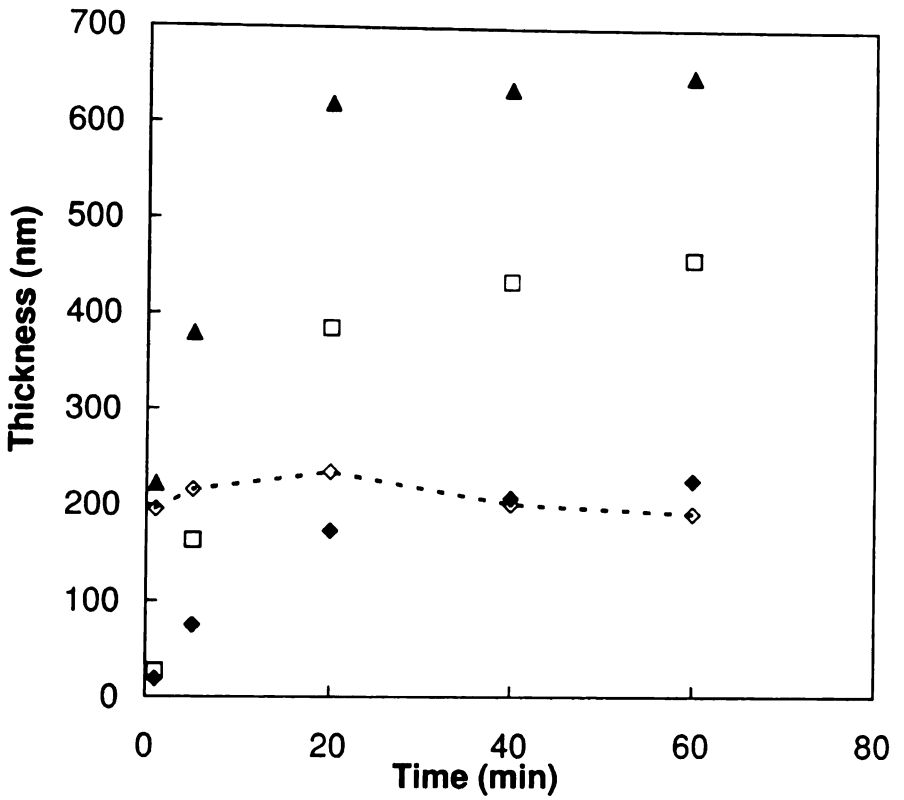

Figure 3.3b: Surface polymerization study of the formation of P*t*BA-*block*-PMMA films on SiO_2 surfaces. □ P*t*BA brushes grown from initiators anchored on SiO_2 surfaces for various times; ▲ Total film thickness after 1 hour growth of PMMA from P*t*BA brushes grown on SiO_2; ◇ Net growth of PMMA from P*t*BA (total film thickness – P*t*BA brush thickness) after 1 hour of polymerization (The broken line drawn as a guide to the eye) ◆ a PMMA brush grown from initiators anchored on SiO_2 for various times, shown for comparison.

3.3.3. Formation and polymerization from a cross linked initiator

The previous data do not distinguish between radical quenching and thiol desorption as the primary factor leading to thinner films growing on Au surfaces compared to SiO_2. However, preventing desorption of thiols from the Au surface should test the validity of the thiol desorption mechanism. To that end, we formed cross-linked initiators on gold surfaces, similar to those of Holzinger *et al.*,[17] and compared polymerizations from cross-linked initiator layers to substrates with initiators based on standard thiols. Scheme 3.3 shows the formation of a cross-linked initiator layer on a gold surface. The thicknesses of the cross-linked and standard thiol initiator layers were comparable, and therefore, radical quenching by the gold surface should be comparable for both initiator layers. Immersion of Au-coated slides in a 2 mM solution of MPS in methanol formed an MPS monolayer. During hydrolysis, the trimethoxysilane group at the MPS terminus condensed to form a dense poly(siloxane) network. The siloxane layer provides lateral stabilization through inter-chain cross-linking and generated a hydroxylated surface for the subsequent attachment of the trimethoxysilane-ATRP initiator.

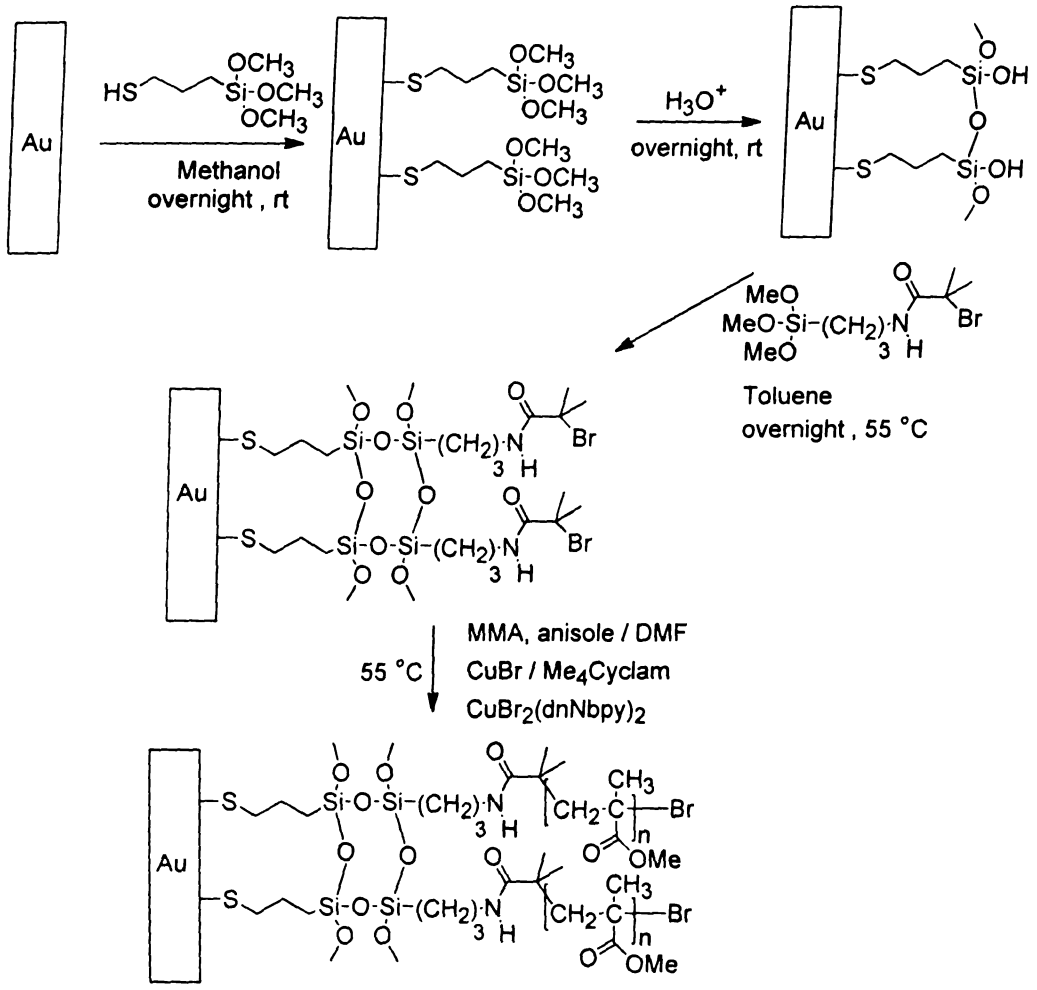

Scheme 3.3: Formation of cross linked initiators on gold surface

We used FTIR spectroscopy and ellipsometry to follow the attachment of the ATRP initiator to MPS. The reflectance FTIR spectrum of the MPS layer on Au (not shown here) shows vibrational bands characteristic of MPS (2938 cm^{-1} for overlapping CH_3 and CH_2 bands, 2846 cm^{-1} for the CH_2 symmetric stretch, and 1114 cm^{-1} for the Si-O-C stretch). After hydrolysis, the methyl peaks disappeared and the peak at 1114 cm^{-1} greatly decreased, indicating nearly complete hydrolysis of the MPS layer. The ellipsometric thickness of the hydrolyzed MPS was 1.0 nm. The above results are in good agreement with literature data.[11,18,19,20] After attachment of the ATRP initiator, the film

thickness increased to 2.2 nm and amide peaks (1652 and 1548 cm^{-1}) appeared in the reflectance FTIR spectrum confirming successful attachment of the ATRP-initiator.

Figures 3.4 and 3.5 show data for the surface polymerization of MMA and styrene from gold and silicon surfaces with the crosslinked initiator. For both MMA and styrene, films grown from the crosslinked initiator on gold had thicknesses comparable to those grown on SiO_2 surfaces. Additionally, the data in Figure 3.5 show increases in the characteristic IR peaks of the respective polymers consistent with the ellipsometry data. Therefore, stabilizing the initiator layer via cross-linking efficiently restricts thiol desorption, and there is no evidence for radical quenching by gold.

To explore the stability of the cross-linked thiol initiator, we ran polymerizations from room temperature to 115 °C using standard initiators immobilized on Au and SiO_2 surfaces. The data (Figure 3.6) show that thinner films are formed on Au substrates, which suggests significant thiol desorption even at low temperatures. In contrast, the polymerization data for the cross-linked initiator track the data for films grown on SiO_2. Furthermore, the crosslinked initiator enables polymerization of MMA and styrene from Au surfaces up to ~100 °C, providing 300 nm and 120 nm films grown in 1hr, respectively. The apparent temperature limit for growth from Au surfaces is ~110 °C. Inspection of a polystyrene film grown at 115 °C showed large-scale delamination of the polymer films (Figure 3.7), which is absent in films grown at 90 °C. Kim *et al.* made similar observations for poly(hydroxyethyl methacrylate) brushes grown on Au.[21]

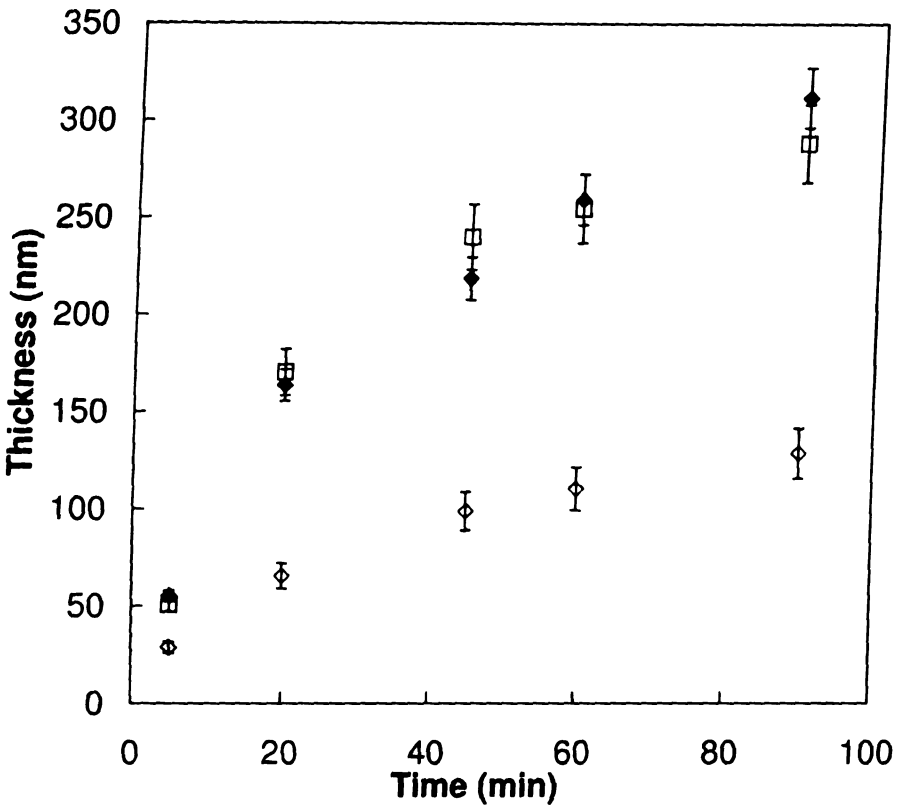

Figure 3.4a: Surface initiated polymerization of MMA from gold and SiO_2 surfaces. ◇ PMMA grown from a standard (non-crosslinked) initiator on gold; ◆ PMMA grown from a crosslinked thio initiator; □ PMMA grown from SiO_2.. The points are the average of data from three independent runs, and the limits of the error bars are the measured film thicknesses from the three runs.

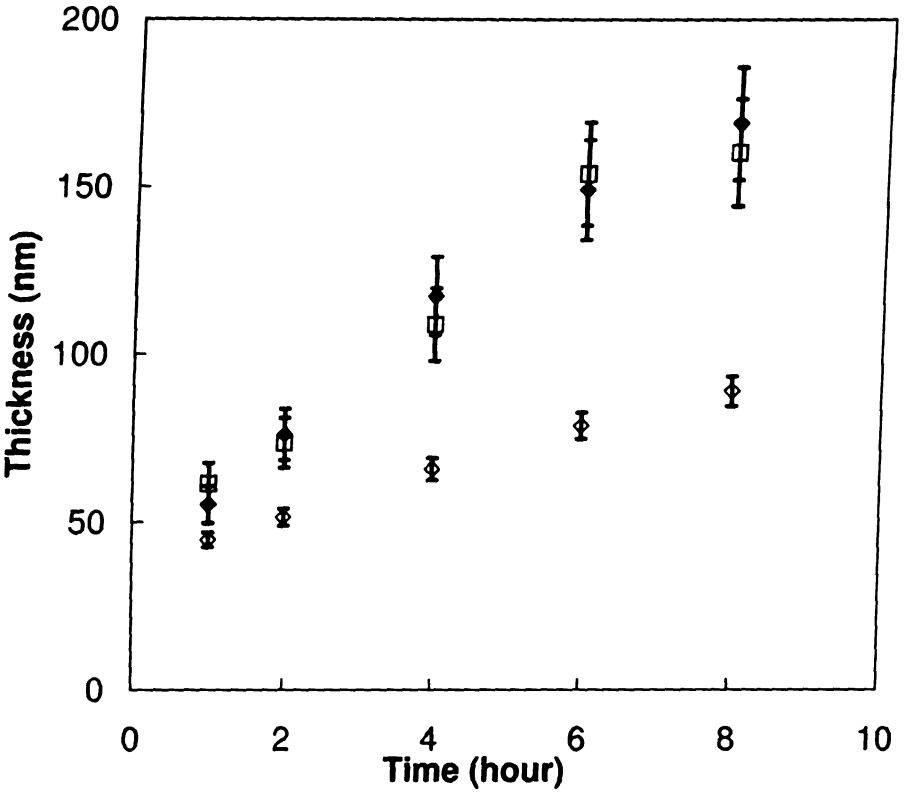

Figure 3.4b: Surface initiated polymerization of styrene from gold and SiO_2 surfaces. ◇ Polystyrene grown from a non-crosslinked thio-initiator on gold ◆ Polystyrene grown from a crosslinked thio initiator □ Polystyrene grown from SiO_2.The points are the average of data from three independent runs, and the limits of the error bars are the measured film thicknesses from the three runs.

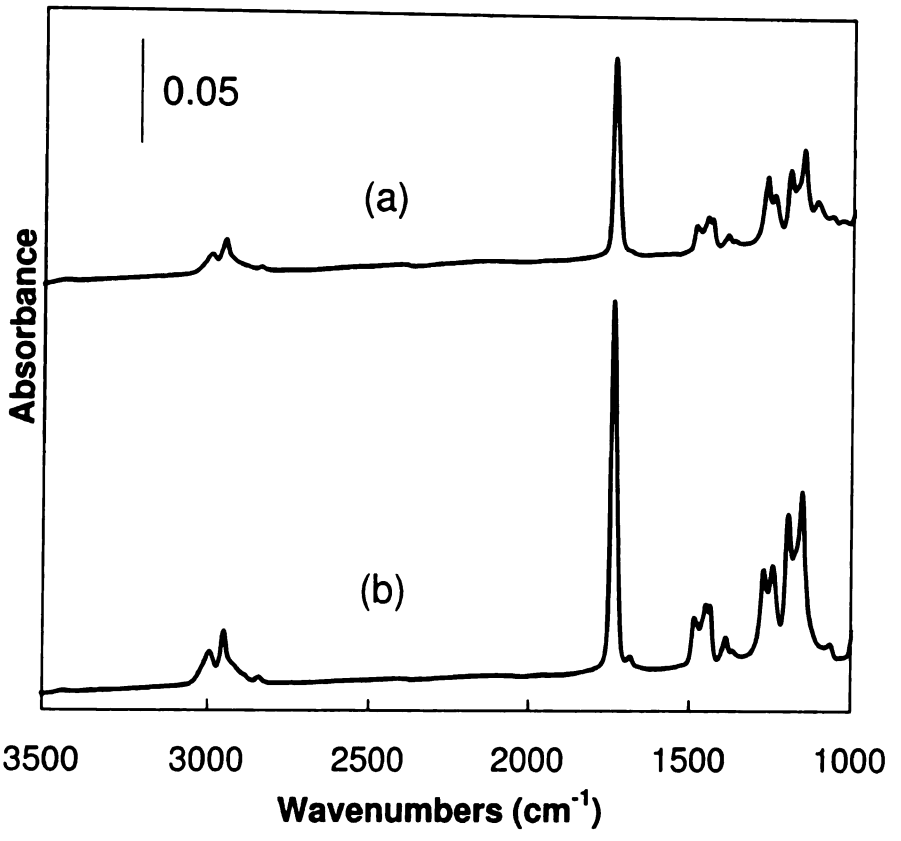

Figure 3.5a: Reflectance FTIR spectra of gold substrates with (a) PMMA brushes grown from a non-crosslinked thio initiator in 1 hour (b) PMMA brushes grown from a crosslinked thio-initiator in 1 hour

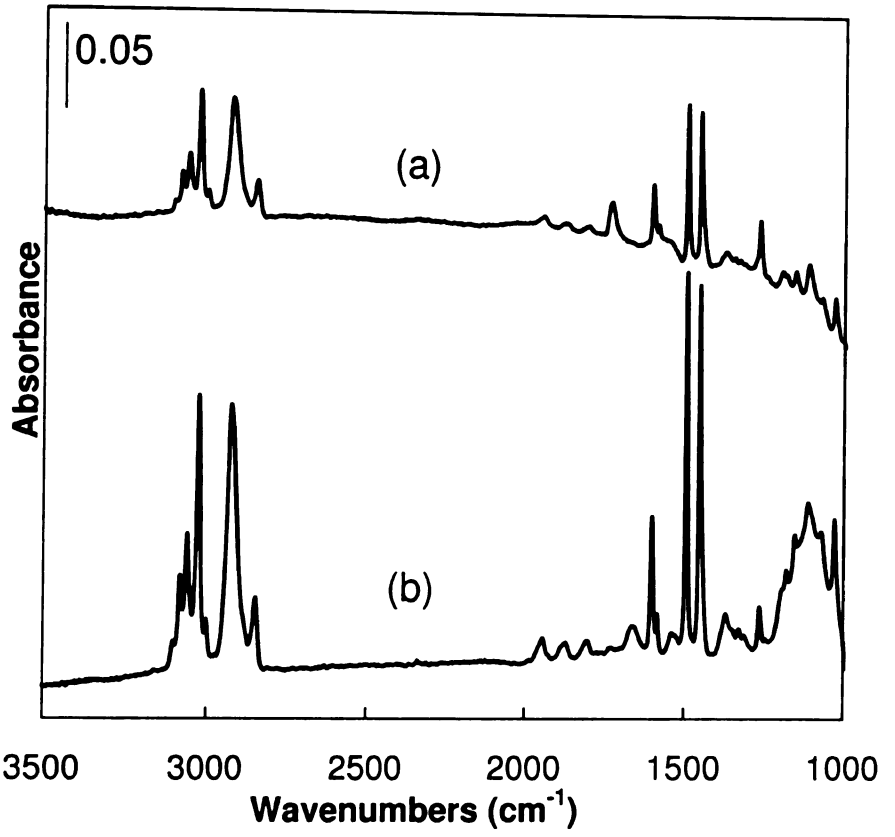

Figure 3.5b: Reflectance FTIR spectra of gold substrates with (c) PS grown from a crosslinked thioinitiator in 8 hours (d) PS grown from a crosslinked thioinitiator in 8 hours

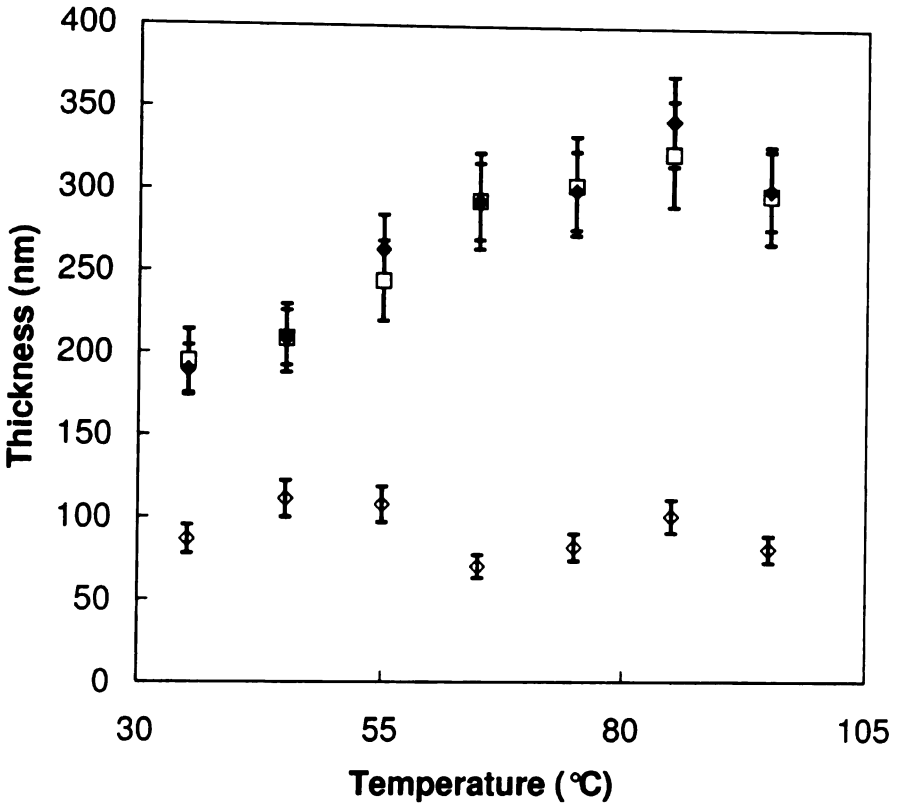

Figure 3.6a: Temperature-dependent surface-initiated polymerization of MMA from various initiators; ◇ PMMA grown from standard thioinitiators anchored to Au surfaces; ◆ PMMA grown from the crosslinked thioinitiator shown in Scheme 3.3; and □ PMMA grown from SiO_2 as shown in Scheme 3.3. Each data point indicates the film thickness after 1 hour of growth. The points are the average of data from two independent runs, and the limits of the error bars are the measured film thicknesses from the two runs. All polymerizations were run for 1 hour.

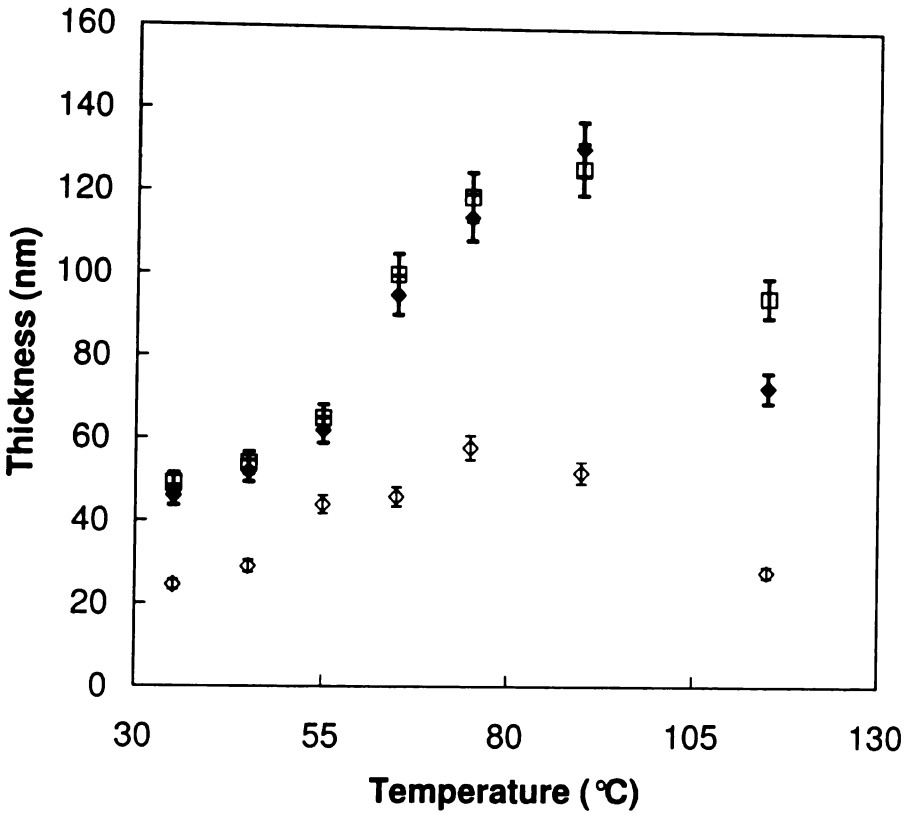

Figure 3.6b: Temperature-dependent surface-initiated polymerization of styrene from various initiators; ◇ polystyrene grown from standard thioinitiators anchored to Au surfaces; ◆ polystyrene grown from the crosslinked thioinitiator shown in Scheme 3.3; and □ polystyrene grown from SiO_2 as shown in Scheme 3.3. Each data point indicates the film thickness after 1 hour of growth. The points are the average of data from two independent runs, and the limits of the error bars are the measured film thicknesses from the two runs. All polymerizations were run for 1 hour.

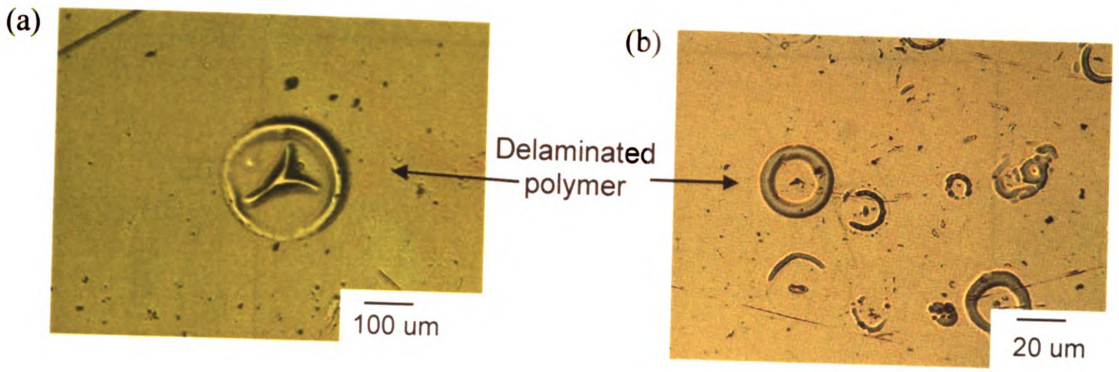

Figure 3.7: Optical micrographs of polystyrene brushes grown from crosslinked initiators immobilized on gold surfaces: (a) and (b) show a 70 nm thick film grown for 1 hour at 115 °C.

The use of cross-linked initiators to improve polymer film growth from Au surfaces can be generalized to other monomers such as poly(vinyl pyridine) (PVP). Despite its potential utility as polyelectrolyte brush, we are unaware of examples of thick PVP brushes grown from Au surfaces (20 nm in 2 hours by Bao *et al.*[12b] and 6 nm in 5 hours by Husson *et al.*[22]). However, Rühe [23] grew 430 nm thick PVP films from surface-anchored azo initiators on SiO_2 in 14 hours. Growing PVP from cross-linked initiators should provide films on Au with thicknesses that approach those of Rühe. Polymerization of vinyl pyridine for 8 hours at 50 °C provided 200 nm films from both Au and SiO_2 surfaces (Figure 3.8), approximately 10× thicker than previous examples. The increase in IR intensities, shown in Figure 3.9, is consistent with the ellipsometric data.

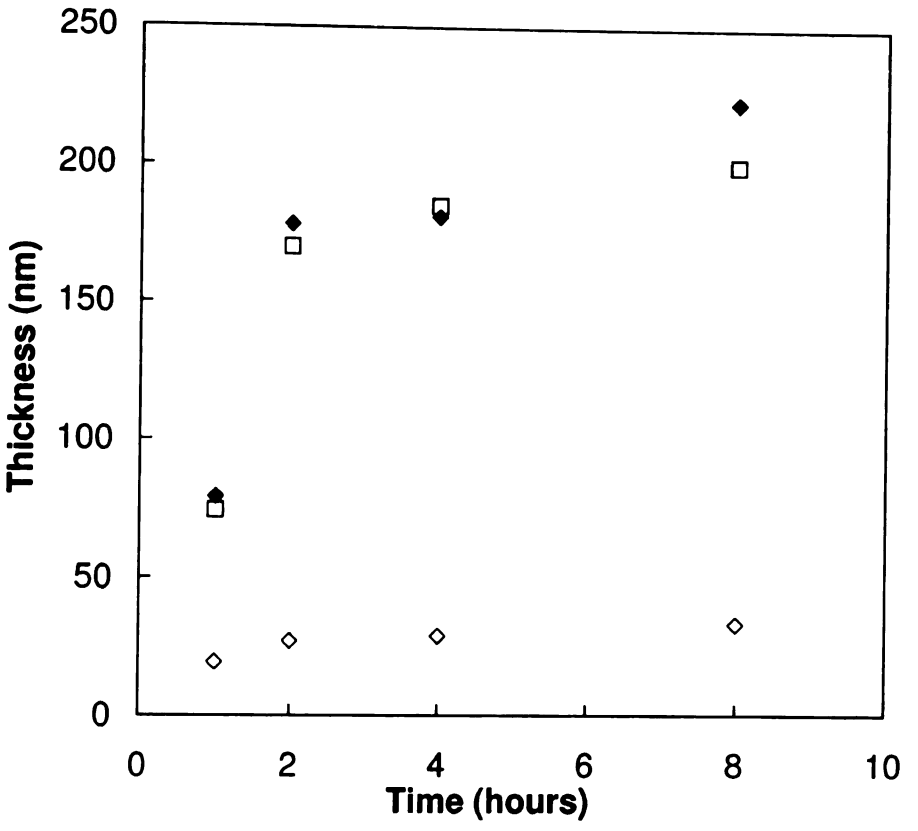

Figure 3.8: Surface-initiated polymerization of vinyl pyridine from various initiators at 50 °C; ◇ poly(vinyl pyridine) grown from a non-crosslinked thio-initiator on gold ◆ poly(vinyl pyridine) grown from a crosslinked thio initiator on gold □ poly(vinyl pyridine) grown from a SiO_2 surface

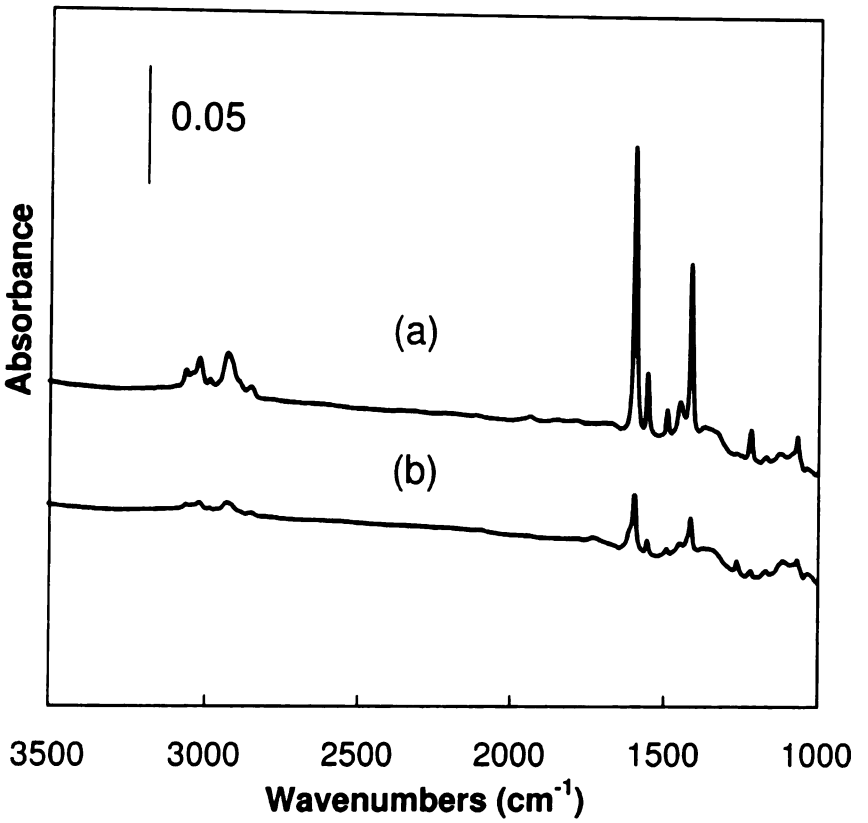

Figure 3.9: Reflectance FTIR spectra of poly(vinyl pyridine) brushes grown for 8 hours from gold surfaces (a) using a crosslinked thioinitiator and (b) a standard thioinitiator.

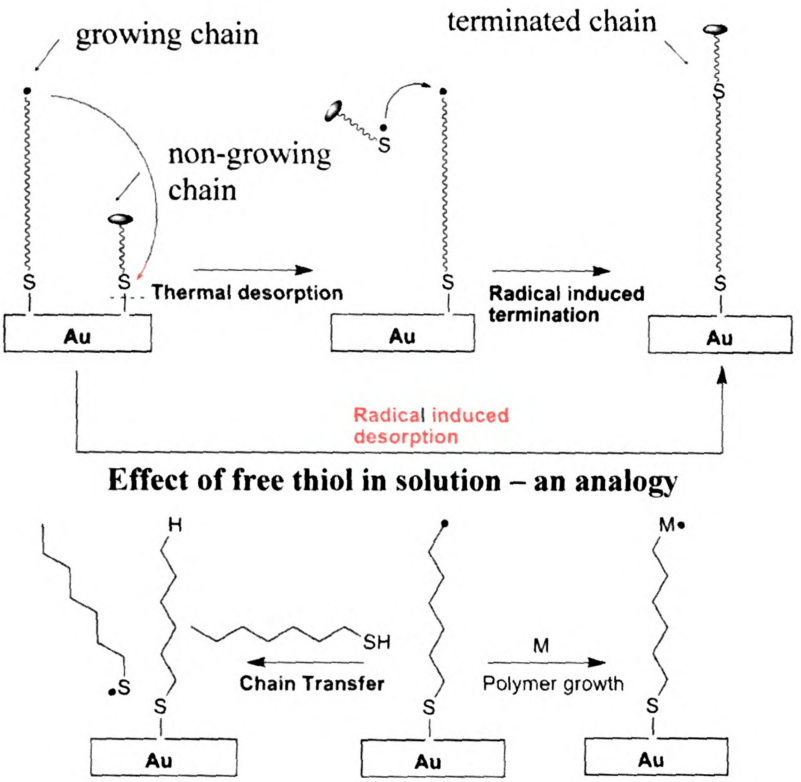

Figure 3.10. Proposed pathways for terminating surface-bound radicals on Au: (top) thermal or radical-induced desorption of surface thiol radicals terminate growing chains, (bottom left) radical termination by reaction with a thiol (analogous to chain-transfer), which competes with propagation (bottom right).

Our experiments using cross-linked initiators indicate thiol desorption as the main limitation to growing thick polymer brushes on Au. However, the desorption mechanisms are unknown. Figure 3.10 depicts some pathways that lead to termination of surface-bound radicals on Au surfaces. The thermal instability of thiol SAMs on Au may not be important for low temperature polymerizations (< 60 °C), but likely more important at high temperatures. Radical-induced desorption of thiol SAMs from growing chains can

be important over a broad temperature range. The copper catalyst also may contribute to thiol desorption. We have observed chain desorption (reduction of the carbonyl peak height in the FTIR spectra of PMMA brushes) at high copper concentrations. Though the copper concentration used here is small, the effect may not be negligible since partial desorption of initiator-containing monolayers from the Au surface would result in a decreased surface initiator concentration.

3.4. Conclusions

Polymerizations initiated from Au surfaces generally provide thinner polymer brushes than comparable polymerizations initiated from SiO_2 surfaces from room temperature to 100 °C. This disparity can be eliminated by forming a crosslinked poly(siloxane) primer layer on gold surfaces, which prevents thiol desorption. Using the crosslinked initiator, polymerizations from Au provide film thicknesses comparable to polymerizations initiated from SiO_2. These results implicate thiols in terminating growing polymer brushes, and polymer chains with low molecular weights and low film thickness. These results also exclude radical quenching by gold or the difference in initiator density between gold and silicon as significant factors. Crosslinked initiators extend the temperature range for polymerizations initiated from Au surfaces to 100 °C, enabling rapid polymerization of monomer less active than methacrylates, such as styrene and vinyl pyridine. Above 100 °C, we observed macroscopic delamination of polymer films grown on Au surfaces.

References:

1 Milner, S. T. *Science* **1991**, *251*, 905.

2 Huang, X.; Doneski, L. J.; Wirth, M. J. *Anal. Chem.* **1998**, *70*, 4023.

3 Bruening, M. L.; Zhou, Y.; Aguilar, G.; Agee, R.; Bergbreiter, D. E.; Crooks, R. M. *Langmuir* **1997**, *13*, 770.

4 Sidorenko, A.; Minko, S.; Schenk-Meuser, K.; Duschner, H.; Stamm, M. *Langmuir* **1999**, *15*, 8349.

5 Prucker, O.; Naumann, C. A.; Rühe, J.; Knoll, W.; Frank, C. W. *J. Am. Chem. Soc.* **1999**, *121*, 8766.

6 Edmondson, S.; Osborne, V. L.; Huck, W. T. S. *Chem. Soc. Rev.* **2004**, *33*, 14.

7 Ulman, A. *Chem. Rev.* **1996**, *96*, 1533.

8 Schlenoff, J. B.; Li, M.; Ly, H. *J. Am. Chem. Soc.* **1995**, *117*, 12528.

9 (a) Huang, W.; G, Skanth; Baker, G. L.; Bruening, M. *Langmuir* **2001**, *17*, 1731. (b) Fan, X.; Xia, C.; Fulghum, T.; Park, M.-K.; Locklin, J.; Advincula, R. C. *Langmuir* **2003**, *19*, 916. (c) Dong, H.; Zhu, M.; Yoon, J. A.; Gao, H.; Jin, R.; Matyjaszewski, K. *J. Am. Chem. Soc.* **2008**, *130*, 12852. (d) Shan, J.; Nuopponen, M.; Jiang, Hua; K., Esko; T., Heikki *Macromolecules* **2003**, *36*, 4526.

10 Bao, Z. "Surface-Initiated Polymerizations on Initiator Anchored Substrates: Synthesis and Characterization of Nanometer Thick Functional Polymer Films." Ph.D., Michigan State University, East Lansing, MI, **2006**.

11(a) Fan, X.; Xia, C.; Fulghum, T.; Park, M.-K.; Locklin, J.; Advincula, R. C. *Langmuir* **2003**, *19*, 916. (b) Kawai, T.; Saito, K.; Lee, W. *J. Chromatogr. B* **2003**, *790*, 131.

12 (a) Bao, Z.; Bruening, M. L.; Baker, G. L. *Macromolecules* **2006**, *39*, 5251. (b) Bao, Z.; Bruening, M. L; Baker, G. L. *J. Am. Chem. Soc.* **2006**, *128*, 9056.

13 Henglein, A.; Lilie, J. *J. Am. Chem. Soc.* **1981**, *103*, 1059.

14 Sakata, Y.; Imahori, H. *J. Phys. Chem. B* **2000**, *104*, 1253.

15 Ganesh, V.; Lakshminarayanan, V. *J. Phys. Chem. B* **2005**, *109*, 16372.

16 (a)Yoon, K. R.; Chi, Y. S.; Lee, K.; Lee, Jungkyu K.; Kim, D. J.; Koh, Y.; Joo, S.; Yun, W. S.; Choi, I. S. *J. Mater. Chem.* **2003**, *13*, 2910. (b) Mulvihill, M. J.; Rupert, B.

L.; He, R.; Hochbaum, A.; Arnold, J.; Yang, P. *J. Am. Chem. Soc.* **2005,** *127,* 16040.

17 Holzinger, D.; Liz-Marzan, L. M.; Kickelbick, G. *J. Nanosc. Nanotech.* **2006,** *6,* 445.

18 Yan, Y.; Bein, T. *J. Phys. Chem.* **1992,** *96,* 9387.

19 Mihailova, B.; Engstrom, V.; Hedlund, J.; Holmgren, A.; Sterte, J. *J. Mater. Chem.* **1999,** *9,* 1507.

20 Mintova, S.; Schoeman, B.; Valtchev, V.; Sterte, J.; Mo, S. Y.; Bein, T. *Adv. Mater.* **1997,** *9,* 585.

21 Kim, J. B.; Huang, W. X.; Wang, C. L.; Bruening, M. L.; Baker, G. L. "*Bottle Brush Brushes: Ring-Opening Polymerization of Lactide from Poly(hydroxyethyl methacrylate) Surfaces*" in *Polymer Brushes*, Advincula, R. C.; Brittain, W. J.; Caster, K.C.; Rühe, J., Eds., Wiley-VCH, Weinheim, Germany, pp. 105-117 (**2004**).

22 Li, X.; Wei, X. L.; Husson, S. M. *Biomacromolecules* **2004,** *5,* 869.

23 Biesalski, M.; Rühe, J. *Langmuir* **2000,** *16,* 1943.

Chapter 4

Surface Tethered Conducting Polymers via a Grafting-from Approach

4.1. Introduction

Over the past several decades, π-conjugated organic polymer materials have been extensively investigated as the active element in sensors,[1a] optoelectronic[1b] and semiconducting devices,[2] and as electroluminescent, photoconducting, electron-transporting, hole-transporting, and ion-dopable materials.[3] One of the most widely used materials is poly(thiophene), which has attractive properties such as high electrical conductivity, electrochromism and electroluminescence.[4] Poly(thiophene) and related polymers are synthesized by two general methods, electro-polymerization directly from electrode surfaces, or step-growth methods such as chemical coupling of di-bromo monomers, or chemical oxidation by $FeCl_3$ and other oxidants.

Electropolymerization conveniently deposits electroactive polymers directly onto sensor substrates, and permits control over the coating thickness, since the polymerization proceeds by application of a precisely controlled potential. In spite of these advantages, poor interfacial adhesion between the conducting polymer and the electrode is a major problem.[5,6,7,8,9,10] One strategy for improving adhesion is to form conducting polymers from polymerizable precursors preadsorbed on a metallic substrate (gold, nickel, or platinum) via thiol functional groups.[5-7] An alternative approach is to graft conducting polymers onto metal oxide surfaces, such as indium tin oxide (ITO),[9]

where the key step is the chemisorption of a preformed conducting polymer or its precursor.

Recently, conjugated polymer network films were formed on conducting surfaces by the synthesis of precursor polymers from monomers with pendant electroactive units and then elaborating the pendant unit by electropolymerization or chemical oxidation.[11,12,13,14,15,16,17] The resulting polymer films are intrinsic conducting polymer networks with having both inter- and intramolecular cross-links between the pendant monomer units.

Surface-initiated ATRP is attractive for modifying surfaces since surface properties are easily modified by varying the composition of the polymer brush, grafting density, the degree of polymerization[18] and most importantly, delamination of polymer layer from surface can be eliminated. Recently, Carter *et al.* reported the successful grafting of disubstituted polyacetylene brushes grown from modified silicon and quartz surfaces using a transition-metal-catalyzed polymerization technique.[19] Huck and Friend used surface-initiated ATRP to produce tethered poly(triarylamine acrylate) hole transport materials for use in photovoltaic devices.[20] Compared to devices prepared by solution-casting methods, devices prepared from tethered polymers showed enhanced conductivity, which was attributed to control over polymer architecture and morphology. Advincula *et al.* grew poly(vinyl carbazole) brushes from ITO by surface initiated free radical polymerization, controlling the graft density and brush length. In a second step, they cross-linked the poly(vinyl carbazole) brush electrochemically.[21]

Herein, we report the growth of poly(terthiophene methacrylate) from gold and ITO substrates using ATRP. Electropolymerization of the pendant terthiophene groups forms conducting cross-linked polymer network films of oligo- and polythiophene.

4.2. Experimental section

4.2.1. Materials

Unless otherwise noted, all chemicals were obtained from Aldrich. 11-Mercapto-1-undecanol (MUD, 97%), 2-bromopropionyl bromide (2-BPB) (97%), 3-thiophenemethanol, thiophene-3-carboxaldehyde, tetrakis(triphenylphosphine) palladium, thiophene-2-boronic acid, methacryloyl chloride (98%), 3,4-ethylenedioxythiophene (EDOT, 97%), *N*,*N*-dimethylformamide (DMF, 99.8%), dimethoxyethane (98%), $NaBH_4$, Cu(I)Cl (99.999%), Cu(I)Br (99.999%) and hexmethyltriethylenetetraamine (HMTETA, 99%) were used as received. Triethylamine and acetonitrile were distilled from calcium hydride under reduced pressure and under an inert atmosphere. Tetraethylammonium perchlorate (TEAP) was dried under vacuum at 80 $^{\circ}C$ for 12 hours and stored in glove bag. ITO (indium tin oxide) coated glass slides were obtained from Delta technologies.

4.2.2. Characterization Methods

^{1}H and ^{13}C NMR analyses were carried out at room temperature on a Varian UnityPlus-500 spectrometer at 500 and 300 MHz, respectively, with the chemical shifts reported in ppm and referenced to signals from residual protons in the solvent. Film thicknesses were measured using a rotating analyzer ellipsometer (model M-44, J. A. Woollam) at an incident angle of 75°. The data were analyzed using WVASE32 software, and thickness and refractive index determinations were performed on at least three spots

on each substrate. The refractive index of the films was assumed to be 1.5 and then fitted with the film thickness. Reflectance FTIR spectroscopy was performed using a Nicolet Magna-IR 560 spectrometer containing a PIKE grazing angle (80°) attachment. UV-vis measurements were taken on an Agilent technologies 8453 spectrometer. Atomic force microscopy (AFM) images were obtained in tapping mode with Multimode AFM and NanoScope IV software (Digital Instruments, Santa Barbara, CA) at room temperature. A tapping mode probe (NSC15) with a nominal frequency of 300 kHz was used for all experiments.

4.2.3. Synthesis of 3-methylthienyl methacrylate (MTM)

3-Thiophenemethanol (5.7 g, 50 mmol), dry triethylamine (7.3 g, 71 mmol), and CuCl 25 mg were dissolved in 35 mL of dry diethyl ether. A solution of methacryloyl chloride (5.35 g, 51 mmol) in 35 mL of dry diethyl ether was added slowly at 0 °C. The mixture was stirred for 2 h, and then filtered through a silica gel column to remove triethylammonium chloride. After solvent evaporation, the residue was stirred overnight in a 1:1 mixture of methylene chloride and 2 M NaOH. The organic layer was separated, washed twice with water, and dried over $CaCl_2$. After solvent evaporation, the residue was distilled under vacuum (Vigreux column). bp (1 mmHg): 90 °C. Yield: 70%. ^1H NMR ($CDCl_3$): δ 1.9 (s, *CH_3*), 5.1 (s, *OCH_2*), 5.5 (s, *vinyl H*), 6.1 (s, *vinyl H*), 7.06 (m, *ring H*), 7.2 (m, *ring H*).

4.2.4. Synthesis of [2, 2':5', 2''-terthiophen]-3'-ylmethyl methacrylate (TTMM)

4.2.4a. Synthesis of 2,5-dibromoformyl-3-thiophene (*1*): A solution of Br_2 (0.562 mL, 20 mmol) in anhydrous $CHCl_3$ was added drop wise and under vigorous stirring, to a solution of thiophene-3-carboxaldehyde (0.500 mL, 5.5 mmol) in anhydrous $CHCl_3$ (1.5 mL) in a 10 mL flask, at 60 °C under inert atmosphere. The reaction mixture was refluxed for 5 h, and brought to room temperature and then poured into ~10 mL of water at 0 °C. The organic phase was neutralized with a Na_2CO_3 saturated solution, dried with $MgSO_4$, filtered, and evaporated to dryness. The residue was chromatographed on flash silica gel 60 using 90/10 hexanes/ethyl acetate as eluant to give a yellowish orange solid. Crystallization from heptanes affords pale yellowish needlelike crystal in 40% yield. ^{1}H NMR ($CDCl_3$): δ = 9.80 (s, 1H, *CHO*), 7.34 (s, 1H, *H4*).

4.2.4b. Synthesis of 3'-formyl-2,2':5',2''-terthiophene (2): A 50 mL 3-neck flask, equipped with condenser, magnetic stirrer and N_2 inlet, was charged with **1**, (0.2086 g, 0.77 mmol), tetrakis(triphenylphosphine) palladium(0) (0.0531g, 0.046 mmol) and 8 mL of 1,2-dimethoxyethane. After stirring for 10 min at room temperature, thiophene-2-boronic acid (0.2362 g, 1.84 mmol) was added, and followed immediately by 5 mL of aqueous 1M $NaHCO_3$ solution. The reaction mixture was refluxed for 4 h under nitrogen. After cooling to room temperature, the mixture was filtered and the organic solvent was evaporated under reduced pressure. After removal of the solvent, 10 mL of water were added to the residue, and the mixture was extracted with diethyl ether (3×50 mL). The combined organic phases were washed with water and with saturated

NaCl solution, and dried over $MgSO_4$. After filtration and solvent evaporation, the crude product was chromatographed on flash silica gel 60, using 90/10 hexanes/ethyl acetate as the eluant. Removal of the solvent yielded greenish-yellow powdery solid. Yield 75%, ^{1}H NMR ($CDCl_3$): δ 10.09 (s, 1H, *CHO*), 7.57 (s, 1H, *H4'*), 7.51 (dd, 1H, *J* = 5.1 Hz, *J* = 1.2 Hz, *H5*), 7.32 (dd,1H, *J* = 3.6 Hz, *J* = 1.2 Hz, *H3*), 7.30 (dd, 1H, *J* = 5.1 Hz, *J* = 1.2 Hz, *H5''*), 7.23 (dd, 1H, *J* = 3.6 Hz, *J* = 1.2 Hz, *H3''*),7.17 (dd,1H, *J* = 5.1 Hz, *J* = 3.6 Hz, *H4*), 7.05 (dd, 1H, *J* = 5.1 Hz, *J* = 3.6 Hz, *H4''*).

4.2.4c. Synthesis of 3'-hydroxymethyl-2,2'5',2''-terthiophene (3): Compound **3** was synthesized by the procedure of Zanardi *et al.*[23] in 95% yield. ^{1}H NMR($CDCl_3$): δ 7.33 (dd, 1H, *J* = 5.1 Hz, *J* = 1.0 Hz, *H5*), 7.23 (s, 1H, *H4'*), 7.22 (dd, 1H, *J* = 5.1 Hz, *J* = 1.0 Hz, *H5''*), 7.20 (dd, 1H, *J* = 3.6 Hz, *J* = 1.0 Hz, *H3*), 7.17 (dd, 1H, *J* = 3.6 Hz, *J* = 1.0 Hz, *H3''*), 7.07 (dd, 1H, *J* = 3.6 Hz, *J* = 5.1 Hz, *H4*), 7.02 (dd, 1H, *J* = 3.6 Hz, *J* = 5.1 Hz, *H4''*), 4.74 (s, 2H,CH_2), 1.78 (s (br), 1H, *OH*).

4.2.4d. Synthesis of [2,2':5',2''-terthiophen]-3'-ylmethyl methacrylate (TTMM): Compound **3** (4.5 g), 3.15 mL of dry triethylamine, and CuCl (25 mg) were dissolved in 50 mL of dry diethyl ether. A solution of freshly distilled methacryloyl chloride (1.68 mL) in 50 mL of dry diethyl ether was added slowly at 0 °C., and the mixture was stirred for 2 h. The solution was filtered a silica gel column to remove triethylammonium chloride, and the solvent was evaporated to dryness. The residue was stirred overnight in a 1:1 mixture of methylene chloride and 2 M NaOH. The organic

layer was separated, washed twice with water, and dried over $CaCl_2$. After solvent evaporation, the residue was re-crystallized from diethyl ether to provide TTMM as green crystals. Yield: 50%. ^{1}H NMR ($CDCl_3$): δ 7.37 (dd, 1H, J = 5.5 Hz, J = 1.0 Hz, *H5*), 7.25 (dd, 1H, J = 5.5 Hz , J = 0.5 Hz, H4′), 7.22 (m, 2H, H5′′), 7.20 (dd, 1H, J = 3.5 Hz, J = 1.0 Hz, H3), 7.11 (dd, 1H, J = 4.0 Hz, J = 5.0 Hz, H3′′), 7.04 (dd, 1H, J = 4.0 Hz, J = 5.5 Hz, H4), 6.18 (s, vinyl H), 5.62 (s, vinyl H), 5.24 (s, OCH_2), 2.0 (s, CH_3). ^{13}C {^{1}H} NMR ($CDCl_3$): 167.41, 136.84, 136.38, 136.15, 134.65, 134.52, 133.32, 128.14, 128.12, 127.0, 126.79, 126.76, 126.29, 125.09, 124.29, 60.49, and 18.61. High resolution MS: m/z calc. for $C_{17}H_{14}O_2S_3^+$: 346.0156; Found: 346.0150.

4.2.5. Synthesis of the silane initiator: The trichlorosilane initiator was synthesized following previously published procedures.[18b] 2-Bromoisobutyryl bromide (1.85 mL, 15.0 mmol), was added dropwise to a stirring solution of allyl alcohol (1.02 mL, 15.0 mmol) and triethylamine (2.51 mL 18.0 mmol) in dichloromethane (10 mL) at 0 °C, under nitrogen atmosphere. After 1 hour of stirring the temperature was raised to room temperature and the reaction mixture was stirred for a further 3 hours. The precipitate was then removed under reduced pressure and the organic layer was washed with an aqueous saturated NH_4Cl solution, followed by a wash with water. The organic layer was then dried over anhydrous $MgSO_4$ and the solvent removed in vacuo. The product was purified by column chromatography (silica) using 9:1 hexane: ethyl acetate as the eluent. The solvent was then removed under reduced pressure to yield the clear,

liquid product prop-2-enyl-2-bromo-2-methyl propionate (1.72 g, 8.31 mmol, 55.4% yield). ^{1}H NMR ($CDCl_3$, 500 MHz): δ = 1.94 (6H, s), 4.66 (2H, d), 5.27 (1H, d), 5.38 (1H, d), 5.93 (1H, m).

A solution of hexachloroplatinic acid (21 mg, 51 μmol) in 1:1 (v/v) ethanol: 1,2-dimethoxyethane (3.75 mL) was added dropwise to a solution of prop-2-enyl-2-bromo-2-methyl propionate (0.97 g, 4.7 mmol) in trichlorosilane (15 mL, 0.15 mol) under nitrogen atmosphere. The reaction was stirred (in the dark) for 18 hours. Toluene (5.0 mL) was then added and unreacted trichlorosilane was removed under reduced pressure. Dichloromethane (20 mL) was added and then removed in vacuo to remove all remaining trichlorosilane. The resulting product, 2-bromo-2-methyl-propionic acid 3-trichlorosilanyl-propyl ester was used without further purification. ^{1}H NMR ($CDCl_3$, 300 MHz): δ = 1.50 (2H, m), 1.93 (8H, m), 4.20 (2H, m).

4.2.6. Preparation of initiator immobilized flat substrates: ITO slides (~1 cm^2) were first sonicated in acetone (10 min), followed by sonication in IPA (10 min). All substrates were cleaned using UV/O_3 chamber for 1 hour. ITO substrates were then placed in a ~1 mM solution of the trichlorosilane initiator, containing ~10 mM triethylamine in toluene. Substrates were left, covered, in the solution, at room temperature, for 18 hours under N_2 atmosphere. The substrates were then removed and, successively: washed with toluene, sonicated for 1 minute in toluene, washed with acetone, washed with ethanol, and dried under a stream of nitrogen. The surfaces were stored under nitrogen until further use.

4.2.7. Surface initiated polymerization on gold and ITO substrates: In a N_2-filled drybox, 0.7 mg of CuBr and 5.55 mg of HMTETA were added to a round-bottom flask containing 1 mL of a degassed solution of TTMM monomer (500 mg) in DMF (DMF : monomer ~1:1 (v:v). The mixture was well-stirred and heated with an oil bath to 50 ^{o}C until a transparent, green solution formed. The prepared solution was then transferred into a small vial containing an initiator-modified Au substrate to start the surface-initiated polymerization. After a set reaction time at 50 ^{o}C, the substrate was removed from the vial, washed with THF and isopropanol sequentially, and then was dried under a flow of N_2. The similar polymerization condition has been applied for growing MTM from surfaces.

4.2.8. Electrochemistry: All electrochemical modifications were performed using a CHI650a computerized potentiostat (CH Instruments, Inc., Austin, TX).The electrochemical experiments, i.e., CV (cyclic voltammetry) were carried out in acetonitrile containing tetraethyl ammonium perchlorate (TEAP~5×10^{-2} M) as a conducting salt. For heterocoupling experiments, the solution contained 10^{-2} M of EDOT along with TEAP. All experiments were carried out in a glovebox under an inert and dry atmosphere at room temperature. In a three electrode system, the working electrode (gold or ITO-coated glass substrate) was placed between the reference electrode (Pt wire) and the counter-electrode (graphite). All potentials were measured in this work with respect to a Pt wire used as a quasi-reference electrode. For this reason, the potentials may not be directly compared.

4.3. Results and Discussion:

4.3.1. Monomer synthesis: As shown in Schemes 4.1 and 4.2, the synthesis of 3-methylthienyl methacrylate (MTM) and the precursors to 3'-methylterthienyl methacrylate (TTMM), i.e. compounds **1**, **2** and **3**, were synthesized by modified versions of the procedures of Yagci[22] and Seeber[23] *et al.* TTMM was obtained in high purity by the reaction of 3 with methacryloyl chloride in dry diethyl ether, similar to the synthesis of monomer MTM. Methacrylate monomers were chosen for their facile polymerization via ATRP, while the polymerizable thiophene and terthiophene groups have shown good conducting properties in related polymers.[24,25,26]

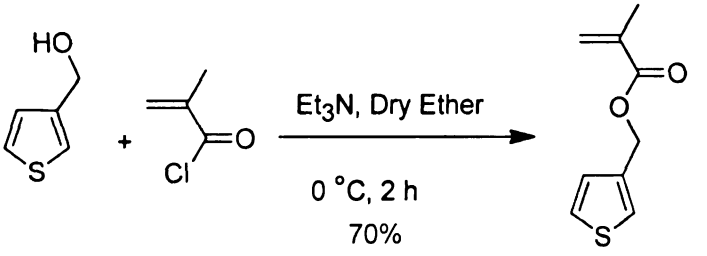

Scheme 4.1: Synthesis of 3-methylthienyl methacrylate (MTM)

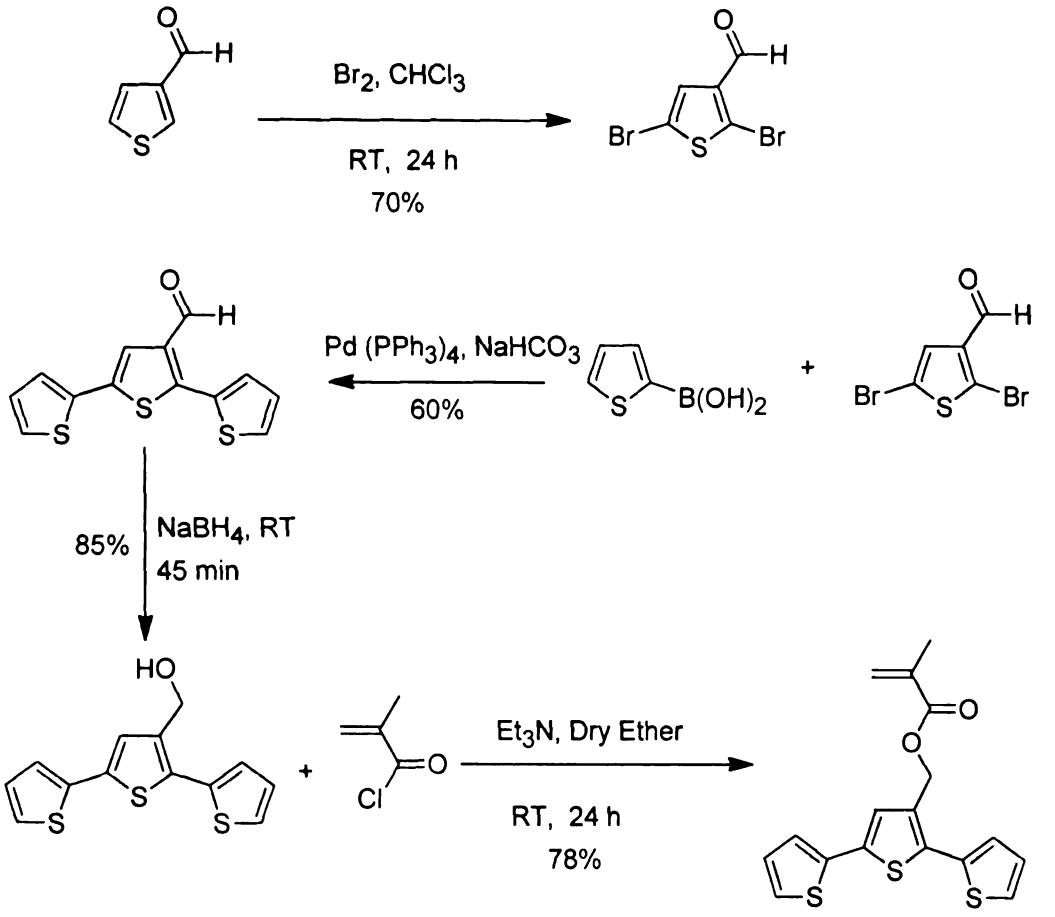

Scheme 4.2: Synthesis of [2,2':5',2"-terthiophen]-3'-ylmethyl methacrylate (TTMM)

4.3.2. Synthesis of silane initiators for ITO substrates

Typically, we use a 11-carbon long alkyl chain in trichlorosilane initiators to ensure a well-defined SAM on ITO. However, we used a short alkyl chain since the longer chain may act as a resistive element and inhibit the polymerization of the pendent thiophene methacrylares. The initiator was synthesized following the method of Huck *et al.*[20] (Scheme 4.3), esterification of 2-bromoisobutyryl bromide with allyl alcohol, followed by hydrosilation of the intermediate ester to give the trichlorosilane initiator. The trichlorosilane functionality was chosen because trifunctional organosilanes are more reactive towards surfaces than their monosubstituted analogues.[27] These SAMs are

expected to be stable due to formation of polysiloxane networks bound to the substrate surface[28,29] For gold surfaces, we used a 11-carbon long ATRP initiator as shorter chain initiators failed to form uniform self-assembled monolayers on gold surfaces.

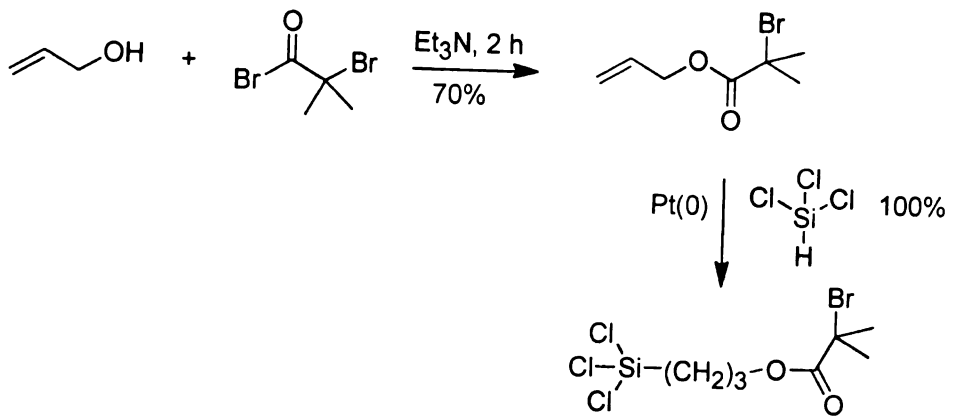

Scheme 4.3: Synthesis of the trichlorosilane initiator

4.3.3. Deposition of SAMs on ITO surface

The formation of trichlorosilane-based SAMs on silica surface is well known.[28] However, generating a well defined SAM on an ITO surface was expected to be more difficult because of the high surface roughness of ITO and the low coverage of hydroxyl groups.[30] Nevertheless, some methods have produced SAMs on ITO. Examples include microcontact printing,[31] a one-hour soak in a 1 mM solution of the chlorosilane at room temperature,[32] and refluxing a solution of trimethoxysilane in toluene over ITO for 7 days.[30] For the latter case, Markovich, *et al.* achieved about 90% coverage of surface sites. Considering the higher reactivity of a trichlorosilane compared with a trimethoxysilane, the reaction was carried out similar to the method of Huck *et al.*,[20] at room temperature for 18 hours to avoid polymerization (Scheme 4.4). In addition, triethylamine was added[18b] to drive the reaction to completion. While this SAM

deposition method may not provide complete surface coverage, estimates of initiator efficiency suggest that ~10% of surface bound initiating molecules initiate a polymer brush,[33] and therefore having less than full surface coverage should not be a significant factor in the polymer brush synthesis. Typically, a full ITO wafer was completely derivatized, stored under nitrogen, and fractured into (~1 × 2 cm^2) pieces just before use. The surfaces were stable and polymerizations carried out with 1-year old initiator monolayers gave similar film thicknesses when used in similar polymerization conditions.

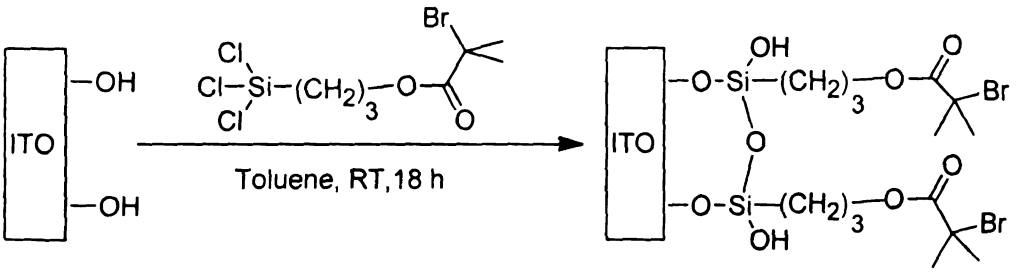

Scheme 4.4: Initiator SAM deposition on ITO surfaces

4.3.4. Synthesis of polymer brushes from gold and ITO surfaces

The syntheses of polyMTM and polyTTMM brushes from gold and ITO surfaces are shown in Scheme 4.5. Films on gold surfaces were characterized using ellipsometry, but for ITO surfaces, tapping mode AFM was used to measure PolyTTMM film thicknesses since the film absorbs light, which makes ellipsometric measurement ambiguous.

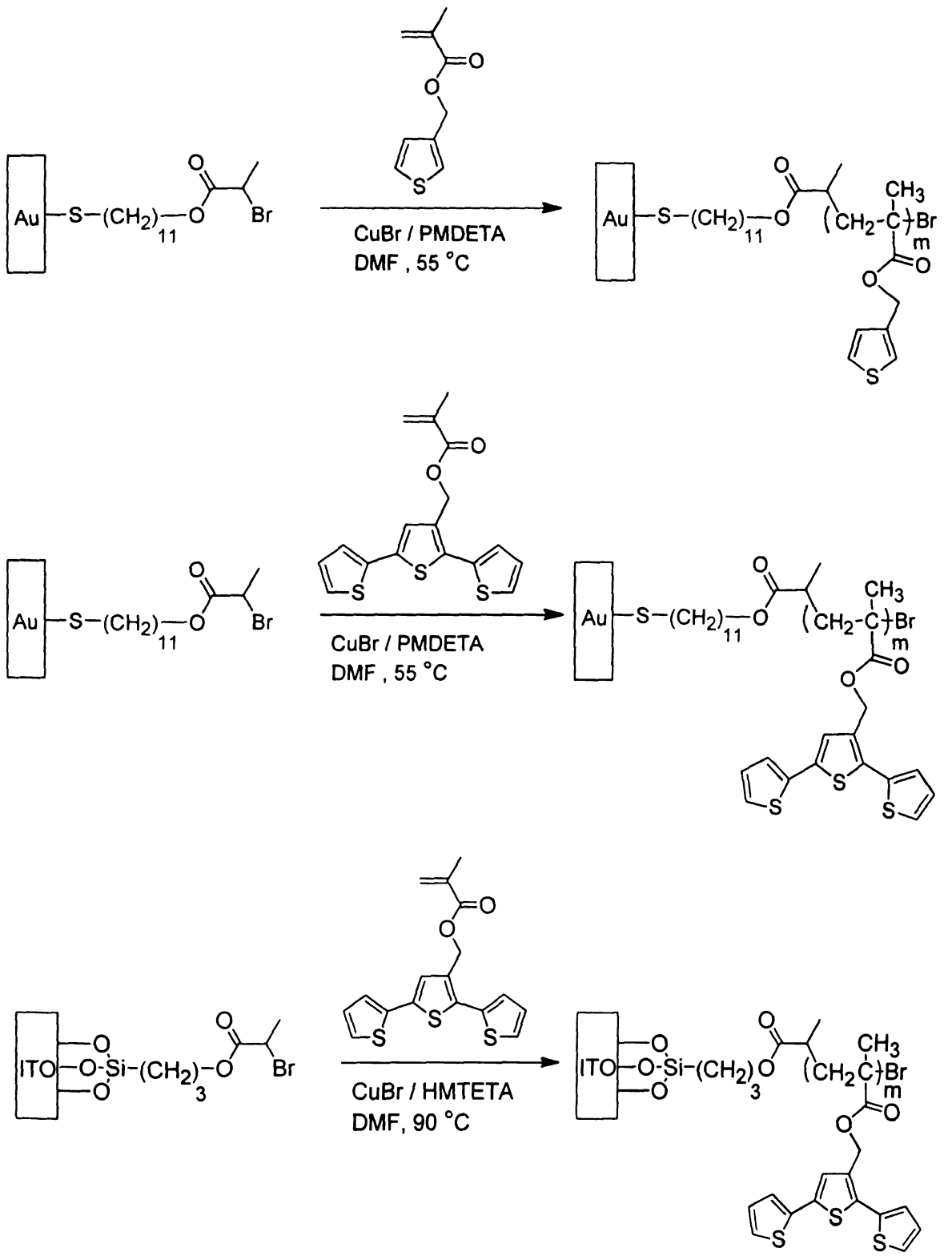

Scheme 4.5: Surface initiated polymerization of MTM from gold surface (top), TTMM from gold surface (middle) and TTMM from ITO surface (bottom).

PMTM brushes were grown from gold surfaces at 55 °C in anhydrous DMF using a CuBr/HMTETA catalyst. This system was previously shown to be compatible with the synthesis of methacrylate monomers via ATRP,[34] and also proved successful for the synthesis of polyMTM brushes. The polyMTM brush was typically synthesized from a concentrated polymerization solution (1g/mL), which allowed access to a greater range of film thicknesses. Similar solutions were used for the synthesis of polyTMM brushes.

The kinetic plots for the synthesis of both brushes (Figure 4.1) show the characteristics of significant termination during ATRP;[35] the polymer chains initially grow rapidly, and as termination consumes growing chain ends, the plots plateau. Complete termination occurs more quickly for the polyTTMM systems than than for polyMTM. High radical concentrations result in increased probability of radical combination and termination of growing polymer chains. Usually, increasing the reaction temperature provides thicker films, but when the polymerization temperature was increased from 55 °C to 90 °C, the growth rate for polyTTMM brushes grown on ITO surfaces did not increase.

No $CuBr_2$ was explicitly added to the polymerizations, but Cu(II) should be present as a consequence of of CuBr with the initiator. For polyTTMM brushes, early termination may be related to the stronger complexing ability of terthiophene units with Cu(II) than for monothiophenes, as evidenced by Rajesh *et al.*[36] Thus, Cu(II) generated during initiating of polymerization is sequestered by the pendent terthiophene of TTMM, leading to a high concentration of radicals and almost no deactivation.

The polyTTMM film thicknesses were intentionally kept low to ensure their crosslinking by electrochemical methods. In thicker films, electrochemical-based cross-linking may be hindered by low permeation rates of anions or monomer through the polyTTMM matrix. PolyMTM and polyTTMM brushes grown from gold surfaces were characterized by FTIR. The spectra for polyMTM and polyTTMM show the expected bands for the carbonyl peak at 1733 cm^{-1} and sp^2 C-H stretching at 3100 cm^{-1} expected for thiophene rings (Figure 4.2).

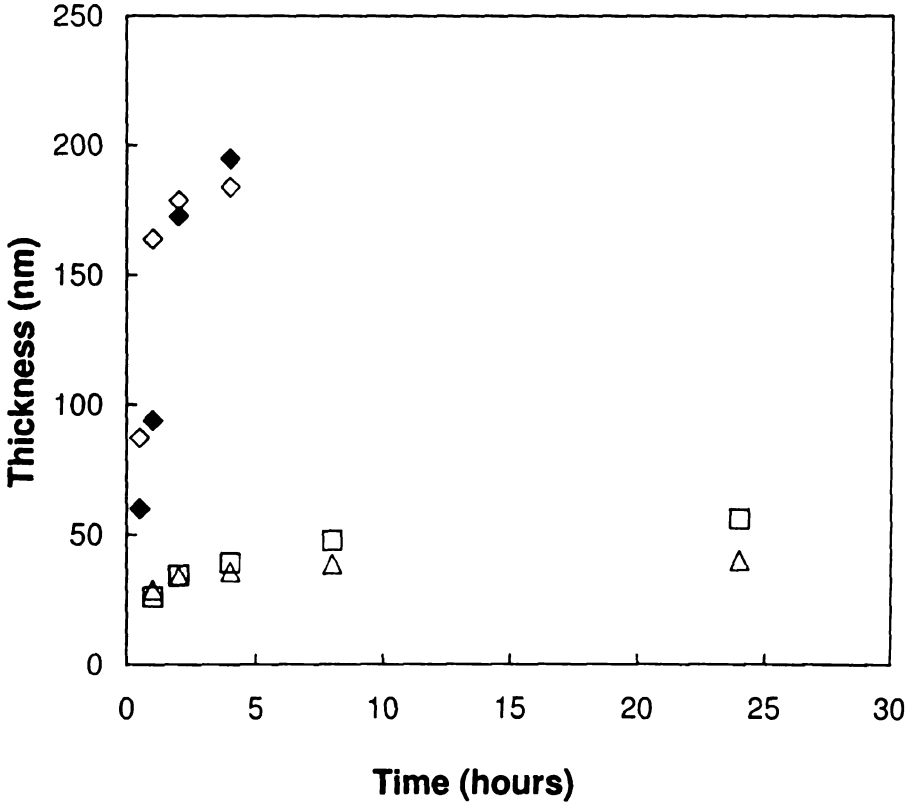

Figure 4.1: Evolution of the ellipsometric brush thickness with time for the polymerization of polyMTM and polyTTMM from gold and ITO surfaces; a polyMTM brush grown on gold surface (◆), a polyMTM brush grown on ITO surface (◇), a polyTTMM brush grown on gold surface (□), a polyTTMM brush grown on ITO surface (△).

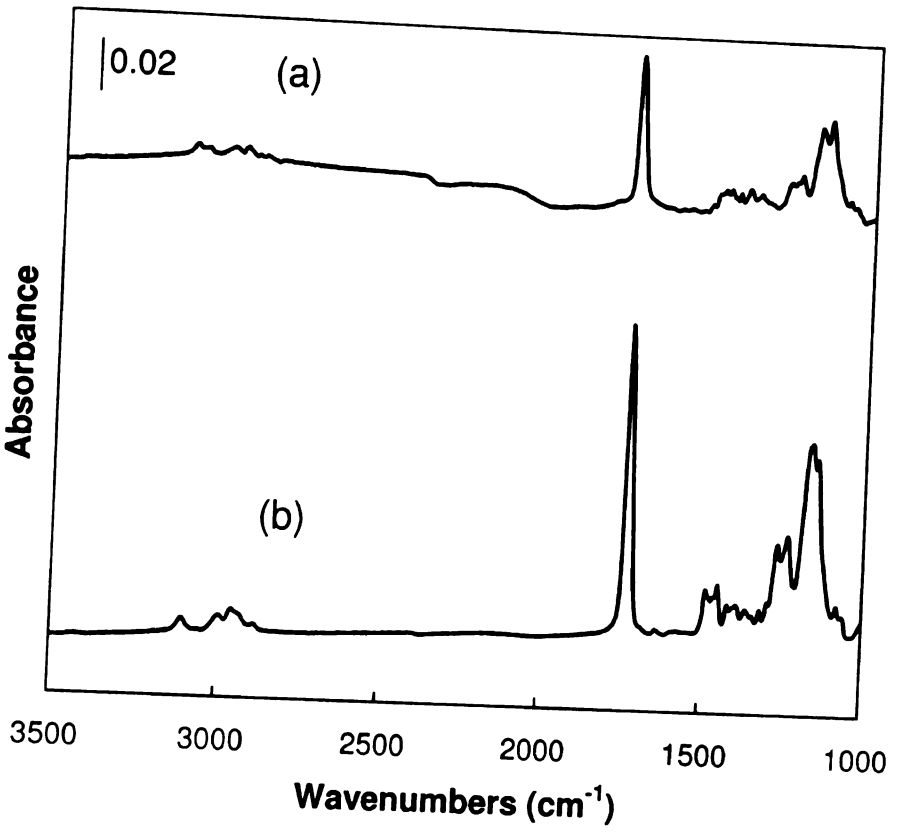

Figure 4.2: Representative examples of reflectance FTIR spectroscopy of gold surface grafted with (a) 50 nm polyTTMM brush (b) 100 nm polyMTM brush.

4.3.5. Electrochemical crosslinking

PolyTTMM films (~30 nm) on ITO and gold substrates were placed in a 0.1 M tetraethylammonium perchlorate (TEAP) solution in acetonitrile under an inert atmosphere to avoid overoxidation, and then crosslinked electrochemically (Scheme 4.6). The substrates served as the working electrode, a graphite electrode as the counter electrode and a Pt wire as the reference electrode. The substrate was scanned at 100 mV/s

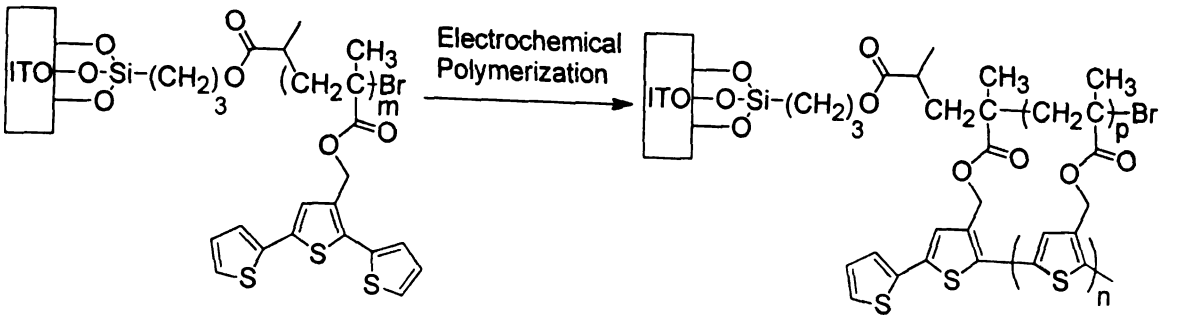

Scheme 4.6: Electrochemical cross linking of polyTTMM brush on ITO surfaces from -25 to +1500 mV for up to 20 cycles in order to cross-link the polyTTMM film (Figure 4.3). The direct electrochemical polymerization of the polyMTM brush was not achievable under our conditions, but consistent with previous reports of the low reactivity of thiophenes substituted with esters in the 3-position.[26] PolyTTMM's higher reactivity stems from the extended π-structure of the terthienyl moiety[26] which lowers the oxidation potential of polyTTMM brush relative to polyMTM. In addition, the terthienyl unit is less sterically challenged with respect to coupling in the 2- and 5"-positions, compared to the 2- and 5-positions of a single thienyl unit.

A well-defined oxidation peak starting at ~1.1 V/Pt (Figure 4.3, first scan) was observed for the polyTTMM brush by cyclic voltammetry. Because films of grafted poly (alkylacrylate), e.g., PEA (poly(ethyl acrylate)), do not react upon anodic polarization, this peak can only be attributed to the oxidation of the aromatic thiophene rings. The reduction peak of the accordingly formed polyTTMM two-component films is observed at ~ 0.63 V/Pt during the reverse scan. These observations confirm that the thienyl rings attached to the conducting substrate (ITO / gold) as a result of the surface initiated polymerization via ATRP of the parent acrylates (TTMM), remain available to electrochemical polymerization and form polymers with a more extended π electron

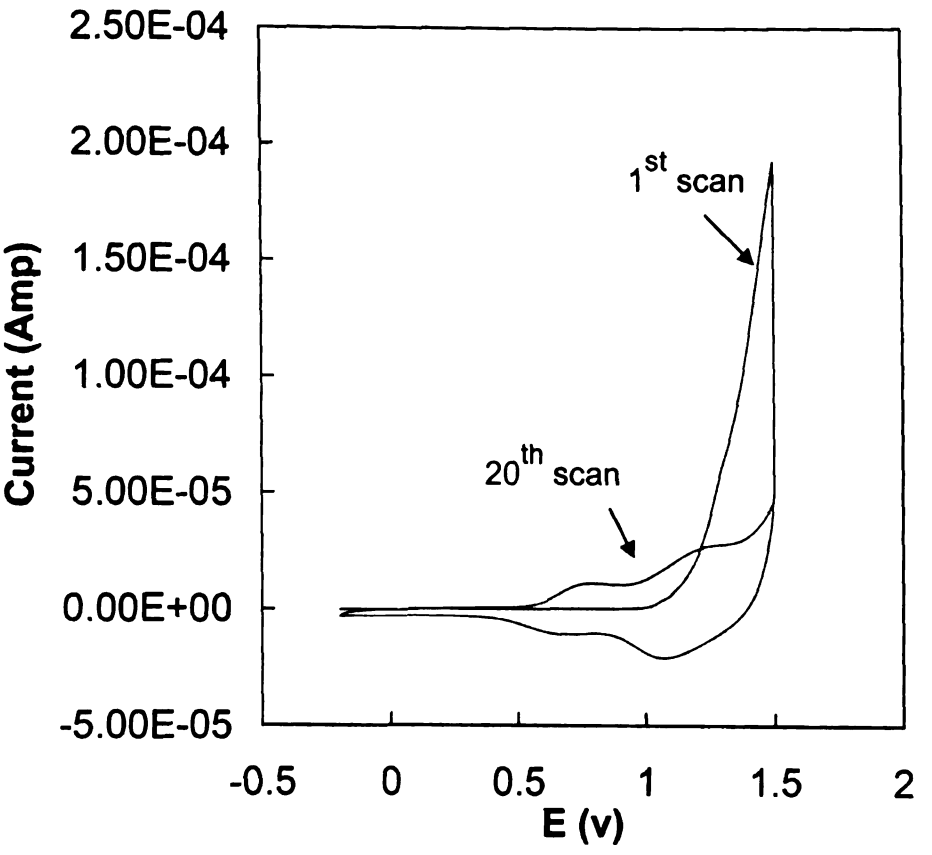

Figure 4.3: Cyclic voltammetry (20 cycles) of ~30 nm polyTTMM brush coated on ITO surface from -25 to 1500 mV at 100 mV/s.

conjugation. The voltammetric scans were repeated (20 times) (Figure 4.3, 20th scan) or less if the polymerization peak was no longer observable. On the last scan (20th scan), the oxidation peak appears at a lower anodic potential (E~0.75 V/Pt), and corresponds to a more extended conjugated system than the monomeric terthiophenes.[37,38,39,40,41] The de-doping peak remains visible. These redox potentials are higher than values reported for terthiophene reduction under the similar conditions[42] but, they are comparable to the data reported by Advincula *et al.*[21] for copolymers of carbazole and terthiophene containing methacrylate (E_c = 0.6 V/Ag/Ag$^+$ and E_a = 1.08 V/Ag/Ag$^+$). The reduced

mobility of a thiophene attached to polymethacrylate chains might explain the formation of polythiophenes with shorter conjugation lengths. Scan rate dependence studies (Figure 4.4) of the cross-linked polyTTMM at scan rates of 20-80 mV/s in a 0.1 M TEAP/CH_3CN electrolyte solution (potentials are reported relative to Pt as a quasi reference electrode) revealed linear behavior (Figure 4.5) similar to data of Sotzing *et al.*[39] for electropolymerized poly(terthiophene) films. This indicates a surface-confined reaction as the sole phenomenon.

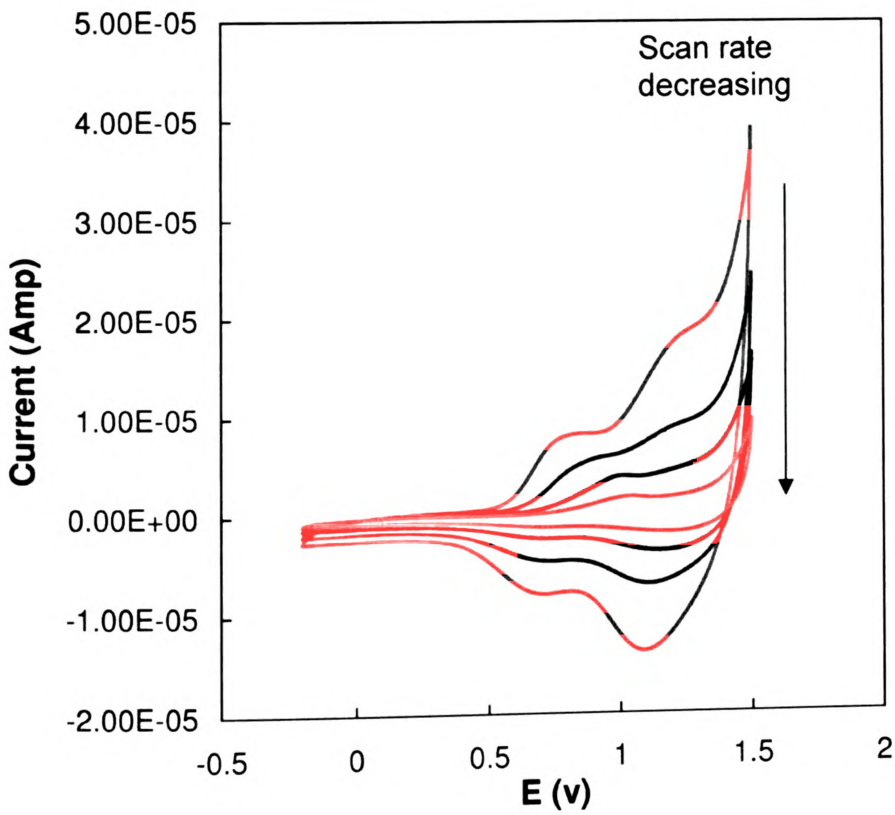

Figure 4.4. Scan rate dependency study of polyTTMM brushes coated on ITO surface at scan rates of 20-80 mV/s in a 0.1 M TEAP/CH_3CN electrolyte solution.

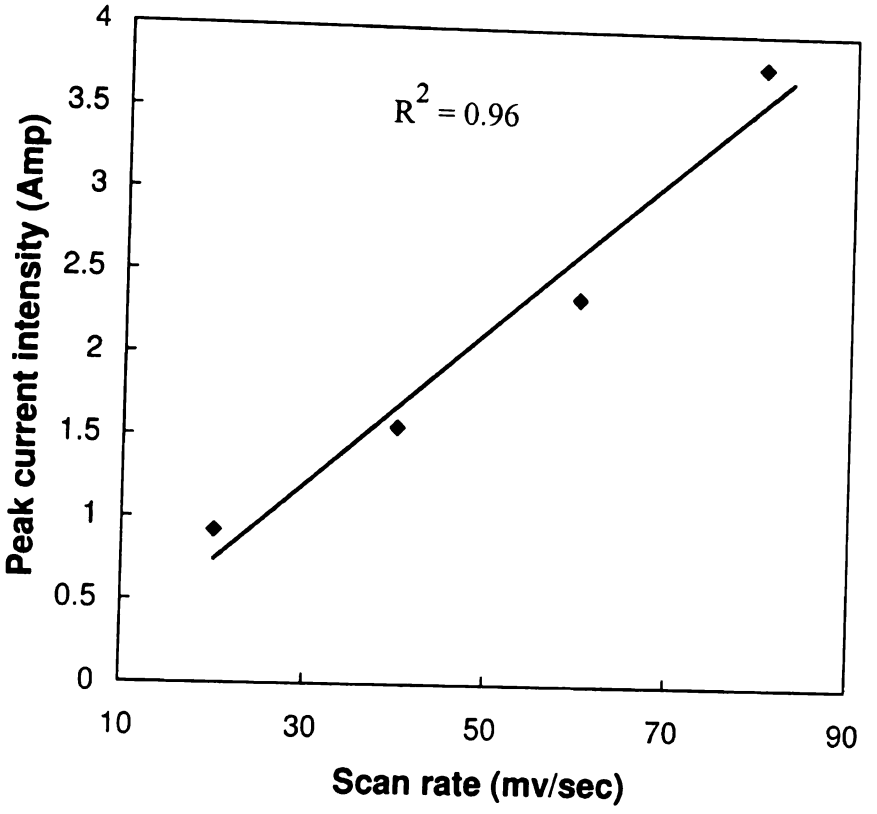

Figure 4.5: Plot of peak current intensity versus scan rate at the maximum of the oxidation wave of polyTTMM brush coated on ITO surface.

Examination of the films by UV-vis before and after the electro-polymerization showed a small spectral difference arising from the formation of conjugated oligothiophene species (Figure 4.7). The λ_{max} for the polyTTMM brush before crosslinking was ~ 360 nm (characteristic vibronic pattern of terthiophene),[39] and shifted to ~ 370 nm after electro polymerization. This pattern is comparable to the sexithiophene based structure investigated previously.[43] IR spectroscopy also suppports terthiophene coupling. The spectrum of polyTTMM (Figure 4.6) shows bands at 3100, 1450 and 790 cm^{-1} due to C-H stretching, wagging and C-H out-of-plane deformation modes from the thiophene rings respectively. After crosslinking, these bands decreased dramatically. A

new band at 1620 cm^{-1}, due to the conjugated thiophene, appears in the spectrum (Figure 4b). The persistence of the carbonyl stretching mode at 1710 cm^{-1} in both spectra confirms that the polymer backbone is apparently unchanged. These results are consistent with a network of conducting polythiophene chains of short conjugation length, perhaps dimers, grown from pristine polyTTMM.

The morphology of the pregrafted polyTTMM films may change upon oxidation of the terthiophene units. Films before and after oxidation were investigated by tapping mode AFM. The surface shows an irregular morphology (Figure 4.8), compared to the smooth films before oxidation. We suspect that anodic oxidation rigidified the polythiophene segments as well as the polyacrylate chains, which resulted in a more heterogeneous surface dominated by grains of various sizes. However, the surface roughness did not change significantly after oxidation.

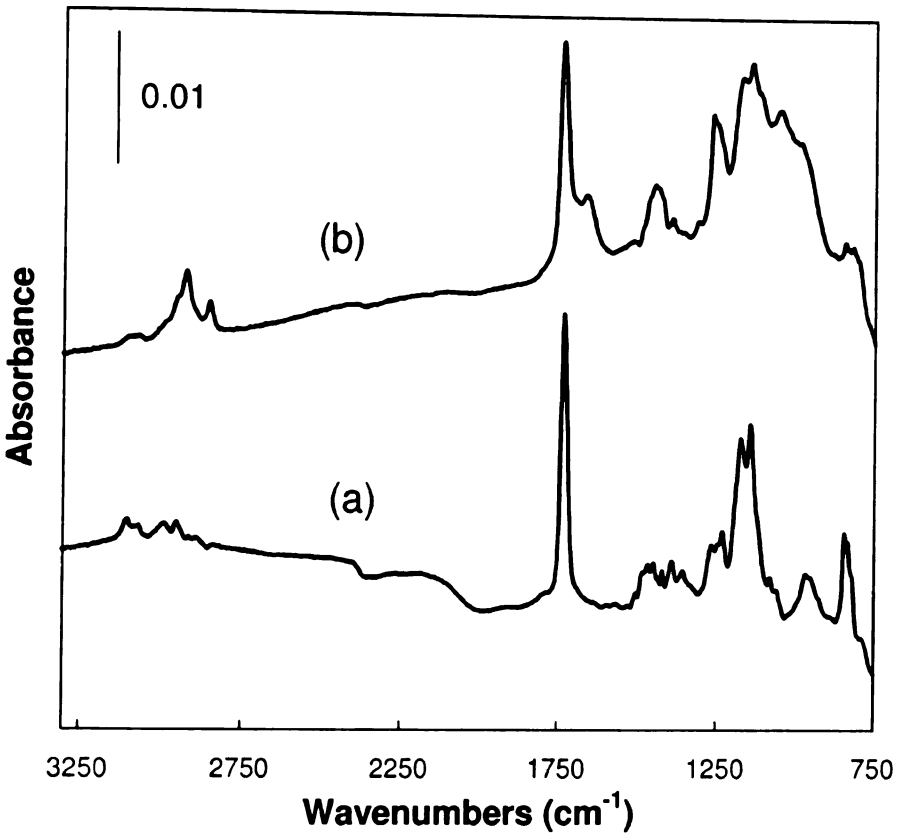

Figure 4.6: Representative examples of reflectance FTIR spectroscopy of gold surface coated with (a) 50 nm polyTTMM brush (b) electrochemically crosslinked polyTTMM brush.

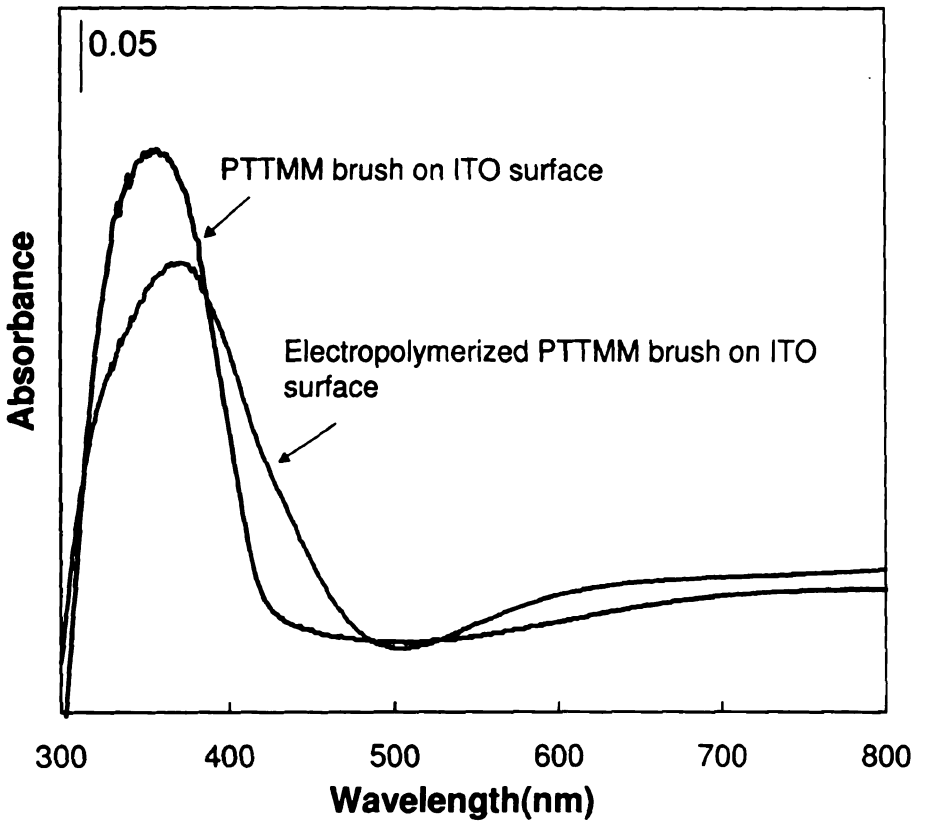

Figure 4.7: UV-vis absorption spectra of polyTTMM brush grown on ITO surface (blue line) and electrochemically cross linked polyTTMM (EPTTMM) brush on ITO surface (red line).

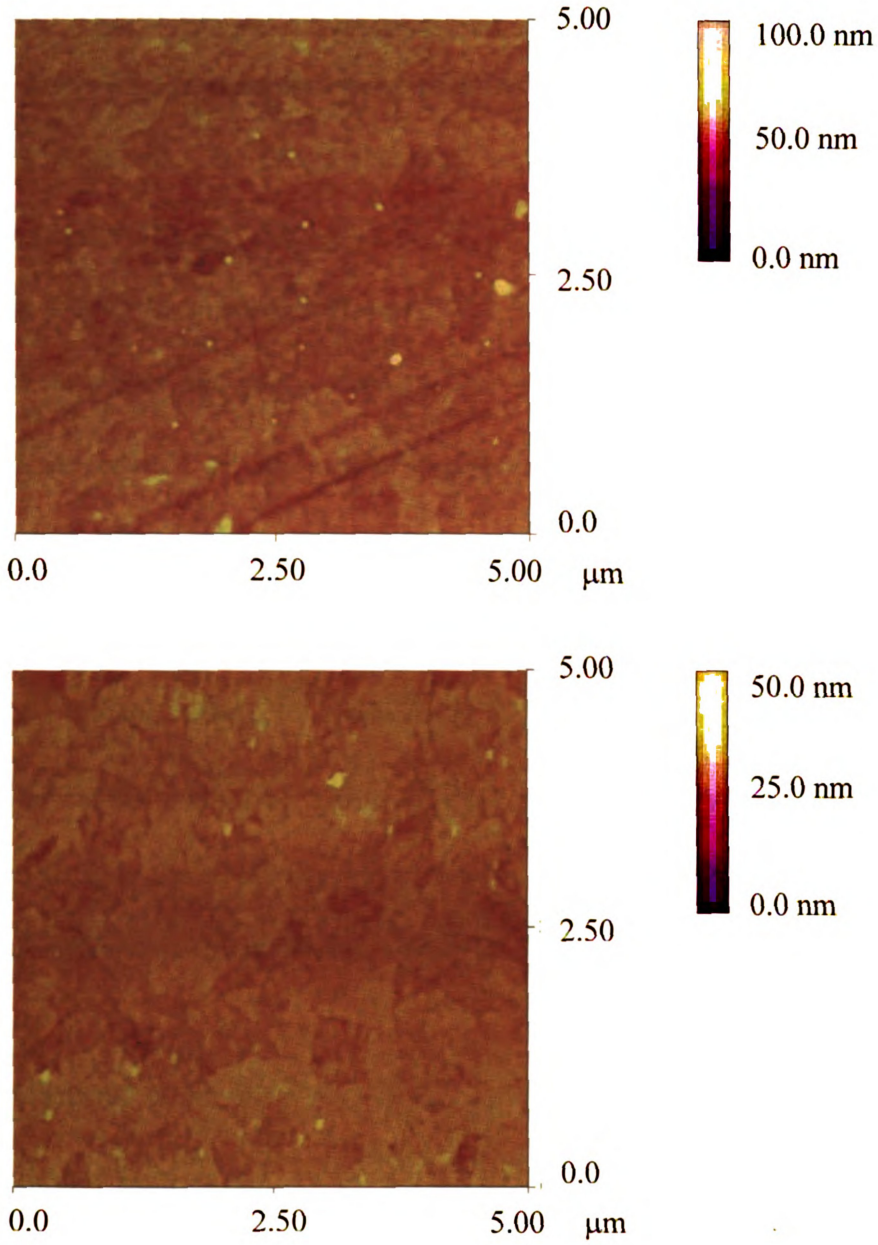

Figure 4.8: Topographical AFM images of ITO surface coated with polyTTMM brush (upper image) and electro polymerized polyTTMM brush (bottom image) taken with tapping mode imaging. Upper image is a 5 × 5 μm survey scan with high surface coverage and an rms roughness of 3.8 nm, as calculated with Nanoscope IV software. The bottom image is a 5 × 5 μm scan with an rms value of 2.9 nm.

4.3.6. Anodic copolymerization of the grafted polythiophene units and additional thiophene derivative in solution - heterocoupling

The data for the electrochemical oxidation of polyTTMM suggest that terthiophene cross-linking was inefficient. To increase the conjugation length of polyTTMM films, the potentiostatic oxidation of polyTTMM can be performed in the presence of thiophene derivatives such as 3,4 ethylenedioxythiophene (EDOT) (Scheme 4.7).[44,46] According to Zotti and coworkers,[42] EDOT is the best choice for heterocoupling terthiophene monolayers as well as polyterthiophene films. Electropolymerization involves the formation of carbon-carbon bonds by reaction between two radical cations,[45,47] and the primary requisite for heterocoupling is the generation of radical cations on the electrode surface (for the polyTTMM brush) and in the solution close to the electrode (for the monomer). Thus, the heterocoupling is favored by a small difference in oxidation potential between the surface and the solution components.

The second factor for the coupling process is the reactivity of radical cations toward coupling. Zotti *et al.*[42] claim the second factor is predominant as the oxidation potential of polyterthiophene films (0.5 V/ Ag/Ag^{+}) is much lower than the oxidation potential of EDOT (1.16 V/ Ag/Ag^{+}). They surmised that the strong positive shift of polyterthiophene oxidation moves it close to EDOT oxidation which should kinetically favor the copolymerization.

Figure 4.9 shows the voltammogram recorded for the oxidation of a polyTTMM film in the presence of EDOT. The polymerization peak starts at ~1.3 V/Pt, nearly the

same potential as the oxidation of the polyTTMM film in the absence of EDOT. Repeated cycling (20 times) of the polyTTMM film between -0.5 V and 1.5 V, while immersed in a dilute solution of EDOT, resulted in the deposition of a polymer film and a concomitant growth of a redox wave in the cyclic voltammogram (Figure 4.9, 20th scan). With each scan, more material deposited onto the electrode, resulting in an increase in the anodic and cathodic peak currents associated with the polymer. The polymerization peak (~1.1V) of the as-prepared conducting polymer occurs at lower cathodic potentials compared to polyTTMM in the absence of EDOT, which is consistent with the formation of chains with longer conjugated length. The UV-vis spectra of a polyTTMM brush before and after heterocoupling with EDOT (Figure 4.10) shows broadening of the absorption band and a shift of oscillator strength to longer wavelengths, consistent with increased conjugation. However, we cannot exclude the possibility of a small amount of EDOT homopolymer adsorbed on the ITO surface after extensive washing.

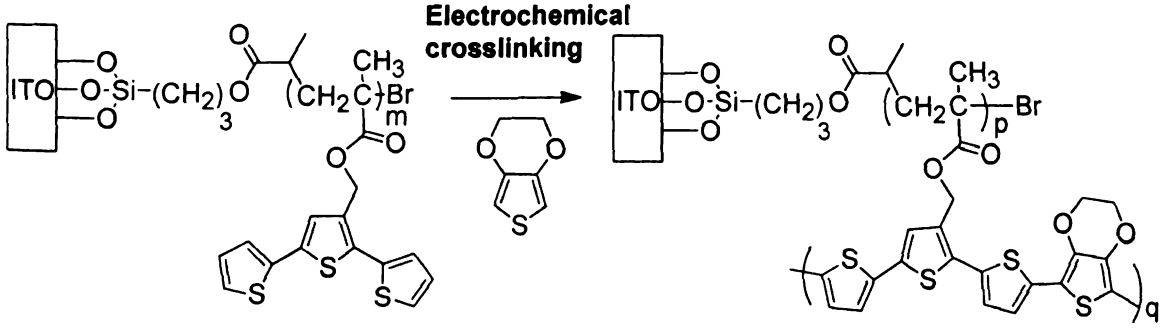

Scheme 4.7: Heterocoupling of polyTTMM brush with EDOT on an ITO surface

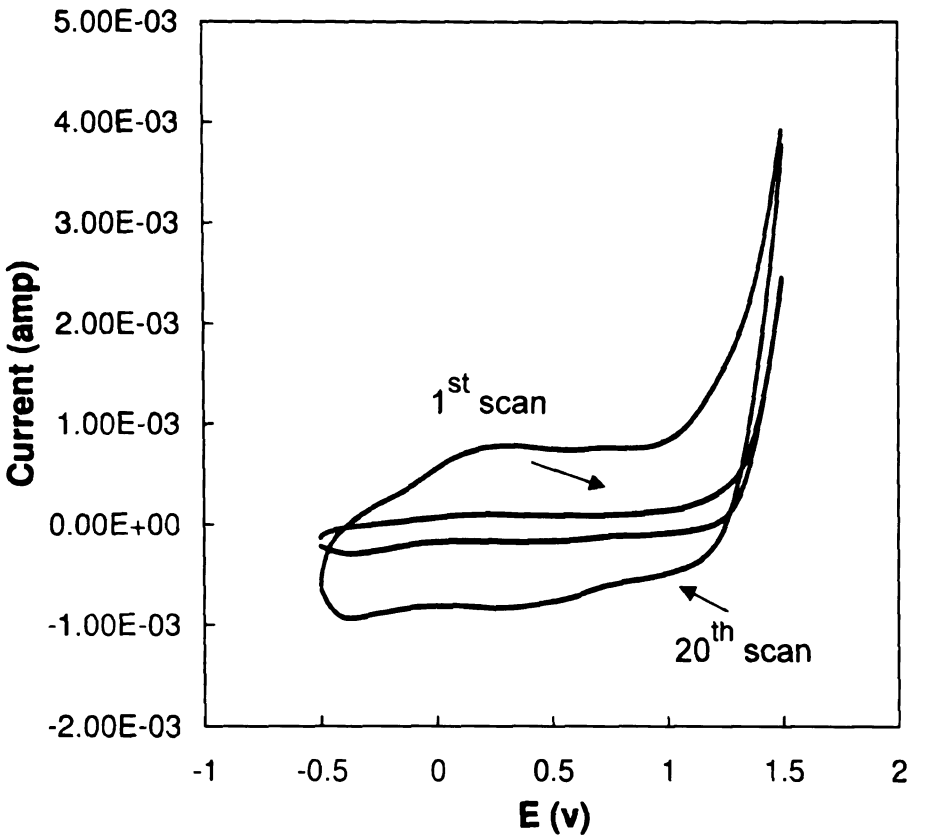

Figure 4.9: Cyclic voltammetry (20 cycles) of ~30 nm polyTTMM brush grafted on ITO surface in CH_3CN added with TEAP (0.05 M) in the presence of EDOT in solution (first (blue line) and 20^{th} scan (red line)) at the scan rate of 20 mV/s

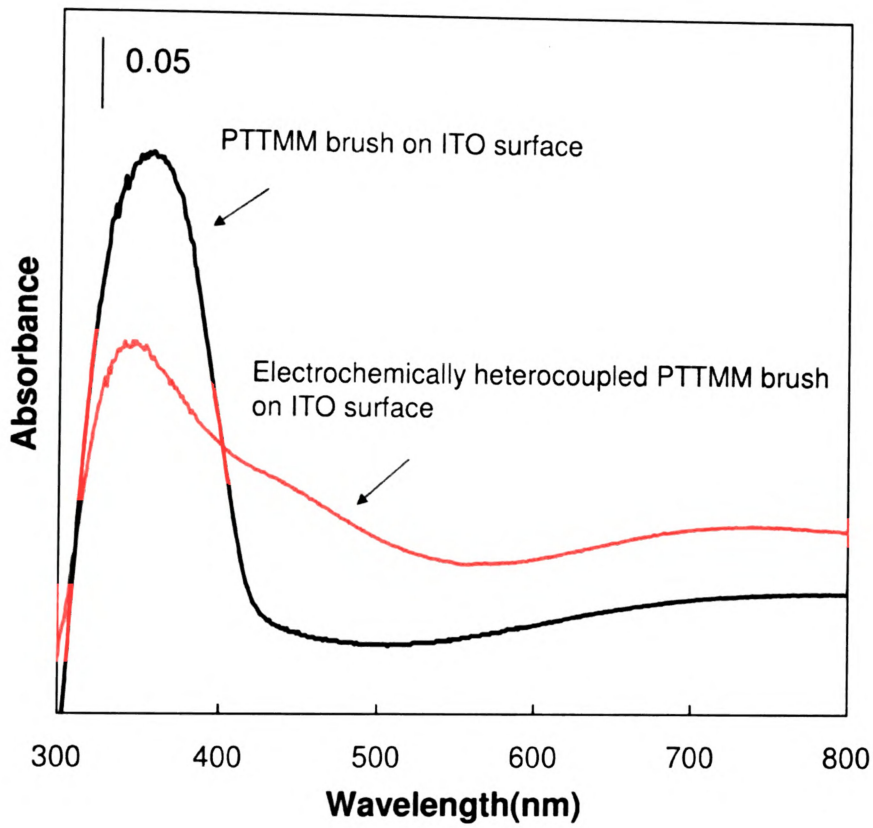

Figure 4.10: UV-vis absorption spectra of polyTTMM brush grown on ITO surface (blue line) and electrochemically heterocoupled polyTTMM brush with EDOT on ITO surface (red line).

4.4. Conclusions

Poly(terthiophene methacrylate) brushes were successfully grown from ITO and gold electrodes using surface initiated ATRP. The resulting films were homogeneous with smooth domains and features. The polyTTMM brush were electrochemically oxidized by cyclic voltammetry, to form a crosslinked polymer network with short segments of conjugated poly(terthiophene) segements. Including EDOT during oxidation resulted in heterocoupled EDOT and polyTTMM with increased conjugation lengths. Uniformly grafted conducting polymer brush may be useful in photovoltaic devices.

4.5. References:

1 (a) Wang, X.; Kim, Y.-G.; Drew, C.; Ku, B.-C.; Kumar, J.; Samuelson, L. A. *Nano Lett.* **2004**, *4*, 331. (b) Tong, H.; Wang, L.; Jing, X.; Wang, F. *Macromolecules* **2003**, *36*, 2584. (c) Murphy, C. B.; Zhang, Y.; Troxler, T.; Ferry, V.; Martin, J. J.; Jones, W. E., Jr. *J. Phys. Chem. B* **2004**, *108*, 1537.

2 Dodabalapur, A.; Torsi, L.; Katz, H. E. *Science* **1995**, *268*, 270.

3 Skotheim, T. A.; Reynolds, J. R. *Handbook of Conducting Polymers*, 3rd ed.; CRC Press: Boca Raton, FL, **2007**.

4 (a) Barbarella, G.; Melucci, M.; Sotgiu, G. *Adv. Mater.* **2005**, *17*, 1581. (b) Kirchmeyer, S.; Reuter, K. *J. Mater. Chem.* **2005**, *15*, 2077. (c) Nalwa, S. H. *Handbook of Organic Conductive Molecules and Polymers*, Wiley–VCH, New York, **1997**. (d) Fichou, D. *Handbook of Oligo- and Polythiophenes*, Wiley–VCH, New York, **1998**.

5 McCarley, R. L.; Willicut, R. J. *J. Am. Chem. Soc.* **1998**, *120*, 9296.

6 Smela, E. *Langmuir* **1998**, *14*, 2996.

7 Sayre, C. N.; Collard, D. M. *Langmuir* **1995**, *11*, 302.

8 Lang, P.; Mekhalif, Z.; Garnier, F. *J. Chim. Phys.* **1992**, *89*, 1063.

9 Nüesch, F.; Si-Ahmed, L.; Francüois, B.; Zuppiroli, L. *Adv. Mater.* **1997**, *9*, 222.

10 Simon, R.; Ricco, A.; Wrighton, M. *J. Am. Chem. Soc.* **1982**, *104*, 2031.

11 Sebastian, R. M.; Caminade, A. M.; Majoral, J. P.; Levillain, E.; Huchet, L.; Roncali, J. *Chem. Comm.* **2000**, 507.

12 Taranekar, P.; Baba, A.; Fulghum, T. M.; Advincula, R. *Macromolecules* **2005**, *38*, 3679. (b) Taranekar, P.; Fulghum, T.; Baba, A.; Patton, D.; Advincula, R. *Langmuir* **2007**, *23*, 908.

13 Deng, S. X.; Advincula, R. C. *Chem. Mater.* **2002**, *14*, 4073.

14 Taranekar, P.; Fan, X.; Advincula, R. *Langmuir* **2002**, *18*, 7943.

15 Inaoka, S.; Roitman, D. B.; Advincula, R. C. *Chem. Mater.* **2005**, *17*, 6781.

16 Park, M. K.; Xia, C.; Advincula, R. C.; Schutz, P.; Caruso, F. *Langmuir* **2001**, *17*, 7670.

17 Jang, S. Y.; Sotzing, G. A.; Marquez, M. *Macromolecules* **2002**, *35*, 7293.

18 (a) Ejaz, M.; Yamamoto, S.; Ohno, K.; Tsujii, Y.; Fukuda, T. *Macromolecules* **1998**, *31*, 5934. (b) Husseman, M.; Malmstrom, E. E.; McNamara, M.; Mate, M.; Mecerreyes, D.; Benoit, D. G.; Hedrick, J. L.; Mansky, P.; Huang, E.; Russell, T. P.; Hawker, C. J. *Macromolecules* **1999**, *32*, 1424. (c) Kamigaito, M.; Ando, T.; Sawamoto, M. *Chem. Rev.* **2001**, *101*, 3689.

19 Jhaveri, S.; Carter, K. *Langmuir* **2007**, *23*, 8288.

20 (a) Snaith, H. J.; Whiting, G. L.; Sun, B.; Greenham, N. C.; Huck, W. T. S.; Friend, R. H. *Nano Lett.* **2005**, *5*, 1653. (b) Whiting, G. L.; Snaith, H. J.; Khodabakhsh, S.; Andreasen, J. W.; Breiby, D. W.; Nielsen, M. M.; Greenham, N. C.; Friend, R. H.; Huck, W. T. S. *Nano Lett.* **2006**, *6*, 573.

21 Fulghum, T.; Taranekar, P.; Advincula, R. C. *Macromolecules* **2008**, *41*, 5681.

22 Cirpan, A.; Alkan, S.; Toppare, L.; Hepuzer, Y.; Yagci, Y. *J. Polym. Sci., Part A: Polym. Chem.* **2002**, *40*, 4131.

23 Zanardi, C.; Scanu, R.; Pigani, L.; Pilo, M.I.; Sanna, G.; Seeber, R.; Spano, N.; Terzi, F.; Zucca, A. *Electrochim. Acta* **2006**, *51*, 4859.

24 Jang, S. Y.; Sotzing, G. A. *Macromolecules* **2002**, *35*, 7293.

25 Jang, S. Y.; Sotzing, G. A. *Macromolecules* **2004**, *37*, 4351.

26 Watson, K. J.; Wolfe, P. S.; Nguyen, S. T.; Zhu, J.; Mirkin, C. A. *Macromolecules* **2000**, *33*, 4628.

27 Fadeev, A. Y.; McCarthy, T. J. *Langmuir* **2000**, *16*, 7268.

28 Ulman, A. *Chem. Rev.* **1996**, *96*, 1533.

29 Zhuang, Y. X.; Hansen, O.; Knieling, T.; Wang, C.; Romback, P.; Lang, W.; Benecke, W.; Kehlenbeck, M.; Koblitz, J. *J. Micromech. Microeng.* **2006**, *16*, 2259.

30 Markovich, I.; Mandler, D. *J. Electroanal. Chem.* **2001**, *500*, 453.

31 Koide, Y.; Such, M. W.; Basu, R.; Evmenenko, G.; Cui, J.; Dutta, P.; Hersam, M. C.; Marks, T. J. *Langmuir* **2003**, *19*, 86.

32 Lee, J.; Jung, B. J.; Lee, J. I.; Chu, H. Y.; Do, L. M.; Shim, H. K. *J. Mater. Chem.* **2002**, *12*, 3494.

33 Jones, D. M.; Brown, A. A.; Huck, W. T. S. *Langmuir* **2002**, *18*, 1265.

34 Patten, T. E.; Matyjaszewski, K. *Adv. Mater.* **1998**, *10*, 901.

35 Huang, W. X.; Kim, J. B.; Bruening, M. L.; Baker, G. L. *Macromolecules* **2002**, *35*, 1175.

36 Mahajan, R. K.; Sood, P. *Int. J. Electrochem. Sci.*, **2007**, *2*, 832.

37 Skompska, M.; Peter, L. M. *J. Electroanal. Chem.* **1995**, *383*, 43.

38 (a) Taranekar, P.; Baba, A.; Fulghum, T. M.; Advincula, R. *Macromolecules* **2005**, *38*, 3679.. (b) Taranekar, P.; Fulghum, T.; Baba, A.; Patton, D.; Advincula, R. C. *Langmuir* **2007**, *23*, 908.

39 Jang, S. Y.; Sotzing, G. A.; Marquez, M. *Macromolecules* **2002**, *35*, 7293.

40 Fulghum, T.; Karim, S. M. A.; Baba, A.; Taranekar, P.; Nakai, T.; Masuda, T.; Advincula, R. C. *Macromolecules* **2006**, *39*, 1467.

41 Taranekar, P.; Fulghum, T.; Baba, A.; Patton, D.; Advincula, R. *Langmuir* **2007**, *23*, 908.

42 Zotti, G.; Zecchin, S.; Vercelli, B.; Berlin, A.; Grimoldi, S.; Groenendaal, L.; Bertoncello, R.; Natali, M. *Chem. Mat.* **2005**, *17*, 3681.

43 Fichou, D.; Horowitz, G.; Xu, Z.; Garnier, F. *Synth. Met.* **1992**, *48*, 167.

44 Labaye, D. E.; Jerome, C.; Geskin, V. M.; Louette, P.; Lazzaroni, R.; Martinot, L.; Jerome, R. *Langmuir* **2002**, *18*, 5222-5230.

45 (a) Waltman, R. J.; Bargon, J. *Tetrahedron* **1984**, *40*, 3963. (b) Waltman, R. J.; Bargon, J. *Can. J. Chem.* **1986**, *64*, 76. (c) Andrieux, C. P.; Audebert, P.; Hapiot, P.; Saveant, J. M. *J. Phys. Chem.* **1991**, *95*, 10158. (d) Audebert, P.; Catel, J. M.; LeCoustumer, J.; Duchenet, V.; Hapiot, P. *J. Phys. Chem.* **1995**, *99*, 11923. (e) Guyard, L.; Hapiot, P.; Neta, P. *J. Phys. Chem.* **1997**, *101*, 5698. (f) Audebert, P.; Catel, J.M.; Duchenet, V.; Guyard, L.; Hapiot, P.; LeCoustumer, J. *Synth. Met.* **1999**, *101*, 642.

Chapter 5

Polymerization of azidomethacrylates on gold surface and its elaboration via click chemistry

5.1. Introduction

Atom Transfer Radical Polymerization (ATRP), one of the most widely developed controlled radical polymerization (CRP) techniques, is extensively used to prepare polymer materials with predetermined molecular weights, narrow polydispersities, and advanced architectures.[1,2,3,4] ATRP is performed under mild conditions, and is applicable to a wide range of monomers and solvents. Recently, the copper-catalyzed Huisgen 1,3-dipolar cycloaddition, one of several chemistries termed as "click reactions", has drawn attention due to their high efficiency, tolerance to various functional groups, technical simplicity and high specificity.[5,6,7] Combining click reactions with ATRP is a versatile strategy for the synthesis of highly functionalized polymers.[8] Generally, polymer functionalization strategies are limited to end-modified and side-modified polymers. In the first approach, an ATRP initiator containing an azide or alkyne moiety is prepared and used to mediate the polymerization of various monomers. The resulting polymers contain terminal alkynyl or azido functionalities, which can be used in click reactions with functional azides or alkynes, respectively. Using this approach, Tsarevsky and Haddleton *et al.* separately synthesized functional telechelic polymers.[9,10] In another approach, a polymer with pendant alkyne or azido groups are first synthesized by ATRP, and subsequently functionalized via click reactions. Recently, Matyjaszewski *et al.* reported the modification of poly(3-azidopropyl

methacrylate) [11] (side-chain functionalization) and linear polystyrene [12] (end functionalization) by click chemistry.

Surface modification with synthetic polymers, especially polymer brushes, is of great interest for industrial and biological applications as well as in academic research.[13] Strategies have been developed for the functionalization of surfaces with polymer brushes to immobilize biomolecules,[14,15,16,17] and to realize "smart surfaces" with responsive and adaptive properties.[18,19] The recent development of ATRP has proved to be a versatile tool for modifying surfaces with a variety of functional polymers with grafted polymer chains ranging from low to high graft densities. Surface-based click chemistry is attracting increasing attention,[20 , 21 , 22 , 23] especially for attaching biomolecules. Bein and coworkers presented a novel approach for the covalent modification of mesoporous silica surfaces (modified with azide monolayer) with intact enzymes (derivatized with an alkyne) via click chemistry.[24] They reported a high density of covalently bound enzyme while retaining enzyme activity and the absence of leaching. Recently, Choi and coworkers demonstrated that the click chemistry could be used to modify the termini of polymeric nanobrushes (synthesized via ATRP) by replacing the bromine at the end of the polymer chain with azide groups.

To expand the versatility of surface-initiated ATRP we report post polymerization modification of polymer brushes by combining surface-initiated ATRP and click reactions. Azidopropyl methacrylate (AZPMA) was polymerized from initiators anchored on gold and indium tin oxide substrates, and via post-polymerization functionalization, dyes and water soluble polymers were attached to the pendent azides via click chemistry.

The AZPMA homopolymer has a high density of azides, and modification of the homopolymer may create a sterically congested system that reduces the efficiency of the click reaction. More importantly, to be suitable for click chemistry in the aqueous environments required for the surface attachment of water soluble molecules (e.g. biological molecules) AZPMA must be copolymerized with hydrophilic monomers. Random copolymer brushes are especially attractive since they should exhibit a uniform distribution of functional groups as well uniform swelling.[25,26] Moreover, if both of the comonomers are functional, then polymer brushes can be created with orthogonal functionalities. In this chapter, we describe the ATRP of AZPMA (hydrophobic functional monomer) with ethylene glycol methyl ether methacrylate (EGMA, hydrophilic) and polyethylene glycol methyl ether methacrylate (PEGMA). The lengths of the ethylene oxide chain in EGMA and PEGMA are different, which permits tuning of the hydrophilicity of the AZPMA copolymers. Click chemistry was used to modify poly(AZPMA) and AZPMA copolymers with an alkynylated organic dye and a water soluble polymer, polyethylene glycol monomethyl ether.

5.2. Experimental Section

5.2.1. Materials

Unless otherwise noted, all chemicals were obtained from Aldrich. Fluorescein, polyethylene glycol monomethyl ether (mPEG, M_n = 5000 g/mol), sodium hydride, propargyl bromide (80% solution in toluene), 11-mercapto-1-undecanol (MUD, 97%), 2-bromopropionyl bromide (2-BPB, 97%), anisole (99.7%), N,N-dimethylformamide (DMF, 99.8%), Cu(I)Br (99.999%), Cu(II)Br_2 (99.999%), Me_4Cyclam (99%) 4,4'-

dinonyl-2,2'-bipyridyl (dnNbpy, 97%) and pentamethyldiethylene triamine (PMDETA, 97%) were used as received. 2,2'-Bipyridine (bpy, 99%) was recrystallized from hexanes and sublimed prior to use. Triethylamine was distilled from calcium hydride under an argon atmosphere at reduced pressure. EGMA (ethylene glycol methyl ether methacrylate, 99%) and PEGMA (poly(oligoethylene glycol methyl ether methacrylate), M_w ~300, 98%) were passed through a 10 cm column of basic alumina to remove inhibitors. Azidopropyl methacrylate (AZPMA) was synthesized using the two step procedure reported in the literature.[11] After purification, monomers and solvents were transferred to Schlenk flasks, de-gassed using three freeze-pump-thaw cycles and then transferred into a drybox. Alkynylated mPEG (M_w ~5000) was synthesis by a published procedure.[27] The alkynylated fluorescein methyl ester was synthesized over two steps starting from fluorescein using the method of Hvilsted *et al.*[28] The process of immobilizing initiators on gold and ITO substrates was described in Chapter 4.

5.2.2. Homo and Copolymerization of AZPMA, EGMA and PEGMA from initiators immobilized on Au and ITO substrates

The procedure for the polymerization of AZPMA is described. In a N_2-filled drybox, CuBr (6 mg, 0.04 mmol), $CuBr_2$ (5 mg, 0.02 mmol), Me_4Cyclam (10 mg, 0.04 mmol), and dnNbpy (16 mg, 0.04 mmol) were added to a round bottom flask containing a 20 mL solution of monomer in DMF/anisole (AZPMA/DMF/anisole = 2:1:1 v:v:v, [AZPMA] = 4.0 M). The well-stirred mixture was heated in an oil bath at 50 °C until a

transparent light green solution formed. The solution was then transferred into small vials containing initiator-modified Au or ITO substrates to start the surface-initiated polymerization. After a set reaction time at 50 °C, the substrate was removed from the vial, washed sequentially with ethyl acetate and THF, and then dried under a flow of N_2 in a drybox. The same conditions were used for homo polymerization of EGMA ([EGMA] = 4 M). The same procedure was used for homo and copolymerizations of the monomers using copper catalysts with PMDETA and bpy. In all cases, the ratio of [monomer]:[Cu(I)]:[Cu(II)]:[ligand] was 300:1:0.1:1.1 and the monomer:solvent was 1:1 (v/v). For copolymerizations, the total monomer concentration was 4 M, and the mole ratio of the co monomers was varied.

5.2.3. Click functionalization of homo and copolymer brushes

Click chemistry was performed in a drybox by placing gold (or ITO) substrates coated with AZPMA homopolymer or copolymer brushes in a DMF solution (5 mL) of alkynylated fluorescein (97 mg, 0.25 mmol), CuBr (9 mg, 0.0625 mmol) and PMDETA (13 μL, 63 μmol) at 50 °C. After a set reaction time, the substrate was thoroughly washed with DMF and THF, sonicated for 1 min in THF, and again rinsed with THF to remove unreacted dye. The rinsed films were then dried in a stream of nitrogen. For modification of polymer brushes by aqueous click chemistry, substrates were transferred inside a glove bag filled with N_2 and placed in degassed solutions (5 mL) of alkynylated mPEG (0.252 g), CuBr (1.8 mg), and bpy (4 mg) in Milli-Q water (18.2 MΩ cm). The reaction was run for 12 hours at room temperature, and then the substrates were rinsed with deionized water and dried in a stream of N_2.

5.2.4. Characterization Methods

^{1}H and ^{13}C NMR analyses were carried out at room temperature on a Varian UnityPlus-500 spectrometer at 500 and 300 MHz, respectively, with the chemical shifts reported in ppm and referenced to signals from residual protons in the solvent. Film thicknesses were measured using a rotating analyzer ellipsometer (model M-44; J. A. Woollam) at an incident angle of 75^{o}. The data were analyzed using WVASE32 software, and thickness and refractive index determinations were performed on at least three spots on each substrate. The refractive index of the films was assumed to be 1.5 and then fitted with the film thickness. Reflectance FTIR spectroscopy was performed using a Nicolet Magna-IR 560 spectrometer containing a PIKE grazing angle (80^{o}) attachment. UV-vis measurements were taken on Perkin Elmer lambda 400 spectrometer. Atomic force microscopy (AFM) images were obtained in tapping mode with Multimode AFM and NanoScope IV software (Digital Instruments, Santa Barbara, CA) at room temperature. A tapping mode probe (NSC15) with a nominal frequency of 300 kHz was used for all experiments. The confocal system was the Olympus FluoView FV1000 Laser Scanning Confocal Microscope (Tokyo, Japan). The images were collected using the 20× UPlanFLN (NA0.5) objectives with a 3× optical zoom. The fluorescence was excited using the 488 nm laser line of the Ar gas laser. The emission was collected using a 535-565 nm band-pass filter.

5.3. Results and Discussion

5.3.1 Synthesis of uniform polyAZPMA brushes from gold surfaces

Scheme 5.1 shows the synthetic route to polymethacrylate copolymer brushes with pendent alkynes and their modification by click chemistry. Initially, we examined the kinetics for the surface initiated homopolymerization of azidopropyl methacrylate (AZPMA) using several catalyst systems (Figure 5.1). Usually, well-controlled ATRPs maintain a low concentration of active radicals to minimize termination, indicated by a linear relationship between film thickness and time, and provide control over the molecular mass and polydispersities. Typically, the rate of ATRP is low, but the use of Me_4Cyclam/dnNbpy as ligands for Cu catalyst systems yields unusually rapid film growth and high film thicknesses. However, Figure 5.1 shows a decline in film growth rate with time for this system, and suggests significant termination as the consequence of a relatively high radical concentration that also leads to rapid polymerization.

Compared to the Me_4Cyclam/dnNbpy catalyst systems, using PMDETA as the Cu ligand provides more controlled polymerizations, as evidenced by a nearly linear increase in thickness with time for the first 4 hours of polymerization (after an rapid rate following initiation). At longer times, the polymerization rate slows and the film thickness reaches 260-300 nm after 12 hours (data not shown here). In prior research, solution polymerization of AZPMA using PMDETA/CuCl and bpy/CuBr provided significant control over the molecular weight distribution and retention of the azide functionality.[11,29] Liu and coworkers found that the PMDETA/CuCl system gave higher monomer conversion and lower polydispersities than catalysts with 2,2′-bipyridyl or

Me_6TREN as the ligands.[29] It has been well-established that the combination of a CuCl catalyst and a bromo-capped initiator results in halogen exchange and increases the relative rate of initiation compared to propagation, and results in a controlled radical polymerization with a high initiating efficiency.[30,31]

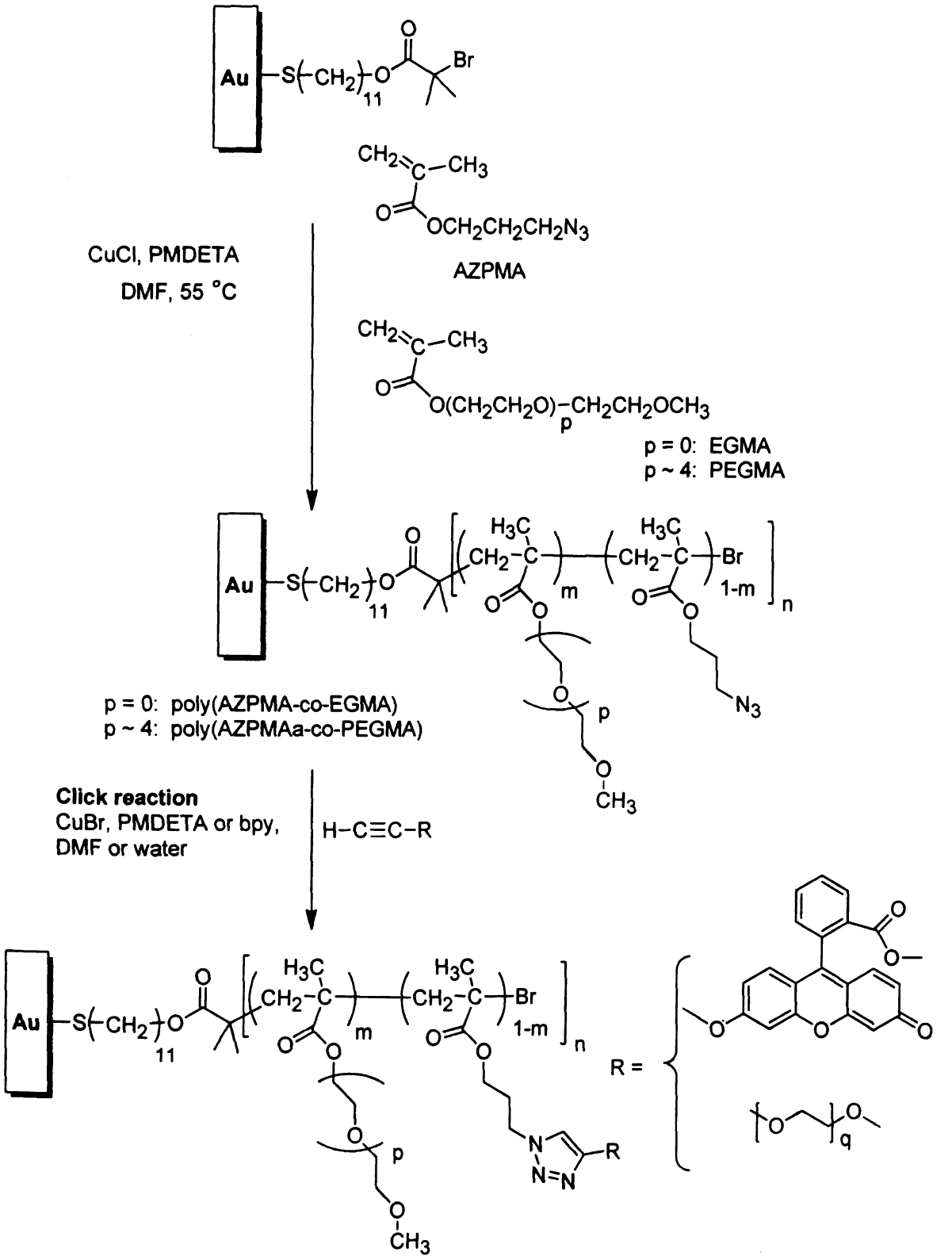

Scheme 5.1. Synthesis of polyAZPMA and AZPMA copolymer brushes grafted on gold substrates and their functionalization by click chemistry.

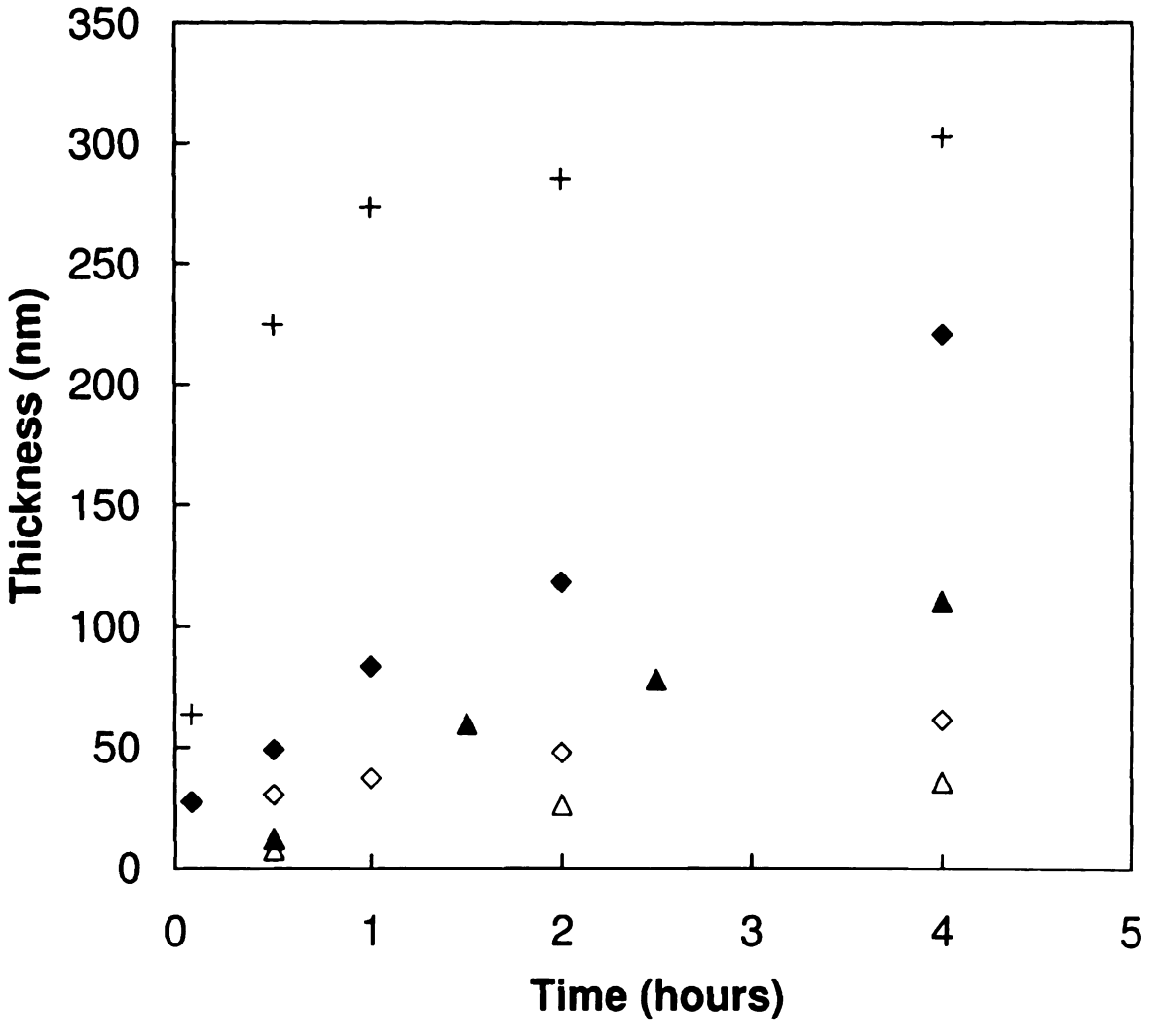

Figure 5.1. Evolution of the ellipsometric brush thickness with time for the polymerization of AZPMA from initiator monolayers on Au substrates using CuBr/Me_4Cyclam/dnNbpy)/DMF at 50 °C (+), CuCl/PMDETA/DMF at 50 °C (◆), CuCl/PMDETA/$CuBr_2$/DMF at 50 °C (◇), CuCl/bpy/$CuBr_2$/isopropanol at 50 °C (▲) and CuCl/bpy/$CuBr_2$/isopropanol at RT (△). Here, each point represents a different film.

However, surface polymerizations of AZPMA using bpy as the catalyst ligand yielded ~100 nm thick polyAZPMA films after 4 hrs of polymerization at 50 °C, compared to ~200 nm thick brushes obtained under similar conditions using PMDETA as the ligand. As proposed by Matyjaszewski,[32] multidentate ligands such as Me_4Cyclam and PMDETA may complex Cu(II) species more efficiently than bpy, shifting the equilibrium toward the Cu(II) complex and providing a higher radical concentration and faster polymerizations than those catalyzed by Cu-bpy complexes.

Previous studies demonstrated that Me_4Cyclam and PMDETA Cu complexes are highly active catalysts for solution ATRP.[33,34] To control the polymerizations, we added 10% $CuBr_2$ to the CuCl/PMDETA catalyst system and observed sluggish, but controlled growth of thick polyAZPMA brushes. As shown in Figure 5.1, the CuCl//PMDETA catalyst system was superior to the other catalyst systems that we tested, and it provides reasonable growth rates with minimal termination. This system was used exclusively in subsequent experiments.

The successful growth of polyAZPMA brushes was apparent in the reflectance FTIR spectra of the film by the appearance of strong carbonyl and azide bands at 1740 and 2150 cm^{-1}, respectively (Figure 5.2). The growth in film thickness matches the changes in the intensity of the IR bands. In addition, a topographical AFM (height) image of a 250 nm thick polyAZPMA brush was smooth and uniform with an rms roughness < 2 nm (< 1% of the film thickness).

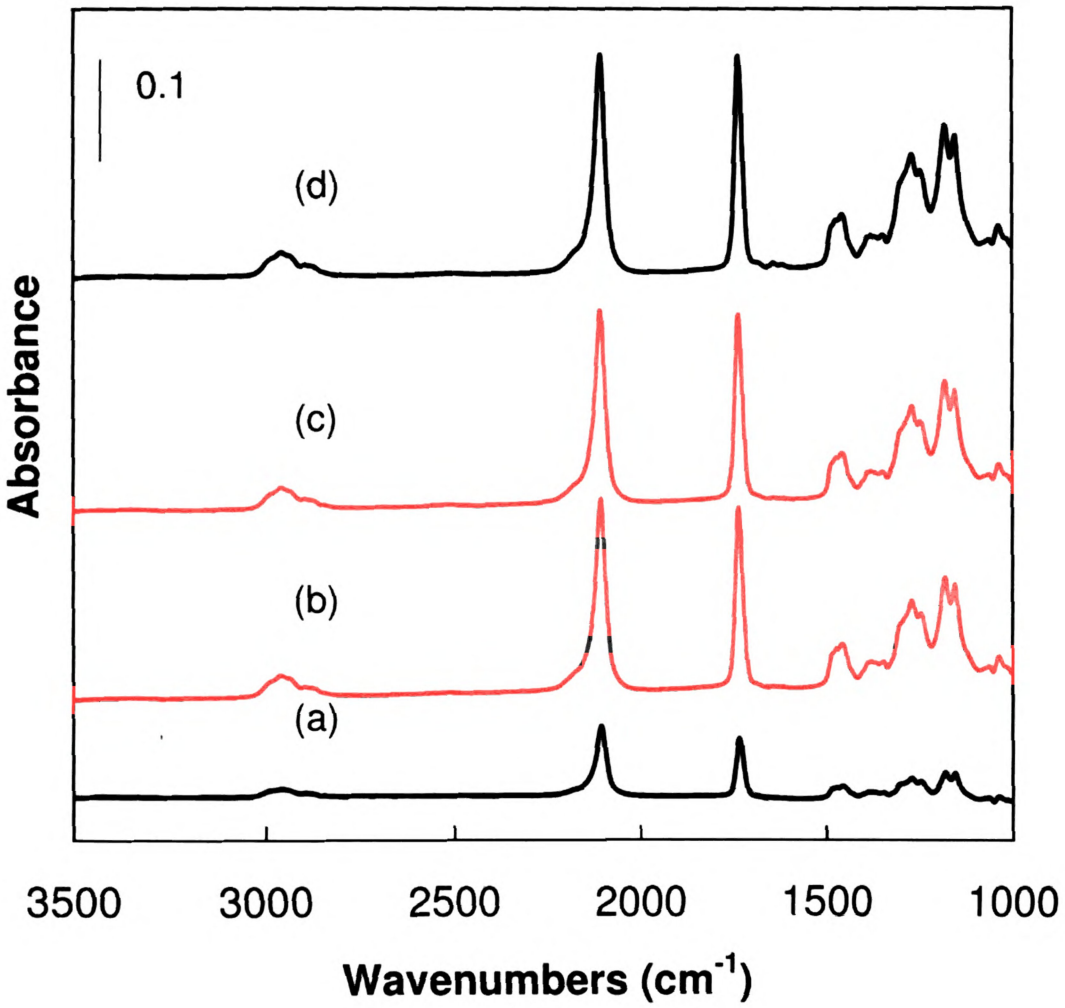

Figure 5.2. Reflectance FTIR spectra of gold substrates coated with polyAZPMA brushes grown for (a) 0.5 h (b) 4 h (c) 6 h and (d) 8 h from the initiator layer. A UV/O_3 cleaned gold slide was used as a background.

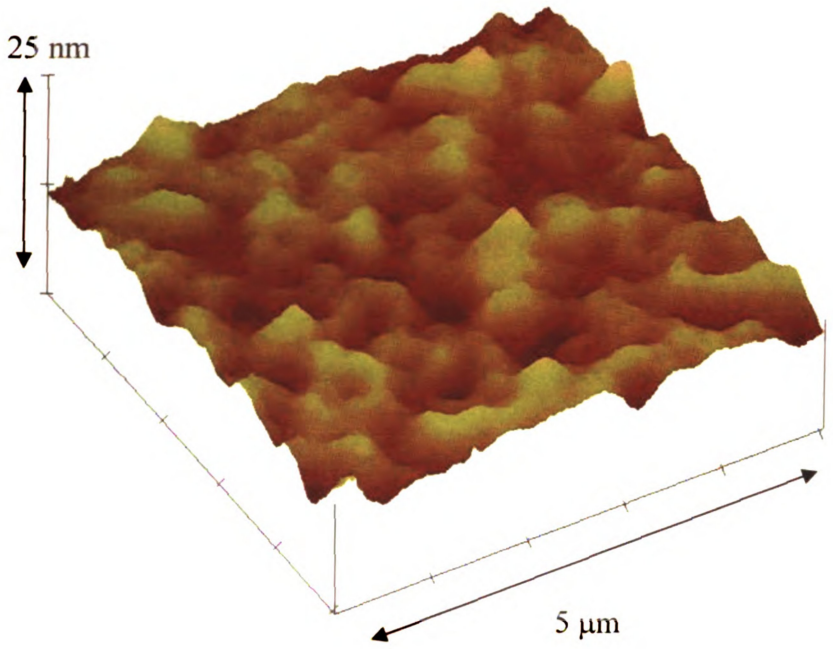

Figure 5.3: Topographical AFM image (tapping mode) of a gold surface coated with a 250 nm polyAZPMA brush. The image is a 5 × 5 μm survey scan with high surface coverage and an rms (root mean square) roughness of 1.9 nm, as calculated by the Nanoscope IV software.

5.3.2 Copolymerization of AZPMA with EGMA and PEGMA from gold surfaces

The conditions used for the homopolymerization of AZPMA were applied to the homopolymerization of EGMA from gold surfaces. Kinetic studies showed that the CuCl/PMDETA system also provided good control over EGMA polymerizations; the CuBr/Me_4Cyclam/dnNBpy system gave higher growth rates but with less control (Figure 5.4). With good control and comparable polymerization rates for AZPMA and EGMA, the CuBr/Me_4Cyclam/dnNBpy system was used for the copolymerization studies.

Copolymerizations were run at various comonomer feed ratios and characterized by ellipsometry and reflectance FTIR (Figures 5.5 and 5.6 respectively). The copolymer composition was calculated from the reflectance FTIR data by integrating the characteristic azide and carbonyl peaks from AZPMA and the carbonyl peak from EGMA. The copolymer composition correlates well with the initial feed ratios of the comonomers (Figure 5.7), consistent with a random copolymer brush. Moreover, copolymers and homopolymer films synthesized at various feed ratios and characterized at identical polymerization times had similar ellipsometric thicknesses, suggesting that the reactivities of AZPMA and EGMA are comparable and consistent with a random copolymerization.[25,26]

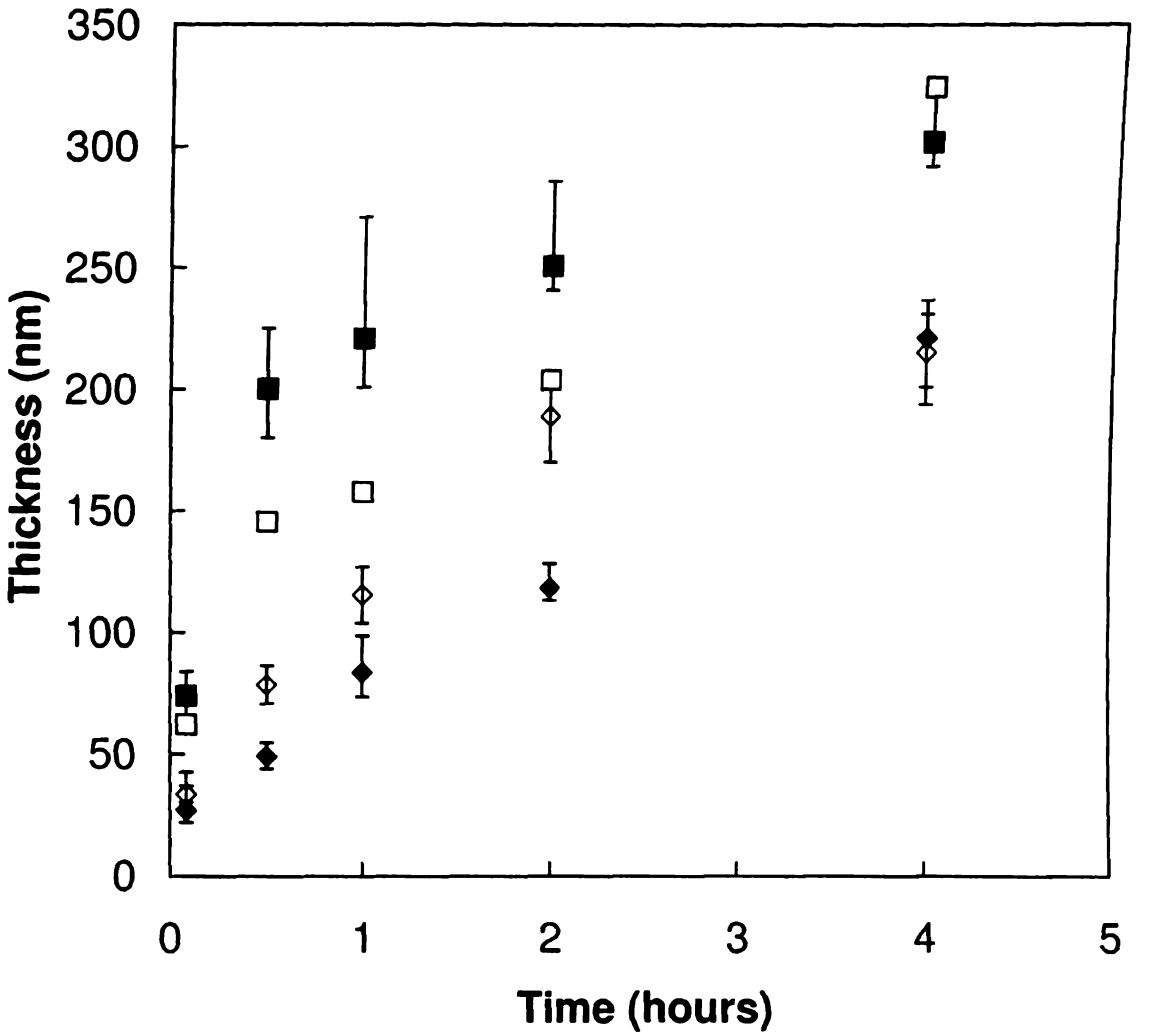

Figure 5.4. The evolution of the ellipsometric brush thickness with time for the homopolymerization of AZPMA and EGMA from initiator monolayers on Au substrates using CuBr/Me_4Cyclam/dnNbpy/DMF as the catalyst at 50 °C (■AZPMA, □EGMA) and CuC /PMDETA/DMF at 50 °C (◆AZPMA, ◇EGMA). Here, each point represents the average of three independent runs, and the error bars correspond to the standard deviation.

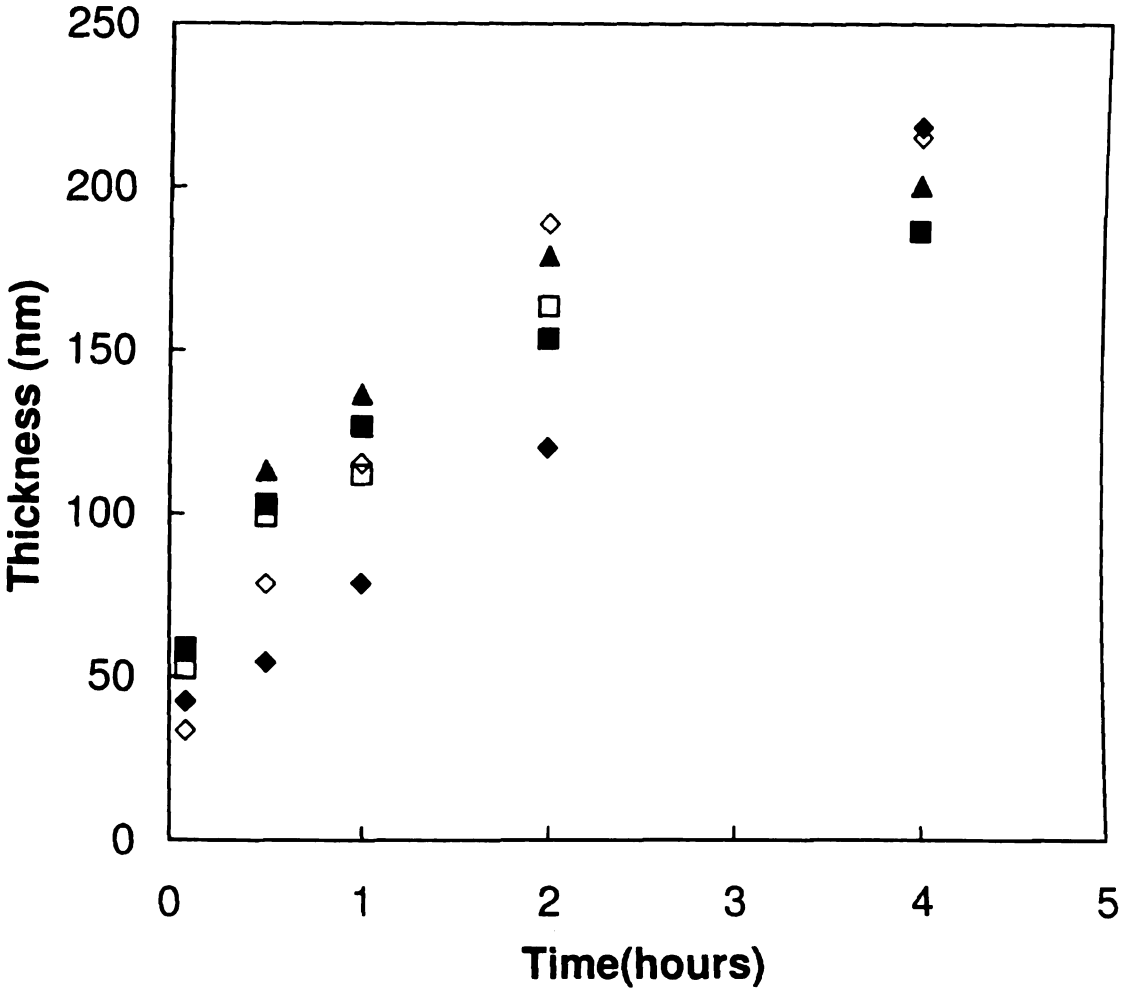

Figure 5.5. Evolution of the ellipsometric brush thickness with time for polyAZPMA and poly(AZPMA-*co*-EGMA) at various initial feed ratios from initiator monolayers immobilized on gold substrates using CuCl/PMDETA/DMF as the catalyst system at 50 °C. ◆AZPMA/EGMA (100/0), ▲AZPMA/EGMA (75/25), ■AZPMA/EGMA (50/50), □AZPMA/EGMA (25/75), ◇AZPMA/EGMA (0/100). Here, each point represents a different film.

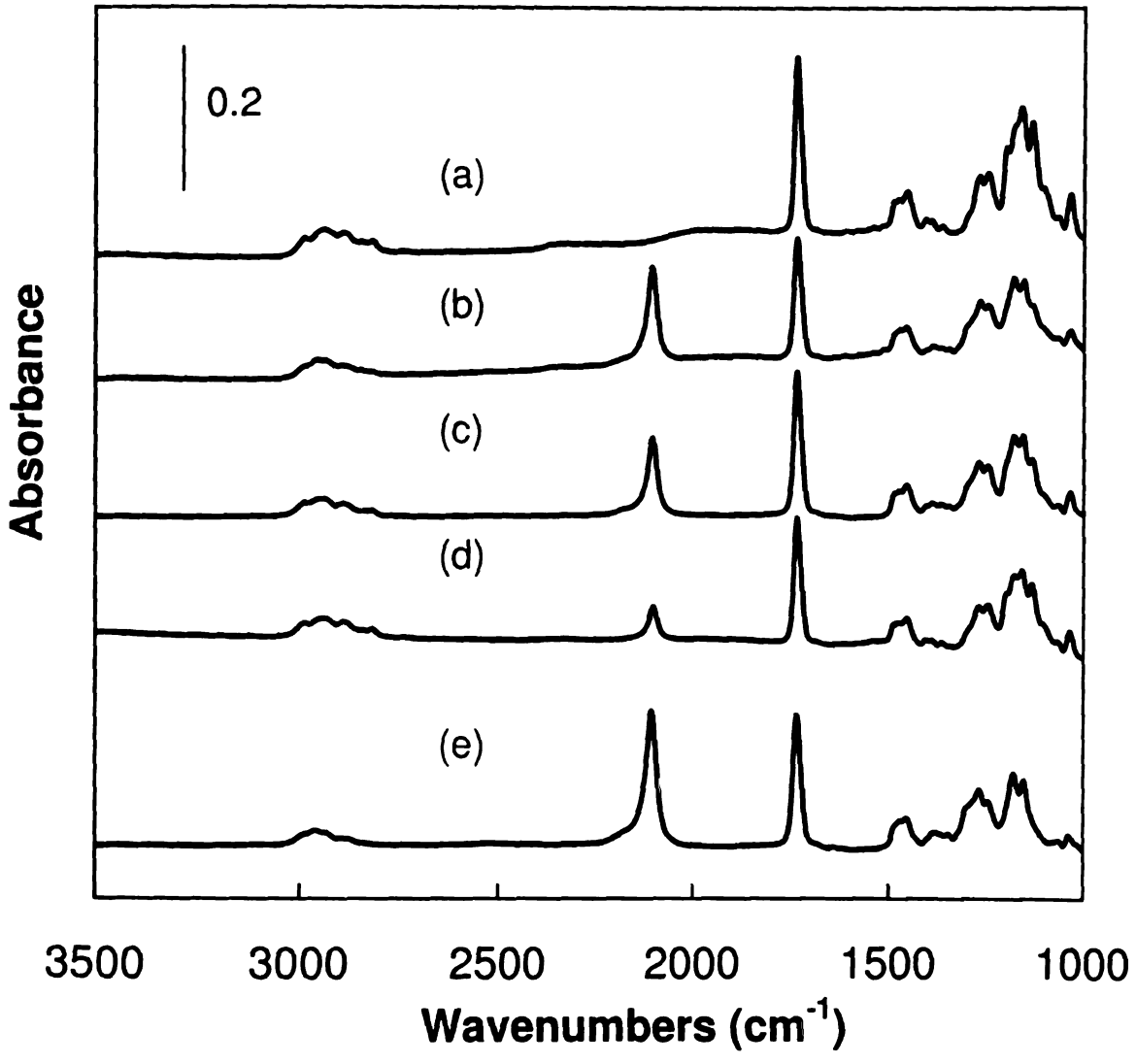

Figure 5.6. Reflectance FTIR spectra of polyAZPMA and poly(AZPMA-*co*-EGMA) brushes grown from gold substrates at different feed ratios. (a) AZPMA/EGMA (0/100) (b) AZPMA/EGMA (75/25) (c) AZPMA/EGMA (50/50) (d) AZPMA/EGMA (25/75) (e) AZPMA/EGMA (100/0).

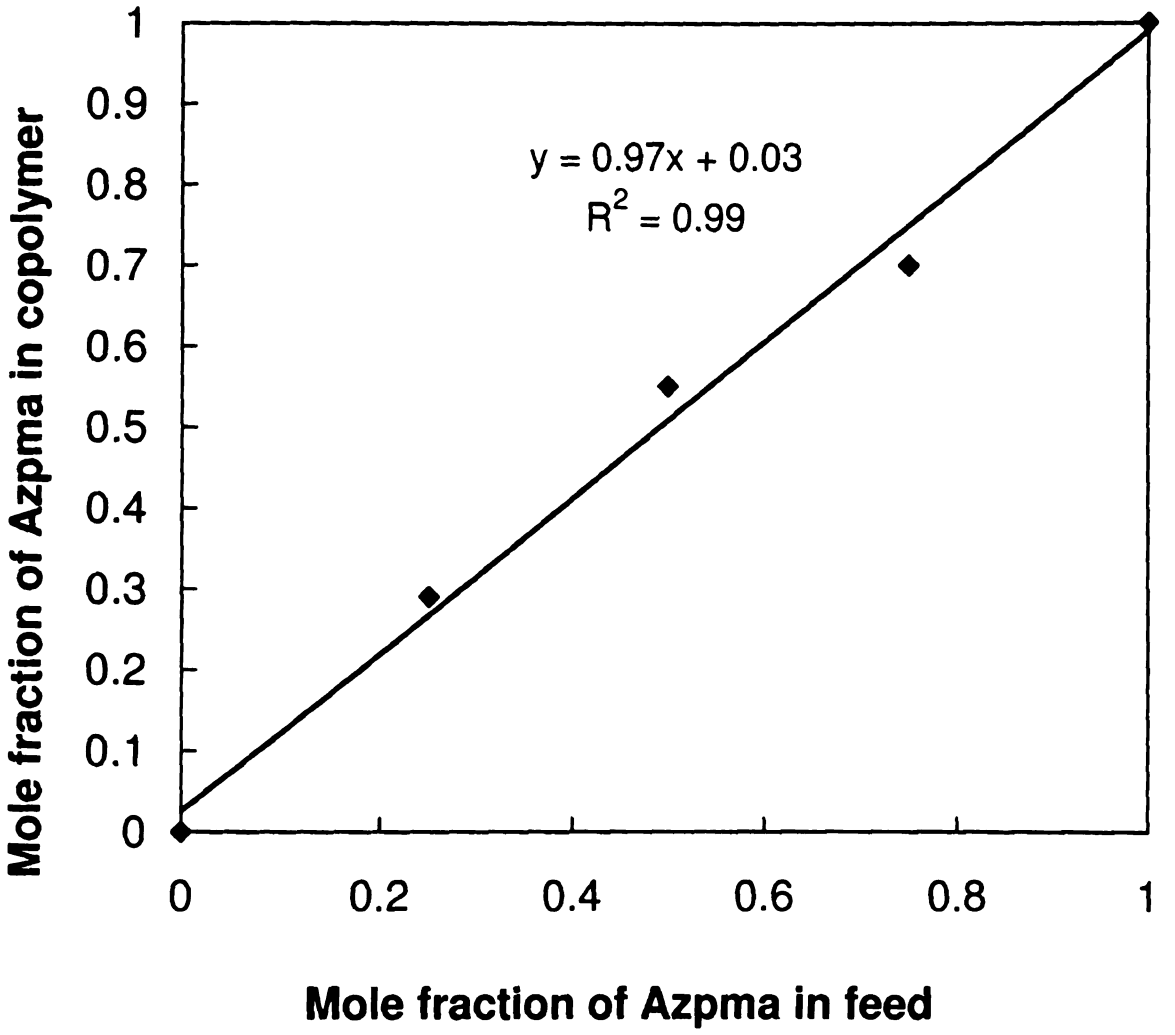

Figure 5.7. FTIR analysis of the copolymer data in Figure 5.6. The ratio of the comonomers in the copolymer was determined by integrating the azide and carbonyl peaks and then normalized by the carbonyl peak area.

We also copolymerized AZPMA and PEGMA. The ethylene oxide side chain of PEGMA (average molecular weight ~ 300) is significantly longer compared to EGMA, and copolymer brushes with PEGMA are more hydrophilic. Because of the large difference in side chain length in AZPMA and PEGMA, we carried out a similar copolymerization study to assess the randomness of copolymerizations. We first used reflectance FTIR to analyze several gold surfaces coated with poly(AZPMA-*co*-PEGMA) ([AZPMA] = [PEGMA] in the feed) corresponding to different polymerization times from 5 min to 4 h. Figure 5.8 shows that the mole fraction of AZPMA, determined from the peak ratios of the azide and carbonyl bands, was 0.50 ± 0.02 for samples from 90 nm to 250 nm. We then synthesized poly(AZPMA-*co*-PEGMA) brushes at different feed ratios and characterized them by ellipsometry and FTIR (Figures 5.9 and 5.10). Figure 5.9 shows that the polymerization profiles of PEGMA and AZPMA are similar, but copolymerizations were faster than homopolymerizations. This behavior suggests that copolymerization favors alternation, i.e. the growing chains preferentially add the comonomer. However, analysis of the FTIR data for the copolymer brushes (Figure 5.11) indicates that the copolymer compositions match the feed ratios, as expected for a random copolymerization. Returning to the copolymerization data for poly(EGMA-*co*-AZPMA) in Figure 5.5, there may be similar rate enhancements for copolymerizations, but not as significant as poly(PEGMA-*co*-AZPMA). However, the IR data indicate that irrespective of their side chain length, EGMA and PEGMA form random copolymer brushes with AZPMA.

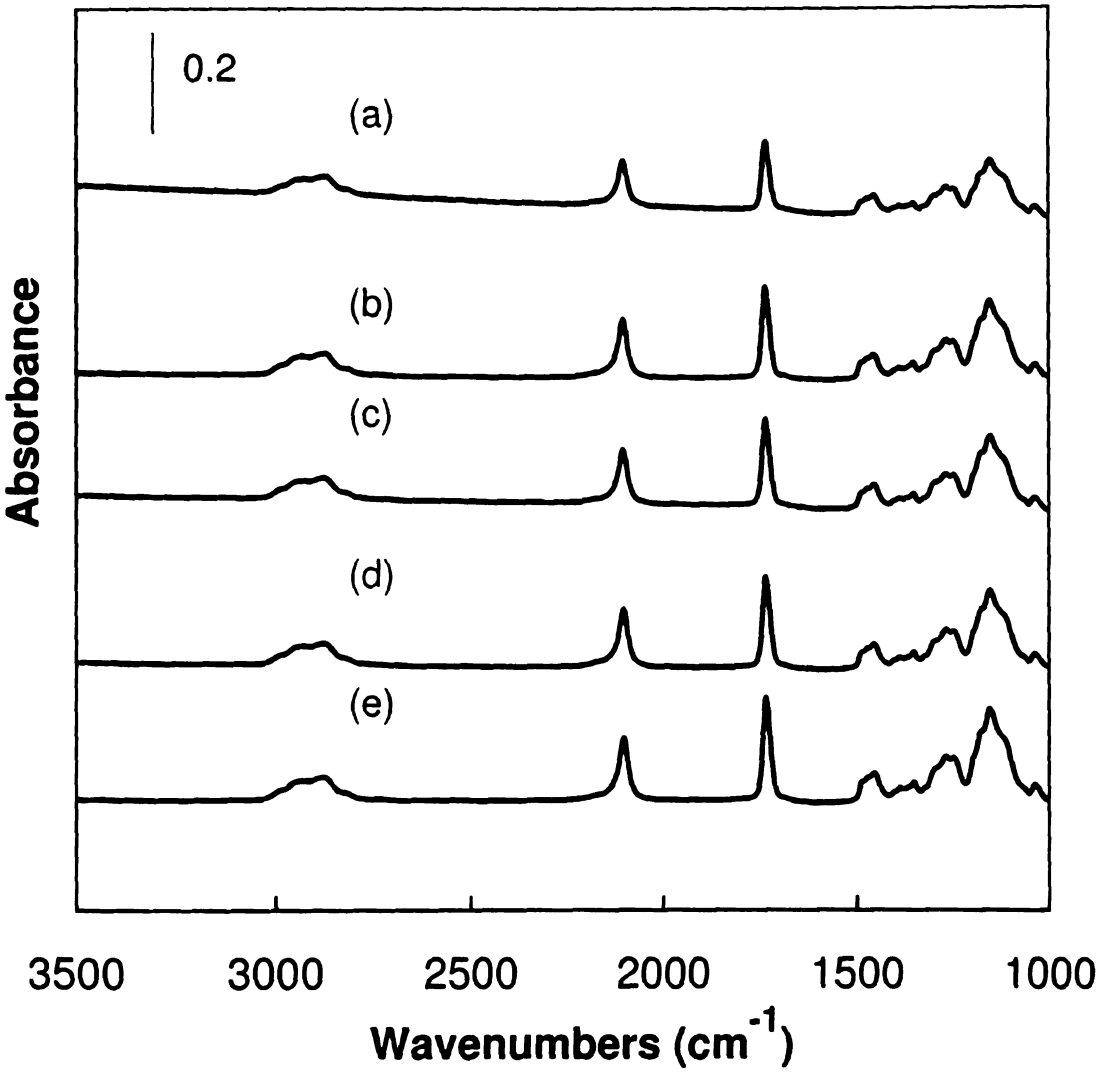

Figure 5.8. Reflectance FTIR spectra of gold substrates coated with poly(AZPMA-*co*-PEGMA) brushes at 50 °C using an equimolar feed ratio at different polymerization times (a) 5 min (b) 30 min (c) 1 h (d) 2 h and (e) 4 h. The polymerization system was CuCl/PMDETA/DMF.

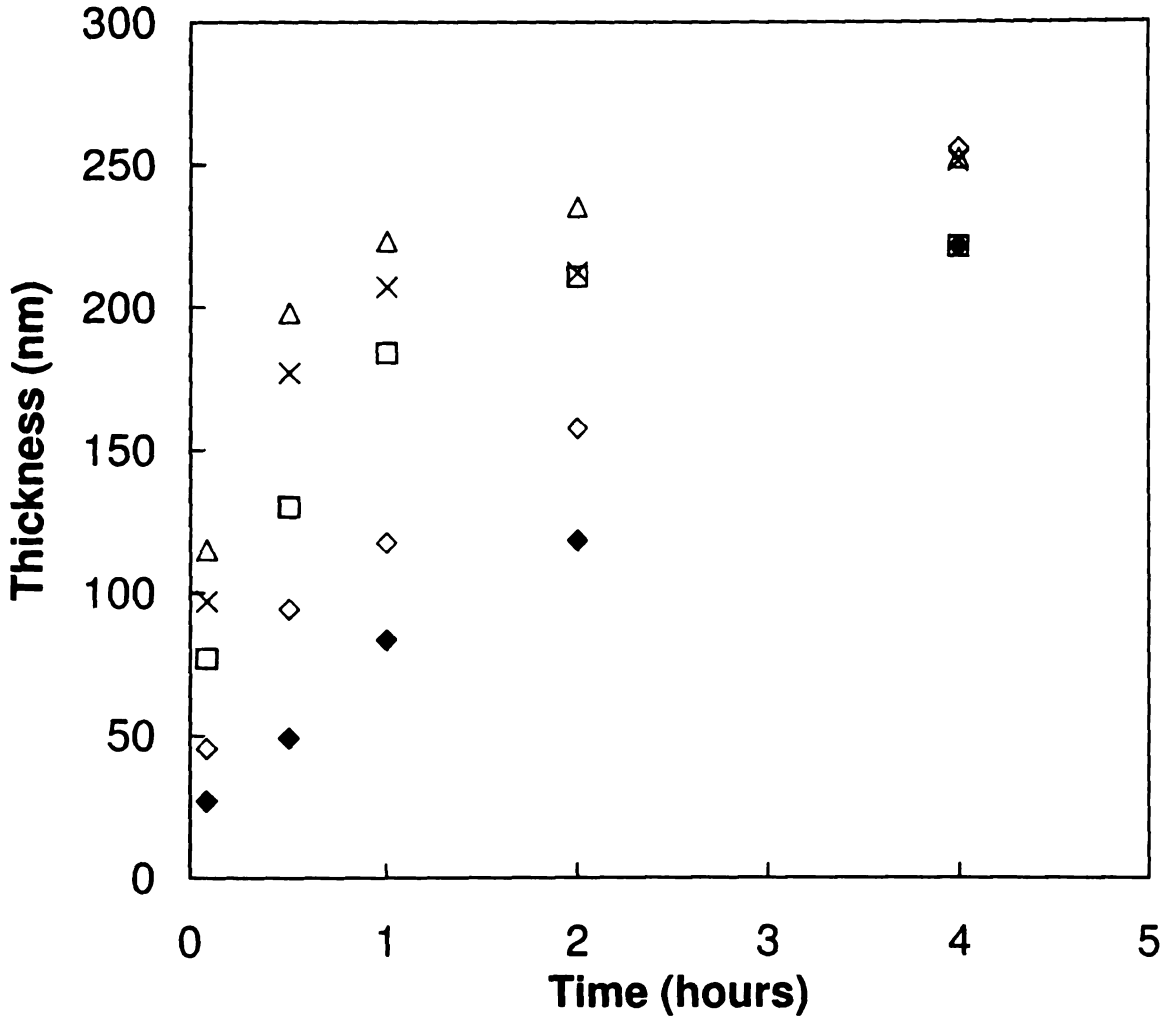

Figure 5.9. Evolution of the ellipsometric thickness with time at 50 °C for polyAZPMA and poly(AZPMA-*co*-PEGMA) brushes with time grown from initiators immobilized on gold substrates at various initial feed ratios, using the CuCl/PMDETA/DMF system. ◆AZPMA/PEGMA (100/0), △AZPMA/PEGMA (75/25), ×AZPMA/PEGMA (50/50), □AZPMA/PEGMA (25/75), ◇AZPMA/PEGMA (0/100). Each point represents a different film.

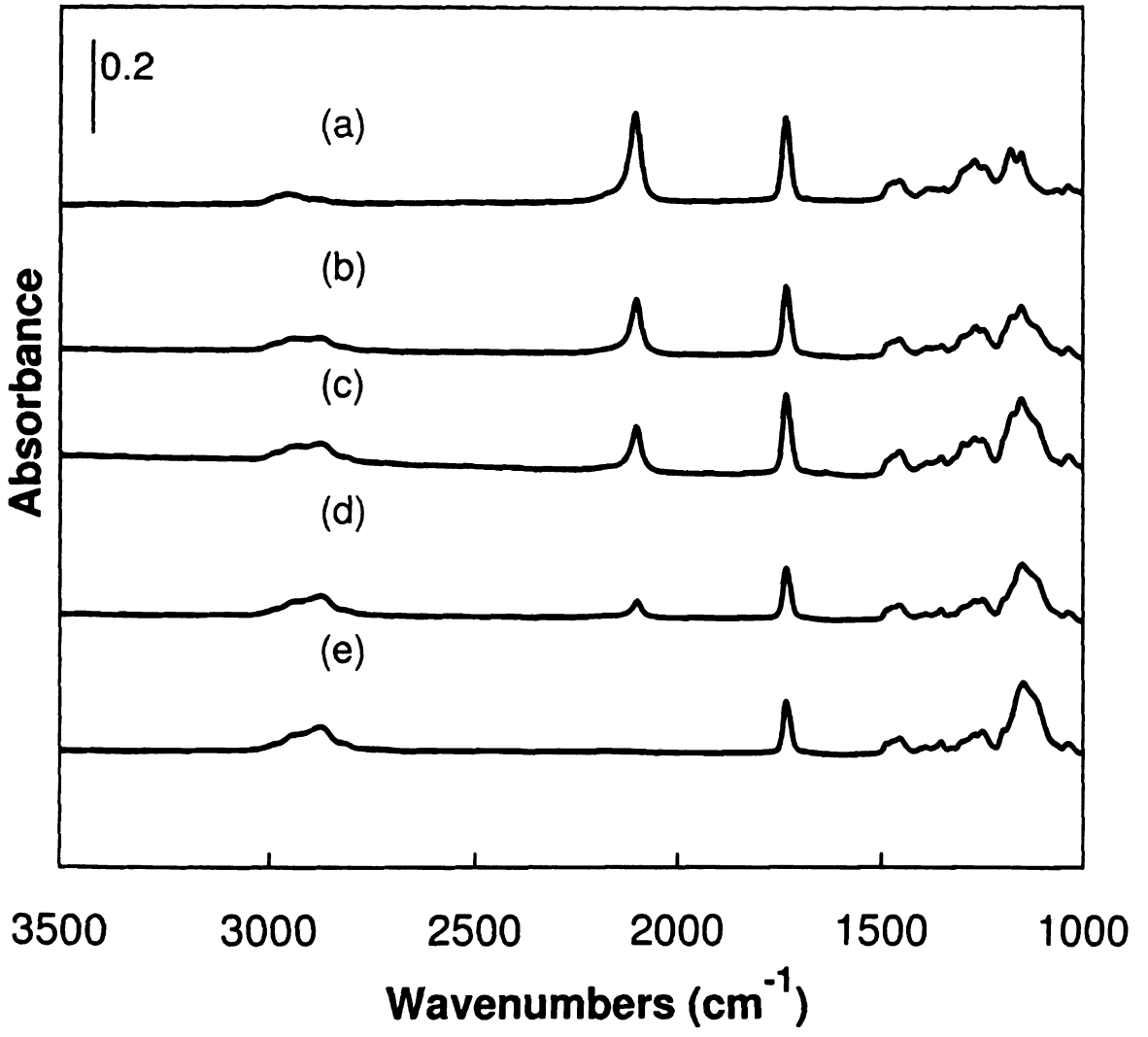

Figure 5.10. Reflectance FTIR spectra of gold substrates coated with polyAZPMA, poly(AZPMA-*co*-PEGMA) and polyPEGMA brushes grown at different feed ratios. (a) AZPMA/PEGMA (100/0) (b) AZPMA/PEGMA (75/25) (c) AZPMA/PEGMA (50/50) (d) AZPMA/PEGMA (25/75) (e) AZPMA/PEGMA (0/100). The polymerization system was CuCl/PMDETA/DMF at 50 °C.

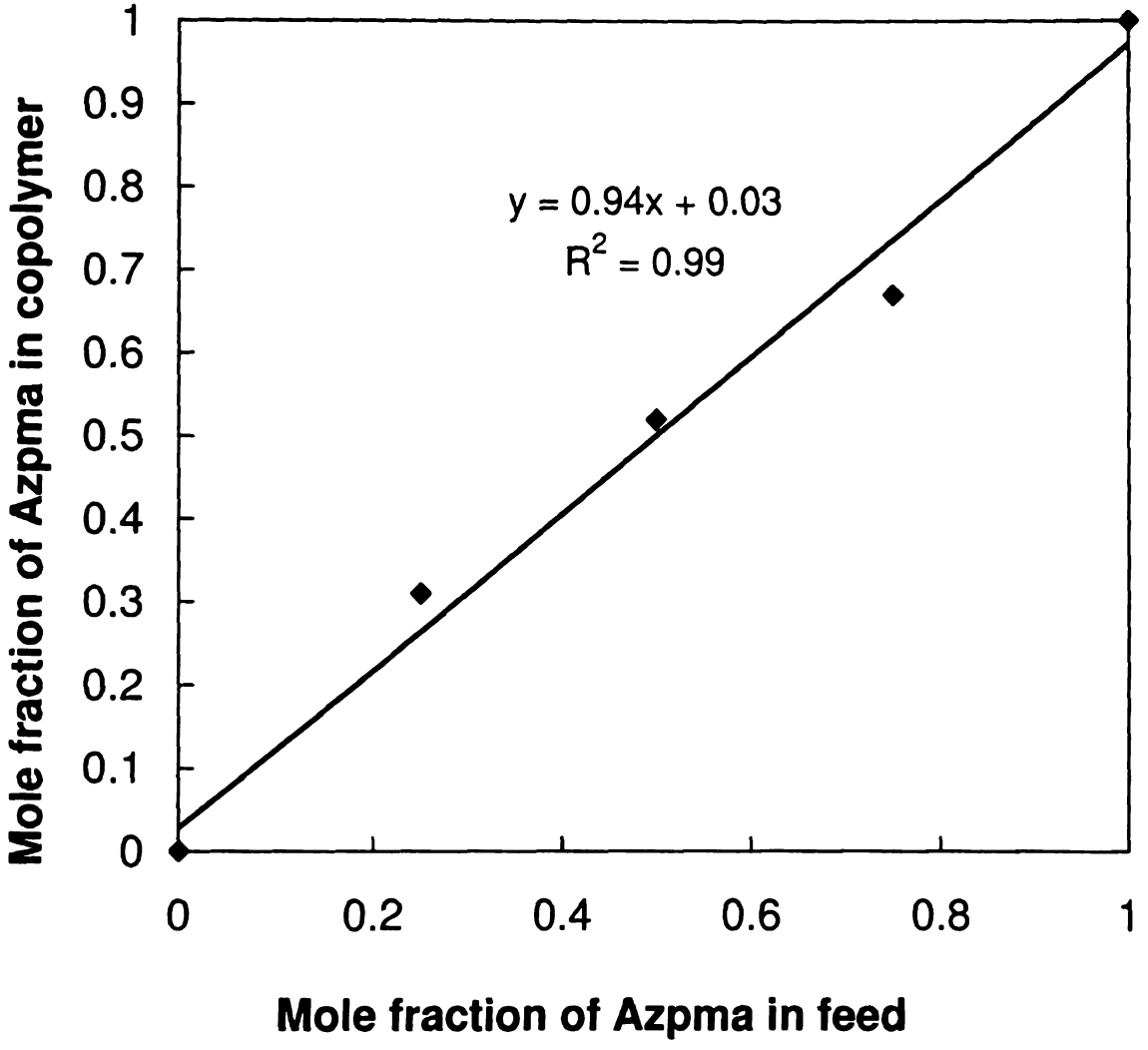

Figure 5.11. FTIR analysis of the copolymer brush data of Figure 5.10. The copolymer composition was determined by integration of the azide and carbonyl peaks and normalized by the carbonyl peak area.

5.3.3. Derivatization of copolymer brushes with dyes via click chemistry

Surface grafted polyAZPMA and AZPMA copolymers are excellent substrates for the synthesis of modified polymer brushes via click chemistry. The number of reactive azide groups can be controlled by the copolymer composition, which is simplified by the apparent random incorporation of PEGMA and EGMA comonomers into the brush. Copolymers are particularly useful since they reduce the high local concentration of azides within the polymer film which may reduce the efficiency of click functionalization compared to reactions in dilute solutions of polyAZPMA.[11] To improve click efficiency, increase polymer hydrophilicity, and reduce the functional group density, we synthesized copolymer brushes with the hydrophilic comonomers, PEGMA and EGMA. To assess the click reaction rate for grafted copolymer brushes, we appended a fluorescent dye, modified with a terminal alkyne, to AZPMA homopolymers and copolymers in DMF using CuBr/PMDETA as the catalyst at 50 °C. Both gold and ITO surfaces were used as substrates; gold for analysis by reflectance FTIR, and ITO for UV-vis spectroscopy. Figure 5.12 shows representative UV-vis spectra of ~200 nm thick poly(AZPMA-*co*-PEGMA) (50/50) brushes grown from ITO surfaces for different reaction times. The click reaction was almost complete within 5 min, as the absorbance marginally increased from 5 min to 1 hour.

To quantify the click reaction kinetics, we used reflectance FTIR to monitor the disappearance of azide peak at ~ 2100 cm^{-1} and the appearance of aromatic C=C stretching at ~1600 cm^{-1} during the first hour span of the reaction, where desorption observed was negligible. The kinetic study (Figure 5.13 and Figure 5.14) confirmed that

the click reaction is fast, with > 60% of the azides reacted within 1 min. The rate was nearly independent of the brush architecture, with copolymers having fewer azides reacting slightly faster than polyAZPMA. There are several reasons for the rapid click reaction: (1) the local concentration of azide groups in a brush is much higher than soluble polyAZPMA, as observed by Li *et al.* in the case of azide grafted on silica nanoparticles;[35] (2) while the azide is immobilized on a polymer brush, the dye molecule is small and readily diffuses through the brush; (3) the azide group forms triazoles, which bind and stabilize Cu(I)[36,37] and hence enhances the local concentration of copper catalyst; and (4) CuBr/PMDETA is a highly efficient click catalyst.[11]

Interestingly, the click reaction never went to completion when the substrate was polyAZPMA brushes or copolymer brushes with >50% AZPMA. This may reflect reduced diffusion of the alkynes through the brush architecture, especially near the substrate surface. The effect seems to be limited to azides near the surface, since the reaction rates are similar for homopolymers, and copolymers with varying ethylene oxide chain lengths. The rapid click reaction may be assisted by the DMF solvent, since DMF at 50 $^{\circ}$C is a good solvent for homopolymer and copolymer brushes, enabling the dye molecule and catalysts to diffuse through the brush.

An important observation is that prolonged soaking the brush-coated substrate in the click solution results in brush desorption. After 24 h of reaction, the dye absorbance decreased instead of increasing. A similar phenomenon was observed via reflectance FTIR spectroscopy where the intensities of the characteristics peaks of thick films (>150 nm) decreased over time.

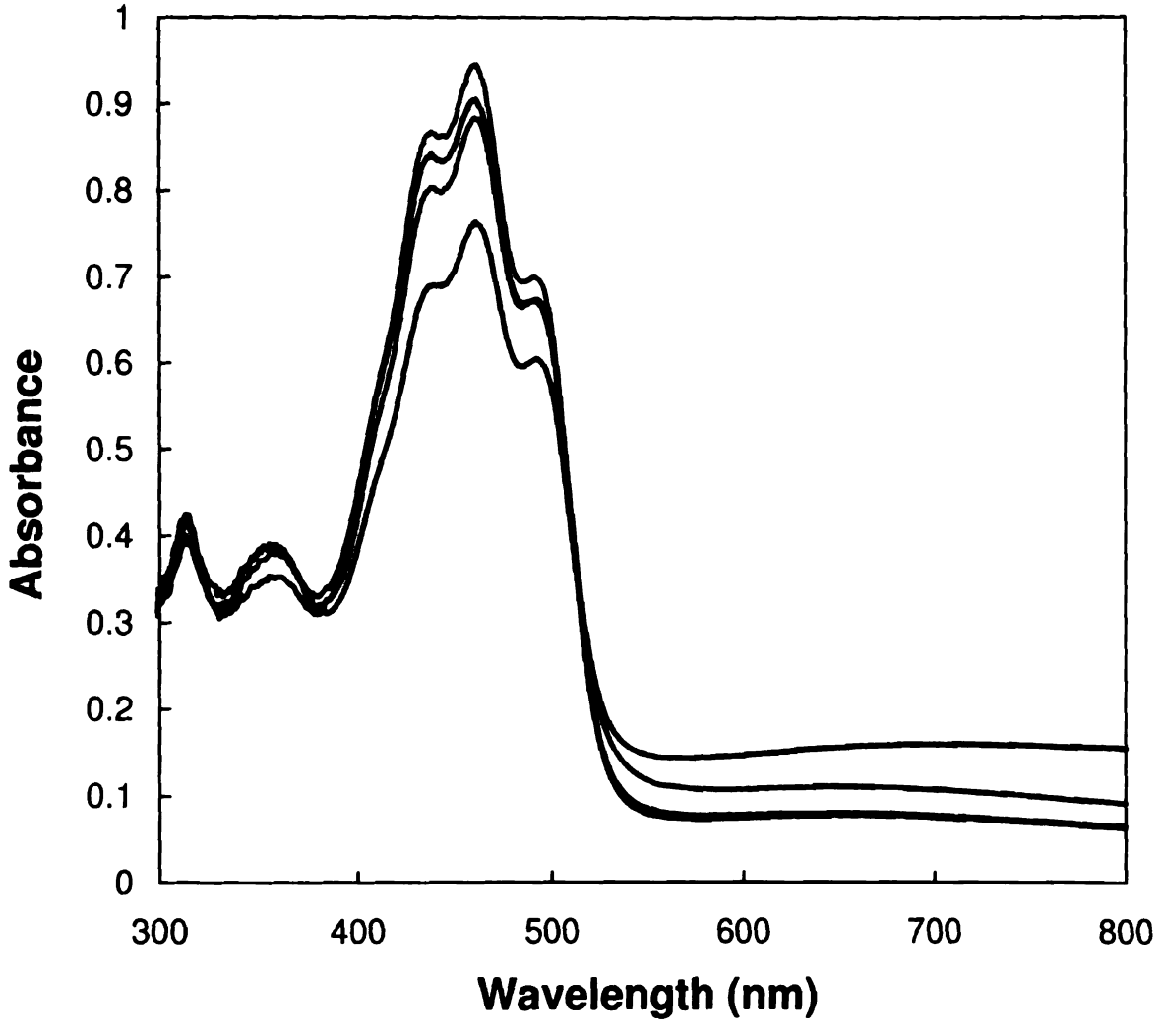

Figure 5.12. UV-vis spectra of ITO substrates coated with ~180 nm of poly(AZPMA-*co*-PEGMA) (50/50) showing the evolution of the click reaction between the copolymer and a fluorescent dye . Blue line: 5 min, pink line: 1 h, red line: 4 h and green line: 24 h.

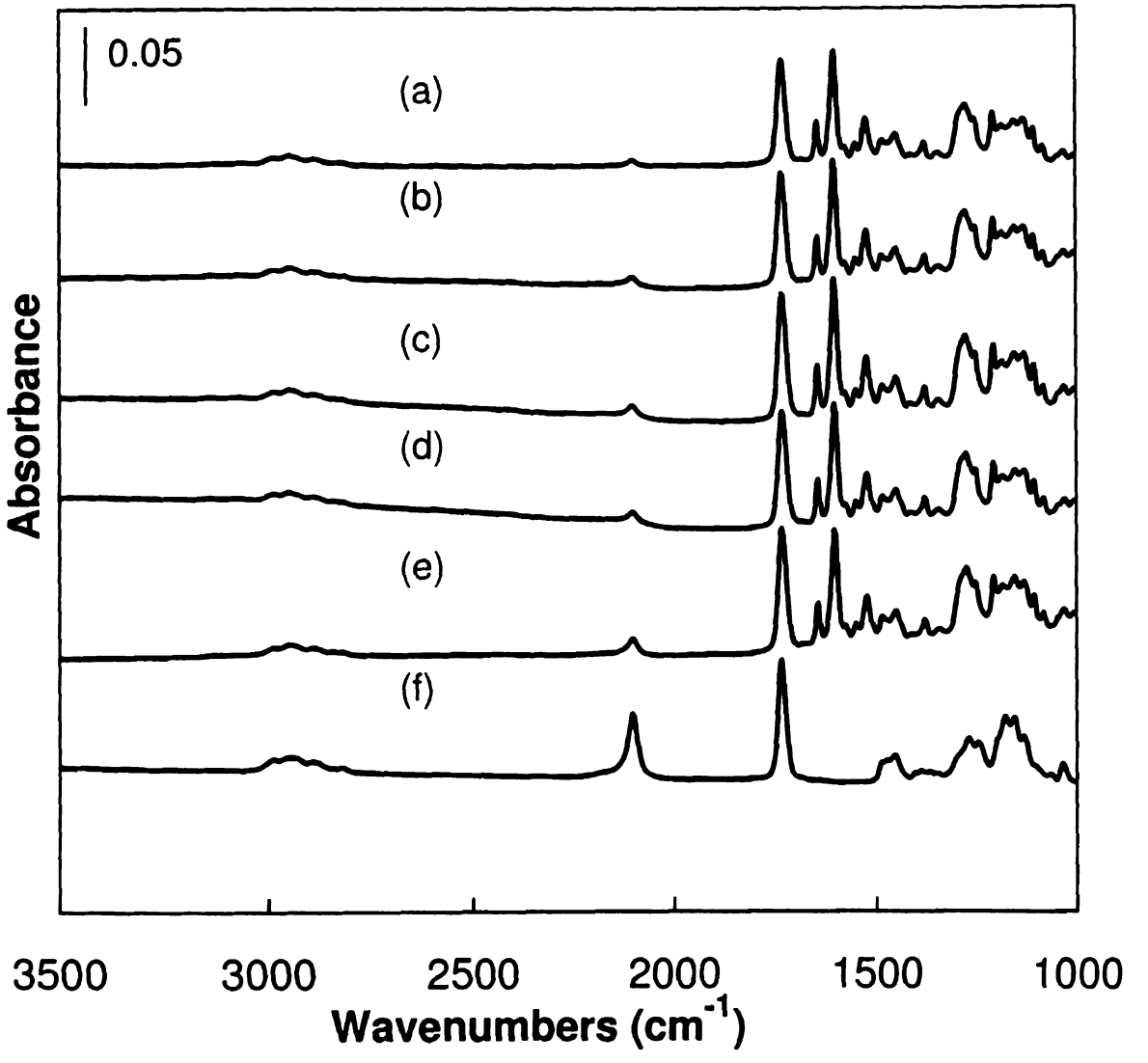

Figure 5.13. Reflectance FTIR spectra of gold substrates coated with ~200 nm copolymer brushes of poly(AZPMA-*co*-PEGMA) (50/50) showing the evolution of the click reaction between the copolymer and a fluorescent dye. (a) 1 h (b) 30 min (c) 15 min (d) 5 min (e) 1 min (f) 0 min.

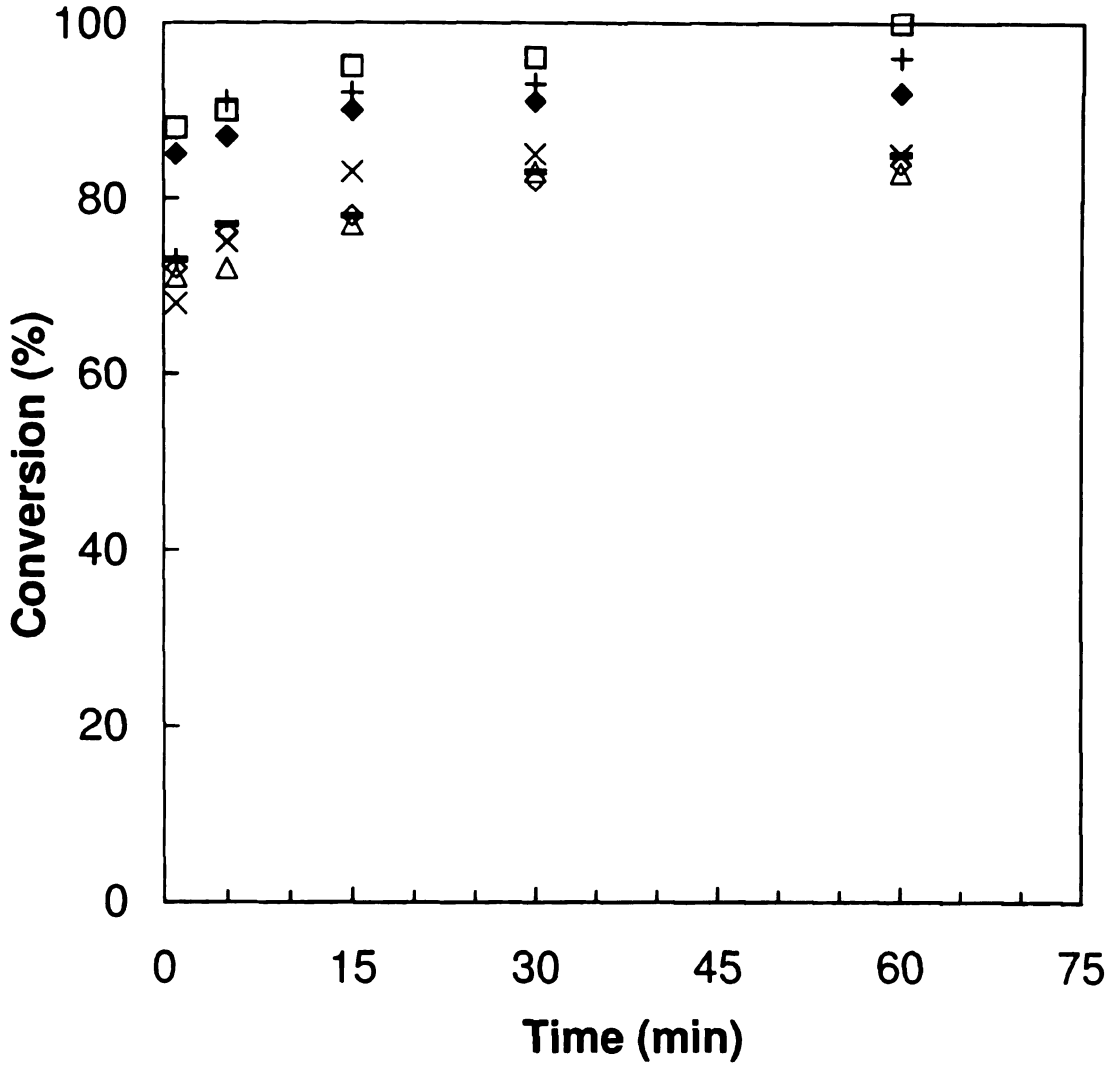

Figure 5.14. Kinetics of the click reaction between a fluorescent dye and ~200 ± 30 nm films of poly(AZPMA), poly(AZPMA-*co*-EGMA) and poly(AZPMA-*co*-PEGMA) grown from gold substrates. The data were extracted from reflectance FTIR spectra analogous to those shown in Figure 5.13. ◇AZPMA/EGMA (100/0), —AZPMA/EGMA (75/25), ◆AZPMA/EGMA (50/50), □AZPMA/EGMA (25/75), ×AZPMA/PEGMA (75/25), △AZPMA/PEGMA (50/50), +AZPMA/PEGMA (25/75). Here, each point represents a different film.

We used the absorbance values at λ_{max} to quantify the covalently bound dye in the copolymer brushes. Alternative methods such as measuring the change in molecular weight or using ellipsometry to monitor changes in film thickness after the click reaction were less precise. UV-vis spectra of the dye were obtained in air and in various solvents, and since we found no changes in the spectra, we assumed that the molar extinction coefficients for the dye in solution and on surfaces is identical. Rearranging the Lambert-Beer's law, $A = \varepsilon\ b\ c$; where A = absorbance, ε = molar extinction coefficient, b = path length, and c = concentration of the solution to $A = (\varepsilon/a)\ a\ b\ c$; where, a = area of the solution exposed to the light, provides $\mathbf{A = \varepsilon\ \Gamma}$; where Γ = the grafting density, (moles/area). To calculate the grafting density (Γ), we need to know the surface absorbance at λ_{max} and molar extinction coefficient of the dye. The molar extinction coefficient of the dye (ε = 52227 cm^2/mol) was calculated from the absorbance values at λ_{max} in THF at 4 different concentrations (Figure 5.15). We estimated the dye molecule grafting density (Γ) from ε and the data from Figures 5.16, 5.17 and 5.18. The dye absorbance tracks the azide content in poly(AZPMA-*co*- PEGMA), until it reaches its maxima for the homopolymer (100% azide).

Figure 5.19 shows fluorescence microscopy images from ITO coated with ~180 nm of poly(AZPMA-*co*-EGMA) (1:1) after a 5 min click reaction with the alkynylated dye, and a control surface, treated identically but without the copper catalyst. The fluorescence of the clicked surface confirms that the dye has been bound to the surface, while the lack of fluorescence for the control surface confirms that physical adsorption of the fluorescent reactant can be disregarded, as observed by Hvilsted and coworkers.[28]

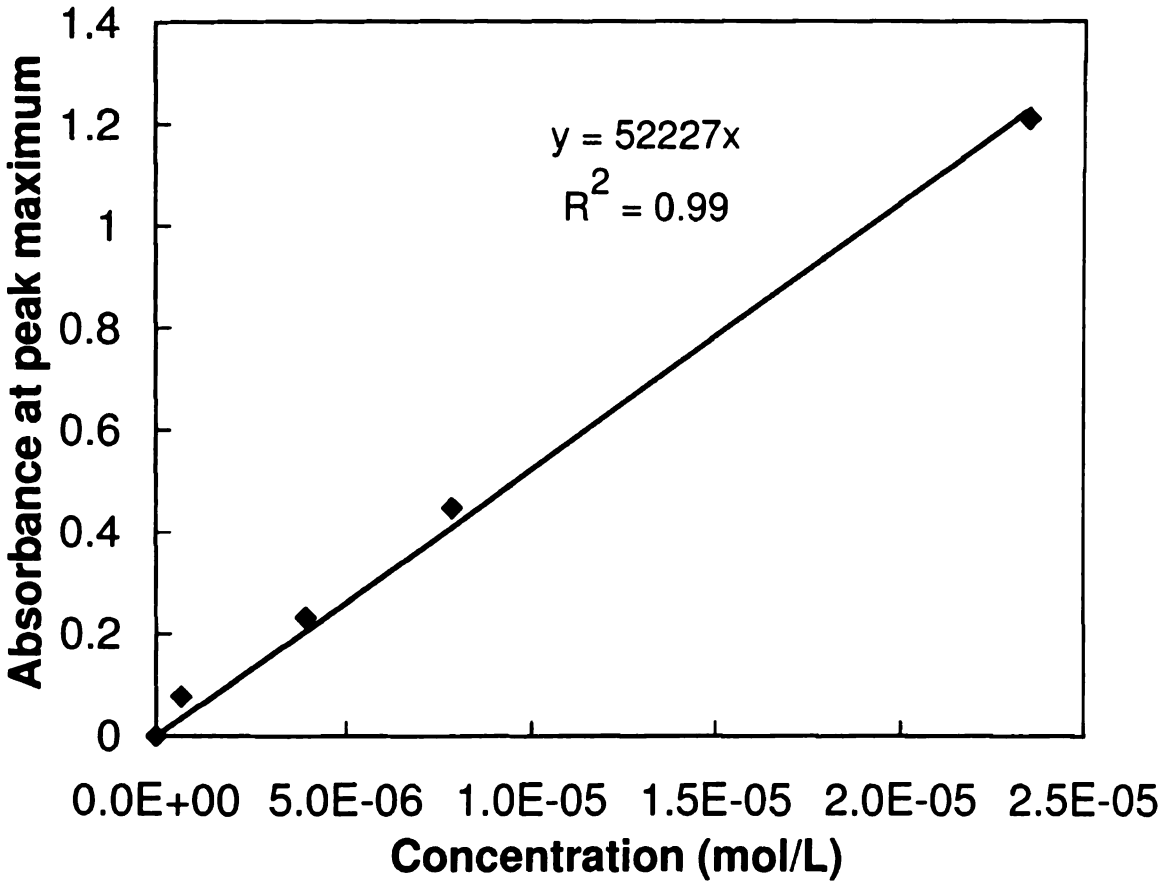

Figure 5.15. Measurement of the molar extinction coefficient of the alkyne modified fluorescein dye.

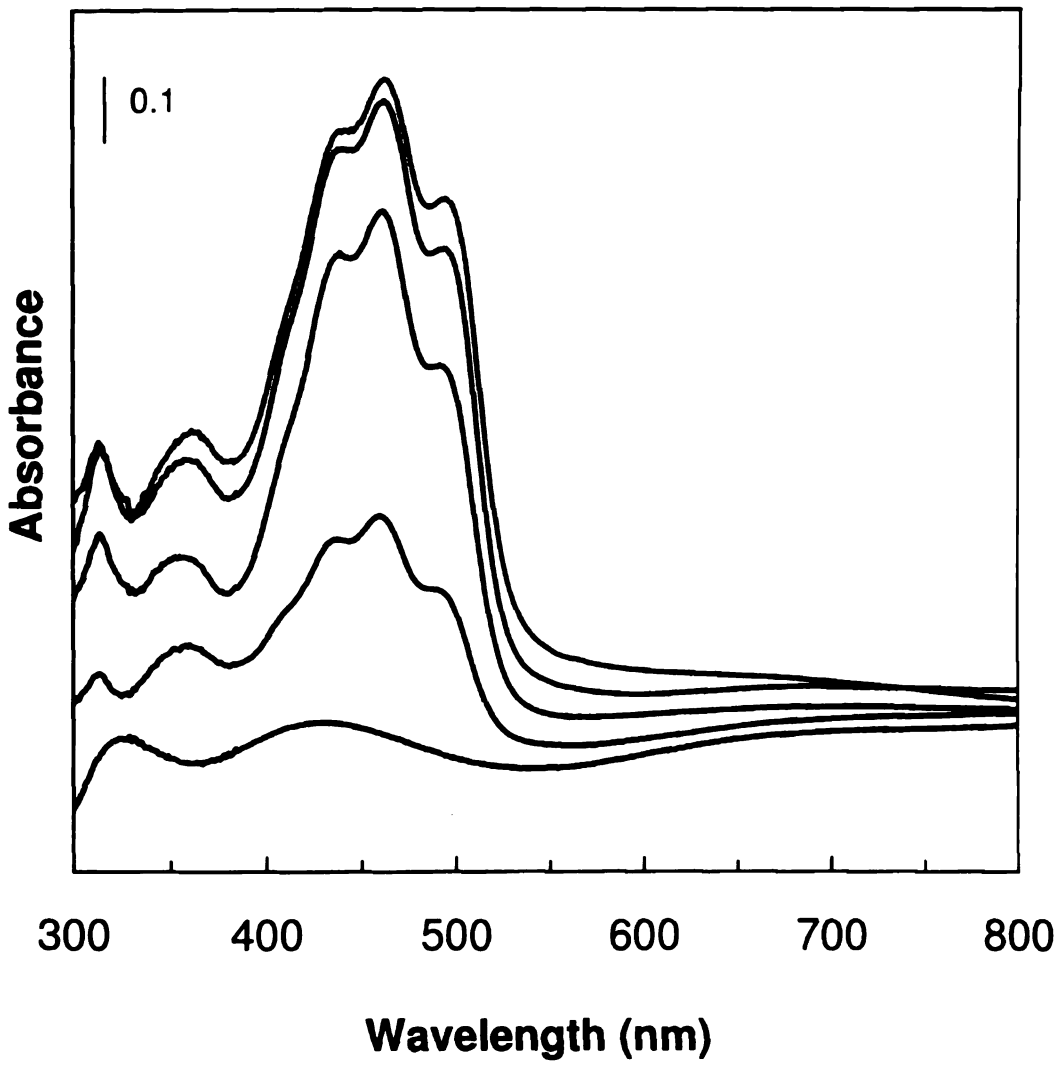

Figure 5.16. UV-vis spectra of ~ 200 ± 30 nm thick polyAZPMA and poly(AZMPA-*co*-PEGMA), and polyPEGMA brushes grown from ITO substrates after a 5 min click reaction with a alkynylated fluorescent dye. Green line: before clicking to AZPMA (100/0), blue line: after clicking to AZPMA (25/75), magenta line: after clicking to AZPMA/PEGMA (50/50), black line: after clicking to AZPMA/ PEGMA (75/25), red line: after clicking to AZPMA/ PEGMA (100/0).

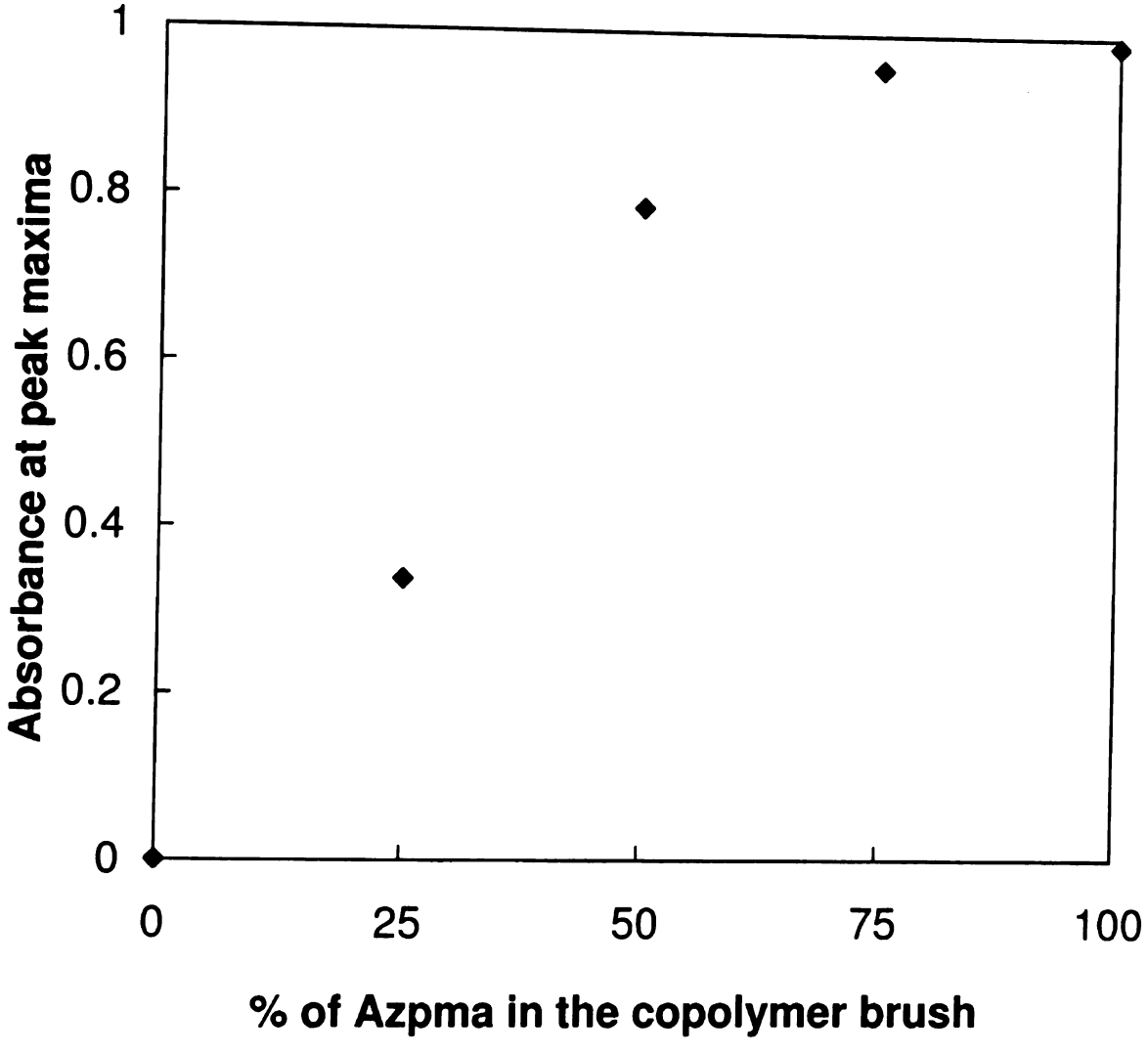

Figure 5.17. Absorbance at λ_{max} (463 nm) obtained from the UV-vis spectra in Figure 5.15.

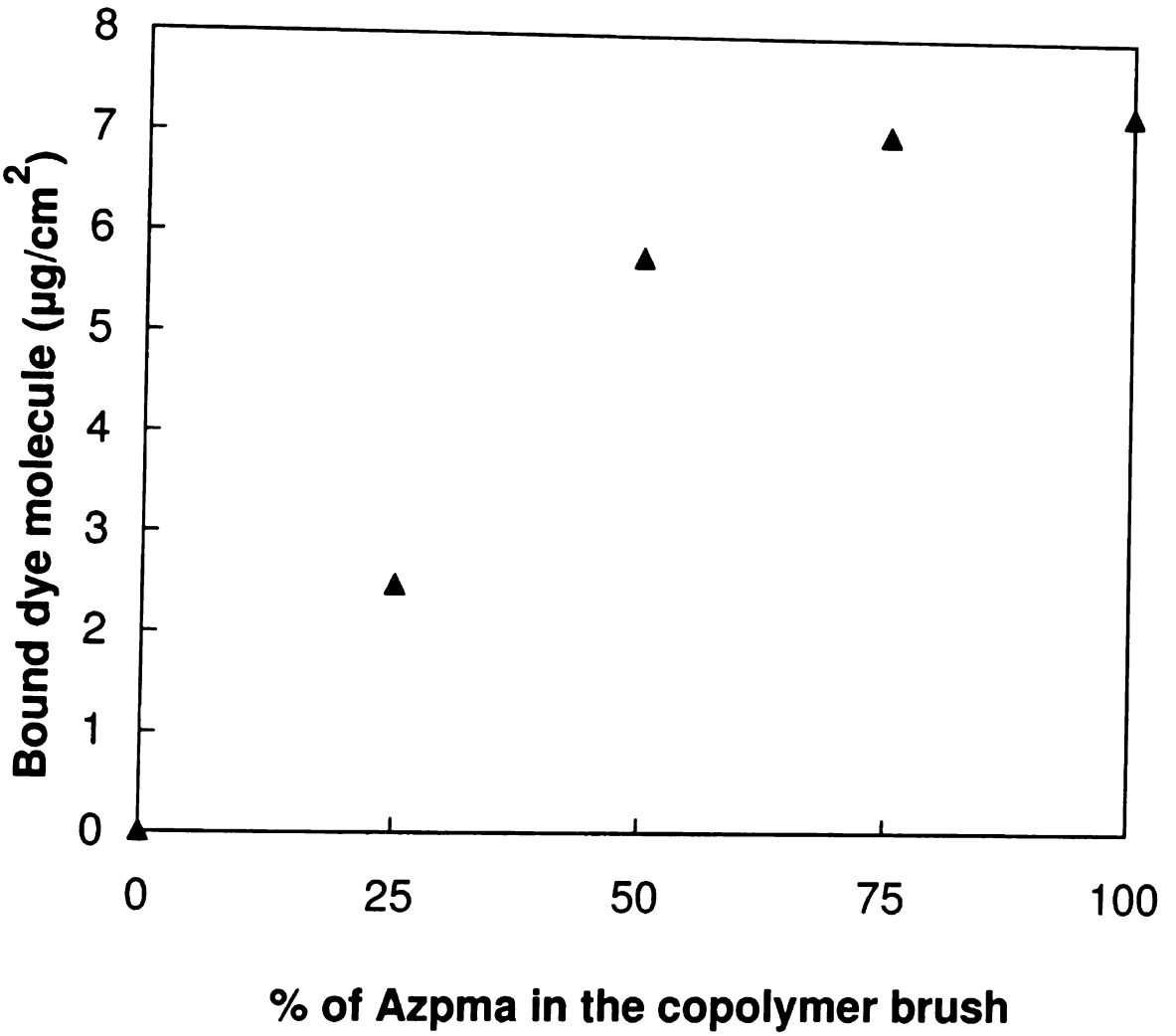

Figure 5.18. Dye molecule binding as a function of the per cent AZPMA in a 200 ± 30 nm poly(AZMPA-*co*-PEGMA) brushes on ITO surface. The dye molecule binding was determined by dividing the UV-vis spectral peak maxima of the different copolymer brushes (Figure 5.17) with the molar extinction coefficient obtained from Figure 5.15.

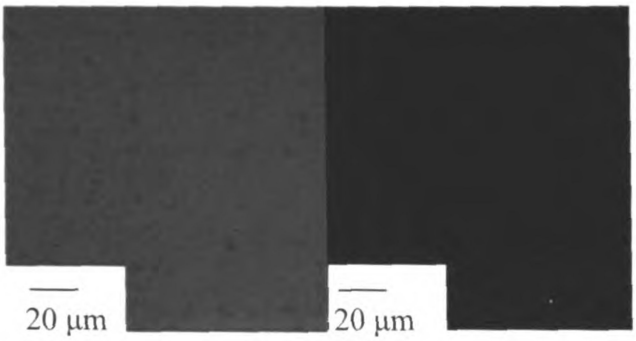

Figure 5.19. Representative fluorescence microscopy images of the clicked surface (left image) and the control (right), prepared without the copper catalyst but under otherwise equivalent conditions. The images were recorded using equal lighting and camera settings.

5.3.4 Derivatization of copolymer brushes via click chemistry with a water soluble polymer

The previous data show that dye molecules in DMF show comparable reactivity in click reactions with homopolymer and copolymer substrates. However, tethering biomolecules to brushes requires an aqueous environment, and therefore we synthesized a water soluble copolymer brush to test whether the click reaction would be successful in aqueous environments. For this experiment, alkynylated mPEG 5000, a water soluble polymer, was used for the click reactions. Figure 5.20 shows reflectance FTIR spectra for ~50 nm thick films of polyAZPMA and poly(AZPMA-*co*-PEGMA) grown from gold surfaces, before and after click reactions with an alkynylated mPEG 5000 in water at room temperature for 12 hours. Compared to click reactions with the alkynylated dye, the reaction of the alkynylated mPEG polymer was slow, likely due to slower diffusion of the higher molecular weight of the polymer (5000 g/mol).

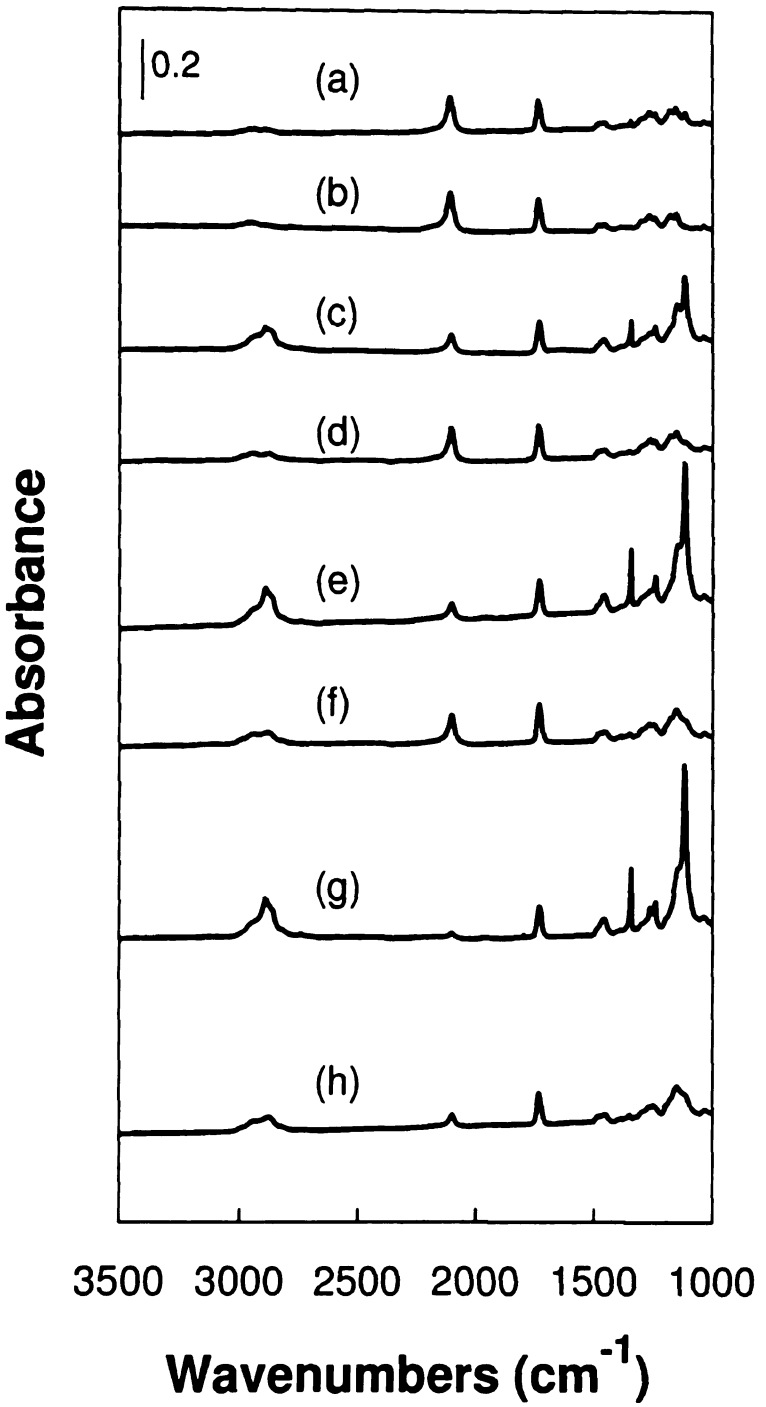

Figure 5.20. Click reactions for 12 hours with a water soluble polymer (alkynylated mPEG 5000) monitored by reflectance FTIR spectra of gold substrates coated with ~ 50 ± 10 nm of poly(AZPMA) and poly(AZPMA-co-PEGMA) brushes (a) after clicking to AZPMA/PEGMA (100/0), (b) before clicking to AZPMA/PEGMA (100/0), (c) after

clicking to AZPMA/PEGMA (75/25), (d) before clicking to AZPMA/PEGMA (75/25), (e) after clicking to AZPMA/PEGMA (50/50), (f) before clicking to AZPMA/PEGMA (50/50), (g) after clicking to AZPMA/PEGMA (25/75), (h) before clicking to AZPMA/PEGMA (25/75).

Other reasons for the slow click reaction may include (1) the hydrophobicity of azide-containing polymer which could collapse and restrict access to the azide, (2) the lower reaction temperature (ambient temperature vs. 50 ^{o}C, and (3) the water soluble catalyst, CuBr/bpy, may be less efficient than the CuBr/PMDETA complex.[38]

Integrating the azide peaks at ~2100 cm^{-1} in FTIR spectra before and after the click reactions (Figure 5.20) reveals that click conversion increases as the PEGMA mole fraction in the polymer brush increases and becomes more hydrophilic (Figure 5.21). In addition, the changes in the intensities of the C-O stretching bands at 1100 and 1350, and C-H stretching at 2900 cm^{-1} are consistent with the azide peak analysis. Moreover, the thickness of the most hydrophilic brush, poly(AZPMA-*co*-PEGMA) (AZPMA/PEGMA = 25/75) nearly doubled, from 47 nm to 92 nm, after the click reaction. The thickness of the poly(AZPMA) brush was almost unchanged after the click reaction (< 10% change) under identical conditions (Figure 5.22).

The expansion of clicked poly(AZPMA-*co*-PEGMA) (25/75) film, and the IR analyses confirm that the click reaction occurs in the bulk film, while poly(AZPMA) films react primarily on the surface. Figures 21 and 22 also show that the click conversion and copolymer compositions, inferred from the change in film thickness, (Figure 5.22), are consistent for all polymers tested. Also, the more hydrophobic

poly(AZPMA-*co*-EGMA) films (shorter ethylene oxide chain, p=0, see Scheme 1) was marginally better than poly(AZPMA) films in terms the water-based click reactions (data not shown here). Therefore, the longer ethylene oxide chains in poly(AZPMA-*co*-PEGMA) films (p ~4, see Scheme 1) make the polymers sufficiently hydrophilic to effect immobilization of water soluble polymers by the click reaction.

70

60

5

Conversion (%)

4

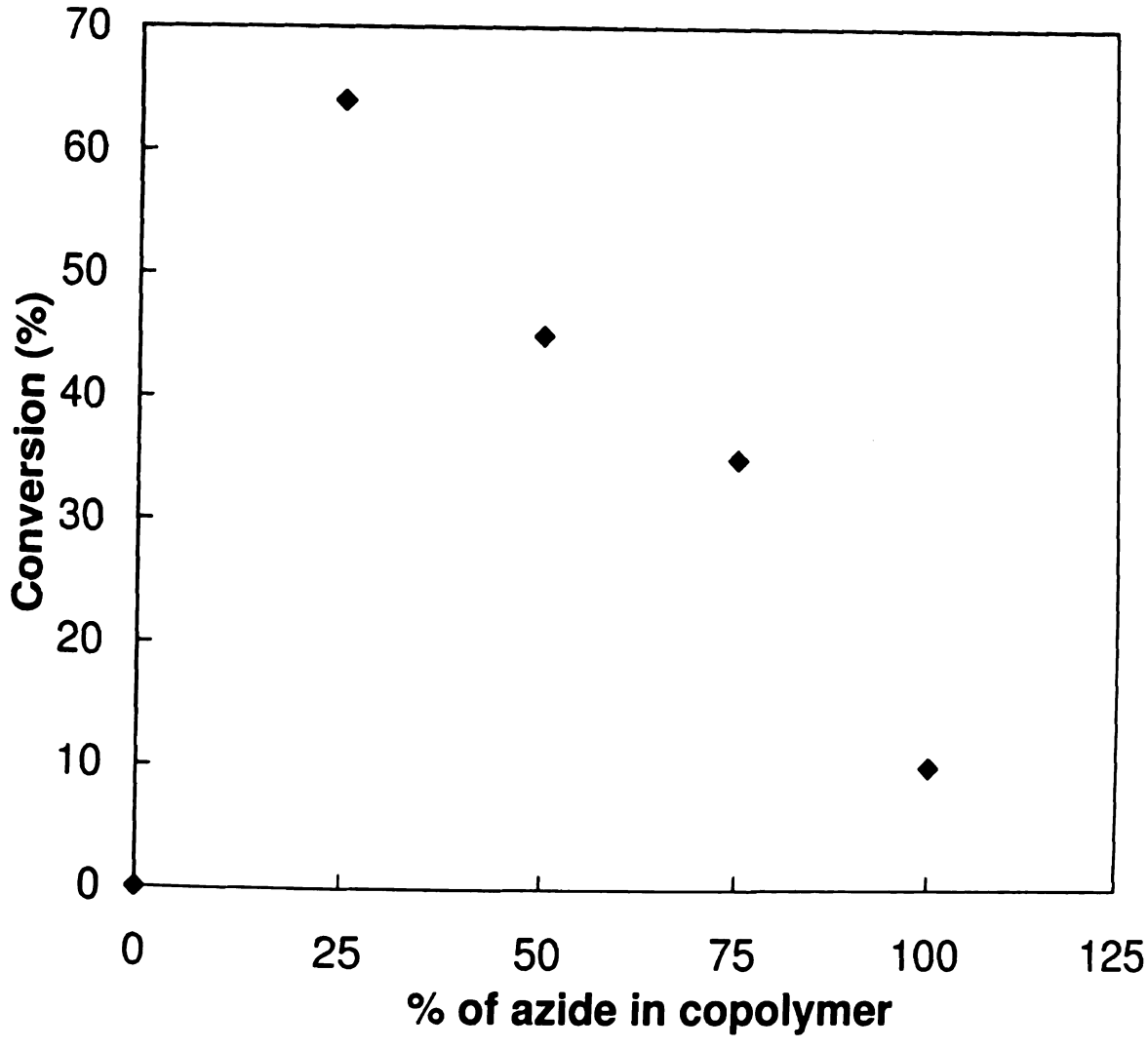

Figure 5.21. The disappearance of azide the via click reaction with alkynylated mPEG 5000 for 12 hours at room temperature as a function of the molar per cent azide in the copolymer brush for different feed ratios (see Figure 5.20). The conversion was calculated from FTIR spectra by integrating the azide peak before and after the click reaction.

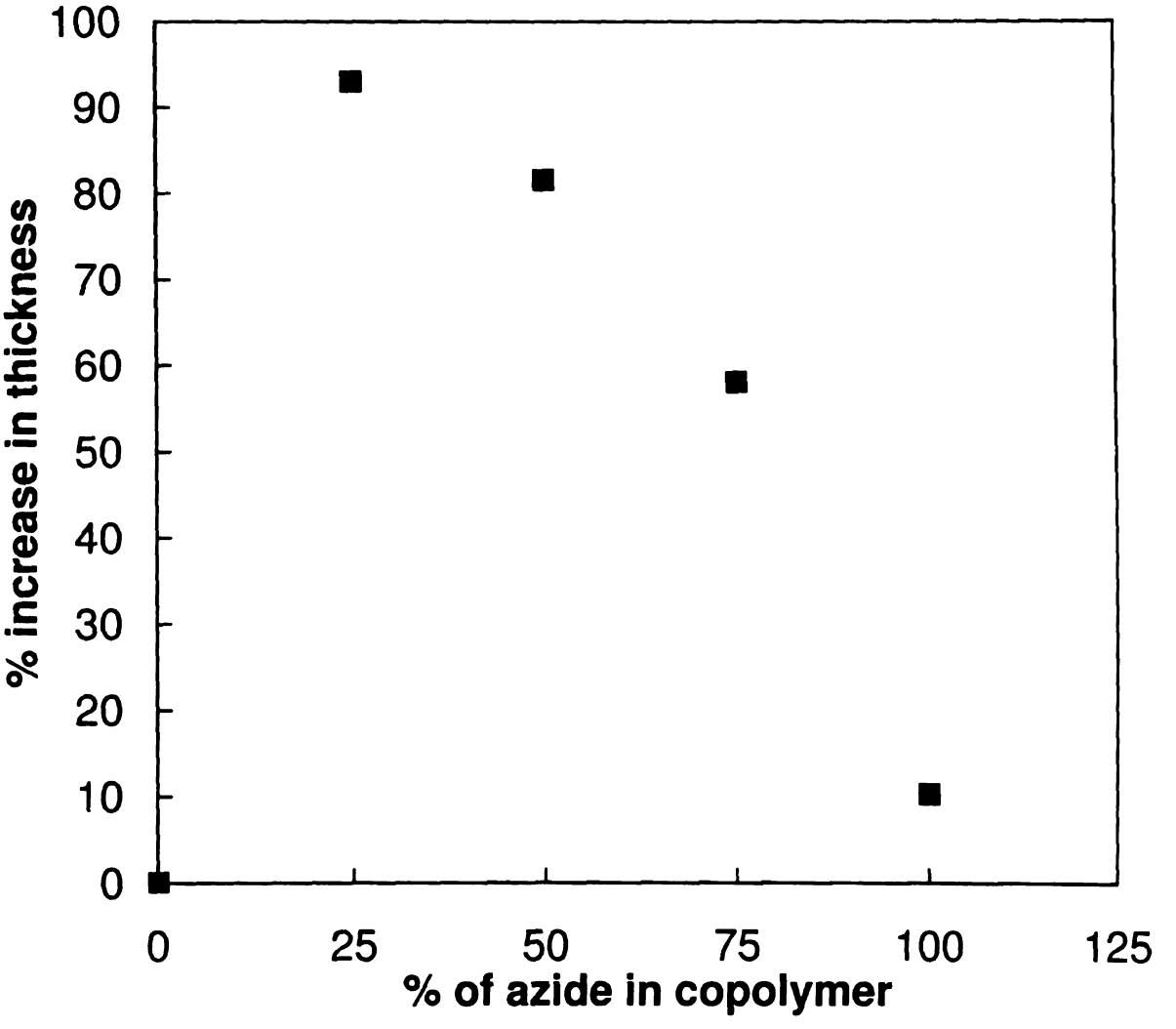

Figure 5.22. Increase in thickness after the click reaction with alkynylated mPEG 5000 for 12 hours at room temperature as a function of the molar per cent azide in the copolymer brush.

Interestingly, FTIR spectroscopy detected significant chain desorption while immobilizing alkynylated mPEG onto thick copolymer brushes (> 150 nm), and the click reaction was reasonably fast (significant conversion within 30 min). However, no desorption (no change of carbonyl peak height) occurred for thin films (~ 50 nm) even after 12 h of reaction. The severe desorption for poly(AZPMA-*co*-PEGMA) brushes, may be due to the long water-soluble side chains[39] and extreme steric crowding of the thick film. However, this needs to be investigated in detail.

5.4. Conclusions

Azidopropyl methacrylate (AZPMA) a functional monomer with a pendent clickable moiety, was grown from gold and ITO surfaces using surface-initiated ATRP. AZPMA enables post-polymerization modification of polymer brushes via the 1,3-dipolar cycloaddition of azides with acetylenes, and copolymerization with PEGMA and EGMA, provides control over the hydrophilicity and functional density of AZPMA polymers. Post-polymerization modification of homo and copolymer brushes was demonstrated by reacting with an alkyne-modified dye via click reactions. Kinetic studies showed that click reactions on surface-grafted homo/copolymer brushes were fast when run in DMF at 50 ^{o}C (> 60% conversion in 1 min) irrespective of the copolymer composition. The outcome of aqueous click reactions depends on the composition of the polymer brush. Using a alkynylated polyethylene glycol methyl ether (mPEG, M_n ~5000), the most hydrophilic copolymers, i.e. those with the highest fraction of PEGMA, immobilized the most mPEG, as evidence by the increase of the dry film thickness. Aqueous click reactions offer an alternative to ester or amide formation for the covalent immobilization of biomacromolecules.

References:

1 Wang, J. S.; Matyjaszewski, K. *J. Am. Chem. Soc.* **1995**, *117*, 5614.

2 Xia, J.; Gaynor, S. G.; Matyjaszewski, K. *Macromolecules* **1998**, *31*, 5958.

3 Matyjaszewski, K.; Xia, J. *Chem. Rev.* **2001**, *101*, 2921.

4 Kamigaito, M.; Ando, T.; Sawamoto, M. *Chem. Rev.* **2001**, *101*, 3689.

5 Rostovtsev, V. V.; Green, L. G.; Fokin, V. V.; Sharpless, K. B. *Angew. Chem. Int. Ed.* **2002**, *41*, 2596.

6 Tornoe, C. W.; Christensen, C.; Meldal, M. *J. Org. Chem.* **2002**, *67*, 3057.

7 Kolb, H. C.; Finn, M. G.; Sharpless, K. B. *Angew. Chem., Int. Ed.* **2001**, *40*, 2004.

8 Golas,P. L.; Matyjaszewski, K. *QSAR Comb. Sci.* **2007**, *26*, 1116.

9 Tsarevsky, N. V.; Sumerlin, B. S.; Matyjaszewski, K. *Macromolecules* **2005**, *38*, 3558.

10 Mantovani, G.; Ladmiral, V.; Tao, L.; Haddleton, D. M. *Chem. Commun.* **2005**, 2089.

11 Sumerlin, B. S.; Tsarevsky, N. V.; Louche, G.; Lee, R. Y.; Matyjaszewski, K. *Macromolecules* **2005**, *38*, 7540.

12 Gao, H.; Louche, G.; Sumerlin, B. S.; Jahed, N.; Golas, P.; Matyjaszewski, K. *Macromolecules* **2005**, *38*, 8979.

13 Advincula, R. C.; Brittain, W. J.; Caster, K. C.; Rühe, J. Eds.; *Polymer Brushes*; Wiley-VCH Verlag: Weinheim, **2004**.

14 Cullen, S. P.; Liu, X.; Mandel, I. C.; Himpsel, F. J.; Gopalan, P. *Langmuir* **2008**, *24*, 913.

15 Dai, J.; Bao, Z.; Sun, L.; Hong, S. U.; Baker, G. L.; Bruening, M. L. *Langmuir* **2006**, *22*, 4274.

16 Tsarevsky, N. V.; Braunecker, W. A.; Vacca, A.; Gans, P.; Matyjaszewski, K. *Macromol. Symp.* **2007**, *248*, 60.

17 Jain, P.; Dai, J.; Baker, G. L.; Bruening, M. L. *Macromolecules* **2008**, *41*, 8413.

18 Rühe, J.; Ballauff, M.; Biesalski, M.; Dziezok, P.; Gröhn, F.; Johannsmann, D.; Houbenov, N.; Hugenberg, N.; Konradi, R.; Minko, S.; Motornov, M.; Netz, R.; Schmidt,

M.; Seidel, C.; Stamm, M.; Stephan, T.; Usov, D.; Zhang, H. *Adv. Polym. Sci.* **2004**, *165*, 79, and references therein.

19 Minko, S. Ed.; *Responsive Polymer Materials: Design and Applications*; Blackwell Publishing: Boston, **2006**.

20 Lummerstorfer, T.; Hoffmann, H. *J. Phys. Chem. B* **2004**, *108*, 3963.

21 Gallant, N. D.; Lavery, K. A.; Amis, E. J.; Becker, M. L. *Adv. Mater.* **2007**, *19*, 965.

22 Kacprzak, K. M.; Maier, N. M.; Lindner, W. *Tetrahedron Lett.* **2006**, *47*, 8721.

23 Prakash, S.; Long, T. M.; Selby, J. C.; Moore, J. S.; Shannon, M. A. *Anal. Chem.* **2007**, *79*, 1661.

24 Schlossbauer, A.; Schaffert, D.; Kecht, J.; Wagner, E.; Bein, T. *J. Am. Chem. Soc.* **2008**, *130*, 12558.

25 Sanjuan, S.; Tran, Y. *J. Polym. Sci., Polym. Chem.* **2008**, *46*, 4305.

26 Sanjuan, S.; Tran, Y. *Macromolecules* **2008**, *41*, 8721.

27 Schoffelen, S.; Mark, H.; Lambermon, L.; Mark, B.; Eldijk, V.; Jan, C. M.; Hest, V. *Biocon. Chem.* **2008**, *19*, 1127.

28 Daugaard, A. E.; Hvilsted, S.; Hansen, T. S.; Larsen, N. B. *Macromolecules* **2008**, *41*, 4321.

29 Zhang, J.; Zhou, Y.; Zhu, Z.; Ge, Z.; Liu, S. *Macromolecules* **2008**, *41*, 1444.

30 Karanam, S.; Goossens, H.; Klumperman, B.; Lemstra, P. *Macromolecules* **2003**, *36*, 3051.

31 Shipp, D. A.; Wang, J. L.; Matyjaszewski, K. *Macromolecules* **1998**, *31*, 8005.

32 Matyjaszewski, K. *Curr. Org. Chem.* **2002**, *6*, 67.

33 Pintauer, T.; Matyjaszewski, K. *Coord. Chem. Rev.* **2005**, *249*, 1155.

34 Tsarevsky, N. V.; Matyjaszewski, K. *J. Polym. Sci., Polym. Chem.***2006**, *44*, 5098.

35 Li, Y.; Benicewicz, B. C. *Macromolecules* **2008**, *41*, 7986.

36 Chan, T. R.; Hilgraf, R.; Sharpless, K. B.; Fokin, V. V. *Org. Lett.* **2004**, *6*, 2853.

37 Sumerlin, B. S.; Tsarevsky, N. V.; Louche, G.; Lee, R. Y.; Matyjaszewski, K. *Macromolecules* **2005**, *38*, 7540.

38 Golas, P. L.; Tsarevsky, N. V.; Sumerlin, B. S.; Matyjaszewski, K. *Macromolecules* **2006**, *39*, 6451.

39 Lebedeva, N. V.; Sun, F. C.; Lee, H.; Matyjaszewski, K.; Sheiko, S. S. *J. Am. Chem. Soc.* **2008**, *130*, 4228.